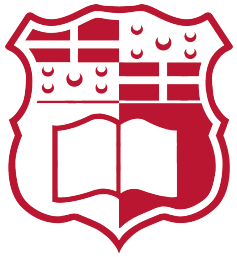

Validation of a motion management and gating protocol on the Elekta Unity MR LINAC for margin reduction in prostate cancer

Kelsey Ann Micallef

Supervised by Mr Martin Pirotta

Co-supervised by Mr Paul B. Bezzina

Department of Medical Physics

Faculty of Health Science

University of Malta

September, 2025

A dissertation submitted in partial fulfilment of the requirements for the degree of M.Sc. in Medical Physics.

WWW.UM.EDU.MT

First edition, September 29, 2025

L-Università ta' Malta

FACULTY/INSTITUTE/CENTRE/SCHOOL Health Sciences

DECLARATIONS BY POSTGRADUATE STUDENTS

(a) Authenticity of Dissertation

I hereby declare that I am the legitimate author of this Dissertation and that it is my original work.

No portion of this work has been submitted in support of an application for another degree or qualification of this or any other university or institution of higher education.

I hold the University of Malta harmless against any third party claims with regard to copyright violation, breach of confidentiality, defamation and any other third party right infringement.

(b) Research Code of Practice and Ethics Review Procedures

I declare that I have abided by the University's Research Ethics Review Procedures. Research Ethics & Data Protection form code FHS-2024-00634.

As a Master's student, as per Regulation 77 of the General Regulations for University Postgraduate Awards 2021, I accept that should my dissertation be awarded a Grade A, it will be made publicly available on the University of Malta Institutional Repository.

To all cancer survivors, those fighting cancer
and those who lost their battle against it

Your approach to life, resilience, and strength inspires
many individuals to keep fighting no matter what.

Acknowledgements

First and foremost, I wish to express my deepest gratitude to my fiancé, Dorian, for his constant encouragement and unwavering belief in me throughout this journey. I am equally thankful to my Mum, Dad, Nannu Charlie, sister Nicole, brother-in-law Christopher, my nephew Harry, and my in-laws for standing by me every step of the way. Your support and faith in me have meant more than words can ever convey. Thank you for keeping me grounded, helping me stay focused, and encouraging me to pursue my dreams, even during the most difficult times.

I am also sincerely grateful to Professor Carmel J. Caruana, head of this course, whose passion for the subject and dedication to lecturing have been a source of inspiration, driving me forward over the past years and months.

Special thanks are due to my main supervisor, Mr. Martin Pirotta, for his invaluable expertise, and to Mr. Paul Bezzina, Head of the Medical Physics Department at SAMOC and my co-supervisor, for his guidance and support throughout this project. I am truly thankful for having the opportunity to work on this study.

My appreciation also goes to all the staff at SAMOC, including the radiographers and oncologists, for their warm welcome and assistance whenever I worked on the Unity MR LINAC.

Finally, I would like to extend heartfelt thanks to my dear friend and colleague, Maronia. Sharing and ending this five-year academic journey with you, through all its challenges and stresses, has been an invaluable source of strength and friendship.

Abstract

Background: The recent installation of Elekta Unity MR-LINAC (MRL) at the Sir Anthony Mamo Oncology Centre (SAMOC) integrates magnetic resonance imaging (MRI) with radiotherapy delivery. The system offers superior soft tissue visualisation and motion management capabilities, particularly relevant for prostate cancer, where intrafractional motion compromises dose coverage and increased exposure to organs at risk (OAR).

Objectives: This study aimed to evaluate the feasibility, performance, and limitations of a reduced margin protocol for prostate radiotherapy on the Elekta Unity MRL. Therefore, the validation of treatment margin reduction was essential to ensure safe margin reduction and effective treatment delivery in a typical clinical setting for prostate treatments.

Research Methodology: The analysis of 360 treatment fractions was performed to characterise prostate motion using Unity log files. Then, a treatment planning study with a phantom was performed to simulate prostate displacements and evaluate dose–volume histogram (DVH) metrics using Monaco® TPS. Lastly, radiochromic film dosimetry validated treatment delivery under static and motion scenarios, with gamma analysis used for dose comparison.

Results: The log file analysis showed minimal motion in the LR and AP directions, but higher variability in the SI axis, especially during the final 30 seconds of treatment. DVH analysis revealed that most treatment plans met dosimetric criteria, though extremely inferior displacements reduced target coverage. Film dosimetry and gamma analysis showed that the film exposed during motion with 2 baselineshifts (BLS) and the film exposed at 97% VOICE performed the best and poorest, respectively.

Conclusions and Recommendations: This study shows that reducing prostate PTV margins to 2 mm is possible. Moreover, it was concluded that BLS can restore margin coverage. Clinically, combining margin optimisation with adaptive work-

flows and quality assurance QA practices enhances safety and precision. Future research should validate results in larger cohorts, consider seminal vesicle motion, and apply such strategies across other anatomically mobile sites.

Keywords: MR-LINAC, prostate, gating, motion management, hypofractionation, radiotherapy

Contents

1 Introduction **1**

1.1 Introduction 1

1.2 Problem Statement 1

1.3 Background and Context 2

1.4 Objectives of the Study 3

1.5 Scope of the Study 4

1.6 Research Methodology 4

1.7 Ethical Considerations 5

1.8 Relevance of the Study 5

1.9 Conclusion 5

2 Literature Review **7**

2.1 Introduction 7

2.2 Literature Review 8

2.2.1 The MRL 8

2.2.2 Comprehensive Motion Management (CMM) in MRgART 8

2.2.3 Patient Workflow in MRL Treatments and Considerations 10

2.2.4 Comparison of Conventional SABR Treatments with MRL SABR Treatments 19

2.2.5 Motion Phantoms . . . 21
2.2.6 Dosimetric Validation Tools: Radiochromic Film Dosimetry . . . 22
2.2.7 Current Literature on Prostate Treatments . . . 26
2.3 Conclusion . . . 35

3 Research Methodology **37**
3.1 Introduction . . . 37
3.2 Research Approach . . . 38
3.3 Research Strategy . . . 38
3.4 Data Collection Technique . . . 39
3.4.1 Prostate Traces . . . 39
3.4.2 Treatment Planning Study . . . 40
3.4.3 Film Dosimetry . . . 41
3.4.4 Summary . . . 41
3.5 Data Collection Procedure . . . 42
3.5.1 Stage 1: Prostate Traces . . . 42
3.5.2 Stage 2: Treatment Planning Study - Modus QUASAR™ MRI 4D Phantom Data Collection . . . 44
3.5.3 Stage 3: Radiochromic Films Data Collection and Analysis . . . 52
3.6 Data Collection Tools . . . 59
3.6.1 Modus QUASAR™ MRI 4D Phantom and its software . . . 59
3.6.2 Monaco® TPS . . . 60
3.6.3 Excel and Python . . . 60
3.6.4 Online Film Analysis Software . . . 60
3.7 Data Analysis Technique . . . 61
3.7.1 Techniques Used . . . 61
3.7.2 Prostate Motion Traces . . . 61
3.7.3 DVH Statistics from Monaco® TPS . . . 62
3.7.4 Film Dosimetry . . . 63

3.8 Ethical Considerations . . . 63
3.9 Limitations of the Research Methodology . . . 64
3.10 Conclusion . . . 65

4 Results **67**
4.1 Introduction . . . 67
4.2 Data . . . 67
4.2.1 Set 1: Prostate Traces . . . 67
4.2.2 Set 2.1 - BLS Planning TPS DVH Statistics . . . 69
4.2.3 Set 2.2 - CTV within PTV TPS DVH Statistics . . . 69
4.2.4 Set 3 - Film Dosimetry . . . 70
4.3 Data Analysis and Results . . . 70
4.3.1 Part 1: Prostate Traces from Log Files . . . 70
4.3.2 Part 2.1: TPS DVH Statistics . . . 75
4.3.3 Part 2.2: 97% VOICE and Associated Translation . . . 83
4.3.4 Part 2.3: CTV movement within PTV . . . 84
4.3.5 Part 3: Film Dosimetry . . . 86
4.4 Conclusion . . . 91

5 Discussion **93**
5.1 Introduction . . . 93
5.2 Discussion . . . 93
5.2.1 Prostate Traces . . . 93
5.2.2 Treatment Planning Study . . . 99
5.2.3 Film Dosimetry . . . 106
5.3 Conclusion . . . 108

6 Conclusions **109**
6.1 Introduction . . . 109
6.2 Summary of Conclusions from the Study . . . 109

6.2.1 Overall conclusion 111
6.3 Recommendations for Professional Practice 111
6.4 Recommendations for Future Research 112
6.5 Conclusion 112

Appendix A Ethical Approval Documents **115**
A.1 UREC Approval 115

Appendix B Prostate Traces Plots **117**

Appendix C Prostate Traces Legend Data **191**

Appendix D Approved Template Coordinate Data **211**

Appendix E Averaged Prostate Motion for Last 30 Seconds Data **227**

Appendix F Treatment Planning Study: Part 1 **243**
F.1 DVH Statistics from TPS - Five Offsets from Prostate's Isocentre 243

Appendix G Treatment Planning Study: Part 2 **261**
G.1 CTV movement within PTV 261

Appendix H Film Dosimetry - Scaling Data **263**

References **269**

List of Figures

2.1 CMM on Elekta Unity MRL during exhale motion, (Brown and Corbett, 2025) 9
2.2 Workflow of the MRgART, (Uno et al., 2023) 11
2.3 Treatment target volumes (Berberoğlu, 2016) 12
2.4 ATS and ATP Treatment Approaches, (Winkel et al., 2019) 13
2.5 Modus QUASAR™ MRI 4D Phantom 22
2.6 Modus QUASAR™ MRI 4D Phantom - Translation and rotation features . . 22
2.7 Film calibration curve example (Zwierzchowski et al., 2016) 23
2.8 Analysis of the observed prostate motion with the mean shift at each time point during 2D cine MR imaging. The standard deviation is represented by the shaded area, (Menten et al., 2020) 28
2.9 Population translation intrafraction motion detected during a VMAT treatment (de Muinck Keizer et al., 2020b) 30
2.10 Prostate motion patterns results, (Oehler et al., 2022) 31
2.11 Boxplots of the intrafraction motion during the beam-on period based on cine-MR concerning the planned anatomy of the PRE scan, (Kontaxis et al. (2020)) 32

3.1 Modus QUASAR™ MRI 4D Phantom on MRL 44
3.2 Structures imported in Monaco® TPS, replicating the setup on the CT and MRL 47

3.3 Anatomical structures included in Monaco® TPS 47
3.4 Film exposure set up which includes a total thickness of cm of solid water with the film inserted beneath the first 5 cm solid water blocks. 53
3.5 Post film exposure set up. 55
3.6 A constructed waveform mimicking the typical prostate intrafraction motion in SI (z) direction 56
3.7 Film placement on Epson Expression 10000XL 57

4.1 A summary of the sample considered for the study 68
4.2 The prostate traces without filter for patient 017 71
4.3 The prostate traces with a `Loess` function with a `Loess` fraction equal to 0.018, for patient 017 72
4.4 Prostate motion traces in x-, y- and z- direction for the total sample considered 76
4.5 A graph of the CTV's V40Gy against translation in z-axis with a dosimteric criteria of V40Gy > 95% (-5%) 77
4.6 A graph of the CTV's D_{mean} against translation in z-axis 78
4.7 A graph of the CTV's V42 against translation in z-axis with a dosimetric criteria of V42Gy <=50% 78
4.8 A graph of the PTV's D95% against translation in z-axis with a dosimetric criteria of D95% > 36.25 Gy 79
4.9 A graph of the PTV's V34.4Gy against translation in z-axis with a dosimetric criteria of V34.4Gy >98% 80
4.10 A graph of the PTV's V36.25Gy against translation in z-axis with a dosimetric criteria of V36.25Gy >95% (-5%) 80
4.11 A graph of the 1_Urethra's V42Gy against translation in z-axis with a dosimetric criteria of V42Gy < 50% 81
4.12 A graph of the Urethra_XX's V42Gy against translation in z-axis with a dosimetric criteria of V42Gy < 50% 82
4.13 A graph of the 1_Urethra V42Gy against Urethra_XX's V42Gy 83

4.14 A graph of 1_Urethra V42Gy against the CTV's V42Gy (V42Gy <= 50%), for all offsets . . . 84
4.15 CTV within PTV: A graph of the CTV's V40Gy against translation in z-axis with a dosimetric criteria of V42Gy > 95% (-5/%) . . . 86
4.16 CTV within PTV: A graph of the Urethra's V42Gy against translation in z-axis with a dosimetric criteria of V42Gy $\leq$ 50% . . . 87
4.17 8.5 mm inferior against reference film - 8 Gy isodose curves . . . 89
4.18 8.5 mm inferior against reference film - 7.25 Gy isodose curves . . . 89
4.19 VOICE 97% against reference film with 8 Gy and 7.25 Gy isodose curves, respectively . . . 89
4.20 2BLS against reference film - 8 Gy isodose curves . . . 90
4.21 2BLS against reference film - 7.25 Gy isodose curves . . . 90
4.22 3BLS against reference film - 8 Gy isodose curves . . . 90
4.23 3BLS against reference film - 7.25 Gy isodose curves . . . 90
4.24 8.5 mm inferior against reference film (left) compared to the TPS 8 Gy isodose curves (right) . . . 91

5.1 The effect of different smoothing fraction parameters on prostate traces . . . 94
5.2 The segments at gantry 0 for the original treatment plan . . . 105
5.3 The segments at gantry 0 for BLS number 1 done on the original treatment plan . . . 105
5.4 The segments at gantry 0 for BLS number 10 done on the original treatment plan . . . 105
5.5 The segments at gantry 0 for BLS number 20 done on the original treatment plan . . . 105

B.1 Filtered traces plot for patient 001 . . . 118
B.2 Filtered traces plot for patient 002 . . . 119
B.3 Filtered traces plot for patient 003 . . . 120
B.4 Filtered traces plot for patient 004 . . . 121

B.5 Filtered traces plot for patient 005 122
B.6 Filtered traces plot for patient 006 123
B.7 Filtered traces plot for patient 007 124
B.8 Filtered traces plot for patient 008 125
B.9 Filtered traces plot for patient 009 126
B.10 Filtered traces plot for patient 010 127
B.11 Filtered traces plot for patient 011 128
B.12 Filtered traces plot for patient 012 129
B.13 Filtered traces plot for patient 013 130
B.14 Filtered traces plot for patient 014 131
B.15 Filtered traces plot for patient 015 132
B.16 Filtered traces plot for patient 016 133
B.17 Filtered traces plot for patient 017 134
B.18 Filtered traces plot for patient 018 135
B.19 Filtered traces plot for patient 019 136
B.20 Filtered traces plot for patient 020 137
B.21 Filtered traces plot for patient 021 138
B.22 Filtered traces plot for patient 022 139
B.23 Filtered traces plot for patient 023 140
B.24 Filtered traces plot for patient 024 141
B.25 Filtered traces plot for patient 025 142
B.26 Filtered traces plot for patient 026 143
B.27 Filtered traces plot for patient 027 144
B.28 Filtered traces plot for patient 028 145
B.29 Filtered traces plot for patient 029 146
B.30 Filtered traces plot for patient 030 147
B.31 Filtered traces plot for patient 031 148
B.32 Filtered traces plot for patient 032 149
B.33 Filtered traces plot for patient 033 150

B.34 Filtered traces plot for patient 034 151
B.35 Filtered traces plot for patient 035 152
B.36 Filtered traces plot for patient 036 153
B.37 Filtered traces plot for patient 037 154
B.38 Filtered traces plot for patient 038 155
B.39 Filtered traces plot for patient 039 156
B.40 Filtered traces plot for patient 040 157
B.41 Filtered traces plot for patient 041 158
B.42 Filtered traces plot for patient 042 159
B.43 Filtered traces plot for patient 043 160
B.44 Filtered traces plot for patient 044 161
B.45 Filtered traces plot for patient 045 162
B.46 Filtered traces plot for patient 046 163
B.47 Filtered traces plot for patient 047 164
B.48 Filtered traces plot for patient 048 165
B.49 Filtered traces plot for patient 049 166
B.50 Filtered traces plot for patient 050 167
B.51 Filtered traces plot for patient 051 168
B.52 Filtered traces plot for patient 052 169
B.53 Filtered traces plot for patient 053 170
B.54 Filtered traces plot for patient 054 171
B.55 Filtered traces plot for patient 055 172
B.56 Filtered traces plot for patient 056 173
B.57 Filtered traces plot for patient 057 174
B.58 Filtered traces plot for patient 058 175
B.59 Filtered traces plot for patient 059 176
B.60 Filtered traces plot for patient 060 177
B.61 Filtered traces plot for patient 061 178
B.62 Filtered traces plot for patient 062 179

B.63 Filtered traces plot for patient 063 180
B.64 Filtered traces plot for patient 064 181
B.65 Filtered traces plot for patient 065 182
B.66 Filtered traces plot for patient 066 183
B.67 Filtered traces plot for patient 067 184
B.68 Filtered traces plot for patient 068 185
B.69 Filtered traces plot for patient 069 186
B.70 Filtered traces plot for patient 070 187
B.71 Filtered traces plot for patient 071 188
B.72 Filtered traces plot for patient 072 189

List of Tables

3.1 BLS coordinates considered for each treatment plan 49

3.2 BLS DVH statistics obtained for each starting position (5 positions in total) . 50

3.3 A table summary of the dose constraints and DVH metrics considered in this study 51

3.4 Coordinates considered for each treatment plan 53

4.1 A table summary of the legend's data statistics averages across the population sample 73

4.2 Template coordinates summary of displacement measurements along X, Y, and Z axes, showing minimum, maximum, and one SD (1SD) values, with measurement uncertainty of ± 0.001 mm. 74

4.3 Summary of X, Y, and Z displacements during the last 30 seconds of beam-on, with average, extrema, and ± 1SD values. 74

4.4 VOICE values at different positions along the axes. 85

4.5 Gamma global pass rates (%) for different profiles at various criteria (10% threshold). 91

C.1 Patient statistics (X, Y, Z directions) 192

D.1 Patient data (column B excluded) 211

F.1 A table of the DVH statistics for the CTV for each BLS, starting from a position of 4 cm inferior . . . 244
F.2 A table of the DVH statistics for the PTV at 2 mm for each BLS, starting from a position of 4 cm inferior . . . 245
F.3 A table of the DVH statistics for the urethra shifted (Urethra_XX) and unshifted (1_Urethra) for each BLS, starting from a position of 4 cm inferior . . 246
F.4 A table of the DVH statistics for the CTV for each BLS, starting from a position of 2 cm inferior . . . 247
F.5 A table of the DVH statistics for the PTV at 2 mm for each BLS, starting from a position of 2 cm inferior . . . 248
F.6 A table of the DVH statistics for the urethra shifted (Urethra_XX) and unshifted (1_Urethra) for each BLS, starting from a position of 2 cm inferior . . 249
F.7 A table of the DVH statistics for the CTV for each BLS, starting from a position of 0 cm . . . 250
F.8 A table of the DVH statistics for the PTV at 2 mm for each BLS, starting from a position of 0 cm . . . 251
F.9 A table of the DVH statistics for the rectum and bladder at 2 mm for each BLS, starting from a position of 0 cm . . . 252
F.10 A table of the DVH statistics for the urethra shifted (Urethra_XX) and unshifted (1_Urethra) for each BLS, starting from a position of 0 cm . . . 253
F.11 A table of the DVH statistics for the CTV for each BLS, starting from a position of 2 cm superior . . . 254
F.12 A table of the DVH statistics for the PTV at 2 mm for each BLS, starting from a position of 2 cm superior . . . 255
F.13 A table of the DVH statistics for the urethra shifted (Urethra_XX) and unshifted (1_Urethra) for each BLS, starting from a position of 2 cm superior . 256
F.14 A table of the DVH statistics for the CTV for each BLS, starting from a position of 4 cm superior . . . 257

F.15 A table of the DVH statistics for the PTV at 2 mm for each BLS, starting from a position of 4 cm superior 258
F.16 A table of the DVH statistics for the urethra shifted (Urethra_XX) and unshifted (1_Urethra) for each BLS, starting from a position of 4 cm superior . 259
F.17 A table summarising the rectum and bladder's DVH statistics for each plan with different offset from the prostate's isocentre 260

G.1 A table of the dosimetric criteria for the Urethra when CTV lies within PTV 261
G.2 A table of the dosimetric criteria for the CTV within PTV 262

H.1 Scaling: Static 0 mm film scaling with morning films 264
H.2 Scaling: Static 8.5 mm inf shift film scaling with morning films 265
H.3 Scaling: Static VOICE 97% film with evening films 266
H.4 Scaling: Motion 2 BLS film with evening films 267
H.5 Scaling: Motion 3 BLS film with evening films 268

List of Abbreviations

AP Anterior Posterior

APM Adaptive Predictive Motion

ART Adaptive Radiotherapy

ATC Anatomic Tolerance Check

ATP Adapt to Position

ATS Adapt to Shape

BLS Baseline Shift

CC Cranio Caudal

CMM Comprehensive Motion Management

CP Completion Plan

CT Computed Tomography

CTV Clinical Target Volume

DVH Dose Volume Histogram

FOV Field of View

GTV Gross Target Volume

ICRU International Commission on Radiation Units and Measurements

IMRT Intensity-modulated Radiation Therapy

ITV Internal Target Volume

kV kilo Volts

LINAC Linear Accelerator

LR Left Right

MDH Mater Dei Hospital

MLC Multi Leaf Collimator

MP Medical Physicist

MRgART Magnetic Resonance Guided Adaptive Radiotherapy

MRI Magnetic Resonance Imaging

MRL MR LINAC

MU Monitor Units

OAR Organs at Risk

PTV Planning Target Volume

QA Quality Assurance

QF Quality Factor

ROI Region of Interest

SABR Stereotactic Ablative Radiotherapy

SAMOC Sir Anthony Mamo Oncology Centre

SBRT Stereotactic Body Radiation Therapy

SD Standard Deviation

SI Superior-Inferior

TPS Treatment Planning Software

UM University of Malta

UREC University Research Ethics Committee

VMAT Volumetric Modulated Arc Therapy

VOICE Volumetric Overlapping Criterion

1

Introduction

1.1 | Introduction

This chapter presents the problem statement, background and context, objectives, scope, summary of research methodology, ethical considerations and relevance of the study.

1.2 | Problem Statement

The installation of MR Linac (MRL), such as the one installed at Sir Anthony Mamo Oncology Centre (SAMOC), offers superior soft tissue visualisation throughout the treatment delivery. In this way, such a system introduces the potential for real-time motion management and gating. This allows precise targeting of tumours such as the prostate while sparing surrounding healthy tissues. These capabilities present an opportunity to reduce planning target volume (PTV) margins, which is important when implementing hypofractionated treatments.

This study aims to evaluate prostate motion comprehensively, providing experimental data to determine whether further PTV margin reduction is practicable while maintaining safe and effective treatment delivery. By doing so, evidence-based motion management strategies can be determined for clinical implementation on the MRL.

1.3 | Background and Context

The Elekta Unity MRL is a medical device that combines a linear accelerator with magnetic resonance imaging (MRI). Such a combination offers significant advantages in cancer treatment; one of which is the system's ability to achieve excellent soft tissue contrast without the use of ionising radiation. Therefore, continuous real-time images can be obtained without the patient being exposed to significant radiation doses related to imaging. Another feature of this device is the ability to manage organ motion via comprehensive motion management (CMM), clinically known as gating. This is crucial as any target volume within the patient's body can experience motion. Like in the pelvic area, bladder and rectal filling can cause motion of the prostate whilst being treated. Therefore, with the help of gating, radiotherapy beams will only be delivered when the volume of interest is within a defined margin. This concept would ensure high geometric accuracy to minimise the treatment target margins whilst sparing healthy tissues or structures.

Prostate motion during radiation is a complex process. This is because, as suggested in the literature, during treatment, regular posterior-inferior shifts, brief random movements, and deformations associated with bladder and rectal distension can occur. Preliminary Unity studies, including the one by Menten et al. (2020), demonstrated quantifiable systematic deviations before and during beam-on. Other recent studies have further measured prostate motion patterns, revealing displacements that vary from small residual variations to sudden shifts of several millimetres, induced by rectal gas or bladder distension (Bosma et al., 2021; Mastella et al., 2024). These findings emphasise the interplay between biological variability and delineation uncertainties, which collectively constrain the safe reduction of PTV margins. Shortening beam-on time, as well as hypofractionated strategies, have been recommended to limit the window for motion and thereby enable tighter margins without compromising coverage (Oehler et al., 2022; Tsekas et al., 2024).

Continuous monitoring and beam-hold gating have been shown to improve safety by interrupting treatment when prostate drift exceeds defined thresholds. For example, Xiong et al. (2022) found that although gated and non-gated fractions produced comparable average dose–volume outcomes, gating remained valuable in preventing severe outliers. Moreover, baseline shift (BLS) corrections can restore coverage for modest displacements but cannot address deformation, while segmented re-optimisation, investigated by Snyder et al. (2024), improved target coverage at the cost of workflow interruption. Together, these studies underline that while Unity workflows can manage small intra-fraction drifts, margin reduction is ultimately constrained by the limited corrective scope of BLS.

1.4 | Objectives of the Study

The objectives of the study include:

1. Analyse the current literature to evaluate how margin reduction in prostate cancer can be achieved on Elekta Unity MRL.

2. To analyse 3D motion data and determine the typical average and maximum prostate motion from a sample of patients who received prostate treatment on Elekta Unity MRL.

3. To design a phantom study related to prostate treatment so as to serve as a basis for end-to-end validation of clinical prostate motion management on the Elekta Unity MRL.

4. To assess the dose coverage, dosimetric effects and accuracy whilst delivering prostate radiotherapy on the Elekta Unity MRL.

1.5 | Scope of the Study

This study focuses on validating a motion management and gating protocol. Concentrating on radiotherapy for the prostate, it seeks to assess whether PTV margins can be further reduced, thereby enhancing treatment precision. The findings may also indicate the potential for clinical adoption of this approach.

1.6 | Research Methodology

The current understanding of intrafraction prostate motion and clinical strategies for margin reduction of prostate treatment was first established through a literature review. With that done, a time-resolved trace of the prostate motion during multiple treatment sessions was obtained from multiple patient log files recorded by the system's software. By averaging the data over a sample of patients, the typical average 3D motion patterns were evaluated through graph plotting. A planning study was carried out to evaluate the dosimetric impact of the exception gating strategy and workflow. This was done by using the Modus phantom, which was available within the radiotherapy department at SAMOC.

For this study to be done, one major assumption was that upon conducting the phantom study on Elekta Unity MRL, the phantom could replicate patient anatomy and prostate motion characteristics. The latter was achieved by analysing the typical prostate trends and generating similar prostate motion characteristics. Besides this, multiple limitations were present, which include the lack of analysis of PTV margin uncertainty, which might provide different results.

1.7 | Ethical Considerations

Since anonymised patient data was used for this study, clearance from Mater Dei Hospital's (MDH's) data protection department was provided. Also, ethical clearance was granted by the University Research Ethics Committee (UREC) within the University of Malta (UM).

1.8 | Relevance of the Study

The relevance of the study for the various stakeholders is as follows:

a) For healthcare professionals:

   i. Increase confidence in SABR prostate treatments in delivery with reduced margins.

   ii. To maintain adequate treatment margins while potentially reducing the frequency or severity of side effects experienced by patients undergoing prostate cancer treatment.

b) For the Medical Physics and Radiation Protection professions/practice:

   i. Reduce margins for SABR and apply such findings to other sites and quality assurance (QA) methods.

   ii. Establish a new evidence-based workflow within the radiotherapy department.

1.9 | Conclusion

This chapter presented a very brief overview of the study. In the chapters which follow, the critical background and literature review will be discussed. These will be followed by the research methodology and the results in chapters three and four, respectively. Chapter five, that is, the discussion, consists of an evaluation of the results.

Lastly, chapter six will summarise the most important conclusions of the study and propose recommendations arising from the study, together with suggestions for future research.

2

Literature Review

2.1 | Introduction

This chapter presents a critical review of the literature, including what is known about the subject, and identifies gaps in the present knowledge of the topic.

This review was initiated using the following electronic research databases: Google Scholar, HYDI, and PubMed/MEDLINE until the 15th of August, 2025. The following keywords were used (derived using the PICO framework where relevant): MRL, prostate, gating, motion management, hypofractionation, and radiotherapy. Published papers in the last 10 years only were considered (2015-2025). Older papers were only included if they were of crucial importance to the project.

An alert option was activated until the final submission date. Selected articles had to satisfy the following inclusion criteria: (1) full-text papers written in the English language, (2) studies that are related to motion management and gating protocol on the Elekta Unity's MRL for margin reduction in prostate cancer. Duplicate findings were discarded to ensure no data overlap. The following criteria were then applied: (1) insufficient data, (2) inadequate methodology, (3) books and case study reports, and (4) subjective expert opinion papers.

2.2 | Literature Review

2.2.1 | The MRL

MRL systems combine MRI with a linear accelerator (LINAC), allowing healthcare professionals to see soft tissue in real time during treatment. Since their initial development, which utilised smaller magnetic fields (0.35 T), systems have been improved mainly by operating at higher magnetic field strengths, typically of 1.5 T, ensuring higher quality images.

Unlike conventional LINAC workflows that rely on planning CT imaging, MRLs allow for MRI-based target localisation, daily plan adaptation, and direct intrafraction monitoring of tumour motion. These capabilities are particularly beneficial in anatomical sites where soft-tissue contrast is poor on CT, such as the pelvis, pancreas, and liver. Having high-resolution MR imaging obtained both pre-treatment and during delivery allows for precise contouring of the target and organs at risk (OARs), while real-time 2D cine MRI enables continuous anatomical visualisation throughout the treatment fraction, (Smith et al., 2025). This is the basis for the development of MR-guided adaptive radiotherapy (MRgART), which allows for treatment to be adapted and improved on a per-fraction basis, resulting in a more accurate treatment, Tsekas et al. (2024). MRL is becoming more popular for both standard and hypofractionated regimens, such as stereotactic ablative body radiotherapy (SABR).

2.2.2 | Comprehensive Motion Management (CMM) in MRgART

Motion management is a crucial component of precision radiotherapy, particularly for targets subject to physiological displacement during treatment. In MRgART, beam gating provides a robust strategy for mitigating intra-fraction motion by synchronising radiation delivery with the tumour's position. On the Unity MRL platform, gating is achieved through continuous monitoring of the target using 2D cine-MRI (Smith et al.,

2025). As shown in Figure 2.1 by Brown and Corbett (2025), for a particular treatment at motion, when the target moves outside a predefined gating boundary, typically derived from the PTV, radiation delivery is automatically interrupted. Such a feature is shown on the bottom trace generated by CMM, where orange regions as shown in Figure 2.1, indicate treatment interruption. This ensures that treatment occurs only when the target remains within the accepted positional range, thereby improving spatial accuracy and reducing the risk of geographic miss (Ocanto et al., 2024).

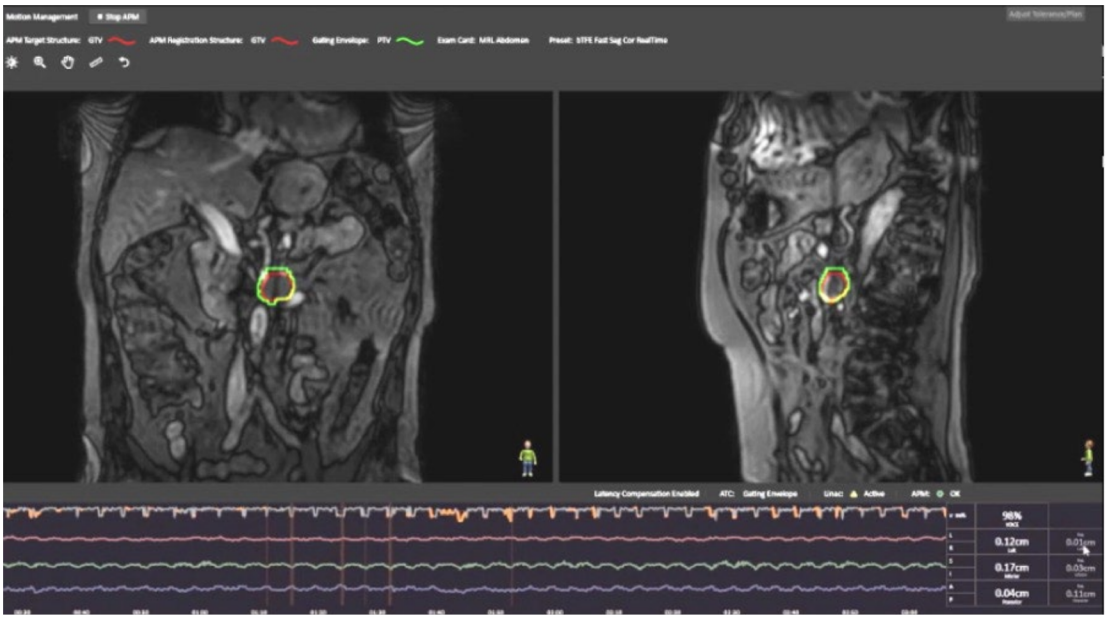

Figure 2.1: CMM on Elekta Unity MRL during exhale motion, (Brown and Corbett, 2025)

Bertholet et al. (2019) emphasises that active motion mitigation techniques such as gating and tracking are essential for the safe reduction of PTV margins, particularly in high-dose, hypofractionated treatments where the dosimetric consequences of small positional deviations can be considerable. By allowing clinicians to respond dynamically to real-time anatomical changes, gating provides a clinically meaningful means of preserving target coverage while maintaining OAR sparing. This is particularly relevant in SABR, where the combination of tight margins and high fractional doses

magnifies the impact of motion. In pelvic treatments such as prostate cancer, for example, intra-fraction displacement caused by bladder filling or rectal distension can be substantial; real-time gating mitigates these effects by ensuring radiation delivery only when the prostate remains within the defined treatment region. Similarly, Tsekas et al. (2024) demonstrated the clinical feasibility of gating on the Unity system in thoracic cases, where the technique enabled margin reduction and improved OAR protection in the presence of respiratory motion.

While gating represents the cornerstone of motion management in MRgART, it also forms part of a broader, integrated framework known as CMM. CMM extends beyond simple beam gating to incorporate systematic detection of BLSs and evaluation of gating signal reliability. By combining real-time monitoring with adaptive decision-making, CMM provides a layered strategy to mitigate motion-related uncertainties, thereby enabling margin reduction and safe dose escalation in MR-guided SBRT.

2.2.3 | Patient Workflow in MRL Treatments and Considerations

Through MRL, tumour shape and position can be effectively managed by adapting the treatment plan for each fraction. This ensures that gating strategies are applied accurately, so that tumour motion is properly accounted for during the actual treatment delivery.

The flowchart in Figure 2.2 by Uno et al. (2023) highlights the whole procedure that the patient follows upon undergoing MRgART. Mainly, this is split into two, where the patient is off the couch (offline) and on the couch (online).

The planning CT provides a reference anatomical image whilst an MR image is then acquired through the MRL to provide complementary soft tissue contrast. Through image registration, CT and MR images are accurately aligned, resulting in a combined anatomical dataset. The CT is essential because it provides information on the electron

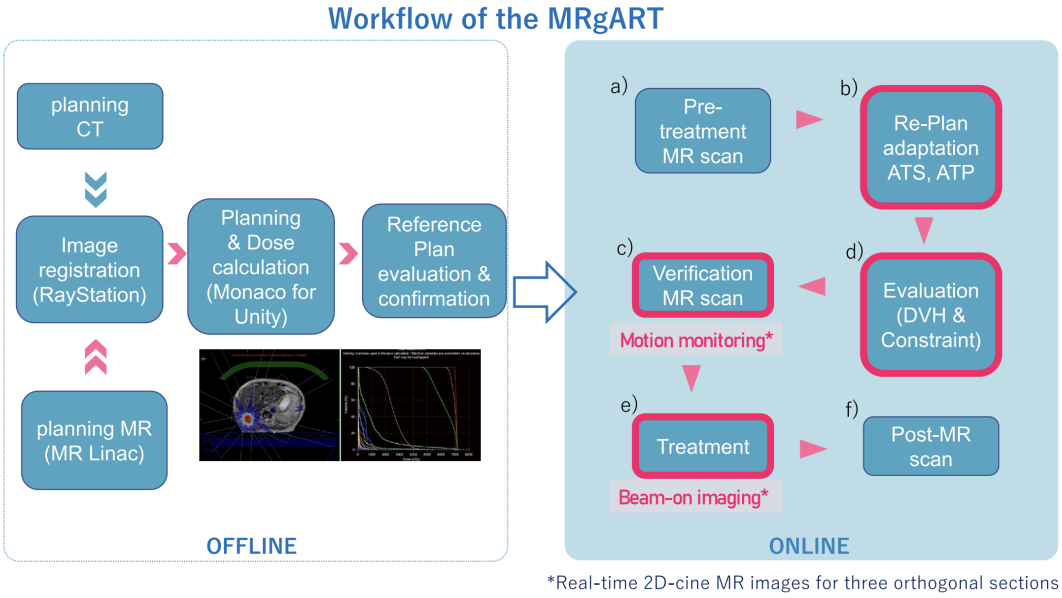

Figure 2.2: Workflow of the MRgART, (Uno et al., 2023)

density, which is required for accurate dose calculations. Without electron densities, the treatment planning system (TPS) cannot correctly model radiation interactions within the patient. Once images are aligned, the radiation oncologist will then define the target volumes and OAR through contouring. Following this, the TPS is used to generate and optimise the treatment plan.

According to the International Commission on Radiation Units and Measurements (ICRU) reports number 50 and 62, these target volumes are crucial to determine the areas of interest and their associated dose prescriptions. Having a total of five volumes, these are important to spare healthy tissues, maximise tumour control and ensure accurate treatment delivery. Such volumes are represented in Figure 2.3.

As defined by EMITEL (2016), the GTV refers to the visible or palpable extent of the tumour identified through imaging or clinical examination. The CTV includes the GTV along with surrounding areas that may contain microscopic disease not visible on scans. The Internal Target Volume (ITV) accounts for the CTV plus an additional

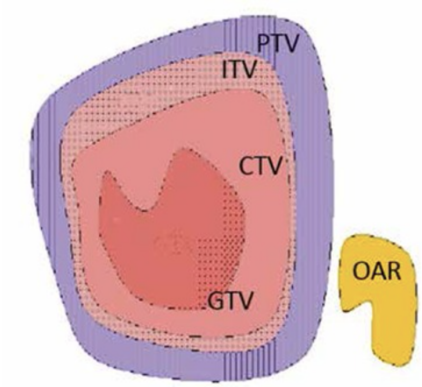

Figure 2.3: Treatment target volumes (Berberoğlu, 2016)

margin to compensate for internal organ motion, such as breathing or bladder filling. Lastly, the PTV encompasses the ITV with an extra margin to allow for patient positioning variations and machine setup uncertainties, ensuring the prescribed dose fully covers the intended area.

In the last stage of the offline process, the planned dose distribution is reviewed and approved by the responsible oncologist to ensure that the treatment goals are met whilst minimising the damage to healthy tissues. All this will eventually serve as a reference plan for the subsequent adaptive treatments.

On the day of treatment, pre-treatment MRI images are again acquired to assess any anatomical changes that may have occurred since the creation of the reference plan. These images are compared to the reference scan using image registration techniques. As highlighted by Ocanto et al. (2024), on the day of the treatment, the treatment plan will be either Adapted-to-Position (ATP) or Adapted-to-Shape (ATS) as shown in Figure 2.4. The purpose of these adaptive strategies is to maintain dosimetric accuracy.

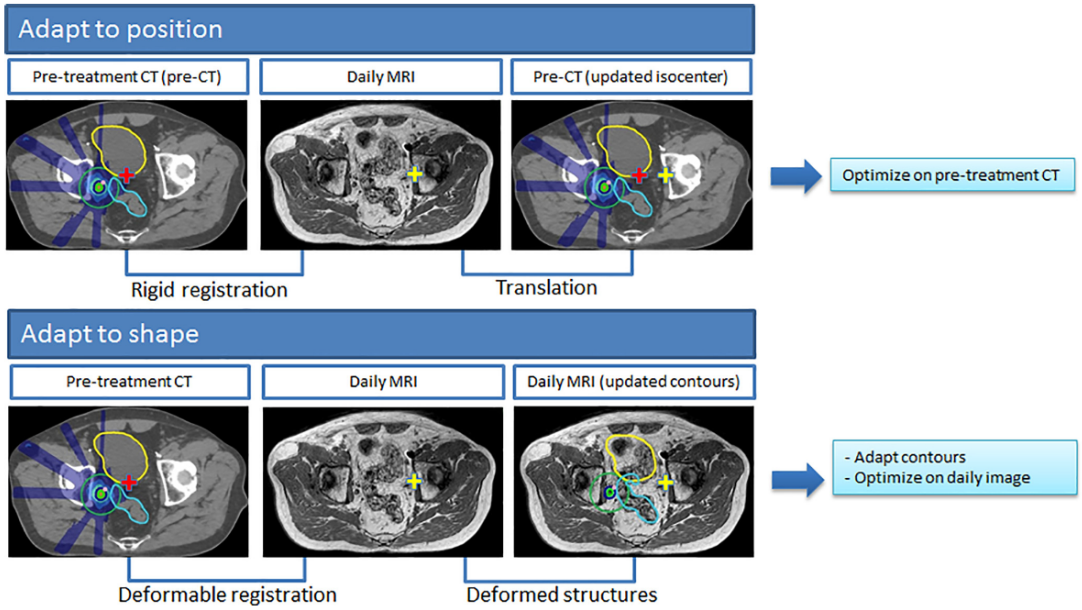

Figure 2.4: ATS and ATP Treatment Approaches, (Winkel et al., 2019)

2.2.3.1 | ATS Workflow

The ATS approach utilises pre-treatment CT or MR and online MRI planning, whereby pre-treatment contours are deformed onto the online MRI. Hence, such an approach will lead to an optimised plan based on the modified contours done by the radiation oncologist, beam geometry, and dose constraints, (Winkel et al., 2019). As further discussed by ELEKTA (2023), this method allows for precise adaptation to anatomical changes such as significant rectal or bladder volume variation, which are common in prostate radiotherapy. Because the beam segments and fluence are fully re-optimised, ATS can offer superior dose conformity and sparing of surrounding healthy tissues.

2.2.3.2 | ATP Workflow

In contrast, the ATP method provides a faster alternative to ATS and is particularly effective when the anatomy remains relatively unchanged in shape but has shifted in position. Within Elekta's Monaco TPS, ATP workflows are implemented by aligning the pre-treatment CT or reference MR with the daily MRI using rigid registration (ELEKTA,

2023). This allows the original plan to be adjusted by adapting the segments and associated dose distribution to match the current position, without the need for re-contouring or full re-optimisation. This is particularly useful in clinical scenarios such as prostate radiotherapy, where small positional changes, rather than structural deformations, are too frequently observed.

The Monaco TPS supports four distinct ATP strategies, allowing clinicians to tailor the adaptation process according to the degree of anatomical change and the time available (ELEKTA, 2024).

1. **Original Segments** - The first and simplest method is "Original Segments", where the original beam segments from the reference plan are used without modification. The dose is recalculated on the daily MRI dataset to verify if the initial plan remains clinically acceptable. This option serves as a quick check and is best suited to highly stable cases (ELEKTA, 2024).

2. **Adapt Segments** - The second strategy is "Adapt Segments", where the shape of the original beam segments is altered to better align with the current anatomy. This adjustment does not involve any change in the relative weighting of the segments, making it a fast solution when minor shape discrepancies are present but a re-optimisation is unnecessary (ELEKTA, 2024).

3. **Optimise Weights** - The third option, "Optimise Weights", adapts the segment's weights to have their intensity recalculated to improve dose conformity. This option offers a balanced trade-off between computational time and plan quality, making it useful when slight changes in anatomy or dose distribution compromise the efficacy of the unmodified plan (ELEKTA, 2024).

4. **Optimise Shapes** - Lastly, "Optimise Shapes" represents the most advanced of the ATP strategies. As highlighted by ELEKTA (2024), it allows both segment shapes and their weights to be re-optimised, offering a level of adaptation that

closely approaches the full ATS workflow. While still operating within the ATP framework, this strategy is computationally more intensive and is generally reserved for cases where simpler ATP methods fail to produce an acceptable plan.

2.2.3.3 | Summary of ATS and ATP - Key Differences

Although ATP and ATS differ in workflows, it is noted that the ATS workflow builds on the "Optimise Shapes" ATP strategy, but with the addition of newly re-contoured anatomy. In ATS, both segment shapes and weights are re-optimised after the radiation oncologist adjusts target and OAR contours on the daily MRI. Therefore, while "Optimise Shapes" modifies the plan to match the new position, ATS ensures it also matches the new shape of the anatomy. This distinction highlights why ATS is preferred in cases with significant organ deformation, while ATP remains a practical solution for managing smaller positional changes efficiently (ELEKTA, 2023).

2.2.3.4 | Anatomic Tolerance Check (ATC) and Anatomic Position Monitoring (APM)

Following adjustments to the patient's plan, the workflow can proceed directly to APM modelling for verification. APM records the translation vector of the target relative to its reference position, thereby accounting for intra-fraction motion during the adaptive planning stage before treatment starts. This reference is defined by a template, which is derived from the reference MR scan and target contours. The template is essentially a 3D representation of the expected anatomy, against which incoming MR images are matched in real time. Before treatment, the template must be checked and approved by the clinical team to ensure that it reliably captures the offset of the target structure and can be safely used for motion monitoring.

The ATC then uses the APM information to determine whether the beam should remain on or be interrupted. This decision is based on user-defined tolerance limits and can be performed in two ways: (i) directly from the measured APM output or (ii)

from the predicted position of the target. In the latter case, a predictive algorithm is applied to anticipate the target position based on motion patterns observed during treatment. For prostate radiotherapy, this approach supports an exception gating strategy, whilst for lung or abdominal treatments, respiratory gating is implemented. Within this framework, two types of thresholds are typically applied:

1. **Displacement threshold** – the target position is checked against predefined tolerances in all three cardinal directions.

2. **Gating envelope** – the percentage overlap between the APM target structure (example the CTV) and the gating envelope (example the PTV) is calculated in 3D, and treatment is only permitted if this overlap exceeds the set threshold.

Together, APM and ATC provide real-time monitoring and beam control, ensuring that dose delivery remains accurate despite intra-fraction tumour or organ motion.

2.2.3.5 | Baseline Shifts

In MR-guided radiotherapy, a BLS refers to a systematic positional deviation of the target anatomy between treatment fractions or during the pre-treatment setup phase. Such deviations are common in prostate radiotherapy, often caused by variations in bladder filling or rectal distension. Clinically, a BLS is not an adaptation method itself but rather a trigger for adaptation.

With close reference to the Elekta Unity MRL environment, once the daily plan adaptation is completed through the adaptive workflows such as ATP and ATS, APM verification is performed before the treatment plan is approved, as otherwise further plan adaptation is no longer possible. Once treatment is initiated, whenever intra-fraction motion occurs and gating persists that inhibits treatment, at such a stage, only two corrective options remain, these being either BLS or generating a Completion Plan (CP).

Comparing the two, a BLS provides a rapid method of correcting for positional drift by translating the prostate. However, this option is limited in scope as it does not permit modification of monitor units (MU) but allows the segment shapes to be adapted. By contrast, a CP is generated if the treatment session is interrupted mid-way through treatment and requires replanning or re-optimisation using an ATP workflow for the remaining dose. This approach allows adjustment of MUs and segment weights for the undelivered part of the initial daily treatment plan, but comes at the cost of workflow interruption and increased treatment time.

Therefore, online BLS serves as a safeguard for modest intra-fraction drifts, while CPs provide a more comprehensive correction pathway when treatment cannot be continued as originally approved.

2.2.3.6 | Dose Volume Histograms (DVHs) Statistics

In MR-guided prostate SBRT, DVH-derived dose–constraint statistics are central to evaluating plan quality and assessing the risk of toxicity. Some key statistical metrics derived from the DVH include:

- D95%, D98%, and D99%: the minimum dose received by 95%, 98%, and 99% of the target volume, respectively, which are indicators of target coverage.
- D_{mean}: the average dose delivered to a structure.
- D_{max}: the maximum dose within a volume, typically relevant for OARs. Other analogous metrics include D1%, D0.1cc, and D1cc.
- V_x (example V40Gy): the volume (in cc or %) receiving at least a dose, x, in Gy, often used to assess OAR sparing.

Furthermore, in motion management studies involving the MRL, comparisons of planned versus delivered DVH statistics have demonstrated how intra-fraction motion

can compromise both target coverage and OAR sparing if not properly managed. Evidence from recent studies highlights the clinical impact of motion-induced deviations in DVH outcomes. Vanhanen et al. (2020) reported that intra-fraction prostate motion during Unity SBRT could result in underdosage of the PTV, with deviations of up to 10–15% in D95% when motion exceeded the applied gating margins. These shifts were also associated with increased rectal and bladder dose spill, reflected in elevated V_x values, underscoring the importance of precise motion monitoring. Similarly, Snyder et al. (2024) demonstrated that while adaptive workflows maintained PTV coverage in most cases, residual anatomical variations, particularly due to bladder and rectal filling, produced measurable increases in rectal V36Gy and bladder V37Gy compared with planned values. Such deviations correlated with higher predicted toxicity risks, reinforcing the necessity of strict adherence to daily adaptation protocols.

2.2.3.7 | Volumetric Overlapping Criterion (VOICE)

In MR-guided radiotherapy, intra-fraction organ motion poses a significant challenge to achieving both adequate target coverage and sparing of adjacent OAR. The VOICE, expressed as a percentage, is a beam-gating metric implemented in the Elekta Unity MRL that quantifies the proportion of voxels from a predefined reference structure that remain within a fixed gating envelope during treatment delivery. Such a predefined threshold allows for beam delivery to be permitted only when the calculated VOICE meets or exceeds this threshold. If the overlap falls below the threshold, irradiation is automatically suspended until the anatomy returns to the predefined tolerance. This approach provides a robust volumetric safeguard compared to centroid- or boundary-based tracking, ensuring that a clinically meaningful proportion of the target remains adequately irradiated. In practice, a 95 to 100% VOICE threshold is typically set.

Such a concept serves two important purposes. Mainly, it prevents systematic underdosage of the target volume that could compromise local control, particularly relevant in SBRT where reduced margins are employed, and secondly, it mitigates the risk

of unintended OAR irradiation by halting treatment whenever organ motion displaces high-dose regions into adjacent critical structures such as the bladder or rectum.

In case of persistent failure to satisfy VOICE thresholds, a BLS or a CP would be appropriate to 'restore' the optimal dosimetric accuracy. Thus, the VOICE percentage provides a real-time quantitative measure of whether the CTV is sufficiently within the gating envelope.

2.2.3.8 | Jitter

In the MRL gating workflows, jitter describes inconsistencies between target displacement estimates derived from sagittal and coronal imaging planes (Tsekas et al., 2024). Ideally, both planes should report similar superior–inferior (SI) motion, but image noise or tracking errors can cause discrepancies that manifest as irregular, non-physiological shifts in the motion trace. Jitter is one of the Quality Factor (QF) metrics, signalling unreliable tracking performance. Its detection is critical, as uncorrected jitter could lead to inappropriate gating decisions, either interrupting treatment unnecessarily or delivering a dose when the target is not adequately positioned.

2.2.4 | Comparison of Conventional SABR Treatments with MRL SABR Treatments

The combination of SABR delivery with MRL technology enables significant improvements in terms of optimisation when compared to conventional technology. Multiple studies highlight various differences:

1. **Imaging and Guidance**

   In conventional radiotherapy, including SABR, CT imaging is commonly used for treatment planning but offers limited soft-tissue contrast. To address this, fiducial markers are often used, particularly for mobile sites such as the prostate, to improve tumour localisation. However, the insertion of fiducials can cause patient

discomfort and is not universally applied across all treatment sites. Additionally, CT-based imaging is performed pre-treatment, making it challenging to account for tumour or organ motion. Alternatively, MR-guided radiotherapy, as enabled by the MRL, overcomes these limitations by providing superior soft-tissue contrast without requiring fiducial markers, as noted by de Muinck Keizer et al. (2020a). APM models in MRL will then allow dynamic monitoring of tumour motion caused by physiological activities. Gating further enhances precision by pausing treatment when motion exceeds defined thresholds. With continuous real-time imaging throughout treatment, the MRL ensures improved treatment accuracy compared to conventional approaches, which rely on pre-treatment imaging alone.

2. **Adaptation During Treatment**

   ART preceeds the development of MR-guided systems. However, in conventional SABR, pre-treatment imaging via CT will be done so as to match it on the day of the treatment. The drawback is that, should significant anatomical changes be present, replanning has to be done. On the other hand, if smaller changes were present upon matching and treatment is still delivered, there is the risk of underdosing the tumour or overdosing healthy tissues. With the incorporation of MRL, ART occurs before treatment starts by using daily MRI to assess anatomical changes in the sites of interest and adapt the plan accordingly. This pre-treatment adaptation enhances tumour control and reduces side effects, (Ocanto et al., 2024).

3. **Treatment Precision**

   The main limitation that conventional SABR treatments have is the implementation of static treatment plans. This is mainly a concern in mobile or irregularly shaped tumours since high doses are difficult to deliver as optimally as possible. Therefore, in the planning process, larger treatment margins are defined to ac-

count for motion or setup uncertainties. With MRL SABR treatments, real-time MRI guidance allows sub-millimeter precision and Multi-Leaf Collimator (MLC) shaping to match the tumour. This concept will allow smaller margins to be defined, hence ensuring an overall higher precision.

4. **Toxicity and Side Effects**

   Provided that in conventional SABR treatments larger margins are generally defined, there will be an increased risk of exposing the surrounding tissues and organs to high radiation doses. On the contrary, with the MRL, since smaller margins are defined and real-time motion is accounted for, the radiation exposure to healthy tissues is significantly reduced, hence lowering the risk of radiation-induced toxicity. Case in point, in the study by Ladbury et al. (2023), which investigated localised prostate cancer treated with SBRT, they found that acute grade ≥ 2 GI toxicity decreased from 10.5% with CT-guided SBRT to 0% with MRgRT, while GU toxicity fell from 43.4% to 24.4%.

2.2.5 | Motion Phantoms

The accurate simulation of tumour motion is fundamental for the validation of motion-adaptive workflows in MRgART. Several motion phantoms have been developed for use in MRL systems, including the Modus QUASAR™ MRI 4D Phantom shown in Figures 2.5 and 2.6.

The Modus QUASAR™ MRI 4D Phantom can be programmed to perform controlled translational and rotational displacements, enabling the simulation of 2D and 3D motion patterns such as those observed in prostate treatments. Adjusting the thumbscrew will activate either motion technique as shown in Figure 2.6. These capabilities allow clinically relevant motion scenarios to be reproduced in a measurable way, thereby providing a practical platform for evaluating motion-induced scenarios and testing adap-

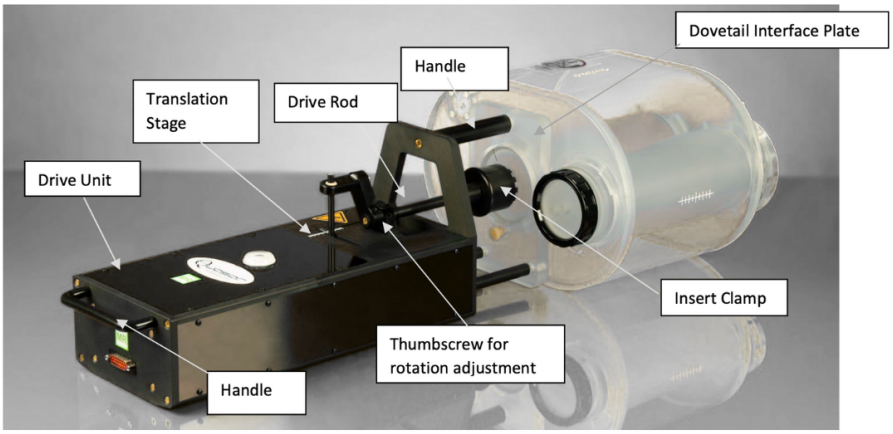

Figure 2.5: Modus QUASAR™ MRI 4D Phantom

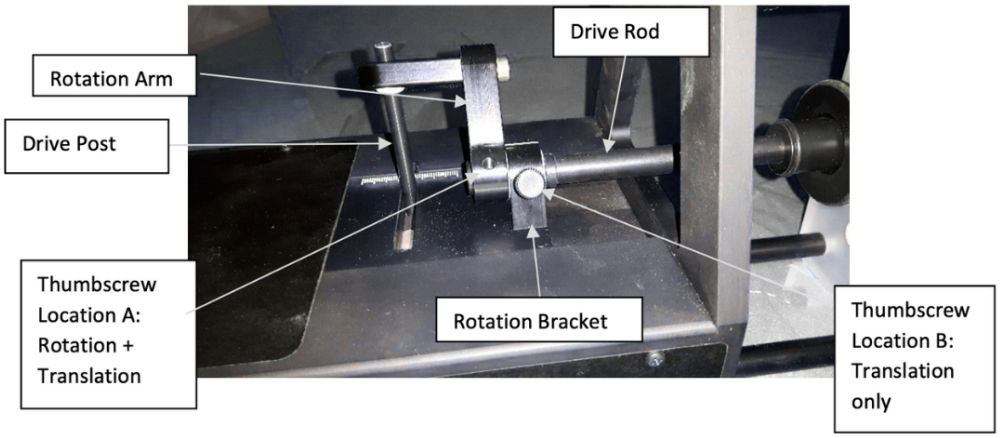

Figure 2.6: Modus QUASAR™ MRI 4D Phantom - Translation and rotation features

tive radiotherapy strategies. Moreover, it also includes an optional film insert, which can be used for dosimetric verification during motion studies.

2.2.6 | Dosimetric Validation Tools: Radiochromic Film Dosimetry

Verification of delivered dose distributions is a critical component of radiotherapy QA. Among the available tools, radiochromic films such as Gafchromic EBT-4 provide a high-resolution and tissue-equivalent dosimetric method. Their self-developing properties eliminate the need for chemical processing, as the active layer undergoes a polymerisation reaction upon irradiation that leads to measurable darkening proportional

to dose. This property allows films to capture 2D dose distributions with sub-millimetre resolution, making them particularly useful in small-field and stereotactic applications. Digitised images of exposed films can then be compared directly against the corresponding treatment plan to confirm accurate dose delivery.

2.2.6.1 | Film Dosimetry Process and Calibration

A robust calibration protocol is essential because the optical density response of EBT-4 films is non-linear with dose and may vary between batches or even within a single sheet. Calibration is typically performed by irradiating multiple film segments with known doses under reference conditions, followed by scanning to establish a dose–response curve. This calibration curve, an example of it shown in Figure 2.7, is then used to convert optical density to absolute dose during patient-specific QA.

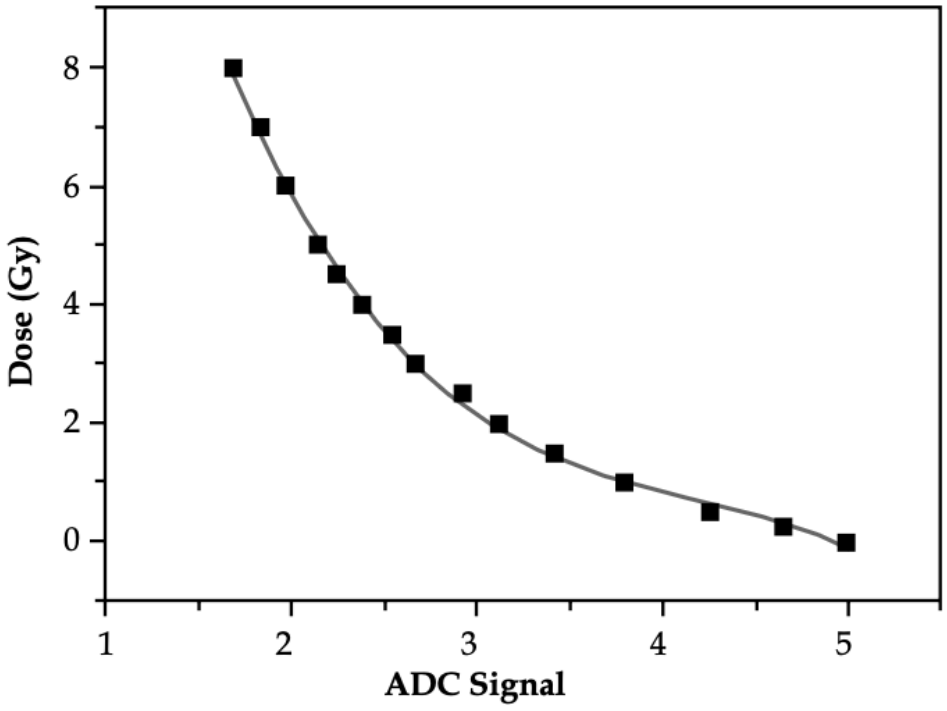

Figure 2.7: Film calibration curve example (Zwierzchowski et al., 2016)

An important consideration is the time dependence of the film response. Given that Gafchromic films do not reach their final optical density immediately after irradiation but continue for several hours, the darkest noticeable optical density occurs within the first 24 hours. Hence, to minimise uncertainty, more than 24 hours should elapse for the films to be scanned, ensuring that both calibration films and measurement films are subject to the same temporal response characteristics.

Without accurate calibration, or if time effects are not standardised, dose estimates can deviate by several percent, particularly in the low-dose and high-gradient regions. Furthermore, repeated calibrations are required for new film batches or changes in scanner conditions to ensure reproducibility (Zwierzchowski et al., 2016).

2.2.6.2 | Scanning and Orientation Effects

Following irradiation, films are digitised using a flatbed scanner under controlled and reproducible settings. The Epson Expression 10000XL scanner is commonly used due to its consistent illumination and large scanning area, but regardless of the model, uniform film placement and fixed scanning parameters are essential to reduce artefacts. In particular, film orientation has been shown to influence measured optical density due to intrinsic anisotropy in the film structure. Therefore, all films should be scanned in a consistent orientation to minimise systematic error. In order to ensure that the dosimetric accuracy is not affected, multiple precautions were highlighted by Grams (nd). These include:

- Allow sufficient scanner warm-up time before acquisition to ensure stable illumination.
- Place all films in a consistent position on the scanner bed, preferably at the centre, to minimise lateral response artefacts. Such an artefact is introduced by the scanner, where it does not respond uniformly across its lateral axis (perpendicular to

the lamp movement), so the same film region may read differently depending on whether it is scanned at the centre or near the edges.

- If multiple films must be scanned simultaneously, apply correction factors or reference films to account for lateral response differences.
- Always scan with the same orientation to avoid anisotropy-related variations.
- Use fixed scanning settings (resolution, bit depth, colour mode) and disable all automatic image corrections.
- Perform background correction or flood-field correction scans to compensate for non-uniformity across the scanning area.

2.2.6.3 | Film Scaling

Once the calibration curve has been established, a scaling procedure is required to adapt the established curve to the day's measurements. This involvs acquiring a set of reference dose levels alongside the experimental films, from which a scaling factor will be determined. The factor accounts for inter-day variations in film response and scanner output, ensuring that the shape of the calibration curve remains valid while being shifted or rescaled to match the current measurement conditions. In this way, the previously determined calibration can be reliably extended to films within the same batch or measurement sessions without the need to repeat the entire calibration process.

The reliability of this scaling process is generally verified by comparing the film-derived doses with independent reference measurements, or with calculated dose distributions from the treatment planning system. Therefore, proper calibration and scaling ensure that the reconstructed dose distribution closely represents the delivered dose and can be robustly compared with planned dose distributions (Zwierzchowski et al., 2016).

2.2.6.4 | Gamma Analysis and Gamma Index

Gamma analysis is a widely used method for comparing two dose distributions in radiotherapy QA. It combines both the dose difference and the distance-to-agreement criteria into a single metric, known as the gamma index. This approach is particularly useful because it accounts for discrepancies in both the magnitude of the dose and the spatial location where the dose is delivered.

The gamma index is calculated by evaluating, for every point in the measured distribution, whether there exists a corresponding point in the reference distribution that satisfies predefined tolerances (example: 3% dose difference and 3 mm distance-to-agreement). A gamma value of less than or equal to 1 indicates that the criteria are met, while values greater than 1 indicate a failure. The gamma index is calculated as follows:

$$\gamma = \sqrt{\frac{\Delta r^2(\mathbf{r}_R, \mathbf{r}_E)}{\delta r^2} + \frac{\Delta D^2(\mathbf{r}_R, \mathbf{r}_E)}{\delta D^2}}$$

where:

- $\Delta r(\mathbf{r}_R, \mathbf{r}_E)$ is the spatial difference between the reference and evaluated points,
- $\Delta D(\mathbf{r}_R, \mathbf{r}_E)$ is the dose difference,
- δr is the respective distance criterion, and
- δD is the dose difference criterion.

In practice, gamma passing rates (the percentage of points with $\gamma \leq 1$) are reported to assess the level of agreement between measured and planned dose distributions. Typical acceptance thresholds (example, 95% of points passing the 3%/3 mm criteria) are used as benchmarks to ensure accurate and clinically safe treatment delivery.

2.2.7 | Current Literature on Prostate Treatments

2.2.7.1 | Prostate Motion

Prostate motion during radiotherapy has been broadly categorised into distinct patterns. Mastella et al. (2024) distinguishes between systematic drifts, which tend to occur posteriorly and inferiorly, and random transient motion, which are more often observed in the anterior and superior directions. Complementing this, Menten et al. (2020) define intrafractional prostate motion as the change in anatomy that occurs after the acquisition of the verification image and the approval of the final treatment plan.

In the study by Menten et al. (2020), continuous motion monitoring with gating was not yet available on the Unity MRL. Instead, treatment log files were combined with 3D MR images acquired before treatment and 2D cine-MRI during beam delivery, allowing motion to be quantified retrospectively as shown in Figure 2.8. Using this method, Menten et al. (2020) demonstrated measurable systematic drifts occurring both before and during beam-on time. Between the acquisition of the 3D verification image and the start of cine-MRI, the CTV was displaced on average by 0.5 mm ± 1.0 mm posteriorly, with shifts of up to 3 mm posteriorly and 1.1 mm ± 2.0 mm inferiorly. Following the initiation of cine-MRI, an additional displacement of 0.0 mm ± 0.8 mm along the SI axis and 0.1 mm ± 0.9 mm inferiorly was observed. While in 2020 this motion could only be characterised retrospectively, in current Unity workflows the equivalent displacement would typically be managed through a BLS correction, applied in combination with continuous motion monitoring and gating to prevent drifts from compromising dose delivery.

Provided that clinically a PTV margin is also added to compensate for uncertainties such as setup variation and organ motion, this ensures adequate CTV coverage despite geometric uncertainties. However, further reduction of this margin requires not only reliable intrafraction motion management but also consideration of delineation variability. Delineation errors arise because no oncologist contours anatomical structures in the same way, and even the same observer may produce slight differences between

sessions. This inter- and intra-observer variability introduces systematic uncertainty into the CTV definition.

In parallel, intrafraction prostate motion represents a biological uncertainty, driven by bowel gas movement and bladder filling. In fact, Tsekas et al. (2024) suggest that such motion can be either gradual or sudden, making it inherently unpredictable.

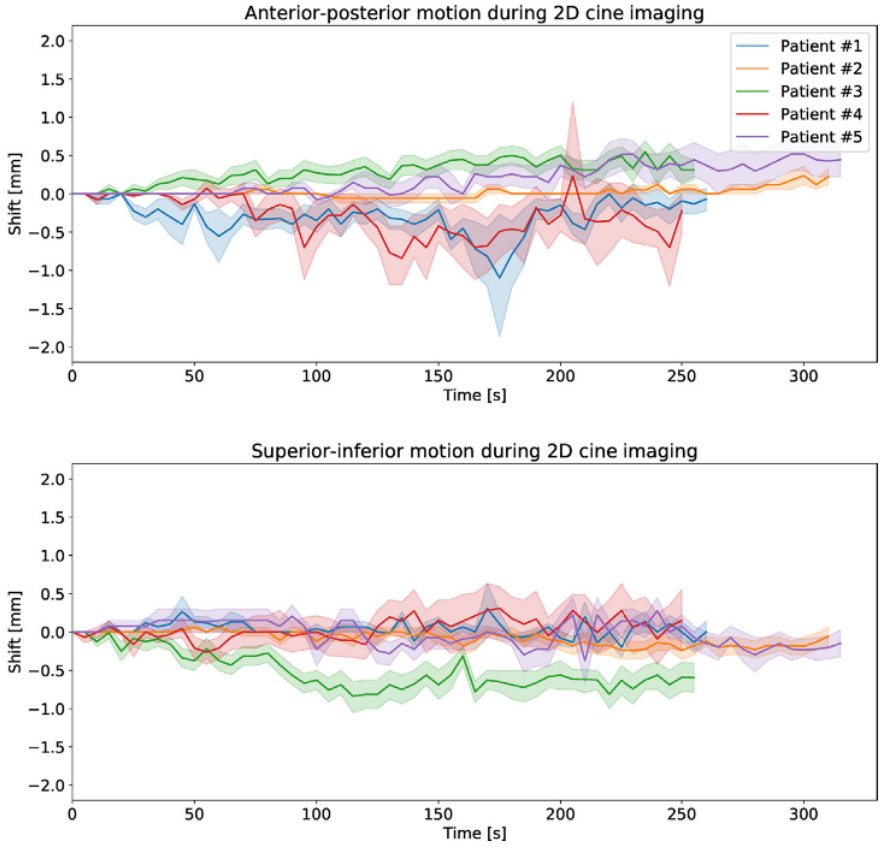

Figure 2.8: Analysis of the observed prostate motion with the mean shift at each time point during 2D cine MR imaging. The standard deviation is represented by the shaded area, (Menten et al., 2020)

.

In the study by Bosma et al. (2021), four different anatomical deformations were studied. These were based on four typical patient observed motion patterns, which

include:

1. **Rectal Filling Motion:** As the rectum fills and expands, mimicking the transit of a gas bubble, it causes the prostate to shift in an anterior-superior direction. This movement pattern was previously observed during the study of de Muinck Keizer et al. (2020a), where in a few individual patients, the prostate shifted by approximately 6 mm anteriorly with a concurrent left–right rotation of around 9°, an abrupt change that persisted for the remainder of the fraction.

2. **Bladder Filling Motion:** The expansion of the bladder exerts pressure on the prostate, displacing it in an inferior-posterior direction. This motion pattern is based on observations of individual patient movement over 6 minutes, as reported by de Muinck Keizer et al. (2020a).

3. **Average Prostate Motion:** Multiple studies have demonstrated that the prostate exhibits a systematic drift predominantly in the posterior and inferior directions. Example de Muinck Keizer et al. (2020b) quantified mean displacements of approximately 1.0 mm posterior and 1.0 mm inferior, with excursions occasionally reaching up to 4–5 mm. over a period of 6 minutes. These findings reinforce that, although motion is generally small, the dominant pattern is a posterior–inferior drift over the course of beam delivery. This observation is shown in Figure 2.9.

4. **Residual Motion only:** Includes the subtle, ongoing physiological activities within the patient's body, such as respiratory fluctuations, and peristaltic movements of the digestive tract. These movements, while often small in magnitude, can still impact the precision of image acquisition and treatment delivery.

With the above considered, such factors should be considered, as larger margins might be necessary to account for any deformation, tumour geometry variations, seminal vesicle deformations and prostate rotation.

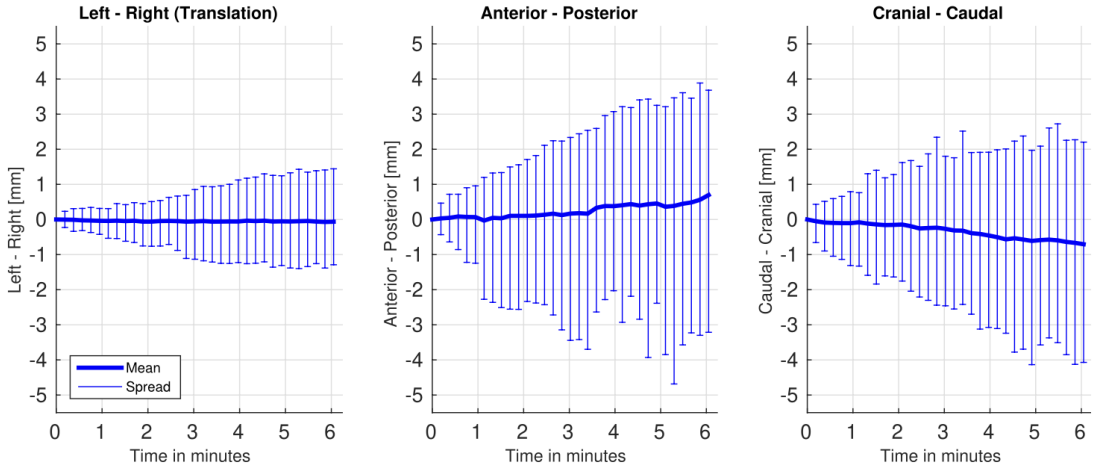

Figure 2.9: Population translation intrafraction motion detected during a VMAT treatment (de Muinck Keizer et al., 2020b)

The time-dependent magnitude of intrafraction prostate displacement is a significant factor in ultra-hypofractionated radiotherapy for prostate cancer. The study by Oehler et al. (2022) highlighted that prolonged treatment durations can lead to larger intrafraction prostate movements, ranging from 3 mm to 7 mm as shown in Figure 2.10. For treatment times under 2.5 minutes, motion is relatively small and can be managed with a 2–3 mm PTV margin. For longer treatments, however, intrafraction monitoring and correction are necessary. In their study, online imaging was performed using fiducial markers tracked with orthogonal kV/kV X-rays on the CyberKnife system, with real-time corrections applied by steering the robotic arm to follow the prostate. By contrast, the Unity MRL at the time of this work lacked intrafraction tracking or beam steering, relying instead on pre-treatment adaptation (ATP/ATS) without the ability to interrupt or correct for drift during beam-on.

2.2.7.2 | Gating Effectiveness and Margin Reduction

Faccenda et al. (2023) compared gated and non-gated SBRT, finding greater dose deviations in non-gated treatments, although fractionation mitigated cumulative effects. These findings underline the need for minimised beam-on time and reduced plan com-

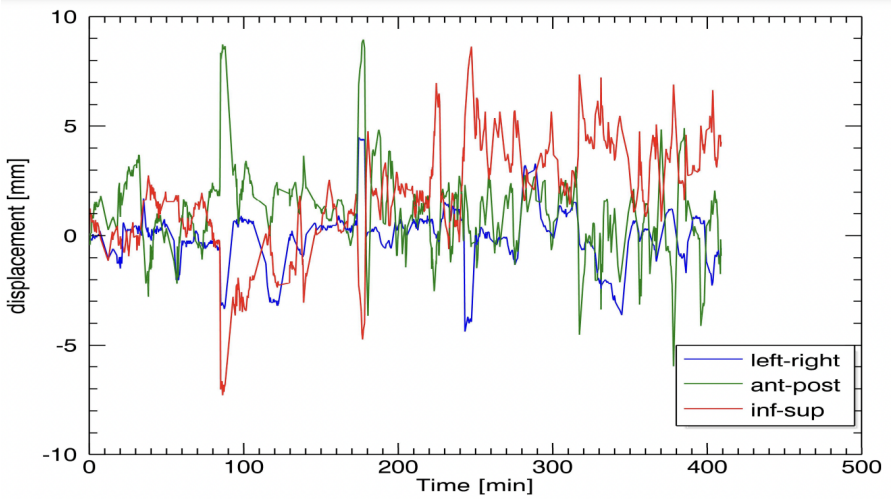

Figure 2.10: Prostate motion patterns results, (Oehler et al., 2022)

plexity to limit motion-related errors (in the absence of gating). The benefits of MRL for prostate SBRT are well documented, and a trial by Kishan et al. (2023) demonstrated that MRI-guided SBRT, through margin reduction, significantly decreased acute toxicities compared with CT-guided treatments, although CT guidance with fiducials can still achieve comparable dosimetric accuracy.

Kontaxis et al. (2020) examined intrafraction prostate mobility during MRL SBRT and its dosimetric implications. The reconstruction of the administered dosage utilising 3D cine-MRI motion data alongside LINAC delivery log files revealed that substantial prostate motion mainly occurred before radiation administration. As shown in Figure 2.11, during beam-on, the prostate demonstrated increased stability, exhibiting reduced mean translations in contrast to the more significant displacements noted during the pre-treatment phase. Nevertheless, random motion instances occurred during irradiation. Concerning the translational motion before and during treatment, the results found in the study are as follows: (LR: 0.1 ± 0.6) mm, (AP: 0.9 ± 1.9) mm, (CC: 0.9 ± 2.0) mm, and (LR: 0.0 ± 0.2) mm, (AP: 0.2 ± 0.9) mm, (CC: 0.3 ± 1.0) mm, respectively. Kontaxis et al. (2020) concluded that due to the diminished intrafraction motion during beam-on, anisotropic PTV margins, perhaps reduced in the CC direction, may be

viable. They observed that the probability of unpredictable motion during treatment constrains the degree of margin reduction, hence highlighting the necessity for real-time adaptive techniques.

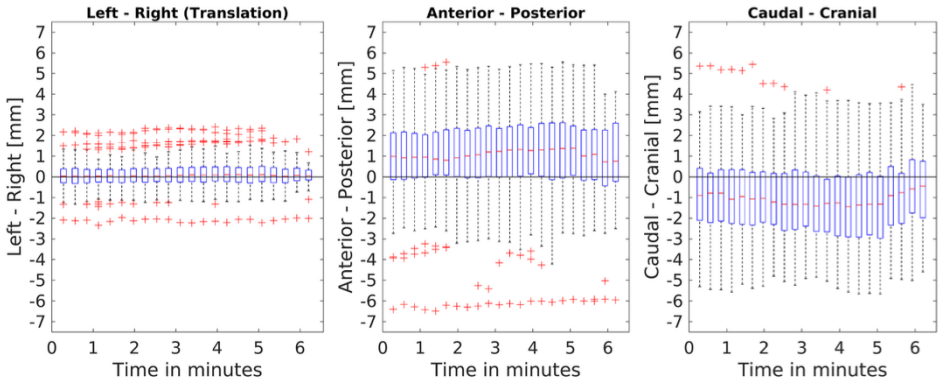

Figure 2.11: Boxplots of the intrafraction motion during the beam-on period based on cine-MR concerning the planned anatomy of the PRE scan, (Kontaxis et al. (2020))

Gated treatments were examined by Xiong et al. (2022) by using a PTV margin of 4.5 mm isotropically around the CTV and 3.0 mm posteriorly towards the rectum. Such margins are important to maintain good CTV coverage whilst minimising rectal dose. (Xiong et al., 2022)'s gating protocol, implemented on the ViewRay MRL, automatically interrupted the treatment beam if 5% or more of the CTV extended beyond a 3.0–5.0 mm isotropic expansion. In cases of prolonged deviation, treatment could be halted entirely and the patient repositioned before resuming. Dose reconstruction based on the static dose cloud approximation. Such a cloud simply represents the planned dose distribution in a fixed space, which ultimately irradiates the structures that lie within it. In the same study, the static dose cloud approximation revealed that residual motion within the gating window led to only small average CTV underdosing, with target coverage generally maintained. While on average, increases in rectal and bladder doses were minor, larger deviations occurred in individual fractions, especially in the rectum. Importantly, the study showed that for most fractions, gated and non-gated deliveries produced nearly identical dose–volume outcomes, indicating that gating offered lim-

ited additional dosimetric benefit under the chosen margins and motion ranges. However, the gating system's ability to interrupt treatment during severe drift was crucial in preventing substantial dosimetric errors. Xiong et al. (2022) further noted that the reliance on the static dose cloud method limited the precision of delivered dose estimates, and highlighted that more accurate segment-by-segment dose reconstruction or even full online dose accumulation would be required to capture the true dosimetric impact of intrafraction motion.

Gradual posterior and cranial drift over time has also been observed, as described by de Muinck Keizer et al. (2020a), who analysed intrafraction motion during fully online adaptive radiotherapy sessions. They found that generally, 5 mm margins are sufficient for prolonged treatments. While prostate motion due to rectal gas pockets was relatively rare, the study noted that intrafraction adaptation may still be necessary in some cases, particularly when anatomical changes introduce significant deviations that could compromise dose accuracy.

To reduce the effect of cumulative motion during delivery, Willigenburg et al. (2022) proposed a sub-fractionation workflow that splits a single fraction into two parts. Using anisotropic margins of 2 mm (LR and CC) and 3 mm (SI), this method improved geometric accuracy without requiring online dose accumulation, with an average beam-on time of 11 minutes per treatment. By limiting intrafraction motion and enabling the safe delivery of high fractional doses, the workflow supports further hypofractionation and may reduce toxicity by enhancing target conformity and sparing surrounding organs.

Tetar et al. (2022) compared 3 mm and 5 mm PTV margins under an adaptive MRgART protocol and observed that while prostate coverage remained acceptable in both cases, coverage of the seminal vesicles was frequently compromised without daily adaptation. This highlighted the importance of either robust margin strategies or dynamic protocols like gating, particularly for irregular or highly mobile structures.

Mitchell et al. (2024) and Lawes et al. (2022) examined workflows using ATP after ATS planning and concluded that although BLSs could be corrected with pre-treatment adaptation, residual motion during beam delivery persisted. Their findings underscore the limitations of relying solely on pre-treatment corrections and highlight the necessity of integrating real-time gating to effectively manage prostate motion throughout the full course of irradiation.

2.2.7.3 | Emerging Technical Strategies and Tools

To address intra-fraction motion dynamically on the Unity MRL, Snyder et al. (2024) investigated a segmented adaptive workflow in which treatment plans were recalculated after each VMAT arc using cine-MRI data. This strategy directly demonstrates how Unity's imaging capability can be leveraged for online adaptation, achieving superior target coverage (minimum dose $\geq$95% in 90% of cases). However, it required repeated planning interruptions and full plan recalculation, making it a time-intensive approach that may be impractical in routine clinical settings. Importantly, the method did not incorporate beam-hold gating or real-time image response during irradiation; instead, motion was managed through episodic re-optimisation. This positions the work of Snyder et al. (2024) as a key step in demonstrating Unity's potential for intra-fraction adaptation, while also underscoring the need to evaluate whether continuous gating could provide similar benefits with less workflow disruption.

The study done by Legge et al. (2017) investigated intrafraction prostate motion during LINAC-based SBRT in patients treated with a rectal displacement device in combination with fiducial-based tracking. Using kilovoltage intrafraction monitoring (KIM), they found that the prostate remained within 1 mm of its initial position for 84.8% of treatment time, with displacements $\geq$3 mm occurring only 0.4% of the time. Most motion occurred in the SI and LR directions, while SI motion was minimal. Nonetheless, it was concluded by Legge et al. (2017) that the idea of targeted anatomic stabilisation

strategies, such as rectal retractors or spacers, can minimise motion and may complement gating protocols in MRgART environments.

2.3 | Conclusion

This chapter presented a deep and critical review of the literature associated with the study. The following chapter will describe and discuss the research methodology adopted in this study.

3

Research Methodology

3.1 | Introduction

The methodological framework of this study was developed to address the central research question of whether prostate radiotherapy margins can be safely reduced on the Elekta Unity MRL while maintaining robust target coverage and sparing of the OAR. Since intrafraction motion of the prostate is a primary challenge in margin reduction, the methodology was designed to capture, quantify, and evaluate this motion in both patient data and phantom experiments. By doing so, the study aimed to generate clinically relevant evidence that could guide the implementation of margin optimisation and motion management protocols at SAMOC.

A mixed research approach was adopted to achieve the study's aims. Patient log files provided retrospective datasets to characterise typical prostate motion patterns over multiple fractions, enabling the evaluation of both average and maximum displacements. Complementing this, experimental work with the Modus QUASAR™ MRI 4D Phantom allowed for a treatment planning study to be implemented by performing controlled testing of motion scenarios. This facilitated dosimetric validation and assessment of treatment workflows under reproducible conditions.

3.2 | Research Approach

To validate prostate motion management and gating procedures, a mixed research method approach was used. For the first part of the study, a quantitative research approach was adopted, closely following the study's objectives. Such an approach allowed a high degree of objectivity to be achieved (Munther et al., 2024). More specifically, through the generation of various plots, the related numerical and/or statistical analysis were retrieved to get a clear idea of how the prostate moves during recent SABR MRL treatments. For the second part of the study, DVH statistics were collected for various dosimetric criteria, followed by the plotting of the related graphs for visual analysis. Lastly, for the third part of the study, the focus was on validating the dose delivery of a simulated clinical delivery through film dosimetry. With all this, the possibility of further margin reduction and improved prostate motion management could be assessed.

3.3 | Research Strategy

Given that the primary aim of this study is to evaluate intrafraction prostate motion on the Elekta Unity MRL in order to determine whether PTV margins can be safely reduced while maintaining accurate dose delivery and OAR sparing, the research strategies for this study are primarily retrospective, experimental, qualitative and quantitative.

The retrospective component of this study involves a sample-based analysis of treatment log files from prostate cancer patients treated at SAMOC. This stage provides an overview of typical prostate motion patterns, enabling an understanding of the magnitude, frequency, and temporal behaviour of intrafraction motion in the clinical setting.

The experimental component involves the creation of a reference treatment plan to

which varying reference plan isocentre offsets and varying BLS plan offsets were systematically applied. This approach allows for controlled testing of BLS plan robustness and the exploration of how far positional offsets can be extended before dosimetric coverage is compromised. DVH statistics from the TPS were obtained for each BLS plan to evaluate the dosimetric impact on the CTV, the PTV and OARs, including the urethra, rectum, and bladder. Such constraints were taken from the SAMOC treatment protocol for prostate SABR treatments on Unity, which are in turn based on the Prostate Advances in Comparative Evidence (PACE) trial by van As and Tree (2020).

The quantitative and qualitative phase consists of experimental dose verification using radiochromic film measurements. Treatment deliveries incorporating the simulated BLS and offsets from the experimental stage were carried out on phantom setups, and the resulting dose distributions were analysed. This enables direct correlation between positional deviations and their dosimetric impact, translating motion data into clinically relevant outcomes. On the other hand, the qualitative phase was incorporated with the objective phase to visually analyse the quantitative data into plots.

By combining retrospective motion analysis, experimental testing with DVH evaluation, and quantitative and qualitative analysis, this multi-phase approach enables a comprehensive assessment of margin reduction strategies and provides evidence-based insights that can be directly translated to clinical treatments, regardless of the specific CTV-to-PTV margin applied.

3.4 | Data Collection Technique

3.4.1 | Prostate Traces

Data for this retrospective analysis was obtained directly from the treatment log files generated by the MRL Elekta Unity at SAMOC. Specifically, the time-stamped posi-

tional coordinates of the prostate target, as recorded by the system throughout each treatment fraction, formed the primary dataset. The associated temporal window for data extraction spanned from the point at which the treating clinician approved the treatment template to the completion of treatment for that fraction. The latter includes data up until the APM session was halted. Specific criteria were established to ensure both the fairness of sampling and the validity of the dataset employed in this study. As elaborated in the subsequent sections, the dataset predominantly comprised five treatment fractions per patient undergoing prostate cancer therapy.

3.4.2 | Treatment Planning Study

The second component of data collection involved the use of Monaco® TPS to extract DVH statistics. With close reference to the PACE trial, the planning aims and dose–volume constraints were used to evaluate five treatment plans, each generated with a different offset of the prostate's centroid relative to the treatment isocentre. These offsets were introduced to plan different BLS scenarios, thereby allowing an assessment of how such displacements could impact target coverage and OAR sparing. This experimental technique enabled the simulation of potential prostate displacements that may occur during online treatment. The selection of offsets was directly guided by the prior examination of motion traces in patient log files. The traces indicate both the most commonly observed ranges and infrequent larger deviations; consequently, the offsets used in the phantom and treatment planning simulations were chosen to encompass this spectrum, accounting for typical displacements while also incorporating extreme scenarios.

Another treatment plan was also created to investigate the movement and the related dosimetric criteria of the CTV and the urethra for minor ungated movements of the CTV within the PTV. This was done because both structures are critical when evaluating the clinical feasibility of margin reduction. In fact, the CTV represents the target volume whose coverage must remain robust under motion, while the urethra, embed-

ded within the prostate, is a dose-limiting OAR. Assessing their behaviour within the PTV allowed for direct evaluation of the trade-off between maintaining tumour control probability and limiting urethral toxicity, which is central to motion management and adaptive prostate SBRT. Metrics and volume values were recorded and analysed to quantify the dosimetric impact on important structures.

3.4.3 | Film Dosimetry

The third stage of the study involved dosimetric validation using radiochromic films placed within a programmable motion phantom, the Modus QUASAR™ MRI 4D Phantom. This setup was designed to approximate clinically observed prostate motion by programming the phantom with a motion trace that incorporates the motion characteristics derived from patient log files, within the constraints of the phantom's degrees of freedom. The films were analysed post-irradiation to evaluate spatial dose delivery accuracy under both static and gated delivery conditions. By comparing the measured dose distributions with those obtained from a static film surrogate, this analysis provided an end-to-end verification of the gating protocol and an evaluation of its ability to compensate for motion during treatment. Ultimately, correlating the results from static and motion films allows confirmation of whether treatment-related motion can be effectively mitigated.

3.4.4 | Summary

While other data collection techniques exist, these three components were considered the most appropriate method for this retrospective validation study. Mainly because such readily available data directly reflects the system's performance during actual patient treatments, on which treatment plans and film studies were based. Thus, this makes it the most relevant and efficient method for achieving the study's objectives.

3.5 | Data Collection Procedure

3.5.1 | Stage 1: Prostate Traces

Data collection for this study focused on recent patients who underwent hypofractionated prostate radiotherapy on the MRL. Such a data sample being retrieved solely by a senior MP included the extraction of the associated patient's log files, which were anonymised as necessary. Following the data sample retrieval and anonymisation, the associated log files per patient per fraction were filtered to keep only the following data columns:

- Translation Vector (x y z)
- Approved Template Registration Values (unit=mm)
- TimeStamp (Translation Computation)
- LINAC State

for further analysis. Besides this, such a sample was chosen based on the following criteria:

- Treatments done between the end of July 2024 (when the Unity MRL entered into clinical service) and September 2024 were not considered to eliminate the inclusion of treatments that may have been affected by procedural delays. This criterion excluded no more than 10 patients.
- Patients were only included if at least 4 out of their 5 treatment fractions were analysable. Fractions requiring a CP were excluded from the analysis, since stitching two MRIs and their associated data to reconstruct a full treatment scenario was not as technically feasible within the scope of this project. Consequently, fractions which had only one CP in the whole treatment were represented as a blank subplot and did not contribute to the final sample statistics.

- Patients who had one or more BLSs performed across fractions were still considered in this study, as this allowed a deeper understanding of greater-than-normal prostate motion traces. This was possible since the translation vector at the point of each BLS was initiated and was available from the records. This could be incorporated from the point onwards where the BLS was applied online. In this way, the impact of BLSs could be accounted for without discarding the fraction entirely, thereby preserving the continuity of the treatment trajectory in the analysis.

Following the careful sample selection procedure, the presence of CPs, BLSs and 'multiple MRIs taken with an ATP after ATS workflow' were identified directly from the audit log files. CPs were indicated by having more than five log files for a given patient (signifying an interrupted session/s), while BLSs were evident from the "Translation Vector (x, y, z)" column, where a sharp drop in offset vector values was observed after the BLS was applied online. Lastly, for the sessions where multiple MRIs were taken with an ATP after ATS workflow, more than one template approval was found within the log file. Therefore, following this procedure, the patient's fraction could be categorised as:

- Normal
- Had one or more MRI taken with an ATP after ATS workflow
- Had one or more BLS
- Had one CP

In cases of difficulty or uncertainty, these records were referred to the senior MP for further evaluation and confirmation.

3.5.2 | Stage 2: Treatment Planning Study - Modus QUASAR™ MRI 4D Phantom Data Collection

Following the first stage of the study, the Modus QUASAR™ MRI 4D Phantom was set up as shown in Figure 3.1. This setup, being replicated on both SAMOC's CT scanner and MRL, allowed for a CT image and a series of MR images to be exported to Monaco® TPS. For the equipment to be set up, the procedure below was followed:

Figure 3.1: Modus QUASAR™ MRI 4D Phantom on MRL

1. Once the phantom was assembled, it was mounted within its cradle. The film insert was placed in a vertical position to consider motion in the SI directions.

2. Adapting the setup described by Uijtewaal et al. (2023), the equipment was inclined at 25.8° by resting the cradle on multiple solid water blocks (total height of 22 cm) placed against the superior index bar at a couch value of 5, as shown in Figure 3.1. Compared to the original 20° ramp configuration described by Uijtewaal et al. (2023), this larger angle was selected to make the AP motion component more evident, thereby better reflecting the multi-directional nature of prostate motion. Then, once the cradle with the phantom was set angled on the solid water blocks, the inferior index bar was placed at the couch index of 25.5 to secure the cradle. For this step, the ceiling laser was used to align the phantom laterally as necessary. It was also ensured that the Modus's motion was set to translation only.

3. For the MRL reference planning scan setup only, the MR anterior coil was placed at the 21.5 index and tilted at 15.9°. The tilt was the maximum feasible angle based on the phantom geometry and coil design. Such a setup still enabled full phantom visualisation within the MR FOV while maintaining image quality.

4. For the MRL reference planning scan setup only, the couch was inserted within the bore until the 48.5 couch index mark, to have the setup placed at the magnet's isocentre.

A CT scan with the Modus QUASAR™ MRI 4D Phantom was obtained with the longitudinal position of the target set at 0 cm. In addition, three T1-weighted MR images were obtained from the MRL, with the longitudinal position of the target set at 0 cm and ±2 cm. The latter images were obtained by using the Modus QUASAR™ MRI 4D Phantom programmable software. In addition, to ensure that the phantom's motor arm was free to move underneath the MR anterior coil, and would not damage the MR

anterior coil set above it, a slow sinusoidal motion of five breaths per minute were set from the same software to simulate the movement as a check.

These four imaging scans were then imported into Monaco® TPS, where the CT image was fused with the MR at 0 mm position, whilst the -20 mm (-2 cm) image was fused with the +20 mm (+2 cm) image, both achieved by doing the 'image fusion' procedure on Monaco® TPS. Through the fusion of the CT to MR, the contours of the Modus phantom and its cradle (and thus the electron densities of these structures) were transferred accordingly, allowing a treatment plan to be done on the MR image. For the ±20 mm fusion, the procedure was performed solely to use the transformation matrix to quantify the angulation of the Modus phantom motion longitudinal axis relative to the couch surface.

For further data to be collected from Monaco® TPS, the CT and MR at 0 mm fused image was first used to generate the required contours. In this way, the cradle, together with the phantom placed on the CT, could be delineated. The structures contoured included: the couch (automatically generated from the MR planning), the cradle frame and its black support rods, the cradle's perspex supports and top and bottom frame, the phantom's surface, film cassette, film cylinder target and registration spheres, the side cavity and its rim, and lastly, the phantom's movable cylinder. Once the structures were delineated, a treatment plan was then created on the MR as highlighted above. The mentioned structures are all shown in Figure 3.2.

More importantly, to simulate prostate shifts and enable film exposures in the next stage of data collection, the senior MP transferred anatomical patient-like structures representing a prostate and surrounding anatomy to the Modus phantom MR dataset, with prostate dimensions typically encountered in clinical experience, but that also fit within the film cassette area. Structures included the urethra, seminal vesicles, bladder and rectum. Besides the inclusion of such OARs, the CTV and the PTV were created

based on the PACE trial. For this study, the CTV was set to be equivalent to the prostate and proximal 1 cm of the seminal vesicles, whilst the PTV was created with a 2 mm margin surrounding the CTV. All this is shown in Figure 3.3.

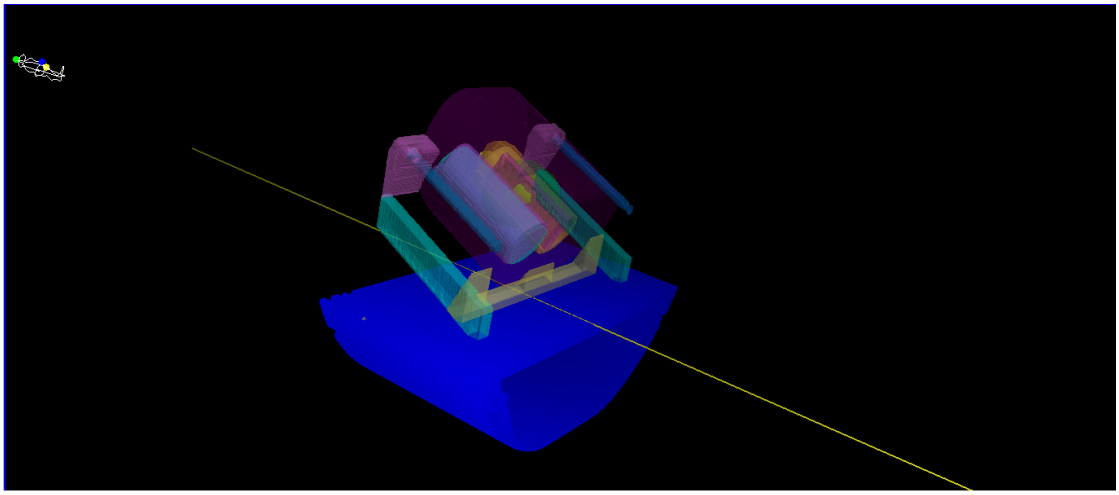

Figure 3.2: Structures imported in Monaco® TPS, replicating the setup on the CT and MRL

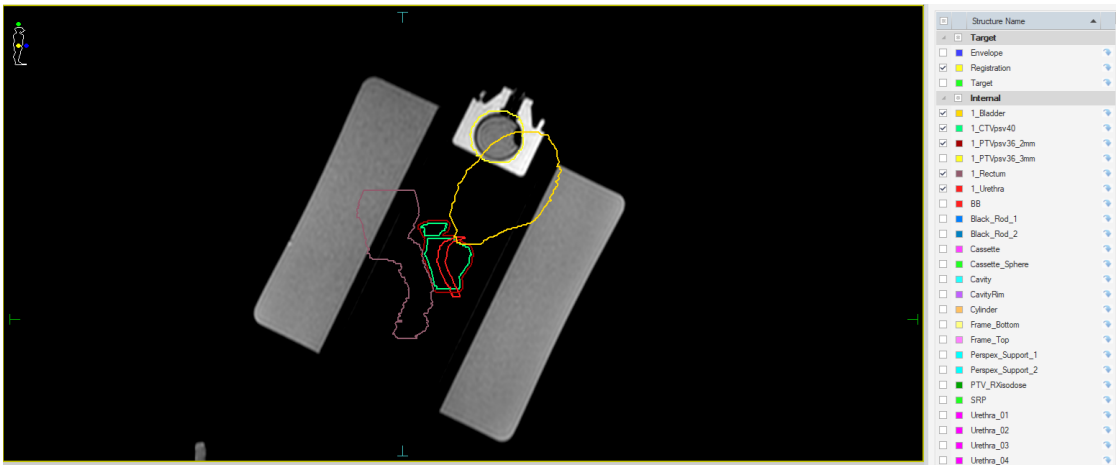

Figure 3.3: Anatomical structures included in Monaco® TPS

A typical clinical 9-beam IMRT reference treatment plan was finalised with a MP such that it meets the clinical dose constraints. Five reference plans were created, with different isocentre offsets from the prostate's centroid position in preparation for the subsequent online BLS stage. These additional isocentre positional offsets were defined at 4 cm and 2 cm superior, 0 cm, and 2 cm and 4 cm inferior relative to the prostate's centroid. These offsets were not applied during the reference plan creation itself within normal clinical routine, but were instead established to simulate realistic offsets encountered during daily plan adaptation.

Common for all iscontre offsets, a corresponding set of BLS coordinates were calculated from the trigonometric relationship present between the setup geometry and the motion direction of interest. The selected offsets were informed by the prostate motion statistics collected during the first stage, covering both the normal displacement ranges typically observed and several 'extreme' cases intended to test the robustness of the approach. The specific BLS increments considered in each scenario are summarised in Table 3.1.

The choice of increments was informed by the phantom's angular orientation, as determined from the TPS transformation matrix, which indicated an actual tilt of 25.82°. In this way, such an angle ensured apparent motion of structures upon creating various offsets from the prostate's centroid. Using a simple trigonometric model, the distances in the AP direction were calculated for a given set of SI displacements.

Table 3.1: BLS coordinates considered for each treatment plan

Direction	**Adjust Tolerance Plan (APM)**		
	***x* in cm (Lt/Rt)**	***z* in cm (Sup/Inf)**	***y* in cm (Ant/Post)**
Inf Post Rt	0.20	-2.00	-1.00
	0.20	-1.00	-0.50
	0.20	-0.80	-0.40
	0.20	-0.60	-0.60
	0.15	-0.60	-0.40
	0.10	-0.40	-0.30
	0.08	-0.40	-0.20
	0.08	-0.30	-0.30
	0.05	-0.30	-0.15
	0.05	-0.20	-0.20
	0.03	-0.20	-0.10
	0.03	-0.10	0.05
Center	0.01	0.00	0.00
Sup Ant Lt	-0.03	0.10	0.05
	-0.03	0.20	0.10
	-0.05	0.20	0.20
	-0.05	0.30	0.15
	-0.08	0.30	0.30
	-0.08	0.40	0.20
	-0.10	0.40	0.30
	-0.15	0.60	0.40
	-0.20	0.60	0.60
	-0.20	0.80	0.40
	-0.20	1.00	0.50
	-0.20	2.00	1.00

For each BLS increment, dosimetric criteria obtained from Monaco® TPS were collected. The statistics were gathered during an online scenario. The statistics include those found in Table 3.2:

Table 3.2: BLS DVH statistics obtained for each starting position (5 positions in total)

Target	**Dosimetric Criterion**	**Range/Tolerances**
CTV	$D_{0.1cc}$	$42.6Gy \leq D_{0.1cc} \leq 48.3Gy$
	$D_{95\%}$	$D_{95\%} \geq 49$ Gy
	V_{40Gy}	$V_{40Gy} > 95\%$ (-5%)
	$D_{99.9\%}$	$D_{99.9\%} \geq 49$ Gy
	D_{mean}	/
	V_{42Gy}	$V_{42Gy} \leq 50\%$ [1]
PTV	$D_{95\%}$	$D_{95\%} \geq 36.25$ Gy
	$D_{98\%}$	$D_{98\%} \geq 34.4$ Gy
	$V_{36.25Gy}$	$V_{36.25Gy} > 95\%$ (-5%)
	$V_{34.4Gy}$	$V_{34.4Gy} > 98\%$
Rectum	D_{1cc}	$D_{1cc} < 36$ Gy
	V_{36Gy}	$V_{36Gy} < 1$cc
Bladder	D_{5cc}	$D_{5cc} < 37$ Gy
	V_{37Gy}	$V_{37Gy} < 5$cc
Urethra	$D_{50\%}$	$D_{50\%} < 42$ Gy
	V_{42Gy}	$V_{42Gy} < 50\%$

[1] The CTV V42Gy $\leq$ 50% threshold was not intended as a clinical criterion but was used as a recording measure for comparison with the urethra's V42Gy.

Following the full set of dosimetric values, separate graphs were generated for the most important parameters against translation in z-axis. The list of graphs generated is

summarised in Table 3.3.

Table 3.3: A table summary of the dose constraints and DVH metrics considered in this study

Dosimetric Criteria	Dosimetric Constraints
■ CTV: V40Gy (V40Gy $>$ 95% (-5%))	■ CTV: V42Gy: $\leq$ 50% [1]
■ CTV: D_{mean}	
■ PTV: D95% (D95% $>$ 36.25 Gy)	
■ PTV: V34.4Gy (V34.4Gy $>$ 98%)	
■ PTV: V36.25Gy (V36.25Gy $>$ 95% (-5%))	
■ 1_Urethra: V42Gy (V42Gy $<$ 50%)	

[1] The CTV V42Gy $\leq$ 50% threshold was not intended as a clinical criterion. Instead, it was used as a recording measure to categorise whether motion along the z-axis, that is, SI, resulted in a substantial reduction of target coverage. This allowed systematic comparison across cases, rather than suggesting a clinically validated constraint.

The above dosimetric criteria (except "CTV: V42Gy: $\leq$ 50%") were chosen from the PACE's Trial and used to monitor the robustness of the BLS plan for each offset considered. From the above dosimetric criteria, multiple copies of the urethra structure were generated for each planned BLS shift in advance, and these were given the name of "Urethra_XX" where the "XX" refers to which BLS the shifted urethra belongs to. These shifted structures were then used to evaluate dose–volume compliance un-

der the different motion scenarios, depending on the coordinates available in Table 3.1. In parallel, the original unshifted urethra structure "1_Urethra" was retained, allowing for direct comparison and assessment of how the unshifted urethra behaves relative to the shifted case. Moreover, another comparison between the unshifted urethra V42 and the CTV within V42 was also made to assess whether the CTV V42 can be a predictor to the unshifted urethra V42.

In a separate procedure, through the phantom's programmable software, the phantom's drive post was moved in small increments along the phantom's longitudinal axis whilst having the phantom being imaged under an online clinical worklow, the longitudinal positions at which 97% and 99% VOICE were achieved on the MRL's CMM, were recorded. From these results, it was then determined to what extent the CTV can move within the PTV that corresponds to the related gating criteria.

With the results used as a guide, the CTV movement within the PTV was then also investigated by paying closer attention to the DVH statistics related to the CTV and the urethra. For this procedure, on Monaco® TPS, the CTV criteria and the criteria for multiple copies of the CTV and Urethra structures were created to analyse the associated DVH statistics. The increments considered for this procedure are shown in Table 3.4. Some additional 'extreme' values were also considered to investigate at what stage the dosimetric criteria will no longer be satisfied.

3.5.3 | Stage 3: Radiochromic Films Data Collection and Analysis

3.5.3.1 | Step 1 - Film Exposure and Scanning

A radiochromic film calibration procedure was performed on the MRL in preparation for the EBT-4 film exposures used in the treatment plan validation, as shown in Figure 3.4.

Table 3.4: Coordinates considered for each treatment plan

Direction	Adjust Tolerance/Plan (APM)		
	X (Lt/Rt) in cm	Z (Sup/Inf) in cm	Y (Ant/Post) in cm
Inf Post Rt	0.200	-0.200	-0.200
	0.075	-0.350	-0.175
	0.050	-0.250	-0.125
	0.050	-0.200	-0.200
	0.025	-0.200	-0.100
	0.025	-0.100	0.050
Center	0.000	0.000	0.000
Sup Ant Lt	-0.025	0.100	0.050
	-0.025	0.200	0.100
	-0.050	0.200	0.200
	-0.050	0.250	0.125
	-0.075	0.350	0.175
	-0.200	0.200	0.200

Figure 3.4: Film exposure set up which includes a total thickness of cm of solid water with the film inserted beneath the first 5 cm solid water blocks.

This setup was replicated from another study by Chetcuti (2025), which was conducted in parallel to this project. With this setup on the MRL, a set of films were exposed at different doses, these being 0 Gy, 0.63 Gy, 1.25 Gy, 2.5 Gy, 5 Gy, 7 Gy, 10 Gy and 14 Gy, so eventually, a calibration curve could be generated to convert optical density to dose.

At each exposure, the blocks in between which the film was placed were sprayed with water to ensure that any air gaps were eliminated. This was important to prevent magnetic-field-induced dose perturbations at interfaces. Post exposure, the film will darken in proportion to the dose delivered as shown in Figure 3.5.

Two sets of three films were also exposed at 7.25 Gy, 8 Gy and 9 Gy, in the morning and at the end of the same session (evening), for scaling to be done as necessary. These three values were chosen, particularly because 7.25 Gy matches the prescription per fraction for SBRT prostate treatments, which is 36.25 Gy in 5 fractions. On the other hand, the 8 Gy and 9 Gy were chosen to represent the higher-dose regions typically observed as hotspots within the target and urethra, ensuring that the scaling check covered the clinically relevant dose range without exceeding the film's reliable response window.

Following the above, film exposure was continued with the use of the Modus QUASAR™ MRI 4D Phantom with a film insert included as discussed earlier in part 2 of this chapter. Having such a setup allowed for another total of 5 films to be exposed for different scenarios, these being:

- **Static film at 0 mm position:** - The film was exposed with the phantom's drive post positioned at a fixed position of 0 mm. Hence, it resulted in such a film to serve as a reference film.
- **Static film at 8.5 mm inferior position:** The film was exposed with the phantom's

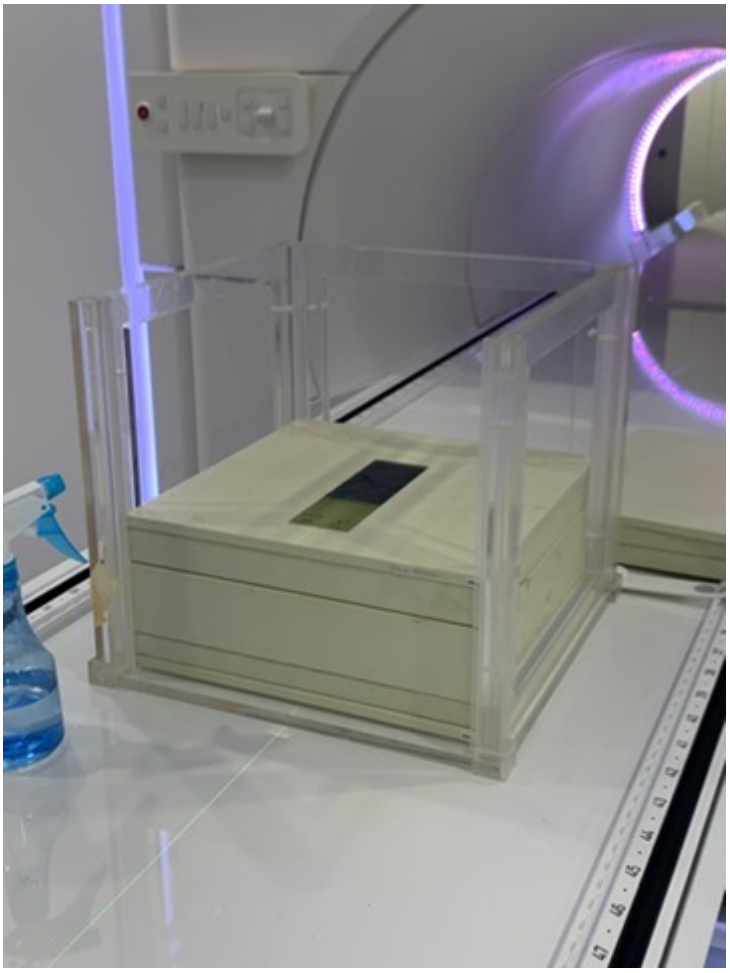

Figure 3.5: Post film exposure set up.

drive post positioned at a fixed position of 8.5 mm inferior to the original position. This was treated by doing a BLS, which in turn represented the maximal shift that could be done.

- **Static film at VOICE of 97%:** This film exposure was done so to assess the dosimetric effect achieved when the CMM's VOICE was set to 97%. Such a value was chosen to represent the extreme displacement which resulted in a VOICE equal to 97%.

- **Motion film with 2 BLSs:** This film was exposed with a live clinical workflow

using the below waveform shown in Figure 3.6, which represents a constructed prostate drift in the most prominent direction, that is, SI (along the z-axis). For this waveform to be constructed, a sine wave with an order of three was considered, starting off with an offset of -1.1 mm so as to mimic the typical patient's offset upon the start of treatment beam delivery. Then, during the live clinical workflow, the treatment was interrupted twice when the target position exceeded the gating criteria of 99% VOICE and a BLS plan was performed each time to mimic a clinical scenario, hence covering a total offset of up to 6 mm by the end of treatment.

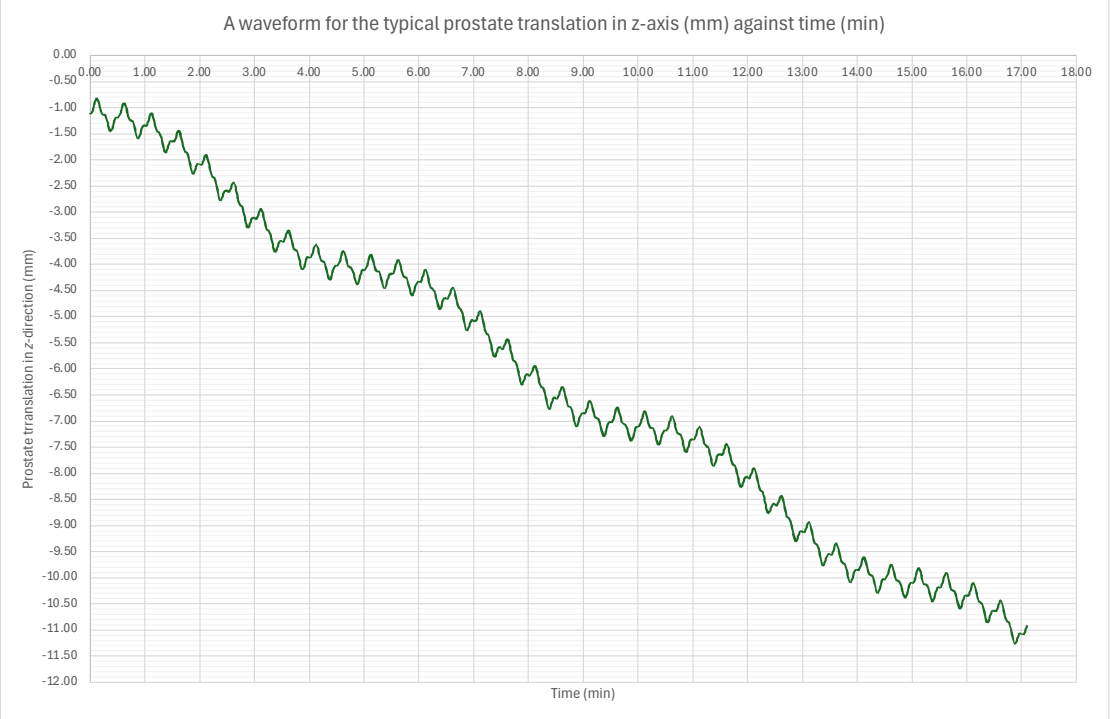

Figure 3.6: A constructed waveform mimicking the typical prostate intrafraction motion in SI (z) direction

- **Motion film with 3 BLSs:** Similar to the "Motion film with 2 BLSs" film, the same waveform was used but three BLSs were done at increments of 1/3 across the

whole treatment duration, meaning that the treatment was inturrupted a total of three times. This was done to cover up to 8 mm of motion with BLS by the end of treatment.

Following the exposure of such films, a maximum of 48 hours was allowed to elapse for the films to self-develop. The films were then scanned on the Epson Expression 10000XL film scanner, as shown in Figure 3.7. For scanning, a glass plate with the same dimensions as the scanning area was used to secure the films in place, preventing curling and ensuring they remained flat whilst in direct contact with the scanner's surface.

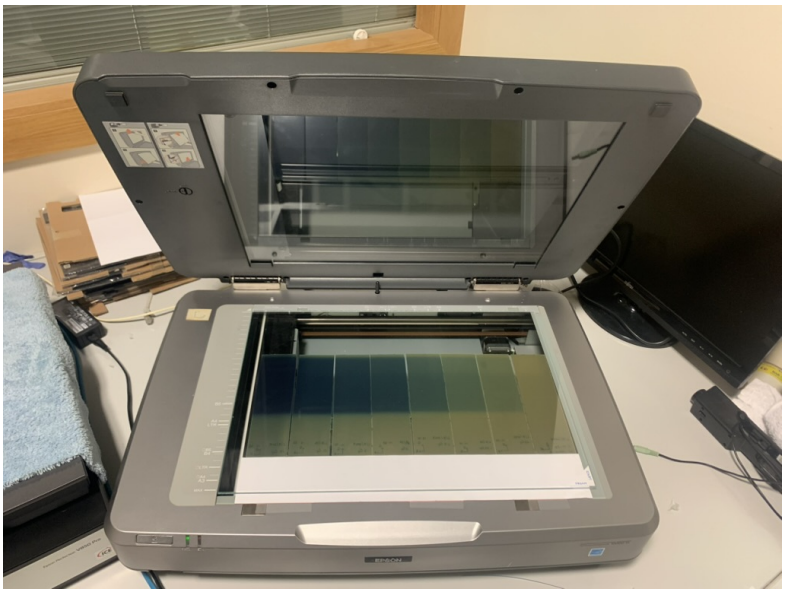

Figure 3.7: Film placement on Epson Expression 10000XL

3.5.3.2 | Step 2 - Calibration

The very first step that was done with respect to film analysis was the calibration procedure. For that to be carried out, a procedure identical to the project by Chetcuti (2025) was followed. Calibration films irradiated with doses of 0 Gy, 0.63 Gy, 1.25 Gy, 2.5 Gy, 5 Gy, 7 Gy, 10 Gy and 14 Gy were processed. This was achieved by selecting a central 10 × 10 mm ROI on each film to capture the high-dose region. The ROI mean pixel values

from the calibration films were assigned to their corresponding dose values to generate a new calibration curve on the radiochromic film analysis software.

3.5.3.3 | Step 3 - No Scaling vs Scaling Analysis

The five sets of scanned films, together with a set of 7.25 Gy, 8 Gy, and 9 Gy scaling strips (morning and evening exposures closest in time to the test film), were scanned together and analysed using the same film analysis software. A ROI measuring 10 mm $\times$ 10 mm was selected at the centre of each scaling strip. The mean dose values within this ROI were recorded, and subsequently, the corresponding percentage error relative to the reference (true) dose was then calculated using the following equation:

$$\text{Percentage Error} = \frac{|\text{Measured Value - True Value}|}{\text{True Value}} \times 100\%$$

The same procedure was repeated without and with the 'Inter-scan correction' and 'dose rescaling' functions enabled within the software, thereby generating percentage errors for the unscaled and scaled analyses.

Comparing the percentage errors obtained allowed for the determination of whether dose rescaling improved agreement with the three check dose values and, consequently, informed the dose accuracy of subsequent analysis.

3.5.3.4 | Step 4 - Registration

To initiate this process, the following set of scanned films were registered with respect to the static film at 0 mm.

- Static film at 8.5 mm inferior position
- Static film at VOICE of 97%
- Motion film with 2 BLSs

- Motion film with 3 BLSs

this was achieved by using the fiducial markings available on the film. In this way, this registration process accounted for potential shifts and rotations mismatches, thereby enabling robust gamma analysis and dose–difference comparisons.

3.5.3.5 | Step 5 - Gamma Analysis

Following the previous step, the 7.25Gy and 8.0Gy isodoses relative to the static 0 mm film were overlaid. Having this procedure repeated for the remaining four films ensured that a qualitative visual indicator of the isodoses were achieved. Then, by setting the parameters of a global normalisation at Dmax, a threshold of 10%, a maximum gamma of 2% and a reference distribution, gamma analysis was then performed as a quantitative substitute for the profile plots.

3.6 | Data Collection Tools

This section outlines the selected tools used for data collection. Both physical instruments and specialised software were employed simultaneously to gather the required information. The tools described below were identified as the most appropriate for conducting the analyses in this study.

3.6.1 | Modus QUASAR™ MRI 4D Phantom and its software

The Modus QUASAR™ MRI 4D Phantom (Modus Medical Devices Inc., London, ON, Canada) was employed to replicate clinically realistic target motion for the validation of motion management strategies. This MR-compatible device allows programmable translation and rotation of inserts to simulate patient-specific motion patterns, such as respiratory or organ drift, without compromising image quality. The phantom's control software enables the import of motion waveforms, precise configuration of movement parameters, and synchronisation with imaging and beam delivery systems. Such pro-

grammable flexibility has been used extensively to evaluate MRgART gating and tracking workflows (Uijtewaal et al., 2023), making it an ideal platform for testing motion-adaptive treatment delivery.

3.6.2 | Monaco® TPS

The Monaco® TPS (Elekta AB, Stockholm, Sweden) utilises a Monte Carlo dose calculation engine, enabling accurate modelling of dose in heterogeneous media (Winkel et al., 2019). In this work, Monaco® TPS was used to generate a treatment plan, to assess how DVH statistics vary in different scenarios. Through the system's adaptive workflows, the features of ATS and ATP were also explored due to being widely implemented in MRL environments for online plan modification in response to anatomical changes (Ocanto et al., 2024; Tetar et al., 2022). Previous studies have demonstrated that Monaco®-based planning in MRgART supports margin reduction while maintaining target coverage and OAR sparing under motion-managed conditions (Kontaxis et al., 2020).

3.6.3 | Excel and Python

Microsoft Excel v16.99.2 served as a data handling tool for cleaning, structuring, and pre-analysing measurement datasets before detailed processing. Also, it has been used to organise other data obtained from Monaco® TPS and film analysis. In this study, Excel was used to collate data exported from the phantom control software, Monaco® TPS, and dosimetric analysis platforms, ensuring dataset integrity. Python Software v3.11 was also used for the prostate traces and statistics handling. For such analyses to be done, various modules were used, including NumPy, pandas, and Matplotlib.

3.6.4 | Online Film Analysis Software

An online film analysis software, `radiochromic.com`, was utilised for the calibration and analysis of radiochromic film dosimetry. Radiochromic film analysis remains a

gold standard for high-resolution dosimetric verification in motion phantom studies and has been used in combination with MR-compatible motion phantoms to assess the spatial accuracy of gated and adaptive delivery (Uijtewaal et al., 2023). In this work, the software processed irradiated Gafchromic EBT-4 films from both static and dynamic phantom experiments to achieve an independent dosimetric analysis of dose delivery accuracy and plan quality.

3.7 | Data Analysis Technique

3.7.1 | Techniques Used

The data analysis for this study combined quantitative statistical evaluation, dosimetric comparison metrics, and motion trace processing, as similarly implemented in the literature. In this way, an assessment of the accuracy and robustness of prostate motion management and gating protocol on the Elekta Unity MRL could be performed. Moreover, the chosen methods were selected for their relevance to the study's objectives, as such an analytical framework is designed to assess both geometric motion and dose distribution, enabling a comprehensive evaluation of the main research question discussed in earlier chapters.

3.7.2 | Prostate Motion Traces

Using Python v3.11, a custom script was developed to analyse the time-resolved displacement traces in the LR, AP, and SI directions. This was done by using the "Translation Vector (x y z)" and converting the "TimeStamp (Translation Computation)" to minutes. To ensure comparability, the global time range and displacement limits were first identified so that every trajectory shared the same temporal and translational windows. Two sets of traces were then generated, one without a filter and another with the `loess` function, which acts similarly to a low-pass filter, assisting in eliminating high-frequency noise related to the system. This was implemented as follows:

```
x_loess = lowess(df['x'], t, frac=SMOOTH_FRAC, return_sorted=False)
```

Considering the x-axis as an example, a simple linear regression was additionally fitted to compute the coefficient of determination (R^2), quantifying the overall trend. The same procedure was repeated for the y- and z-axes, resulting in smoothed trajectories that were subsequently plotted as five subplots per patient (one for each fraction). A sixth subplot was generated by averaging the smoothed displacements across all three axes, using:

$$\bar{x} = \frac{1}{n}\sum_{i=1}^{n} x_i$$

Finally, to capture intra-patient variability, the standard deviation (SD) of displacement at each time point (based on the highest common time value across fractions) was also plotted, representing the dispersion of the data relative to the mean. This was done using the equation below:

$$\sigma = \sqrt{\frac{1}{n-1}\sum_{i=1}^{n}(x_i - \bar{x})^2}$$

The following data sets were collected from the graphs generated. This includes:

- A table with the subplot's legend data calculated for all axes.
- A table of the approved template coordinates for each patient.
- A table of the final 30-second average translation for each treatment fraction per patient. This was achieved using the "Translation Vector (x y z)" and "LINAC State" from the log files.

3.7.3 | DVH Statistics from Monaco® TPS

In line with the studies of Vanhanen et al. (2020) and Snyder et al. (2024), for the second part of this project, various DVH statistics were defined so to compare the difference

between treatment plans created for different offsets. For this to be achieved, SAMOC's protocol for Prostate SBRT was followed. This being based on the "The PACE Trial Protocol Version 12", the dosimetric criteria included in Table 3.2 were considered. Besides this, the DVH metric of V42Gy $\leq$ 50% was also considered for the CTV.

3.7.4 | Film Dosimetry

As discussed in the previous subchapter, for film dosimetry, besides the generation of the isodose distributions, gamma analysis was also employed, so to compare 2D dose distributions quantitatively. In this way, the gamma index (γ) was calculated for various gamma criteria, which include 3%/1 mm, 3%/2 mm, 3%/3 mm, 5%/1 mm, 5%/2 mm, and 5%/3 mm for each of the four films. $\gamma \leq 1$ in such analysis denotes a pass for the chosen tolerance criteria.

The gamma analysis was important to conduct as it helps to identify whether deviations arise from systematic dosimetric errors or geometric inaccuracies. Hence, isodose distributions and gamma analysis were considered as a suitable method to validate the study's objectives.

3.8 | Ethical Considerations

This study received ethical approval from the UREC within the UM. Before commencement, permission to conduct the research was granted by the CEO of MDH and the Chairperson of SAMOC. Furthermore, data protection clearance was obtained from the Data Protection Officer at MDH to ensure compliance with relevant regulations.

To safeguard patient confidentiality, a senior MP was appointed to ensure that the treatment log files extracted from Elekta's software were anonymised, ensuring that no identifiable patient data was directly accessed or handled as the study proceeded.

The coded data files used for collection and subsequent analysis were stored on the hospital's database, with access restricted to hospital staff members.

3.9 | Limitations of the Research Methodology

While this study provides valuable insights into the objectives of the study, a few inherent limitations were encountered. These include:

1. **TPS/Unity MRL Limitations:** The experimental process itself introduced significant time-related constraints. Performing multiple BLS across several treatment plans in succession required repeating many planning and adaptation steps, each of which was computationally intensive and time-consuming. This cumulative workload occasionally led to reduced responsiveness and longer optimisation times within the planning environment. While the final dosimetric accuracy of the plans was not compromised, the overall throughput of testing was limited, extending the experimental workflow. Considering Unity and hence a clinical setting, similar time demands could hinder the efficiency of adaptive workflows that rely on rapid plan generation and re-optimisation following BLS detection. Comparable challenges have been noted in the literature, where repeated online adaptive steps have been identified as a potential bottleneck for efficient treatment delivery (Winkel et al., 2019); (Snyder et al., 2024). These limitations, therefore, reflect the inherent complexity and resource requirements of adaptive planning processes, rather than the performance of a specific TPS.

2. **Computational load:** Another limitation of this study is related to the computational demands of processing the extensive data derived from the Elekta Unity treatment logs. Given the large number of CSV files, each containing multiple entries of positional and temporal data, a computationally expensive analysis would have significantly prolonged the research process. To mitigate this, multiple Python scripts were implemented. This approach allowed for the sepa-

rate processing of specific aspects of the data, thereby ensuring faster and more manageable data analysis. While this strategy enhanced efficiency, it necessitated careful coordination between the individual scripts to ensure data integrity and the accurate synthesis of the overall findings. This approach, while optimising computational resources, inherently introduced a degree of segmentation into the analytical workflow.

3. **Delineation Errors:** Since different oncologists may delineate the prostate and surrounding structures with subtle but clinically relevant differences, both target coverage and OAR sparing could be compromised. As a result, inter-observer variability was present in this study.

4. **Seminal vesicle deformation:** Given that the seminal vesicles can undergo independent motion and deformation relative to the prostate, and their inclusion in the target volume is common in intermediate- and high-risk prostate cancer patients, the deformation achieved by the seminal vesicles was not considered. This resulted in the study to not fully capture the geometric uncertainties and planning challenges encountered in more advanced cases of prostate cancer.

3.10 | Conclusion

This chapter presented a deep insight into the research methodology adopted. The results obtained will be detailed in the following chapter.

4

Results

4.1 | Introduction

This chapter presents the results obtained for each part of the study. Part one contains the findings from the prostate traces collected during the sample acquisition process, along with the corresponding statistical analyses. This is followed by treatment planning study and the investigation of BLS data acquired from the Modus QUASAR™ MRI 4D Phantom. Lastly, the results from the film data analysis are included.

Across all sections, the findings are illustrated through a combination of graphs and tables to provide a clear and comprehensive representation of the outcomes.

4.2 | Data

4.2.1 | Set 1: Prostate Traces

The first set of data gathered for this study was information concerning the sample in use. The sample considered from the 1st of October 2024 to the 22nd of July 2025 included a total of 360 fractions. These are equivalent to 72 eligible prostate patients, from which:

- 82% of the sample (293 fractions) were considered as normal
- 6% of the sample (23 fractions) had one or more MRI taken with an ATP after ATS workflow
- 10% of the sample (37 fractions) had at least one BLS in that session (the BLS was in response to a 3 mm CTV to PTV and 97% VOICE and do not reflect potential number of BLS interventions with a reduced 2 mm margin and 99% VOICE)
- 2% of the sample (7 fractions) had at least one CP and thus were discarded from the sample's statistics

as represented by Figure 4.1. For the same period, 10 patients (equivalent to 50 fractions) had to be discarded, with the most common reason being that they had more than one fraction with CPs done.

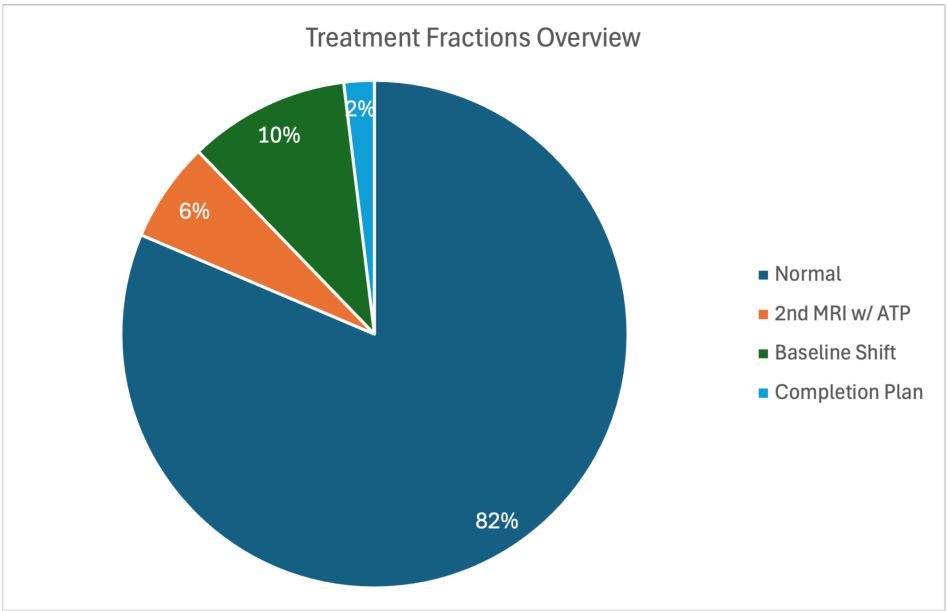

Figure 4.1: A summary of the sample considered for the study

The prostate traces across the x-, y-, and z-axes, that is, the LR, AP, SI, respectively, were investigated with respect to elapsed time. Found in the Appendix Section B, the

first set of data includes all the filtered graphs generated for the population's sample.

From the same filtered graphs, statistics which include the mean, SD and R^2 value were also extracted and stored for further analysis. The resulting data is included in the Appendix Section C.

Following this, records of the approved template coordinates were also stored for each fraction per patient so to investigate the typical prostate position at the start of the treatment. The full list can be found in the Appendix Section D.

For this set, the final 30-second average translation for each treatment fraction per patient was also generated as in the Appendix Section E. This was achieved by considering the last 30 seconds during which the LINAC state was on. This allowed the prostate's position in the last few MUs of treatment to be investigated accordingly.

4.2.2 | Set 2.1 - BLS Planning TPS DVH Statistics

Following closely Appendix Section F, statistical data from the DVH statistics obtained through Monaco® TPS were recorded. These data will eventually represent how well each plan adhered to the dosimetric criteria set in the mentioned TPS. Primarily, this includes information on the CTV, PTV at 2 mm, the rectum, bladder, and urethra. From such data, multiple graphs were generated to assess each criterion throughout all five plans, each of which had a different starting position.

4.2.3 | Set 2.2 - CTV within PTV TPS DVH Statistics

In addition to this, in the Appendix Section G, statistical data was similarly stored for the analysis of the CTV movement within the PTV. For this case, the focus was mainly on the CTV and the urethra.

4.2.4 | Set 3 - Film Dosimetry

The film analysis of Gafchromic EBT4 films primarily yielded results in the form of dose distributions derived through both non-scaling and scaling analysis. From these, 2D isodose plots were generated to visualise the measured dose delivery, and quantitative comparisons were performed using gamma analysis to assess the agreement between measured and planned distributions.

4.3 | Data Analysis and Results

The data from this study was gathered in a series of tables and plots, achieved using Python v3.11 and Microsoft Excel v16.99.2, all aiming to address the study's objectives.

4.3.1 | Part 1: Prostate Traces from Log Files

Upon working on the redacted and anonymised patient log files, the prostate's traces in the x-, y- and z- directions, LR, AP and SI, respectively, were plotted against time.

With close reference to Figure 4.2, the motion in the x-, y- and z-axes for this particular patient was contained within 2 mm; however, the traces evidently included system noise. For this to be minimised, the `loess` function in Python was used, which required a smoothing parameter. By setting a smoothing parameter equal to 0.018, as presented in Figure 4.3, the main trace was still preserved.

Provided that all fractions were smoothed in this way, statistical data from the same plots were saved, and the population's average statistics were obtained as shown in Table 4.1. From this data, it was found that in the LR (x-) direction, the mean displacement was quite minimal (0.075 mm) with a SD of 0.207 mm, and essentially no net drift was observed, yet achieving a R^2 of 0.313. In the AP (y-) direction, the prostate showed a larger average shift of 0.318 mm with a SD of 0.462 mm, accompanied by a slight pos-

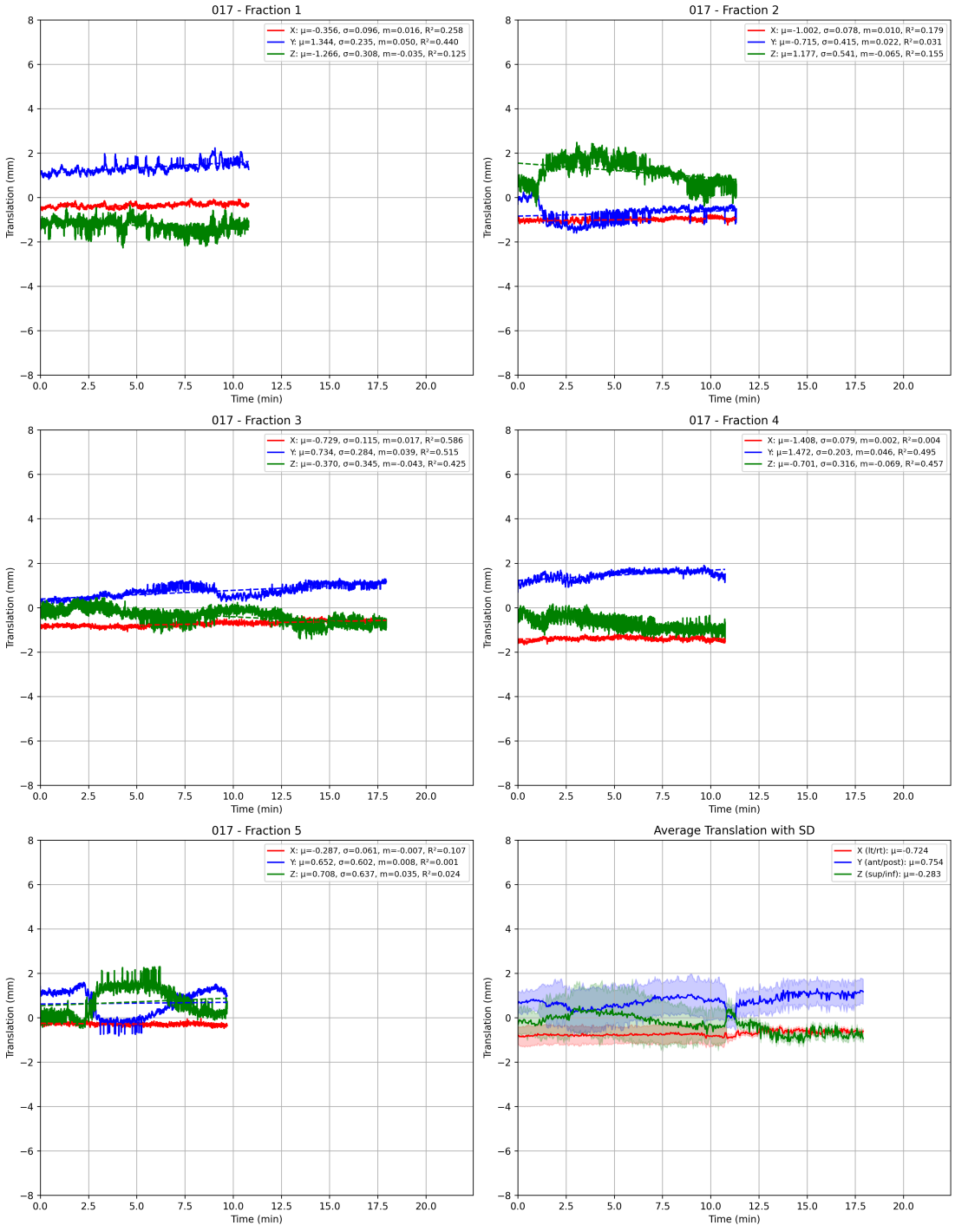

Figure 4.2: The prostate traces without filter for patient 017

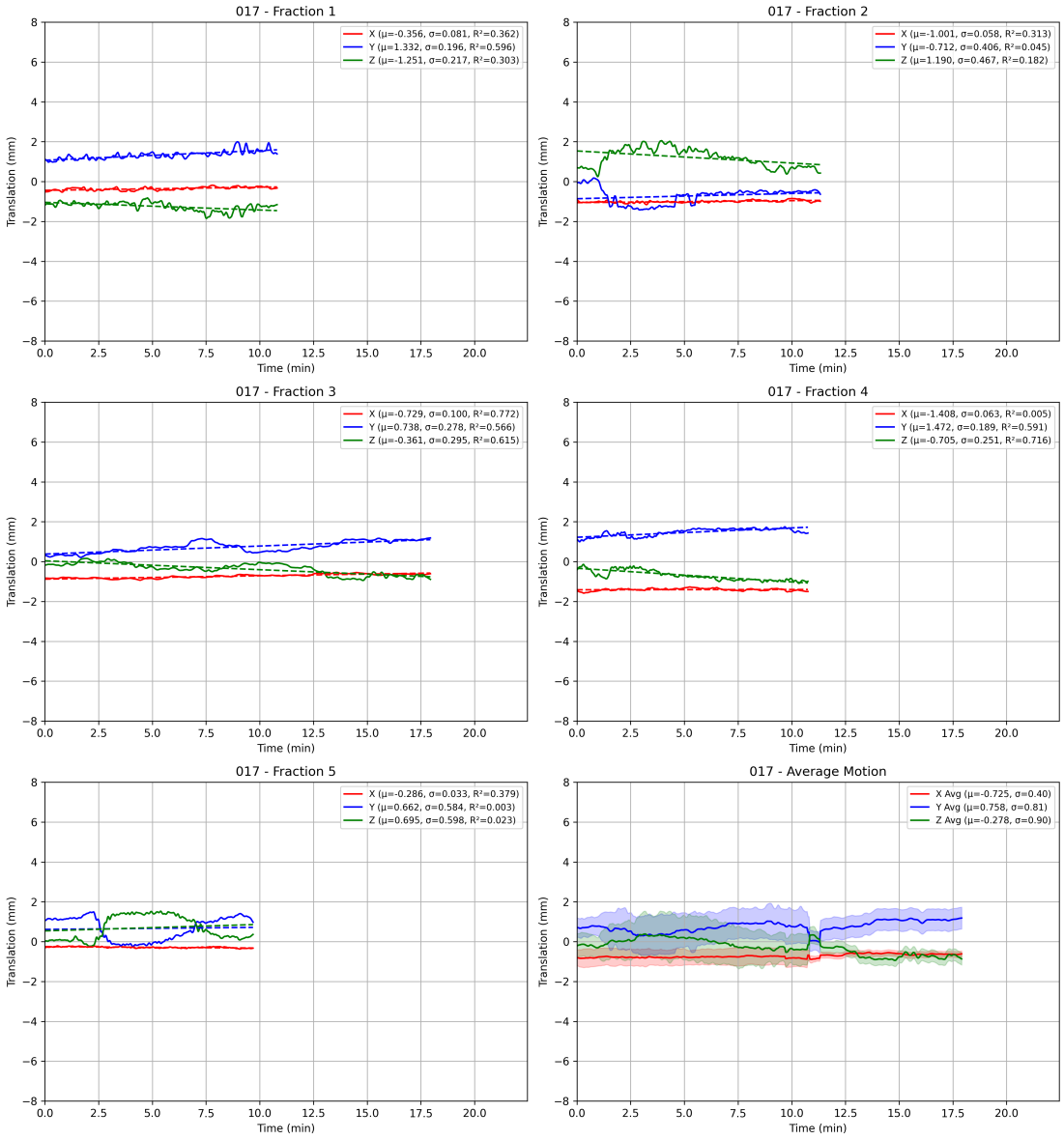

Figure 4.3: The prostate traces with a Loess function with a Loess fraction equal to 0.018, for patient 017

itive drift (0.030 mm/s, $R^2 = 0.399$). In contrast, the SI (z-) direction exhibited a mean displacement of -0.600 mm with the largest variability (0.615 mm), and a small negative drift (-0.043 mm/s, $R^2 = 0.404$).

Table 4.1: A table summary of the legend's data statistics averages across the population sample

Mean X (mm)	**Std X (mm)**	**Slope X (mm/s)**	**R^2 X**
± 0.001	± 0.001	± 0.001	± 0.001
0.075	0.207	0.000	0.313
Mean Y (mm)	**Std Y (mm)**	**Slope Y (mm/s)**	**R^2 Y**
± 0.001	± 0.001	± 0.001	± 0.001
0.318	0.462	0.030	0.399
Mean Z (mm)	**Std Z (mm)**	**Slope Z (mm/s)**	**R^2 Z**
± 0.001	± 0.001	± 0.001	± 0.001
-0.600	0.615	-0.043	0.404

From the log files, the template approval coordinates were also recorded per patient. From such data the averaged statistics found in Table 4.2 were obtained:

From this data, it can be said that for the:

- LR (x-) translation: shows some fluctuation with a wider range of values.
- AP (y-) translation: remains relatively stable, with values clustered around 1 mm.
- SI (z-) translation: presents the most variability.

Upon analysing the last 30 seconds of treatment, that is, during the last 30 seconds of the active LINAC beam, the below averaged statistics were calculated:

Table 4.2: Template coordinates summary of displacement measurements along X, Y, and Z axes, showing minimum, maximum, and one SD (1SD) values, with measurement uncertainty of ± 0.001 mm.

	X (mm)	**Y (mm)**	**Z (mm)**
	± **0.001**	± **0.001**	± **0.001**
min	3.700	3.100	3.600
max	-2.900	-4.100	-3.900
1SD	0.857	1.094	1.073

Table 4.3: Summary of X, Y, and Z displacements during the last 30 seconds of beam-on, with average, extrema, and ± 1SD values.

	X (mm)	**Y (mm)**	**Z (mm)**
	± **0.001**	± **0.001**	± **0.001**
avrg	0.047	0.309	-0.624
max	4.234	3.382	4.716
min	-2.520	-6.504	-9.811
1SD	0.904	1.353	1.646

- LR (x-) translation: fluctuation with a wider range of values compared to the approved template coordinates.
- AP (y-) translation: remains relatively stable, with values clustered around 0.3 mm.
- SI (z-) translation: continues to show variation, ranging from negative to positive values, indicating that the treatment process may cause more dynamic shifts in the z-axis.

Overall, from Tables 4.2 and 4.3, data reflect consistency in the AP (y-) translation but reflect greater variability in both LR (x-) and SI (z-) directions, particularly in the

final 30 seconds of treatment.

Lastly, for this part of the analysis, a filtered plot for the population sample, shown in Figure 4.4, was generated to visually represent the prostate motion trends in each axis. This figure complements the data from Table 4.1.

From Figure 4.4, it is shown that across the cohort, the population–average translation over time remained close to zero, with dispersion increasing from x to the z direction. Linear regressions of translation versus time yielded slopes of $+0.001$, $+0.026$, and $-0.053\,\mathrm{mm/min}$ for x-, y-, and z- axes, respectively, whilst the goodness-of-fit was negligible for the x-axis ($R^2 \approx 0.09$) but substantial for y- and z- directions, ($R^2 \approx 0.85$ and 0.89), respectively.

4.3.2 | Part 2.1: TPS DVH Statistics

The associated tables related to all DVH statistics can be found in the Appendix Section F. Results on eight particular parameters are represented in graphs as follows. The graphs are supported by a traffic light system where the green zones indicate acceptable and robust performance (meet ideal dose constraints), orange highlights borderline values that warrant caution (acceptable dose constraints), and red marks failure, which represent a breach of the clinical tolerance considered.

4.3.2.1 | Criterion 1 - CTV: V40Gy against translation in z-axis (V40Gy >95% (-5%))

Starting with Figure 4.5, it was found that for most BLSs, more than 90% of the 40 Gy volume was covered. However, for the 4 cm inferior offset, some translations in the negative direction, that is, more away from the prostate's isocentre, did not achieve 90% coverage with 40 Gy. There were two points in the 0 cm and 2 cm superior offsets,

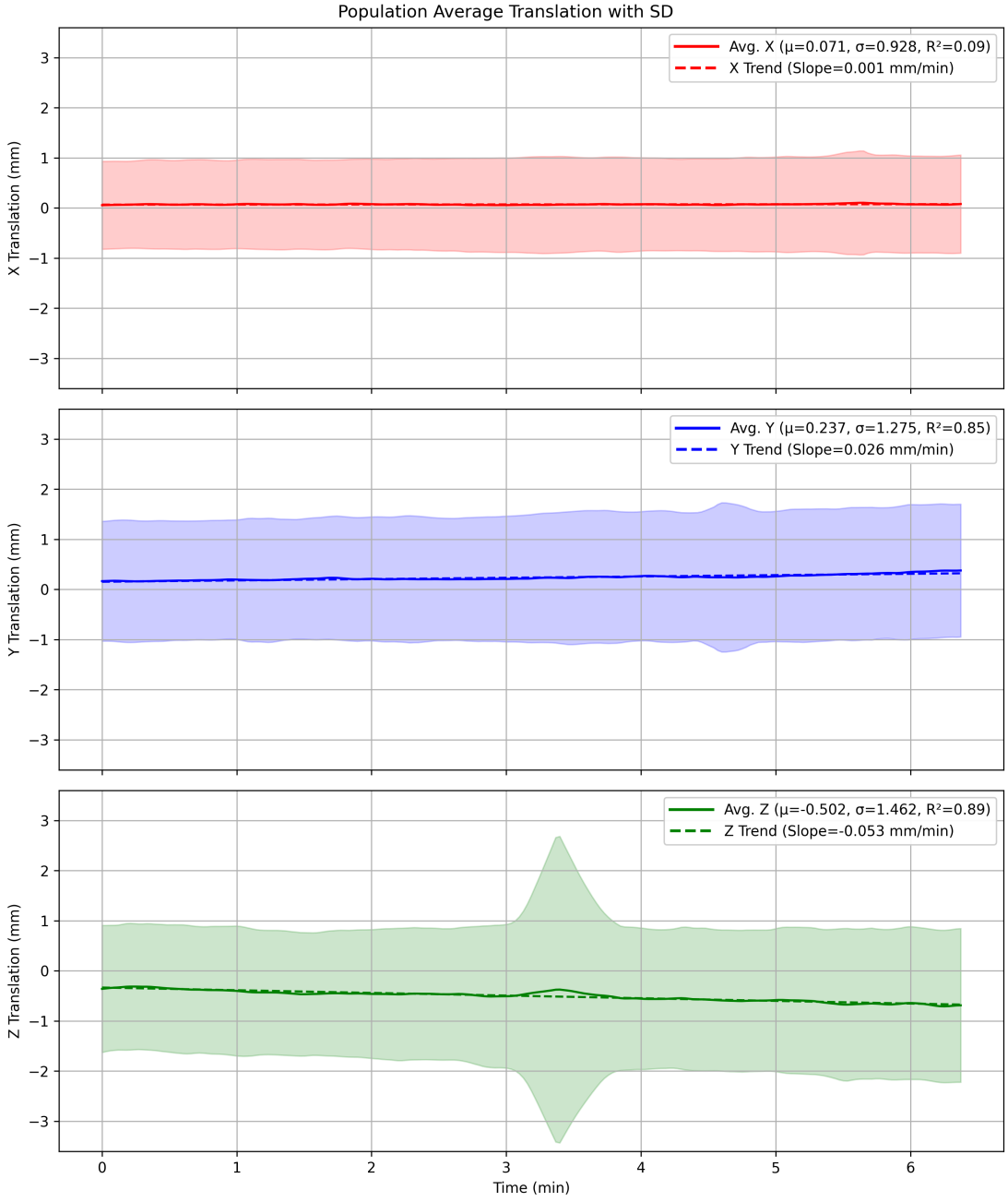

Figure 4.4: Prostate motion traces in *x*-, *y*- and *z*- direction for the total sample considered

which also did not achieve the 90% coverage of the 40 Gy volume. [1]

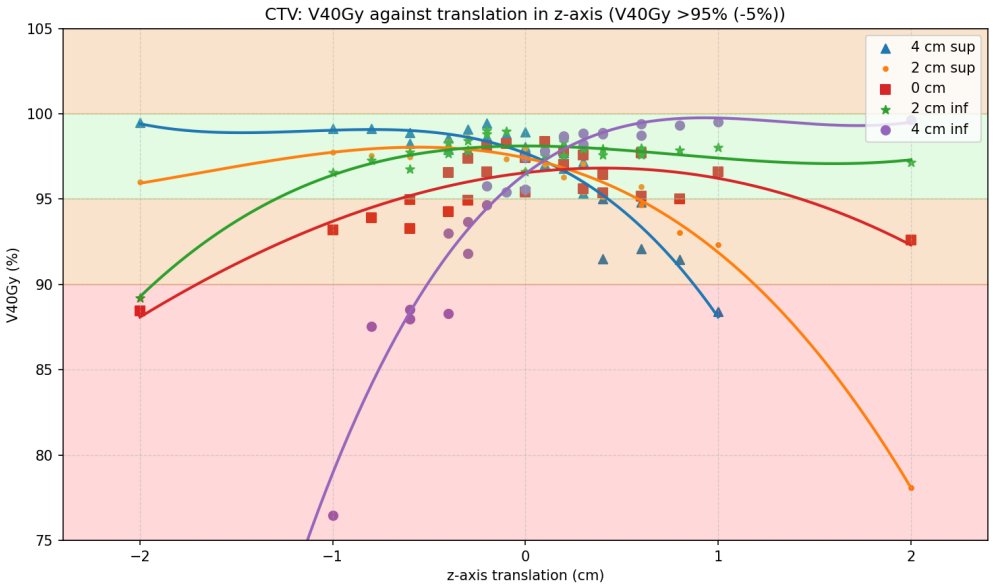

Figure 4.5: A graph of the CTV's V40Gy against translation in *z*-axis with a dosimteric criteria of V40Gy > 95% (-5%)

4.3.2.2 | Criterion 2 - CTV: D_{mean} against translation in *z*-axis

With close reference to the Appendix Section F and Tables F.1, F.6, F.7, F.11 and F.14, it is shown graphically in Figure 4.6 that the maximum mean dose lies within 4 cm superior, this being equal to 44.189 Gy (110.5% of 40 Gy) whilst the lowest mean maximum dose lies within 2 cm inferior this being at 37.258 Gy (93.1% of 40 Gy).

4.3.2.3 | Criterion 3 - CTV: V42 against translation in *z*-axis (V42Gy <=50%)

With close relation to Figure 4.7, it is evidently seen that approximately half of the data achieved less than 50% of the 42 Gy volume, as suggested by the green-area region. On the other hand, the other half of the data exceeded the said coverage, as shown at the points that lie in the shaded-red region.

[1] From the same figure, Figure 4.5, one coordinate which failed the criterion (achieved 36.57% for co-ordinates [0.20, -2.00, -1.00] as also found in the Appendix Section F), was not included so to ensure better graph clarity.

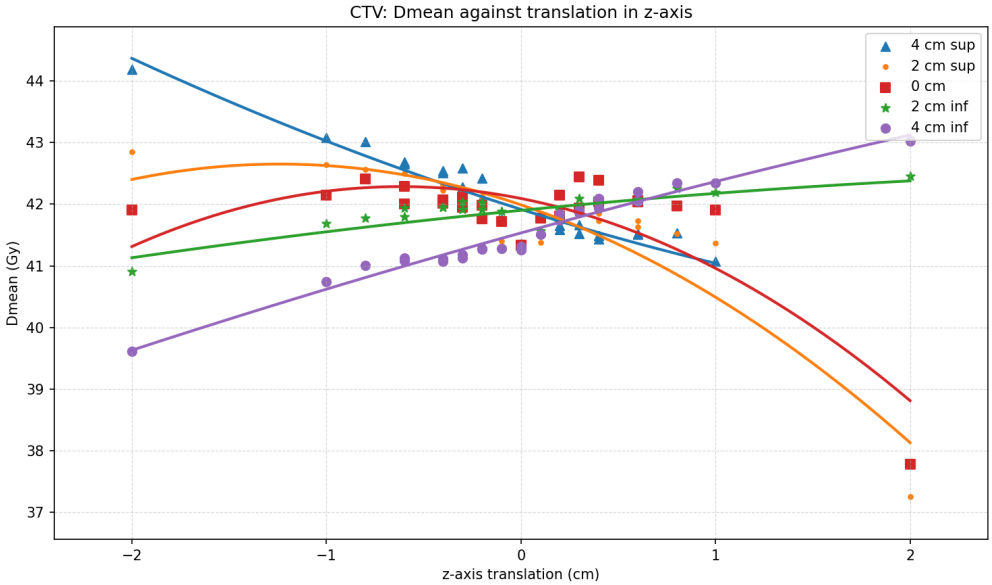

Figure 4.6: A graph of the CTV's D_{mean} against translation in z-axis

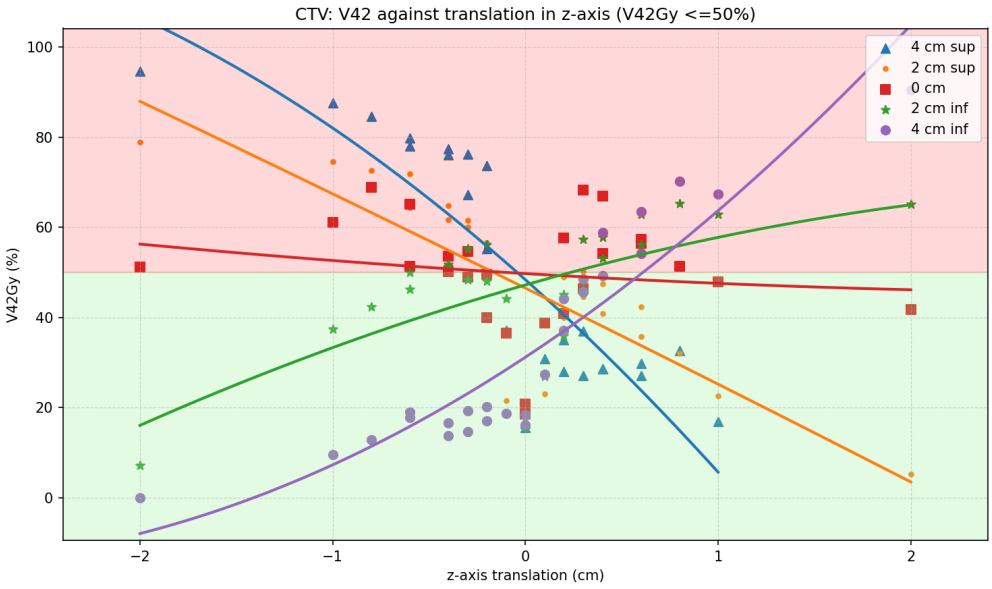

Figure 4.7: A graph of the CTV's V42 against translation in z-axis with a dosimetric criteria of V42Gy <=50%

4.3.2.4 | Criterion 4 - PTV: D95% against translation in *z*-axis (D95% > 36.25 Gy)

With regards to the PTV's coverage, shown in Figure 4.8, all data achieved more than 95% coverage of dose greater than 36.25 Gy.

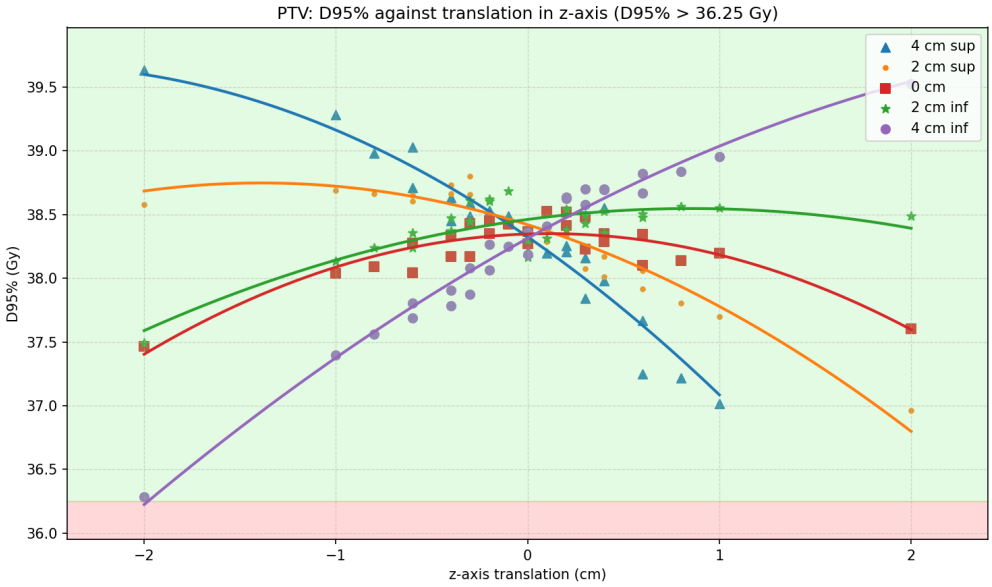

Figure 4.8: A graph of the PTV's D95% against translation in *z*-axis with a dosimetric criteria of D95% > 36.25 Gy

4.3.2.5 | Criterion 5 - PTV: V34.4Gy against translation in *z*-axis (V34.4Gy >98%)

As shown in Figure 4.9, a similar scenario was achieved to the PTV coverage with more than 98% of the volume being covered by 34.4 Gy dose.

4.3.2.6 | Criterion 6 - PTV: V36.25Gy against translation in *z*-axis (V36.25Gy >95% (-5%))

Regarding Figure 4.10, all BLS shift plans lie within the shaded-green portion of the graph, implying that more than 95% of the BLSs achieved 95% volume coverage of at least 36.25 Gy.

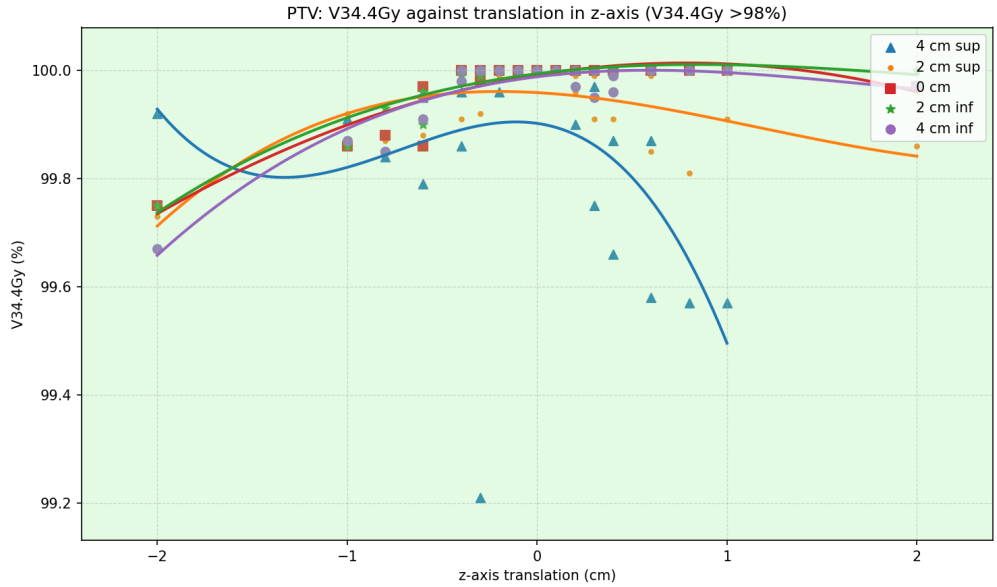

Figure 4.9: A graph of the PTV's V34.4Gy against translation in *z*-axis with a dosimetric criteria of V34.4Gy >98%

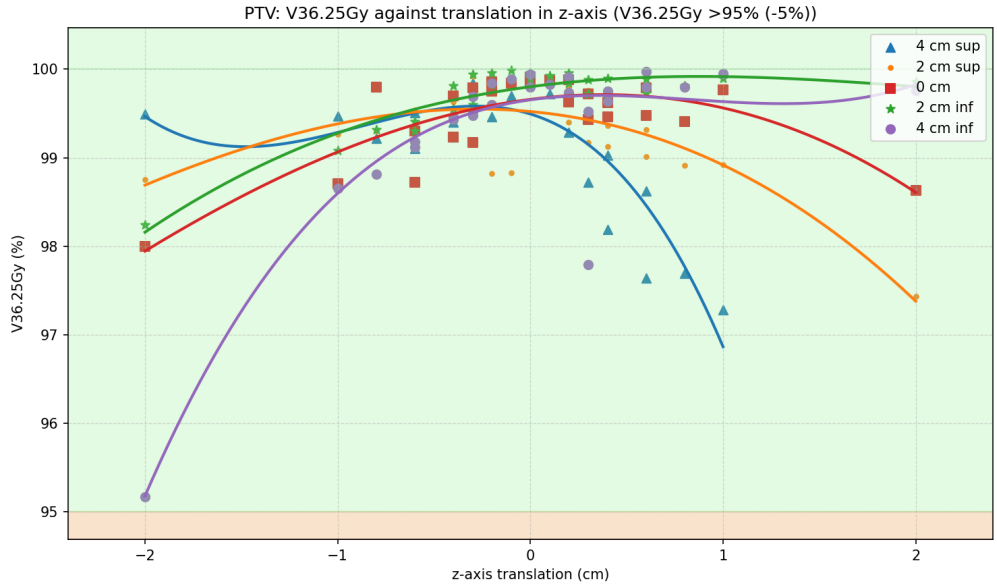

Figure 4.10: A graph of the PTV's V36.25Gy against translation in *z*-axis with a dosimetric criteria of V36.25Gy >95% (-5%)

4.3.2.7 | Criterion 7 - 1_Urethra: V42Gy against translation in *z*-axis (V42Gy < 50%)

Moving on to the statistics obtained for the unshifted urethra, that is, 1_Urethra, from Figure 4.11 it was found that most of the data followed the defined dosimetric criteria of V42Gy < 50%, except for some BLS points ranging from 0 and -1 for the 2 cm and 4 cm superior offset from the prostate's isocentre. [2]

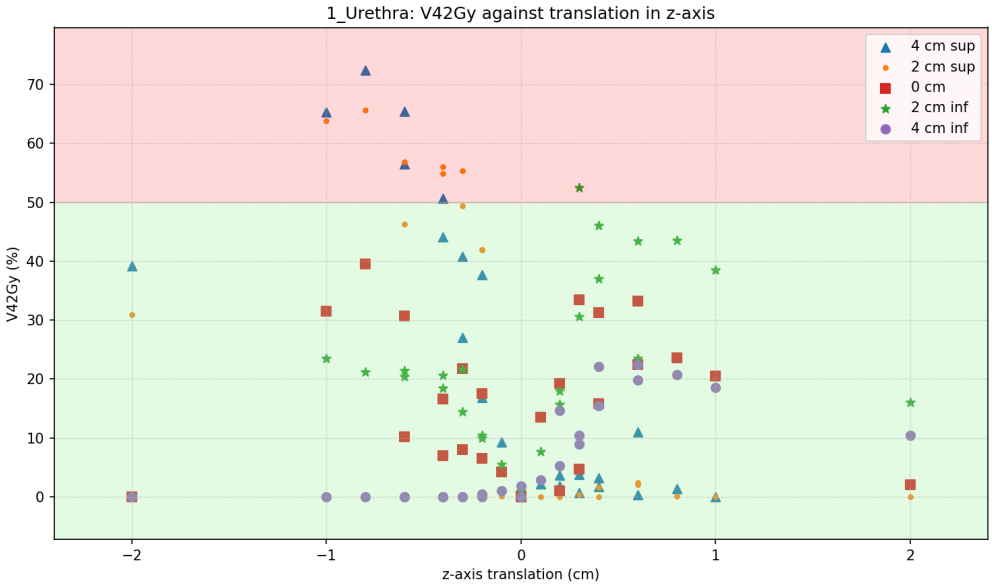

Figure 4.11: A graph of the 1_Urethra's V42Gy against translation in *z*-axis with a dosimetric criteria of V42Gy < 50%

4.3.2.8 | Criterion 8 - Urethra_XX: V42Gy against translation in *z*-axis (V42Gy < 50%)

Focusing on the shifted urethra, that is, Urethra_XX, it is evident from Figure 4.12 that most data satisfied the same criterion, however, some data points for the 4 cm superior, 2 cm inferior and 4 cm inferior offsets from the prostate's isocentre did not remain

[2]For Figure 4.11, it was not possible to generate a polyfit trendline for this data due to its stochastic nature

within less than 50% of the volume coverage, hence exceeding the specified criterion. [3]

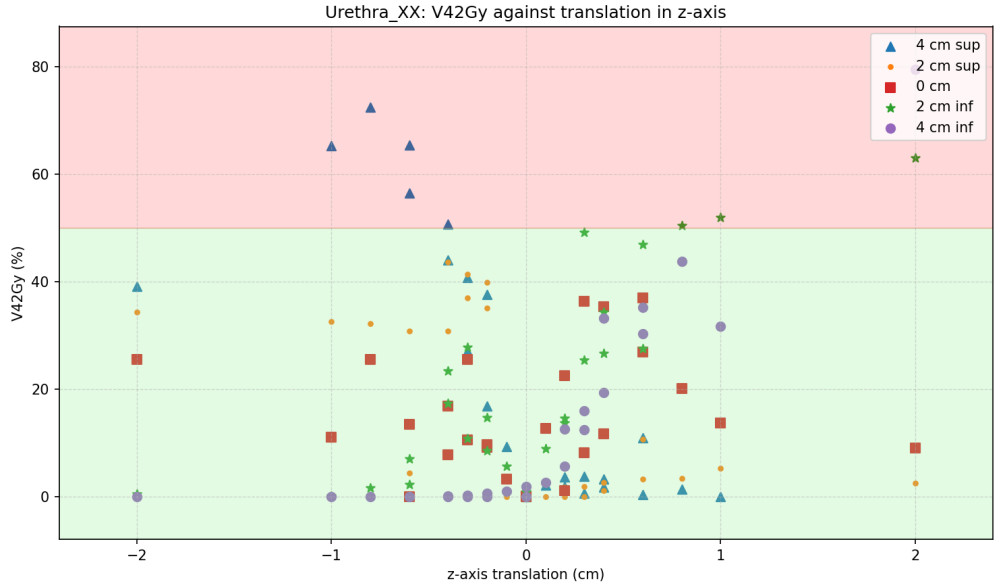

Figure 4.12: A graph of the Urethra_XX's V42Gy against translation in z-axis with a dosimetric criteria of V42Gy < 50%

4.3.2.9 | A graph of 1_Urethra V42Gy against Urethra_XX V42Gy (V42Gy < 50%), for all offsets

In Figure 4.13, the unshifted urethra (1_Urethra) was plotted against the shifted urethra (Urethra_XX) so as to show how the DVH V42Gy statistic for the unshifted urethra can be used as an indication of the DVH V42Gy statistic for the unshifted urethra that is not reported during the online BLS planning. Following the same figure, many of the data points lie close to or above the line of equality ($y = x$), suggesting that in a large number of cases the unshifted urethra V42Gy overestimates the true shifted urethra value. However, at the 4 cm superior and inferior offsets, the spread of points increases and some lie below the line of equality, indicating underestimation in certain cases.

[3]For Figure 4.12, it was not possible to generate a polyfit trendline for this data due to its stochastic nature

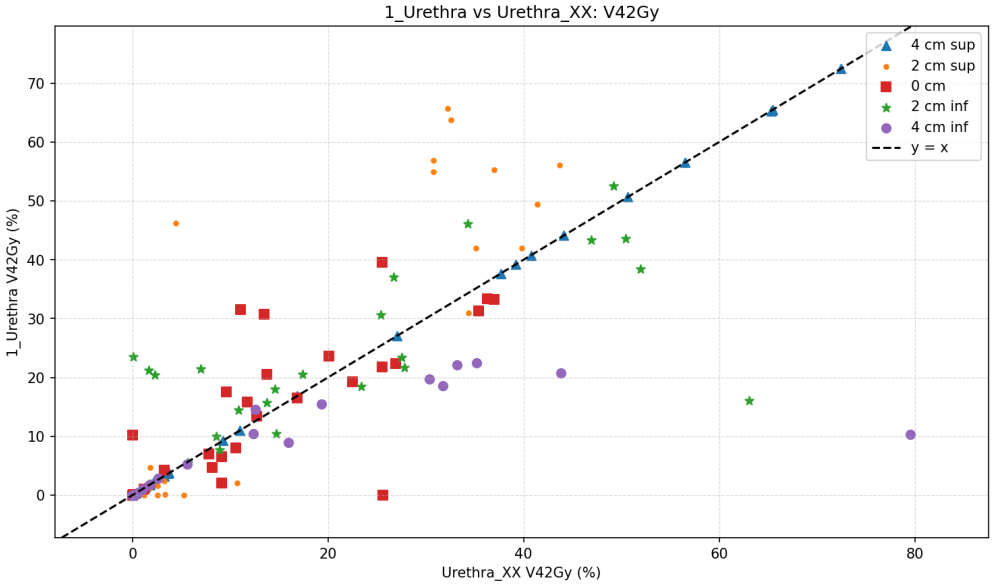

Figure 4.13: A graph of the 1_Urethra V42Gy against Urethra_XX's V42Gy

4.3.2.10 | Graph of Urethra_XX V42Gy against the CTV's V42Gy (V42Gy <= 50%), for all offsets

Shown in the scatter plot in Figure 4.14, a positive correlation is present between the two criteria, as an increase in "CTV V42Gy" generally corresponds to an increase in "Urethra V42Gy." Most of the data points, regardless of their category, are concentrated in the lower-left portion of the graph. However, the 4 cm and 2 cm superior data points tend to have higher values, with many occupying the upper-right section of the plot. The remaining categories, 0 cm, 2 cm and 4 cm inferior, are more tightly clustered in the middle and lower-left areas, indicating lower V42Gy values for both variables.

4.3.3 | Part 2.2: 97% VOICE and Associated Translation

In order to proceed with the following section, the translations that achieved 97% VOICE were first identified, as in Table 4.4. Furthermore, the translations corresponding to a stricter tolerance of "100/99"% VOICE were also noted as in the same Table.

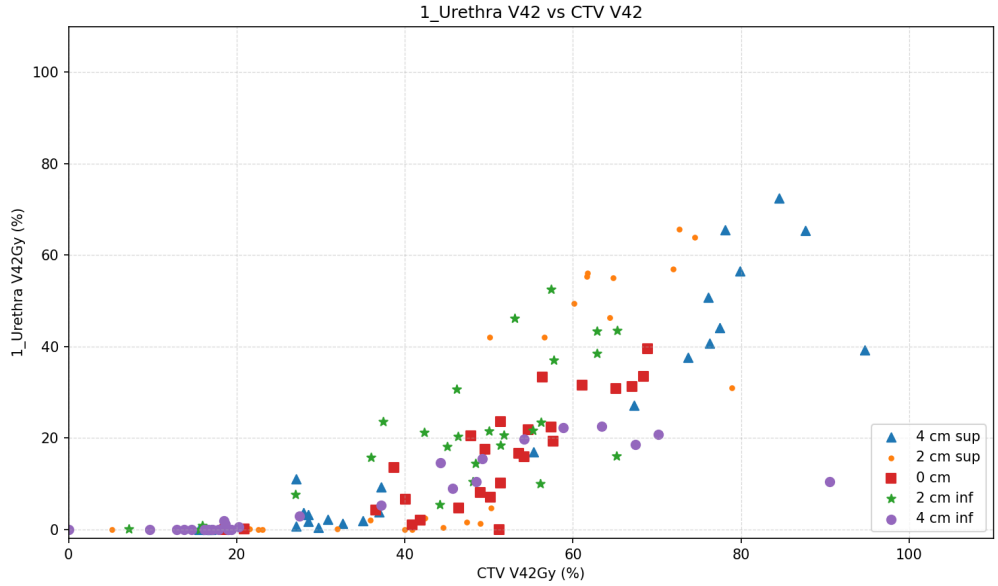

Figure 4.14: A graph of 1_Urethra V42Gy against the CTV's V42Gy (V42Gy <= 50%), for all offsets

Entries like "98/97"% and "99-97"% indicate that the CMM achieved a VOICE of 98% and 97%, and values between 99% and 97%, respectively, when set at particular positions for the SI and AP directions.

4.3.4 | Part 2.3: CTV movement within PTV

Another set of data was collected to show how dose volume metrics for the CTV and urethra structures change when small increments/shifts are considered, so as to lie within the PTV.

4.3.4.1 | Criterion 1 - CTV: V40Gy against translation in *z*-axis (V40Gy >95% (-5%))

By considering the dosimetric criterion of V40Gy > 95% (-5%) as shown in Figure 4.15, the traffic light system in the background shows that only two points lie within the acceptable range of having a volume of the 40 Gy isodose more than 95% covered.

Table 4.4: VOICE values at different positions along the axes.

Modus (Hyp) (cm)	**Sup–Inf (cm)**	**Ant–Post (cm)**	**VOICE (%)**	**Direction**
0.00	0.00	0.00	100	Center
0.50	-1.50	0.02	100	Inferior
1.00	-1.00	0.04	100	
1.50	-0.80	0.07	100	
2.00	-0.60	0.09	100	
2.30	-0.50	0.10	100	
2.50	-0.40	0.11	100/99	
2.70	-0.20	0.12	99	
3.00	0.00	0.13	99/98	
3.50	0.20	0.15	98/97	
4.00	0.40	0.17	97–95	
-0.50	0.50	-0.02	100	Superior
-1.00	0.60	-0.04	100	
-1.30	0.80	-0.06	100/99	
-1.50	1.00	-0.07	100/99	
-1.70	1.50	-0.07	100–98	
-2.00	-0.18	-0.09	99–97	
-2.50	-0.23	-0.11	97/96	
-3.00	-0.27	-0.13	95/94	

Similarly, two points lie within the orange region, and the rest did not achieve the mentioned criterion.

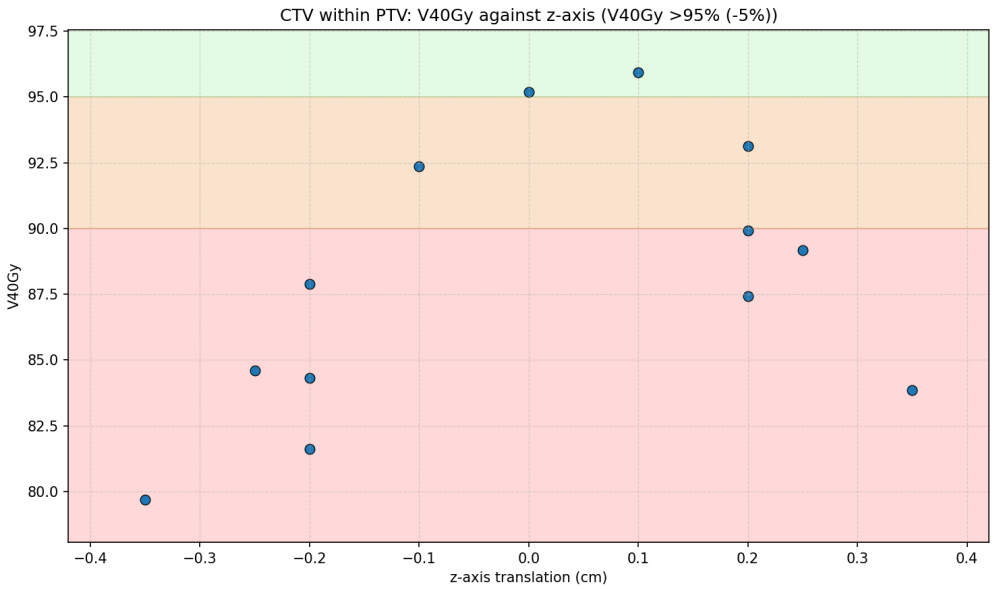

Figure 4.15: CTV within PTV: A graph of the CTV's V40Gy against translation in *z*-axis with a dosimetric criteria of V42Gy > 95% (-5/%)

4.3.4.2 | Criterion 2 - Urethra: V42Gy against translation in *z*-axis (V42Gy < 50%)

Similarly, Figure 4.16 also had all points achieving the pre-defined criteria, where only three points were greater than zero, the maximum being equivalent to 0.29%.

4.3.5 | Part 3: Film Dosimetry

Based on the scaling results included in the Appendix Section G, the static 0 mm and 8.5 mm inf film were scaled on the morning 7.25 Gy, 8 Gy and 9 Gy films whilst the VOICE 97% film and the motion 2 and 3 BLS films were scaled on the evening 7.25 Gy, 8 Gy and 9 Gy films as per indication of the uncertainity, also included in the Appendix

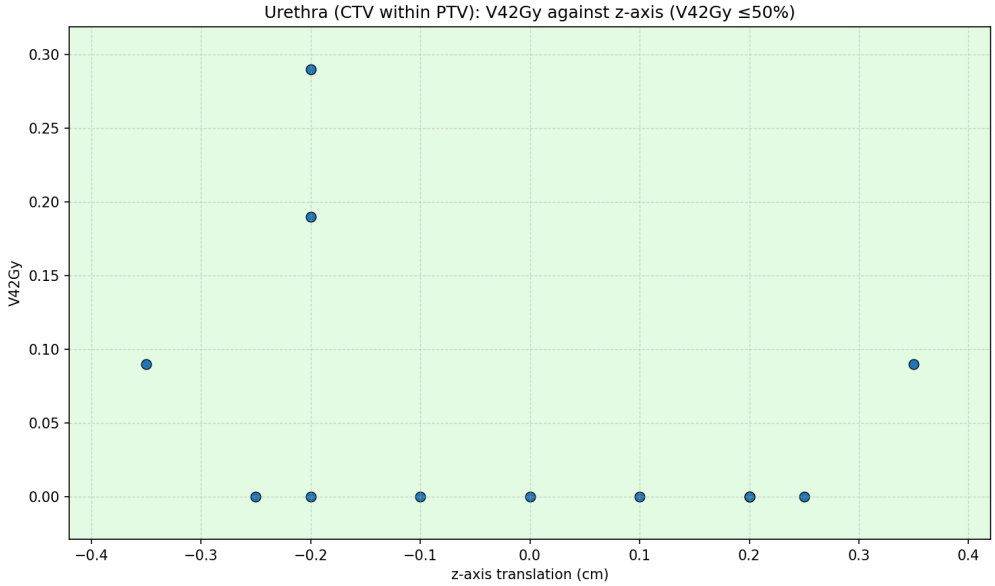

Figure 4.16: CTV within PTV: A graph of the Urethra's V42Gy against translation in z-axis with a dosimetric criteria of V42Gy $\leq$ 50%

Section.

Following the scaling procedure, an analysis was done to establish a visual analysis on the isodose curves of the films with respect to the reference film. Shown from Figures 4.17 to 4.24, the 8 Gy and 7.25 Gy isodose curves were visually inspected. From such figures, the dotted line represents the reference image (that is, static 0 mm film) and the solid line represents one of the four remaining films.

In the case of the 8.5 mm inferior shift film (Figures 4.17 and 4.18), the solid line deviates noticeably from the dotted reference contour. The misalignment is evident across multiple regions, with the solid curve sometimes lying outside and other times inside the dotted line, indicating that the shifted distribution fails to accurately reproduce the reference isodose pattern.

Considering the isodose curve for VOICE 97% at 8 Gy overlaid with the reference

film 7.25 Gy isodose curve, as shown in Figure 4.19, the actual position of the displaced CTV position on the original planned PTV coverage is shown, indicating that the CTV is in this case underdosed.

With regards to the film for which 2 BLSs were done, Figures 4.20 and 4.21 show that there is also a very good agreement between the isodose lines, only having small visible deviations, particularly along the edges. This reflects a moderate but consistent improvement in dose reproduction.

Finally, for the films where 3 BLSs were done, the 3 BLS isodose curves are systematically larger than the reference image isodose curves, implying that a greater portion of the film was exposed with the same dose. This can be seen through Figures 4.22 and 4.23.

In Figure 4.24, it is shown that even though the latter figure is at a different orientation, the 8 Gy isodose distributions are still very close to one another.

Following the visual analysis, the gamma index was also expressed quantitatively so to assess the pass rates for different profiles at various criteria. Following closely Table 4.5, it shows that under strict conditions (3%/1 mm), pass rates are lowest, with VOICE performing particularly poorly followed by the 3 BLS motion film. As tolerances are relaxed to 5%/3 mm, all gamma indices improve, with the “Static 8.5mm inf”, “2BLS Motion”, “3BLS Motion” films reaching 99.7%, 100% and 97.6%, respectively, indicating excellent concordance with the reference film.

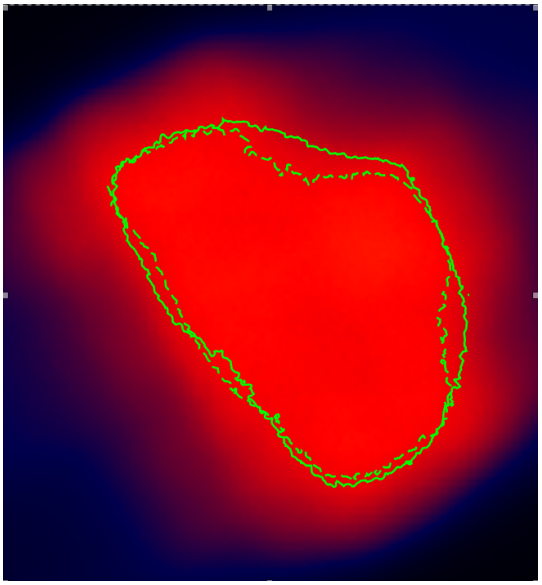

Figure 4.17: 8.5 mm inferior against reference film - 8 Gy isodose curves

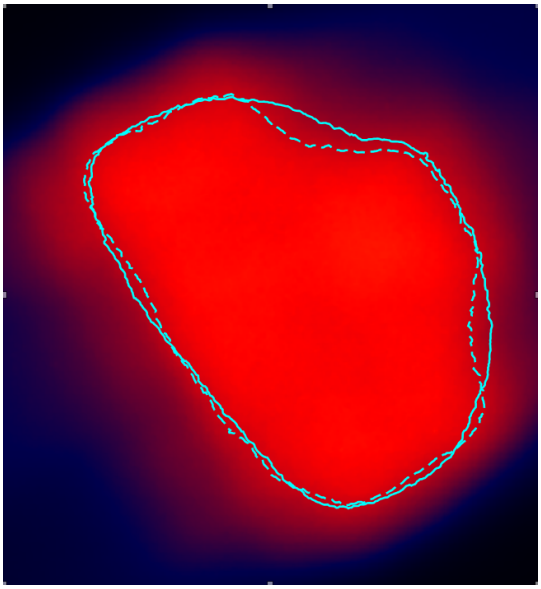

Figure 4.18: 8.5 mm inferior against reference film - 7.25 Gy isodose curves

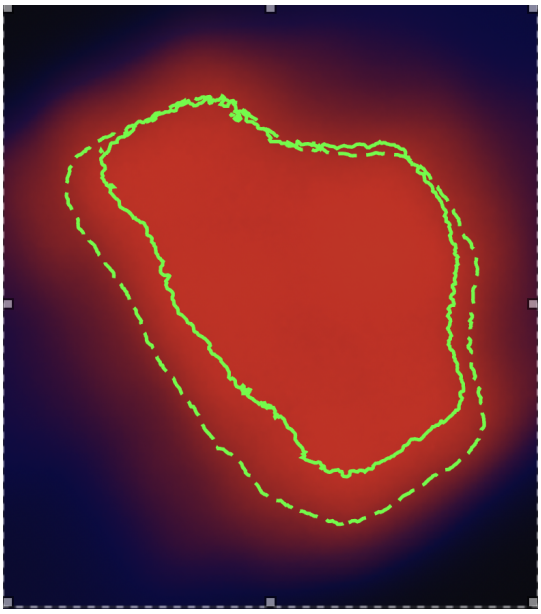

Figure 4.19: VOICE 97% against reference film with 8 Gy and 7.25 Gy isodose curves, respectively

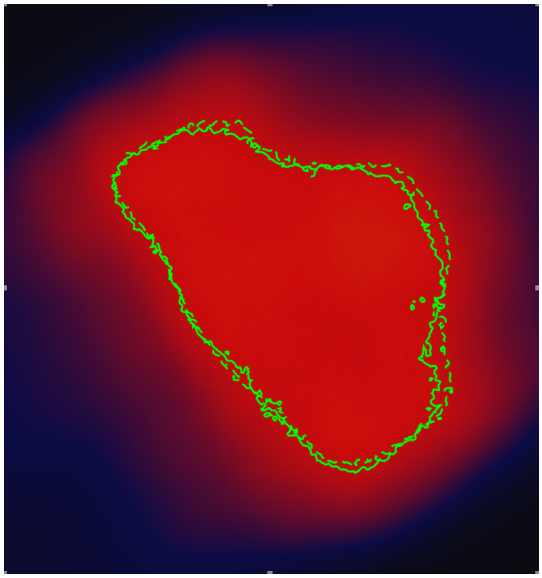

Figure 4.20: 2BLS against reference film - 8 Gy isodose curves

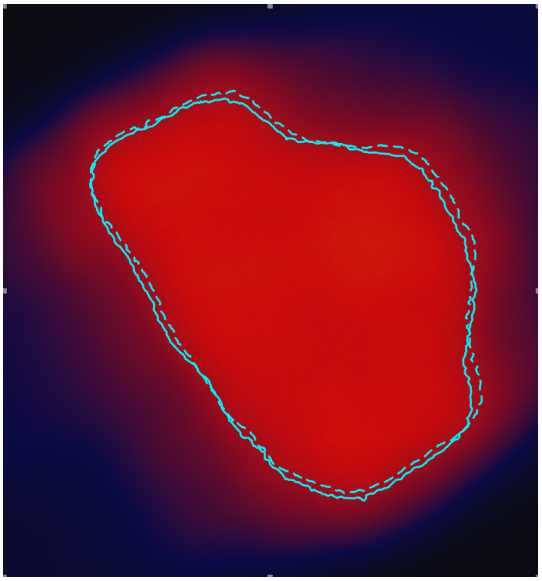

Figure 4.21: 2BLS against reference film - 7.25 Gy isodose curves

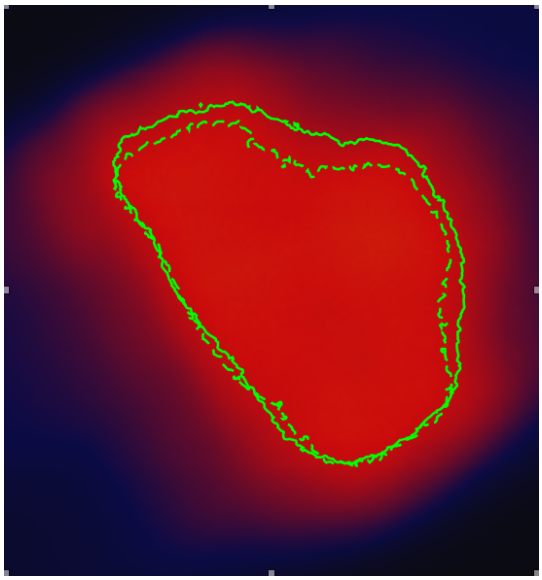

Figure 4.22: 3BLS against reference film - 8 Gy isodose curves

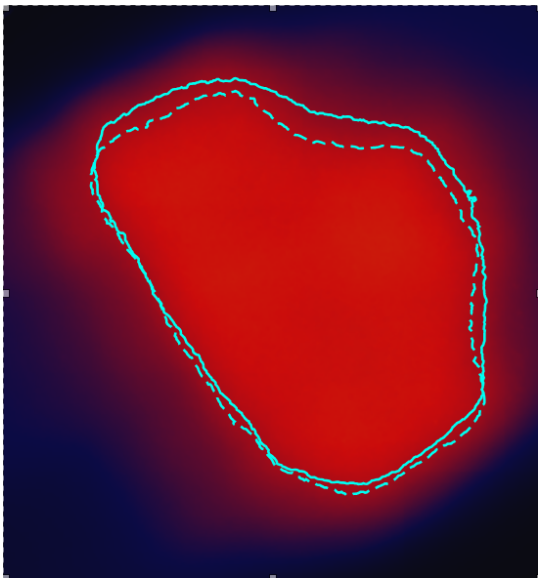

Figure 4.23: 3BLS against reference film - 7.25 Gy isodose curves

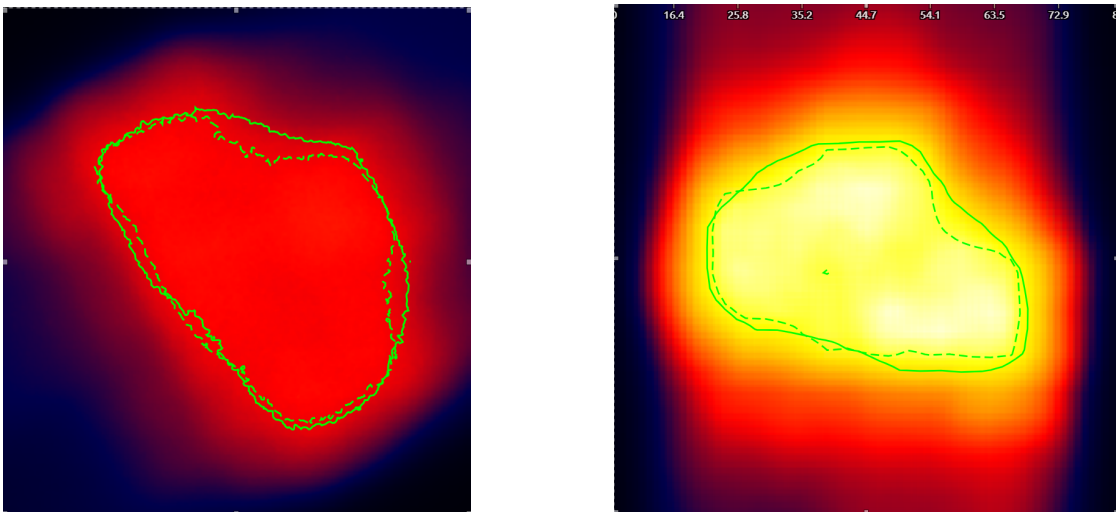

Figure 4.24: 8.5 mm inferior against reference film (left) compared to the TPS 8 Gy isodose curves (right)

Table 4.5: Gamma global pass rates (%) for different profiles at various criteria (10% threshold).

Criteria (10%)	Static 8.5mm inf	97% VOICE	2BLS Motion	3BLS Motion
3%/1mm	82.0%	38.4%	96.0%	52.6%
3%/2mm	92.4%	57.0%	99.9%	81.7%
3%/3mm	96.2%	84.4%	100.0%	92.3%
5%/1mm	93.6%	54.6%	98.6%	73.1%
5%/2mm	98.4%	67.8%	100.0%	91.4%
5%/3mm	99.7%	90.8%	100.0%	97.6%

4.4 | Conclusion

This chapter has outlined the key results from the prostate trace analysis, BLS data from the Modus QUASAR™ MRI 4D Phantom, and film data, supported by relevant statistical and visual representations. These findings address the study's objectives and form the basis for the discussion in the following chapter, where their significance and broader implications will be addressed.

5

Discussion

5.1 | Introduction

This chapter presents a comprehensive discussion and interpretation of the findings obtained across all three components of this study, which include: (1) prostate motion traces analysis, (2) DVH statistics interpretation, and (3) film dosimetry analysis.

This chapter aims to integrate the results from these parts, critically evaluate their implications, and relate them to the objectives outlined in the earlier chapters. The discussion addresses the relevance of the observed trends, explores potential sources of uncertainty, and compares the outcomes with the existing literature. This chapter seeks to provide a deeper understanding of the study's contributions, limitations, and possible directions for future work.

5.2 | Discussion

5.2.1 | Prostate Traces

The first stage of the results involved analysing prostate motion traces across the patient cohort, as presented in Appendix Section B. These plots were generated using the `Loess` function in Python, which acts as a low-pass filter to reduce system noise. At this

stage of the study, care was taken to avoid excessive smoothing so that the true shape of the traces was preserved. This was controlled by selecting an appropriate smoothing fraction. As illustrated in Figure 5.1, the third subplot demonstrates oversmoothing, leading to a noticeable distortion in the trace of interest. In contrast, the middle subplot shows the optimal smoothing fraction, where noise is effectively reduced while preserving the underlying motion pattern shown in the uppermost subplot in Figure 5.1. The smoothing fraction parameter was kept equal to 0.018 and applied it to the rest of the prostate traces under investigation.

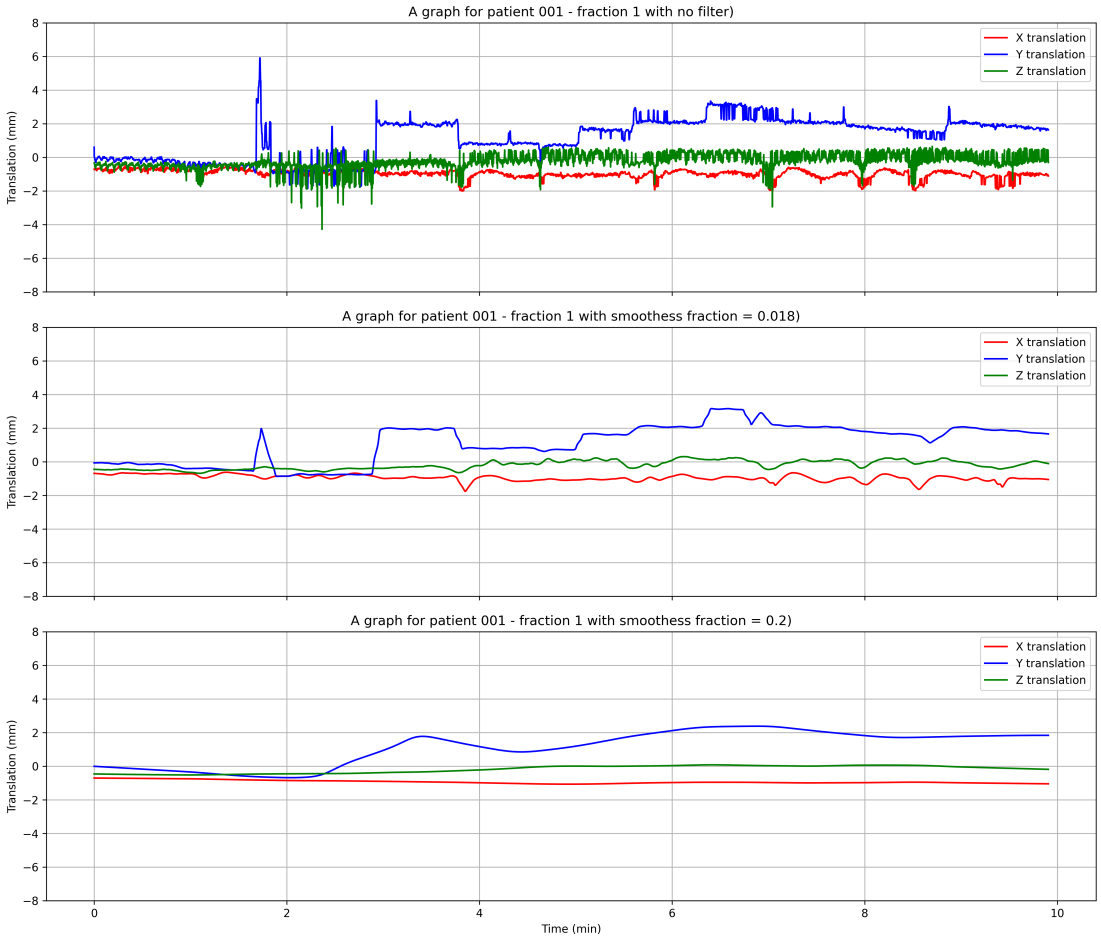

Figure 5.1: The effect of different smoothing fraction parameters on prostate traces

On initial inspection, the data statistics averages across the population sample indicate relatively modest mean displacements, with the prostate generally remaining within a few millimetres of its initial baseline position. However, the SD across all axes was large, reflecting significant inter-patient variability. This highlights an important limitation of population-level reporting: group averages may conceal clinically relevant outliers. Several fractions demonstrated movements beyond the typical gating thresholds. This included fraction 2 for patient 024, fraction 4 for patient 025, and fraction 1 for patient 056. This underscores that while the average patient benefits from stable targeting, individual cases remain at a substantial risk of tumour underdosage. These examples are also found in the Appendix Section B.

The motion gradients averaged across the population sample is of equal importance because they show how the location of the prostate changes over time. The average slopes are very close to zero, as can be seen in Figure 4.4; however, they do show a slow change in direction during treatment administration, especially along the AP and SI directions, that is, the y-axis and z-axis, respectively. Even minor but persistent drifts are important from a clinical perspective when considering tighter margins. For instance, a 3 mm isotropic margin might allow gradual drifts without triggering gating, but with the implementation of a 2 mm margin, such events are more likely to cause gating events. This is especially important in VOICE 97, where the gating techniques are linked to certain thresholds. If drift behaviour is not considered, patients may remain beyond the allowed envelope for extended periods, which could hinder treatment effectiveness and possibly result in more frequent beam interruptions.

Therefore, even though the displacement averages show that a 2 mm margin could work for some patients undergoing treatment, this will probably lead to more gating. Such an increase in BLS performed during an online treatment can be viewed as beneficial, since more frequent corrections allow for greater accuracy in dose delivery and improved protection of OAR. Therefore, this underscores the necessity for individ-

ualised motion monitoring and adaptive gating mechanisms, rather than depending exclusively on population-level averages for PTV definition.

Shifting the focus to the R^2 value, although the regression analysis on the same plots demonstrated what appeared to be linear trends, the statistical outputs showed consistently low R^2 values as shown through Table 4.1. This contradiction has also been reported in other studies on intrafraction prostate motion. One explanation is that when the slope of the regression line is shallow, even when the points fall close to the line, the variance explained remains small because changes in the independent variable translate into very small changes in the dependent variable. As a result, the regression captures the direction of the drift, but not enough variance to yield a high R^2. The second explanation lies in the stochastic nature of prostate motion. As noted by Menten et al. (2020) and Kontaxis et al. (2020), prostate displacement is often subject to small random fluctuations arising from rectal and bladder filling, which superimpose noise on the underlying trend. Even when the drift is visually apparent, this noise reduces the fit quality in terms of statistics. Similar observations have been reported by Oehler et al. (2022), who emphasised that intrafraction motion should be treated as a stochastic process rather than a deterministic one, noting that regression models often underestimate the true clinical relevance of observed trends because the variance is dispersed across multiple unpredictable factors. Willigenburg et al. (2022) also discussed the limited predictive power of regression fits in the presence of baseline shifts, arguing that clinically relevant displacement can be identified even when R^2 values remain low.

Taken together, these considerations suggest that the low R^2 values obtained in this study do not imply that the regression analyses were uninformative or that no clinically meaningful trends exist. Instead, they highlighted that prostate motion is a complex, partially stochastic process in which linear regression can capture the general drift but not fully explain the variance introduced by noise and physiological unpredictability.

Another feature which was noted in some cases, such as fraction 2 of patient 043 (Figure B.43), was that immediate action was necessary very close to the start of the treatment, as shown in the plot. Mainly because if clinically a margin of 3 mm was defined, a drift was immediately present in the z- and y- axes. In fact, for this case, a BLS with x = 2.7 mm, y, and z = 4.0 mm was required for the treatment to continue.

Regarding Table 4.2, the data for the approved template coordinates provides information on the average starting position of the prostate analysis immediately before treatment delivery was initiated. Because these coordinates represent the clinically approved setup position, they acted as a baseline reference for subsequent motion assessments. The reduced variability observed at this stage suggests that the planning and image-guided setup process is effective in bringing the prostate into a stable position before beam delivery. However, although this confirms that the prostate can be aligned within clinically acceptable margins at the start of treatment, it does not capture the full extent of motion that may occur later during beam-on time.

When considering the third table, Table 4.3, motion deviations appear larger relative to the earlier treatment phases. This observation is consistent with progressive bladder filling and rectal distension, phenomena also highlighted by Menten et al. (2020) and Kontaxis et al. (2020) in their analyses of intrafractional motion on Unity, where systematic displacement increased as treatment progressed. The last 30 seconds of data provide an illustrative snapshot of end-of-fraction behaviour, but this period is highly susceptible to statistical noise and outlier effects. For example, an abrupt shift by a single patient at the end of delivery could disproportionately influence the reported average. To mitigate this, a slightly longer evaluation window, such as 120 seconds, could instead be considered; even though this would remain a small fraction of the overall trace.

Figure 4.4 shows the population average displacement and variability in the x-, y-,

and z-directions for the prostate motion across the 360 fractions in this study. In the x or LR-direction, motion was minimal, with an average close to zero, a shallow slope, and a very low R^2 of 0.09. This suggests that motion in this axis was mostly random and not clinically important. The low R^2 here is explained by the very small slope, meaning that noise in the data outweighs any systematic trend. In the y-direction, a clearer trend was seen, with a slope of 0.026 mm/min and an R^2 of 0.85, showing that displacement here was more structured and predictable. While the average displacement was small, several fractions exceeded the 3 mm margin. The z-direction showed the greatest drift and variability. Figure 4.4 recorded a negative slope (that is, an inferior drift) of –0.053 mm/min with the largest SD. This directional drift was also reported in the literature, where bladder filling and rectal changes are known to cause inferior drift during treatment ((Menten et al., 2020); (Kontaxis et al., 2020)).

Figure 4.4 also links closely with Tables 4.2 and 4.3. At the approved template coordinates, variability was lower because the prostate was stably aligned at the start of treatment. This is seen in Figure 4.4, where traces remain flat near time zero. As treatment progressed, however, drift became increasingly noticeable, particularly in the y- and z-directions, consistent with the findings in Table 4.3 for the final 30 seconds. The magnitude and direction of drift have direct implications when considering a reduced margin strategy. For instance, with a conventional 3 mm PTV margin, gradual drifts may remain within tolerance and trigger fewer gating events. By contrast, under a 2 mm margin, the same drift patterns are more likely to exceed gating thresholds, increasing the frequency of interruptions and potentially requiring more adaptive shifts.

Taken together, all the tables and plots generated for this part show that most patients begin treatment with their prostate well aligned, but progressive drift develops, most notably in the z-direction, that is, SI. With close reference to the literature, such a behaviour was also noticed in the studies of Oehler et al. (2022) and Willigenburg et al. (2022). Keeping in mind that in Willigenburg's work, non-gated treatment was per-

formed with motion primarily assessed using start-to-end displacements, this study provides a deeper understanding of the prostate's drift behaviour and the timing of threshold exceedances. Moreover, while the global statistics derived here remain comparable to those reported in the literature, the temporal resolution by continuous trace monitoring highlights why real-time adaptive gating is essential to mitigate clinically significant underdosage. These differences are particularly relevant when considering margin reduction strategies, as time-resolved drift data under gating provide a clearer indication of how often a 2 mm margin would be exceeded compared to the conventional 3 mm, and thus directly inform the balance between tighter margins and increased gating incidence.

5.2.2 | Treatment Planning Study

5.2.2.1 | BLS Data and DVH Statistics

The DVH analysis conducted in this part of the study provided a deeper analysis of how BLS planning to correct for intrafraction prostate displacements influence both target coverage and OAR sparing. Starting by considering the BLS plan offsets, the increments or positions considered at this stage were crucial to investigate the possible displacements which can potentially occur clinically. With this done, the CTV, the PTV and the OARs were analysed deeply for offsets of 2 cm and 4 cm inferior, 0 cm and 2 cm and 4 cm superior to the prostate's centroid. For this analysis, the 0 cm offset considered the two main volumes (the CTV and the PTV) and OARs to capture the full relationship of how BLSs affect them accordingly. This said, for the other offsets, only the CTV, PTV, and urethra were considered, as the urethra was found to be the only relevant limiting OAR from the 0 cm offset. Thus, this further inspection of the DVH parameters revealed that consistent directional dependencies and clinically relevant trade-offs were present between tumour coverage and urethral sparing. In fact, the urethra was the only OAR investigated, as the bladder and the rectum, with the implementation of small BLSs, were assumed not to be affected, hence there was no way

of determining how the DVH stats would vary with different offsets. Another aspect of why the urethra was only investigated from the OAR was because Monaco® TPS only shifts the target structures but not the OARs. Therefore, for the Urethra to be investigated, multiple structures had to be created for each BLS offset (a total of 25 per offset).

5.2.2.2 | TPS DVH Statistics

Starting with the CTV, the V40Gy metric as shown in Figure 4.5, it demonstrated that coverage was generally well preserved, though inferior displacements of 1–2 cm produced marked reductions below the 95% tolerance in certain cases. This trend highlights that the prostate apex is particularly vulnerable to underdosage, owing to its close anatomical relationship to the urethra and anterior rectal wall, where margins are necessarily tighter. By contrast, the shifts with a superior offset were less critical, as most cases still met the V40Gy limits. These findings agree with reports by Kontaxis et al. (2020) and Xiong et al. (2022), who similarly observed that inferior displacements present a greater risk of target undercoverage than superior ones. Clinically, this asymmetry indicates that motion management techniques may need to focus on stricter gating thresholds in the downward direction or use anisotropic margins.

From Figure 4.6, the CTV mean dose (D_{mean}) was less sensitive to motion, varying by only 2–3 Gy across the displacement range. While this relative stability underscores that global target coverage remains intact, the inferior translations again produced small but consistent reductions in D_{mean}. The insensitivity of D_{mean} to localised dose loss is well described in the literature, as mean values average across the volume do not capture the displacement of hotspots outside the target (Winkel et al., 2019). Thus, although D_{mean} provides reassurance regarding overall dose delivery, it may hide clinically important cold spots. Therefore, other metrics were also considered as part of the analysis.

Although the CTV V42Gy criterion was only defined for comparison with the V42Gy of the urethra, its graph against the translation in the z axis was plotted as shown in Figure 4.7. Such a high-dose metric showed greater sensitivity to positional shifts. In fact, inferior displacements led to a rapid rise in V42Gy beyond the 50% limit, while superior shifts also resulted in constraint violations in several cases. This behaviour primarily arises from changes in the overall mean dose with offsets from the isocentre.

Shifting the focus to the PTV, the PTV's V36.25Gy metric revealed a subtle directional dependency. As shown in Figure 4.8, while coverage remained above the recommended clinical limit in all cases, a trend towards reduced V36.25 Gy was evident for inferior displacements. This pattern mirrors that observed for CTV metrics, underscoring that inferior motion poses the greatest challenge for dose conformity. The underlying reason is anatomical: the inferior aspect of the prostate tapers at the apex and lies in close proximity to the urethra and the rectal wall. To spare these sensitive structures, the planning margins at the apex are often reduced, leaving less room for positional uncertainties. Consequently, even small inferior displacements can shift a part of the target volume outside the high-dose region, leading to a measurable reduction in PTV coverage. In contrast, superior or lateral shifts are more easily accommodated because of broader margins and greater surrounding soft-tissue tolerance, indicating that inferior motion uniquely magnifies the risk of underdosage at the target boundary.

The PTV's V34.4Gy parameter, as shown in Figure 4.9 remained largely invariant across all offsets considered, consistently approximating 100%. The stability of this parameter provides additional reassurance that the global target coverage is not compromised by the undesired motion commonly observed in clinical practice.

Similarly, Figure 4.8 illustrates that PTV coverage, expressed as V36.25 Gy, remained above the clinical acceptance criterion of 95% across all simulated z-axis translations, confirming the robustness of the applied 2 mm CTV-to-PTV margin. Again, the data

reinforce that inferior motion is more vulnerable for prostate dose conformity, in agreement with prior reports that highlight apex underdosage as a common limitation in MR-guided prostate radiotherapy (Mastella et al., 2024; Menten et al., 2020).

Figures 4.11 and 4.12 demonstrate that the urethral dose, expressed as V42Gy, is strongly influenced by the z-axis translations, with superior displacements producing the most pronounced dose escalation. In both delineation approaches, the unshifted and shifted urethras, or 1_Urethra V42Gy and Urethra_XX, respectively, showed that several superior shifts drove V42Gy above the clinical tolerance of 50%, whereas inferior displacements generally remained within acceptable limits. This highlights the urethra as a dose-limiting structure, particularly vulnerable to upward prostate movements. A direct comparison of the two contouring methods, as shown in Figure 4.13, further revealed a strong correlation between the V42Gy values; however, Urethra_XX consistently reported higher affected volumes, indicating that more inclusive delineations capture additional hotspots and may provide a more conservative estimate of toxicity risk.

Finally, the scatter plot in Figure **??** shows the relationship between the CTV V42Gy and the urethra V42Gy across all offsets. A strong positive correlation was evident, whereby an increase in CTV V42Gy was consistently associated with an increase in the urethral V42Gy. This suggests that the extent of high-dose coverage within the target can serve as a surrogate predictor of urethral exposure. The figure shows that whenever the CTV V42Gy approached 100%, it almost resulted in urethral V42Gy values exceeding tolerance, whereas lower CTV V42Gy values corresponded to minimal urethral involvement. Importantly, the scatter distribution also demonstrated that superior displacements drive the highest urethral doses for equivalent levels of CTV coverage, reflecting the anatomical overlap between the structures. Collectively, this scatter plot shows that monitoring CTV V42Gy could provide a practical dosimetric indicator of urethral risk, facilitating adaptive decision-making during MR-guided prostate SBRT.

5.2.2.3 | CTV within PTV Data and DVH Statistics

For the second part of this phase, the phantom was set to move at increments corresponding to the SI and AP directions to activate the CMM gating criteria. In this way, the distances which provide a VOICE of 99% and 97% could be determined. These two percentages were particularly chosen to investigate until what point gating occurs at 99% and 97%. Moreover, as shown in Table 4.4, the 99% and 97% VOICE provided an idea of the stage at which it was expected to exceed the PTV margin in the upcoming test. For the subsequent stage, the main focus was on the CTV and urethra structure, as the PTV served as a boundary.

The analysis of small CTV displacements within the PTV demonstrated that the target coverage remained largely preserved across all simulated scenarios. The dose–volume parameters for the CTV showed minimal variation, confirming that the applied PTV margin was sufficient to account for minor positional uncertainties. These findings reinforce the clinical principle that the PTV provides geometric robustness for maintaining adequate CTV coverage under small intrafractional shifts.

In contrast, the urethra exhibited greater sensitivity to internal displacement. While the CTV remained adequately covered, the urethral dose metrics, particularly D_{max} and V42, showed noticeable increases when the CTV shifted closer to the urethra. This observation highlights the urethra as the most dose-limiting OAR in the treatment scenario. Importantly, this effect was observed even for shifts that remained entirely within the PTV, suggesting that target robustness comes at the expense of an increased urethral dose.

5.2.2.4 | Monaco® TPS

Throughout the study, a few limiting factors were encountered when working with Monaco® TPS.

As previously mentioned, upon proceeding with the treatment plan for the second part of this study, it was noticed that Monaco® TPS does not offer the option to set the OARs as a target structure. This necessitated a workaround by creating multiple urethra structures in our case to investigate how the urethra structure is affected by prostate movement during treatment.

Secondly, it was noted that even though a BLS work with the principle of maintaining the MLC segments, it was found, as shown in Figures 5.2 to 5.5, that the between one BLS and the other, the segments' shape was slightly altered. This suggests that the overall volume created by the MLCs is maintained, but the actual segments are slightly shifted for a given gantry angle.

It was also observed that recalculating the same plan in Monaco® TPS at different times resulted in slight variations in dosimetric outcomes, despite unchanged geometry and beam parameters. This behaviour likely stems from the inherent stochastic nature of Monte Carlo dose calculation, where each run samples particle interactions using pseudo-random processes. As documented in the literature, Elekta (2023) highlights that Monaco® TPS allows users to set a level of statistical uncertainty, a parameter governing the trade-off between calculation time and precision, making such a parameter able to influence both dose uniformity and reproducibility across repeated calculations significantly. In fact, for this study, an statistical uncertainty of 1% was maintained throughout to ensure minimal variability.

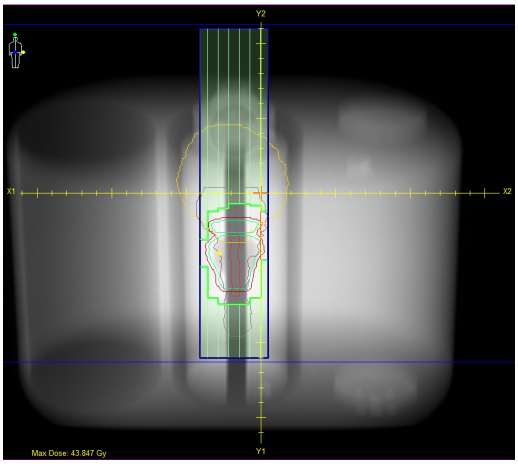

Figure 5.2: The segments at gantry 0 for the original treatment plan

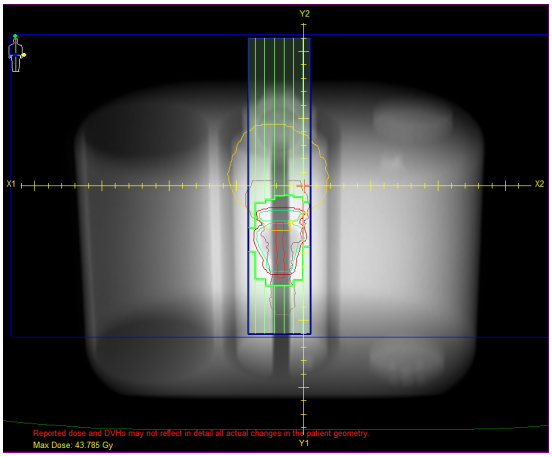

Figure 5.3: The segments at gantry 0 for BLS number 1 done on the original treatment plan

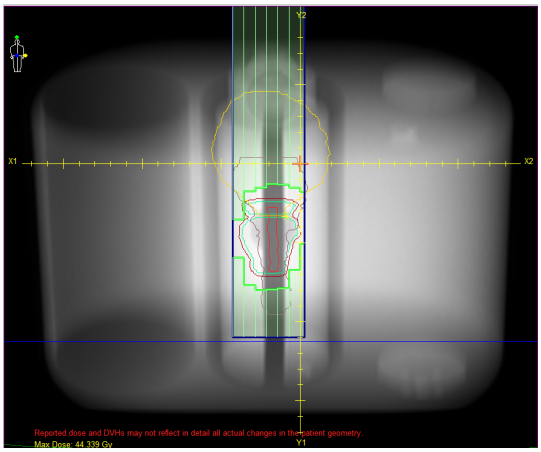

Figure 5.4: The segments at gantry 0 for BLS number 10 done on the original treatment plan

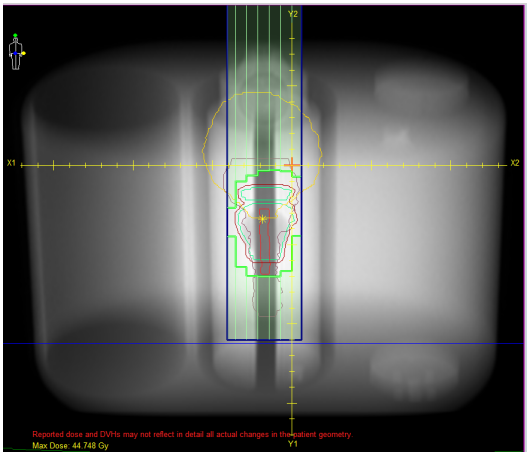

Figure 5.5: The segments at gantry 0 for BLS number 20 done on the original treatment plan

5.2.3 | Film Dosimetry

To validate the prostate's motion and treatment planning study conducted in the early stages of this project, film dosimetry was used to assess the isodose distributions and the gamma indices obtained.

5.2.3.1 | Isodose Distributions and Gamma Index - The Qualitative and Quantitative Point of View

The results obtained for the isodose overlays for an 8.5 mm inferior displacement achieved with a BLS, which refers to Figures 4.17 and 4.18, show that for the static 8.5 mm inferior displacement shows a clear geometric divergence from the reference (0 mm) distribution, particularly in the SI direction. The dotted reference curves extend superiorly beyond the shifted plan's solid isodoses, illustrating underdosage to the superior prostate margin, while inferior regions receive unintended higher doses. This is reflected in the gamma analysis, where only 82.0% of points pass the strict 3%/1 mm criteria, though pass rates improve to 96.2% at 3%/3 mm and nearly 100% under 5%/3 mm criteria. These results highlight a key limitation that is, while gamma passing rates under lenient criteria may appear acceptable, the underlying dose displacement is clinically significant, risking insufficient tumour coverage and excess dose to adjacent normal tissue.

The VOICE-based isodose plots demonstrate a modest improvement compared to the static displacement but still reveal residual misalignment at prescription isodose levels. The superior margin in particular shows persistent undercoverage, reflecting the limited corrective ability of VOICE 97% when large and sustained inferior drifts occur. The gamma analysis supports this interpretation, with passing rates of only 38.4% at 3%/1 mm and 57.0% at 3%/2 mm, increasing to 84.4% at 3%/3 mm. Even at the relaxed 5%/3 mm criteria, VOICE achieves only 90.8%. These results suggest that while VOICE can partially improve dosimetric agreement, it fails to restore reference-level

conformity in the presence of substantial baseline motion. Clinically, this indicates that VOICE alone may not reliably protect against underdosage of the prostate target volume or limit overdosage to nearby OARs, particularly during longer treatments where motion persists or progresses.

With two adaptive BLSs introduced during treatment, the isodose comparisons demonstrate markedly better alignment with the reference curves compared to 97%VOICE or 8.5 mm static displacement. The prescription-level isodoses overlap more closely, with only small residual discrepancies along the SI axis. This is reflected in the gamma analysis, which shows 96.0% passing at the tight 3%/1 mm level, increasing to 100.0% at 3%/3, at 5%/2 mm and at 5%/3 mm. These improvements highlight that even limited intrafraction adaptation can significantly reduce geometric and dosimetric error. Clinically, the 2BLS strategy demonstrates feasibility as a practical compromise, recovering much of the target coverage lost under static conditions. However, two BLS corrections may not be sufficient for all patients, particularly in cases of progressive drift or more complex motion trajectories.

The 3BLS motion film also yields a somewhat good agreement between the measured and reference isodose curves. Visual inspection shows near-complete overlap at both high- and intermediate-dose levels, suggesting that repeated adaptation can effectively manage both baseline displacement and ongoing intrafraction drift. Gamma analysis confirms this high level of concordance, with passing rates of 69.0% at the strictest 3%/1 mm criterion, 94.6% at 3%/3 mm, and >99% under 5%/3 mm tolerances. Upon executing this clinical scenario online, the treatment was not interrupted equally at a 1/3 interval of MU delivery. Mainly because the system happened to gate more often than predicted, leading to two out of the three BLSs to occur at very close time intervals. From a clinical perspective, this turned out to imitate more closely a typical live scenario where an actual patient is being treated. Although it requires more workflow interventions, the dosimetric gain supports its role as a viable approach for managing

patients prone to significant intrafraction motion.

Now considering the subfigures as shown in Figure 4.24, the left-hand figure, which represents the film measurement, and the right-hand figure, which represents the TPS calculation, show the isodose curves for the 8 Gy delivery with an 8.5 mm inferior displacement. While both representations capture the overall shape of the high-dose region, discrepancies between the solid (measured) and dotted (reference) isodose lines are evident. The film demonstrates slightly more irregular isodose contours, which is expected due to scanner noise, film uniformity issues, and the inherently higher spatial resolution of film compared to TPS grids. Conversely, the TPS distribution appears smoother, reflecting the dose calculation algorithm's interpolation and grid resolution.

The agreement between the film and TPS was generally acceptable in the central high-dose region, indicating that the TPS Monte Carlo algorithm reliably predicts dose deposition despite the geometric shift. However, the deviations were most noticeable along the superior and inferior boundaries, where the solid (film) curves deviated from the dotted (reference) TPS lines. This likely reflects a combination of motion-induced geometric misses and the limitations of film calibration under steep dose gradients.

From a clinical perspective, this comparison confirms that Monaco Monte Carlo-based dose calculation reproduces the measured dose distribution to a high degree, supporting its reliability for treatment planning even under shifted geometries.

5.3 | Conclusion

The observations derived from the data presented in the previous chapter are discussed in this chapter. In the final chapter, the key findings, conclusions, and recommendations are outlined.

6

Conclusions

6.1 | Introduction

This chapter brings together the main outcomes of the research, highlighting the implications for adaptive radiotherapy within MRL workflows and quality assurance practices. It reflects on how the study's findings contribute to a deeper understanding of motion management, treatment adaptation strategies, and dosimetric validation methods. The chapter also outlines practical recommendations for clinical implementation, aiming to support medical physicists and radiation therapy professionals in optimising patient treatment and safety. Ultimately, it identifies key limitations of the work and proposes directions for future research, aiming to advance adaptive radiotherapy techniques and enhance the role of MR-guided technologies in clinical practice.

6.2 | Summary of Conclusions from the Study

The main conclusions for the study include:

Part 1: Prostate Motion Analysis:

- Log file data from 360 fractions confirmed that the mean motion in the LR, AP, and SI directions was minimal ($\leq$1 mm mean displacement), but large inter-

fraction and inter-patient variability was present.

- Sudden large inferior drifts were observed, consistent with the systematic and transient motion patterns reported by Mastella et al. (2024) and Menten et al. (2020).
- These findings confirm that although margins can be reduced, intrafraction management strategies are essential to safeguard target coverage.

Part 2: Treatment Planning Study:

- CTV coverage was generally maintained for displacements $\leq$3 mm, but larger inferior shifts caused a notable reduction in V40Gy and D95%.
- The CTV within PTV metric proved to be a sensitive geometric predictor of plan degradation, as even small SI drifts rapidly reduced overlap and directly corresponded to loss of CTV dose coverage.
- The shifted urethra (Urethra_XX) showed a strong correlation with the static urethra (1_Urethra), acting as a conservative predictor of dose escalation.
- Scenarios that preserved CTV coverage tended to exceed urethral tolerance, while cases that met urethral limits often failed to maintain adequate CTV dose. This confirmed the urethra as the critical OAR when margins are reduced.

Part 3: Film Dosimetry

- Monaco's Monte Carlo dose calculations showed strong agreement with film measurements, confirming the reliability of TPS modelling under adaptive workflows.
- Gamma analysis demonstrated poor passing rates for the 8.5 mm inf static and VOICE film scenarios but significantly improved results for 2 BLSs.
- Radiochromic film measurements confirmed high concordance with planned dose distributions, with high gamma passing rates at 5%/3 mm.

- Films showed that repeated BLS corrections successfully restored coverage for modest SI drifts, whereas gating alone could not recover coverage once the target moved outside the treatment envelope.

6.2.1 | Overall conclusion

- The study demonstrates that reducing prostate PTV margins from 3 mm to 2 mm on the Unity MRL is feasible only if margin reduction is coupled with adaptive correction strategies.
- VOICE is effective for beam-hold gating but does not recover coverage after displacement.
- BLSs (2–3 corrections per fraction) provides the most robust safeguard against systematic drifts, restoring both target coverage and plan compliance.

6.3 | Recommendations for Professional Practice

- **Adopt adaptive strategies beyond VOICE gating:** While VOICE remains a useful safeguard, persistent prostate drift necessitates baseline shifts. A workflow integrating two or more BLS interventions per fraction provides a clinically robust approach to safeguarding coverage.
- **Margin optimisation:** A reduced PTV margin from 3 mm to 2 mm is feasible when combined with intrafraction adaptation, and may potentially enable better sparing of rectum and bladder without compromising prostate coverage. This aligns with current trends in MRgART for prostate SBRT (Winkel et al., 2019).
- **Quality assurance integration:** Film dosimetry and independent gamma analysis should remain part of routine QA when introducing new adaptive strategies, as this ensures that TPS predictions translate accurately to delivered dose (Zwierzchowski et al., 2016).

- **Workflow refinement:** Healthcare professionals working on Unity should prepare for the time and resource demands of repeated adaptive steps. Protocols should balance patient throughput with the dosimetric benefits of multiple adaptations.

6.4 | Recommendations for Future Research

- **Larger patient cohort validation:** Expanding prostate motion trace analysis to larger datasets would allow better modelling of population-level variability and identification of subgroups at higher risk of motion-induced underdosage.
- **Seminal vesicle deformation:** Future studies should account for seminal vesicle motion and deformation, which were not considered here but may significantly influence margins and OAR dose.
- The Modus QUASAR™ MRI 4D Phantom used in this study has dimensions smaller than a typical male pelvis. As such, the results could be replicated or confirmed using actual patient imaging data to ensure that organ size, tissue heterogeneity, and anatomical variability are adequately represented.
- **Broader site application:** Similar adaptive strategies should be explored in anatomically mobile sites such as the pancreas and liver, where Unity's MR capabilities are particularly advantageous (Tsekas et al., 2024).

6.5 | Conclusion

This dissertation has demonstrated that margin reduction in prostate SBRT delivered with the Elekta Unity MRL is achievable, provided that intrafraction adaptation is incorporated. While VOICE gating offers a first level of safety, its limitations in scenarios of persistent drift necessitate BLS corrections. Among the strategies tested, 2 BLS proved most effective, restoring agreement with reference plans and films to clinically

acceptable levels.

The combination of motion trace analysis, TPS planning studies, and film dosimetry provided a comprehensive validation framework, reinforcing both the reliability of Monaco's Monte Carlo dose calculations and the clinical necessity of adaptive interventions. Ultimately, these findings contribute to ongoing efforts in MRgART, supporting safe margin reduction, optimised OAR sparing, and improved treatment precision for prostate cancer patients.

A

Ethical Approval Documents

A.1 | UREC Approval

L-Università ta' Malta

Kelsey Ann Micallef <kelsey.micallef.20@um.edu.mt>

The status of your REDP form (FHS-2024-00634) has been updated to Acknowledged
1 message

form.urec@um.edu.mt <form.urec@um.edu.mt> 7 January 2025 at 11:09
To: kelsey.micallef.20@um.edu.mt

Dear Kelsey Ann Micallef,

Please note that the status of your REDP form (FHS-2024-00634) has been set to *Acknowledged*.

You can keep track of your applications by visiting: https://www.um.edu.mt/research/ethics/redp-form/frontEnd/.

This email has been automatically generated by URECA. Please do not reply. If you wish to communicate with your F/REC please use the respective email address.*

B

Prostate Traces Plots

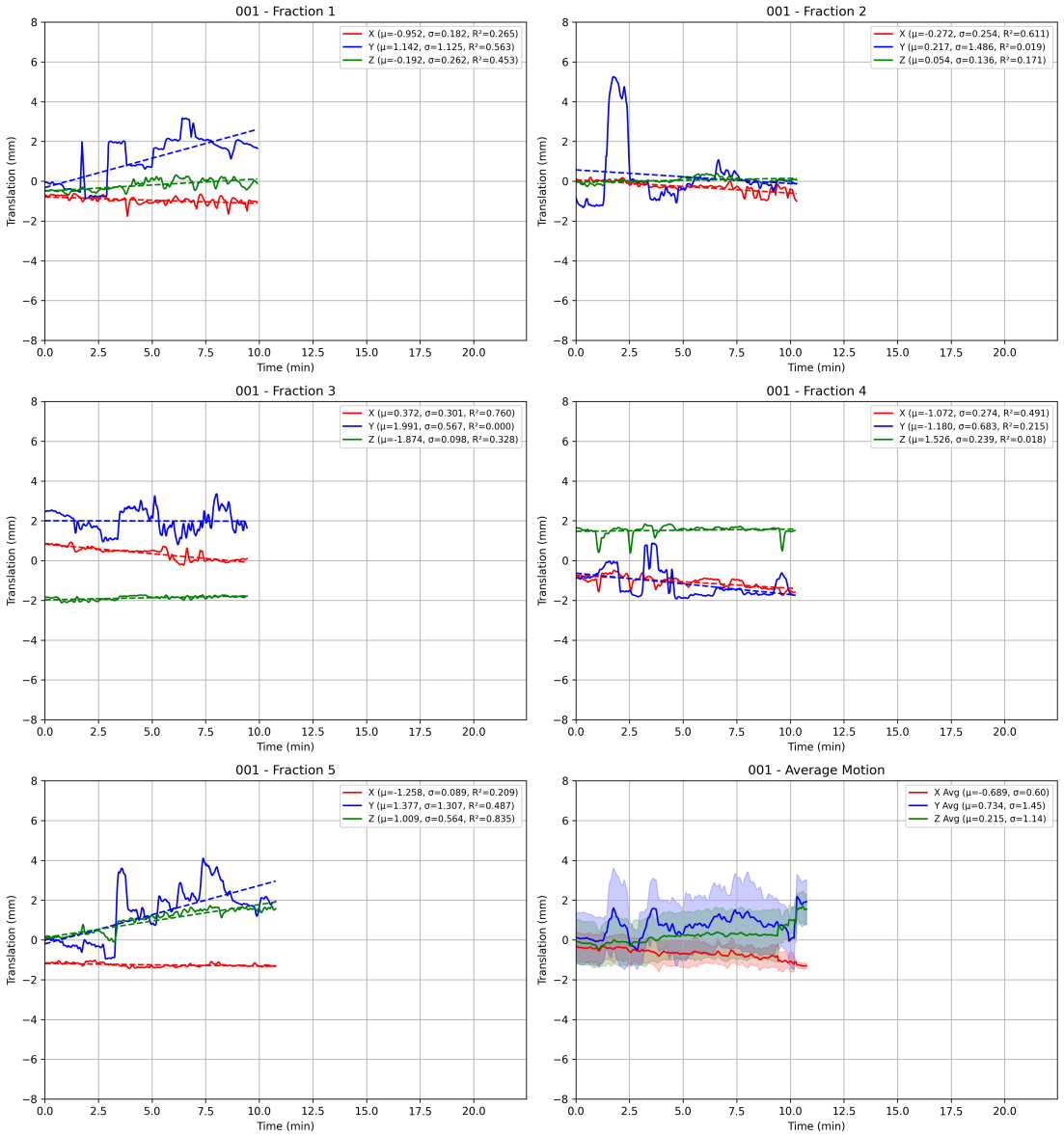

Figure B.1: Filtered traces plot for patient 001

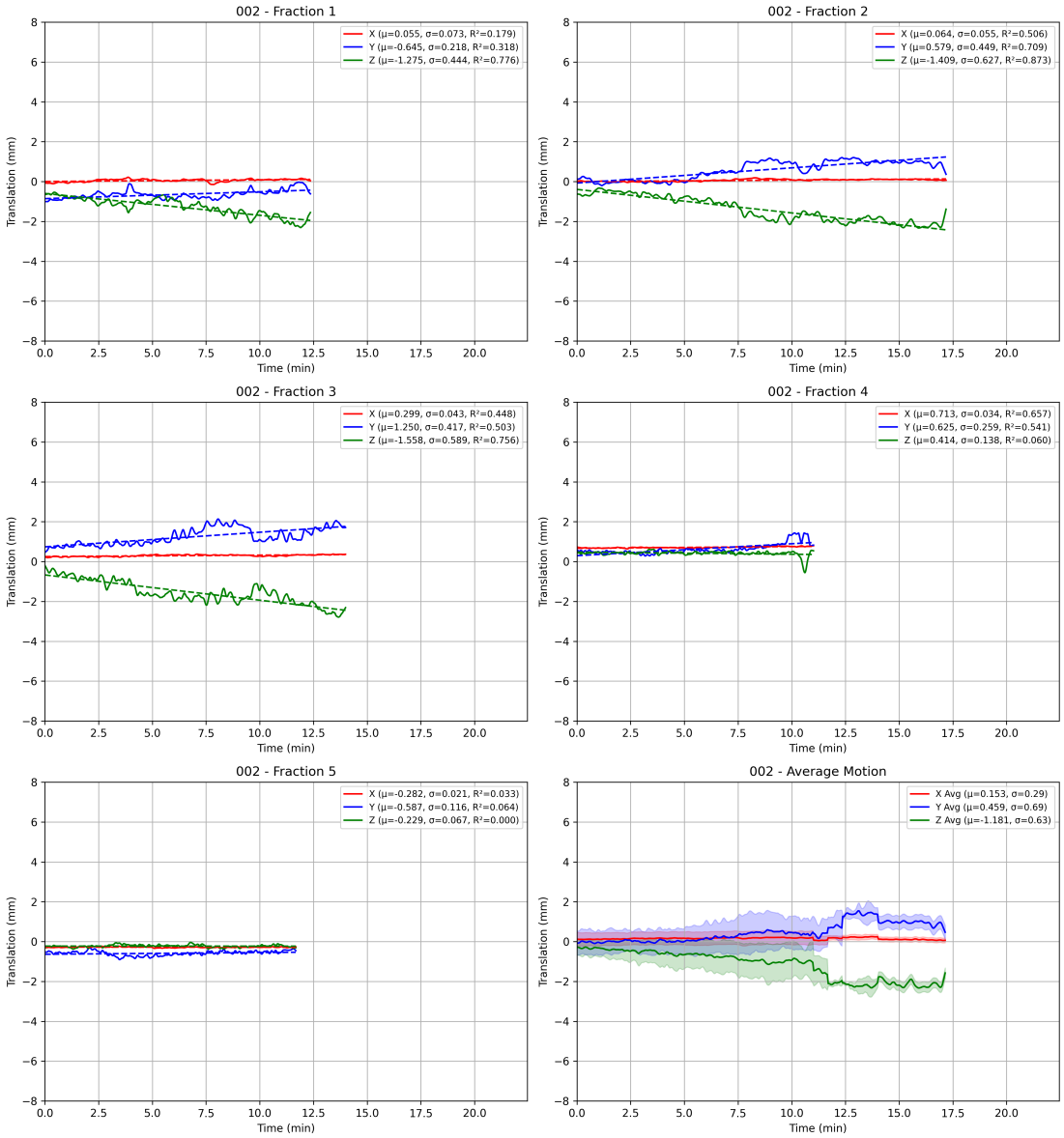

Figure B.2: Filtered traces plot for patient 002

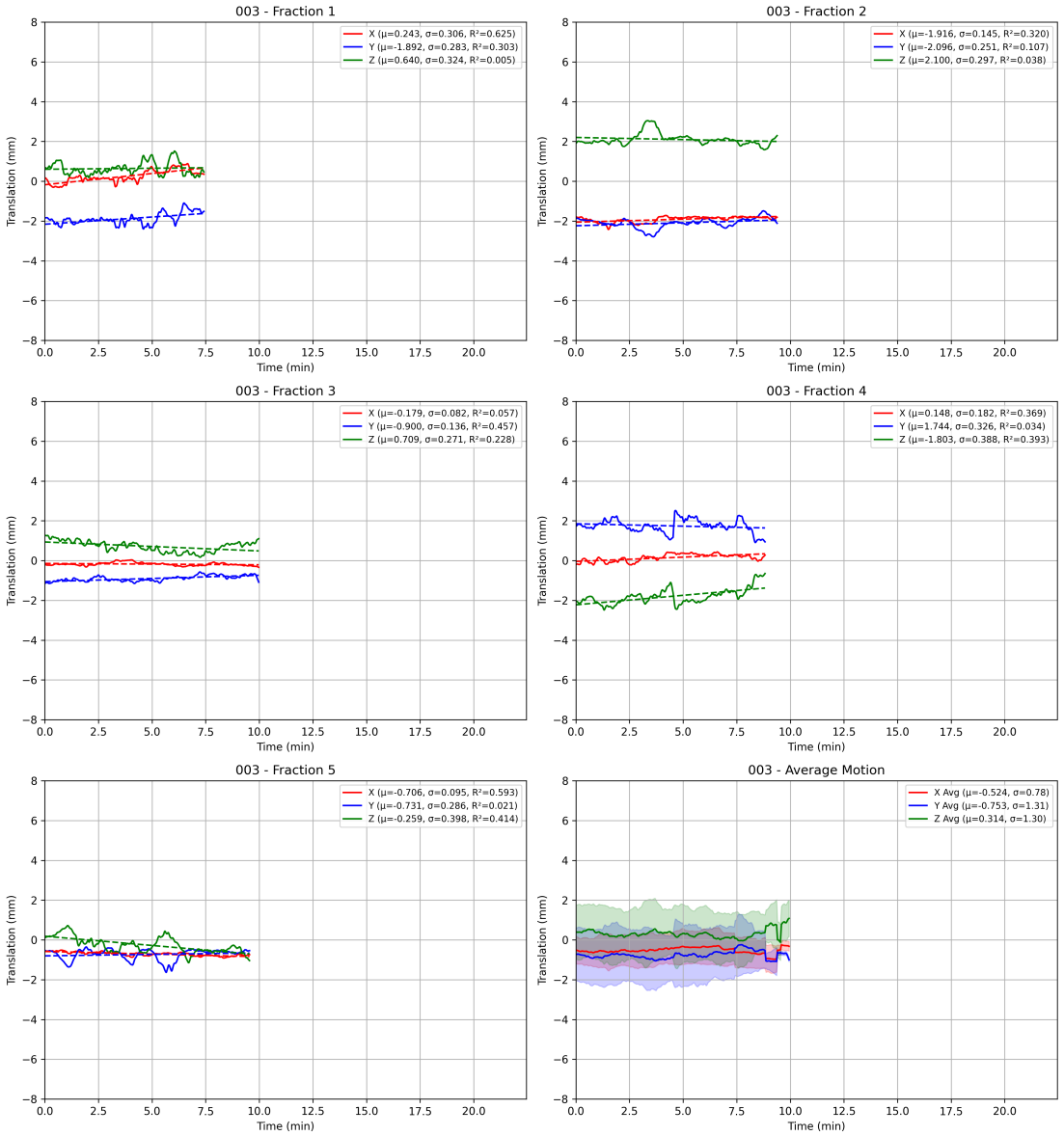

Figure B.3: Filtered traces plot for patient 003

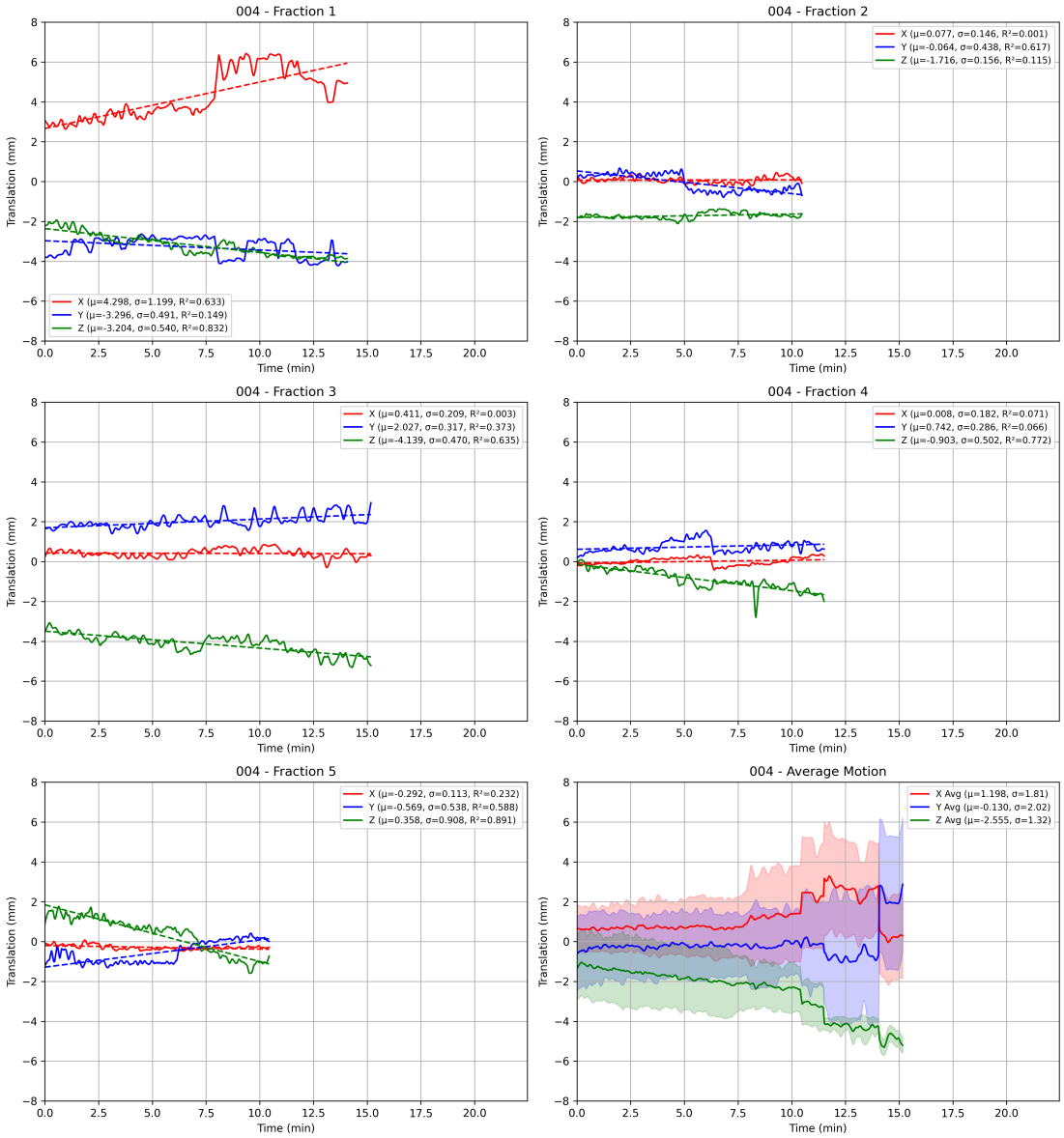

Figure B.4: Filtered traces plot for patient 004

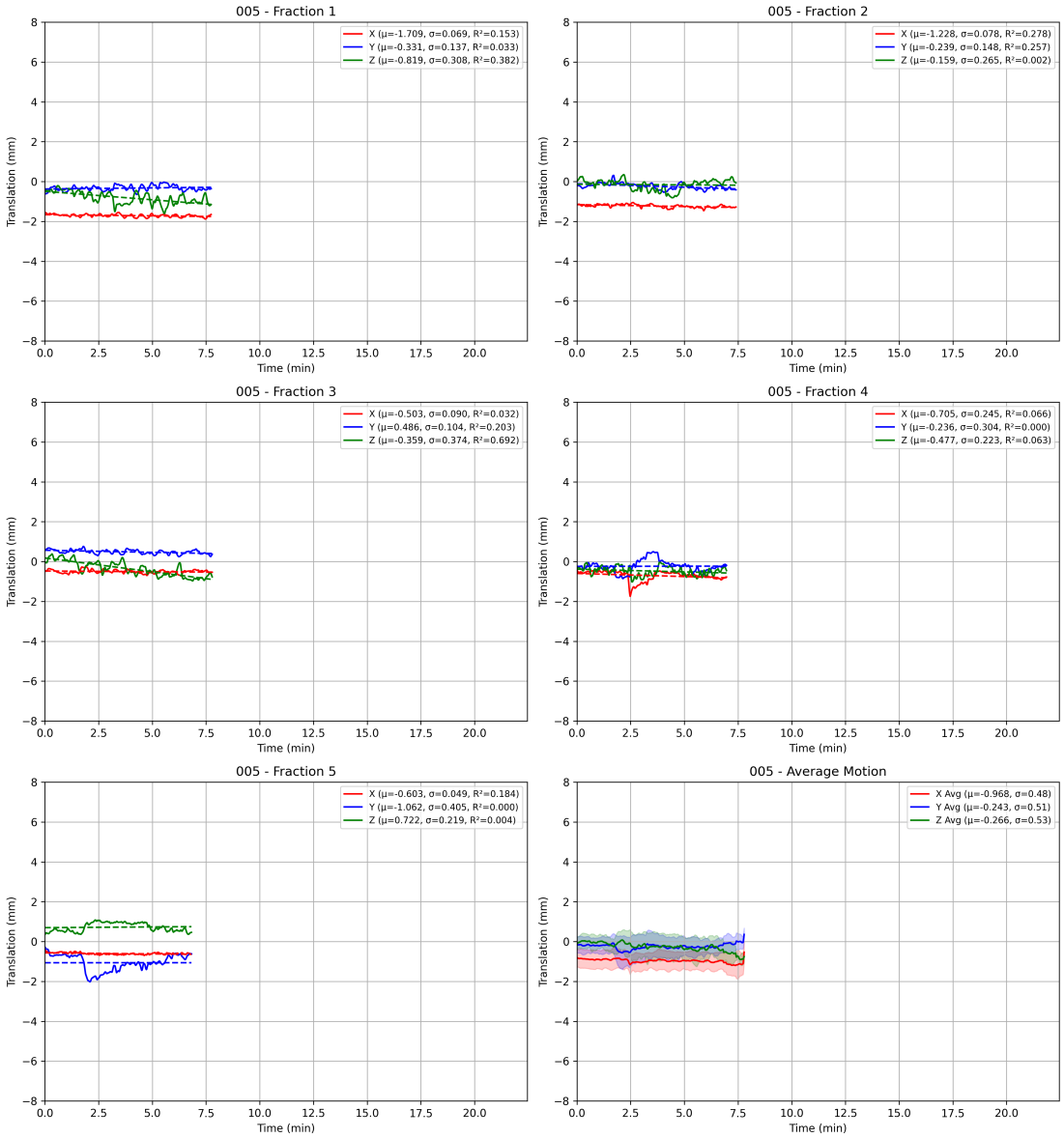

Figure B.5: Filtered traces plot for patient 005

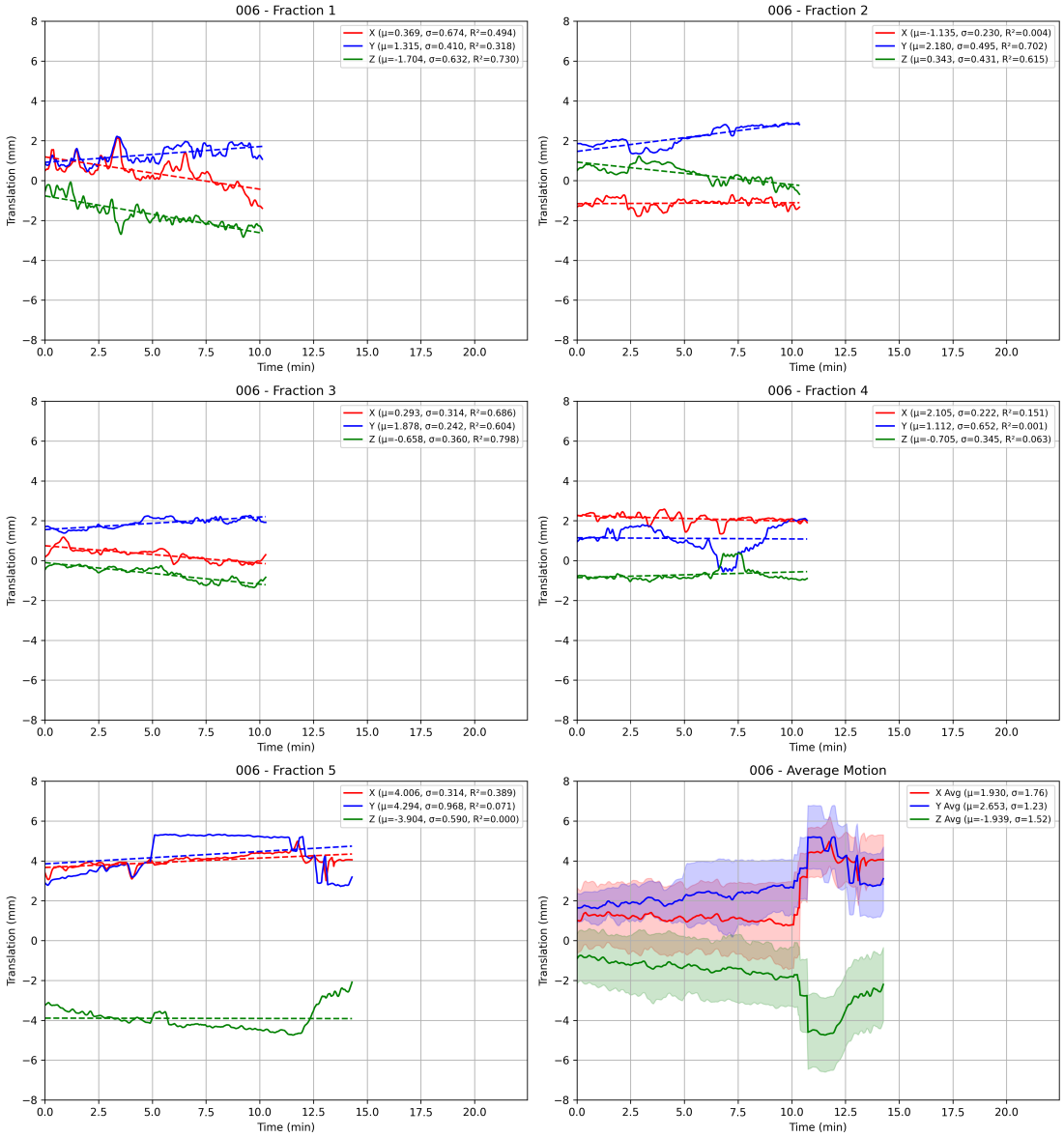

Figure B.6: Filtered traces plot for patient 006

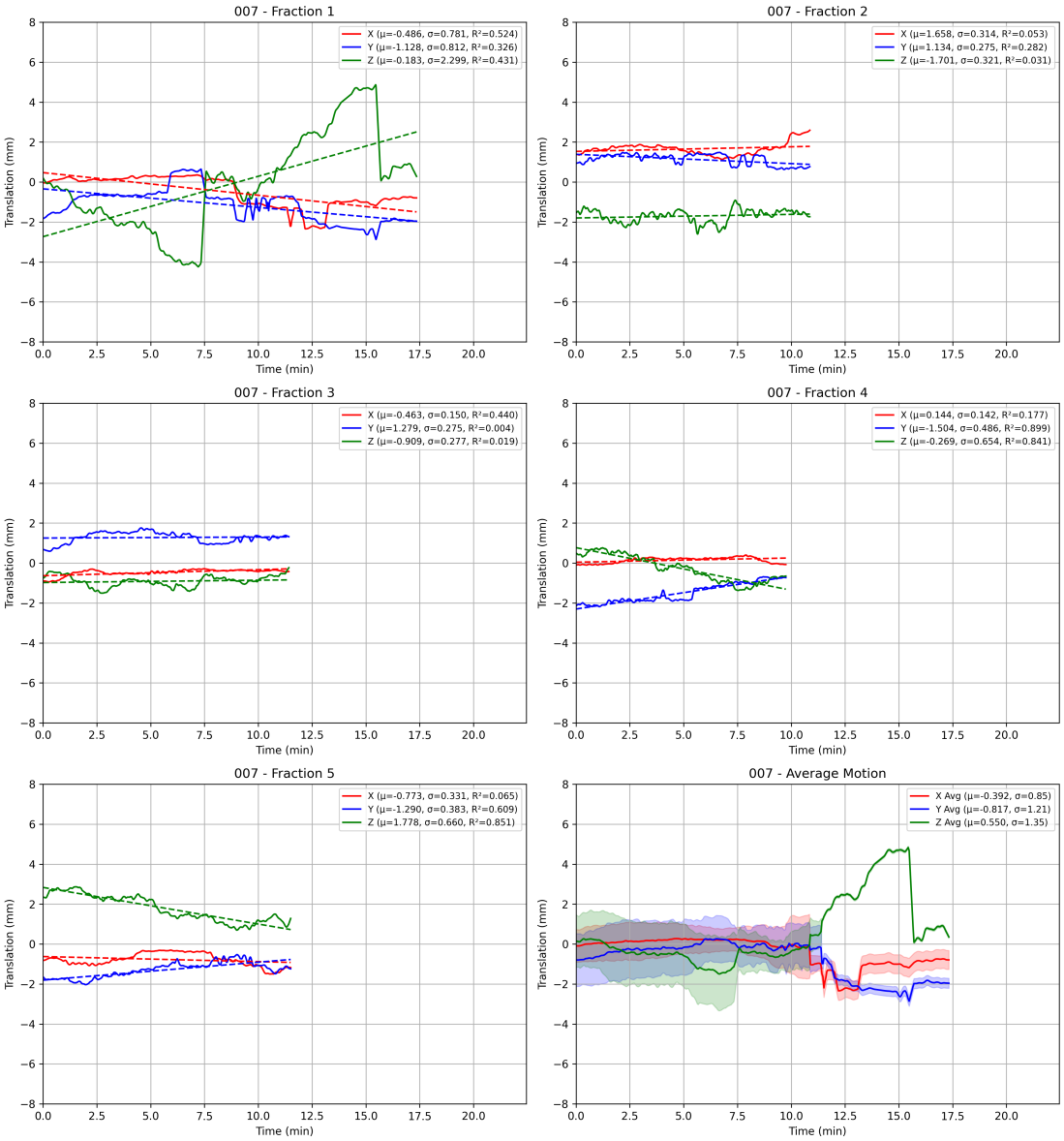

Figure B.7: Filtered traces plot for patient 007

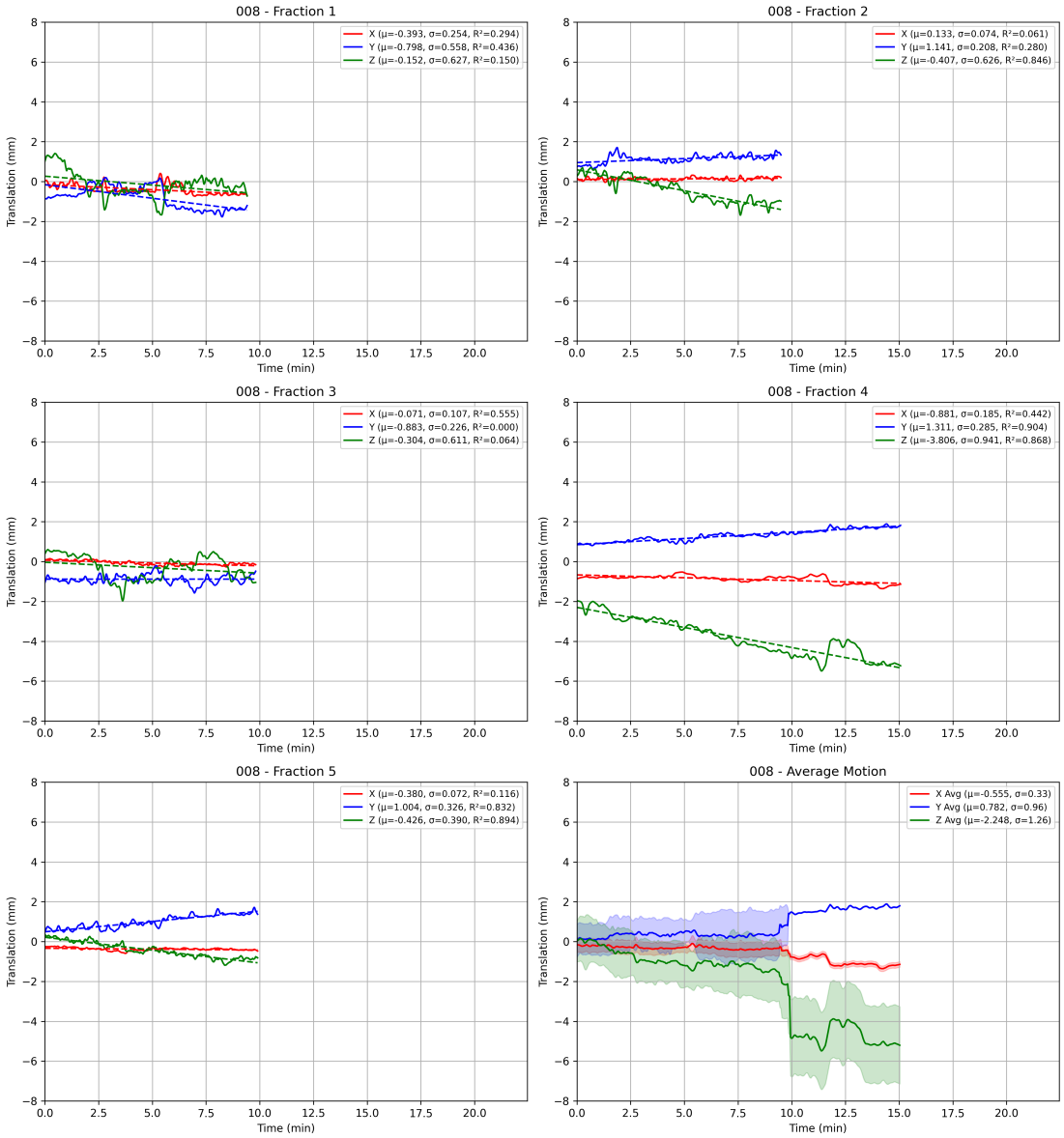

Figure B.8: Filtered traces plot for patient 008

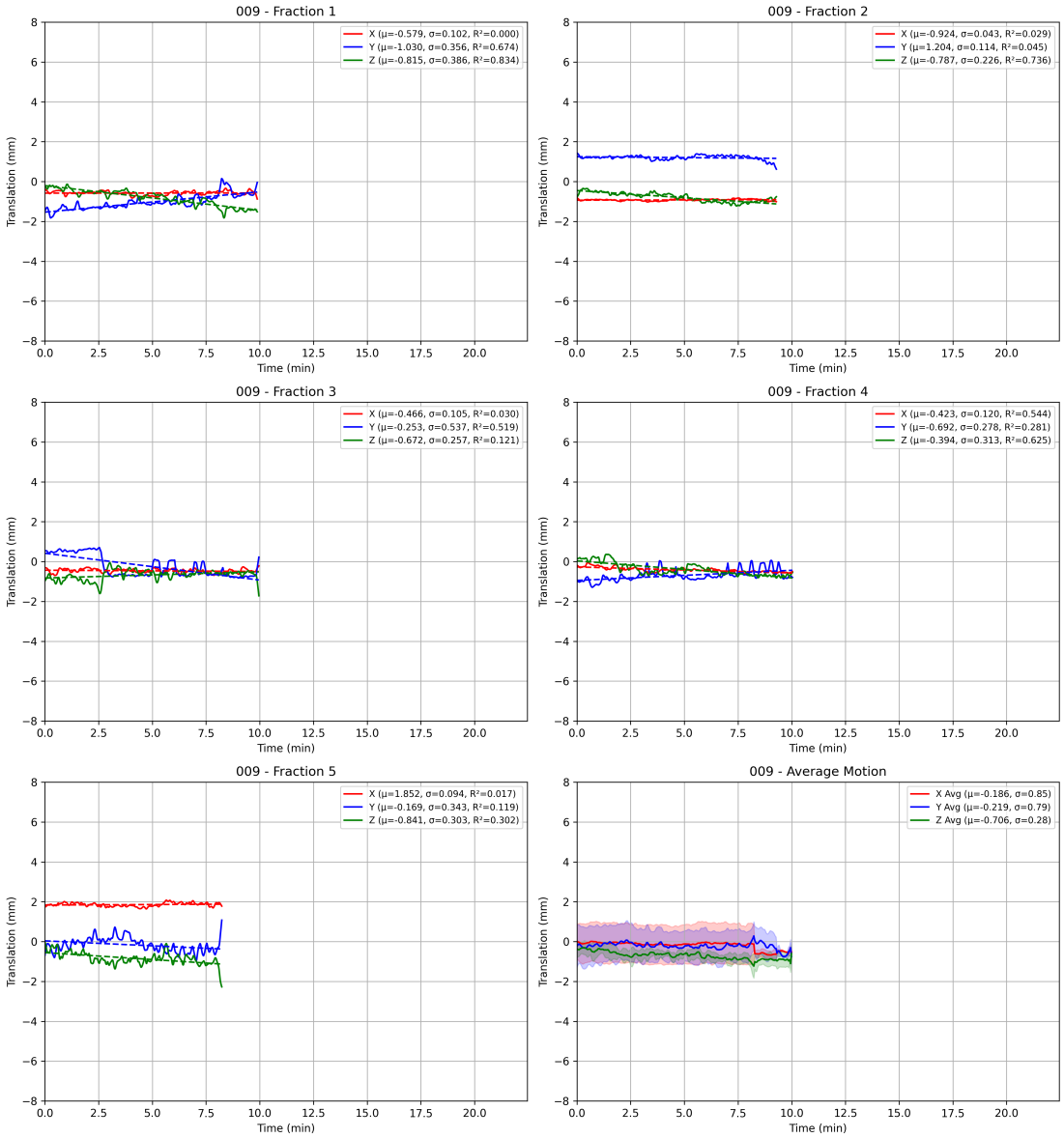

Figure B.9: Filtered traces plot for patient 009

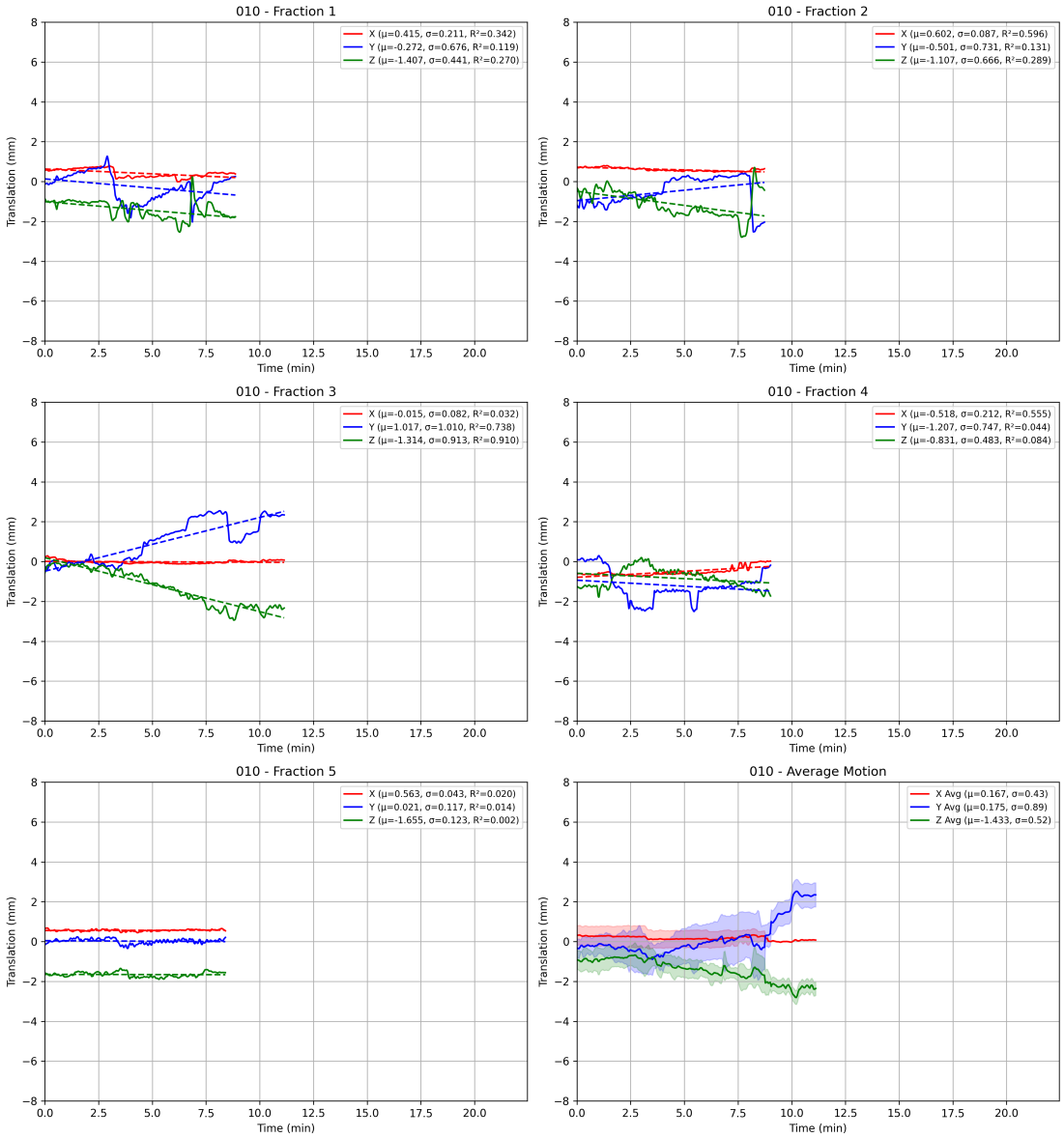

Figure B.10: Filtered traces plot for patient 010

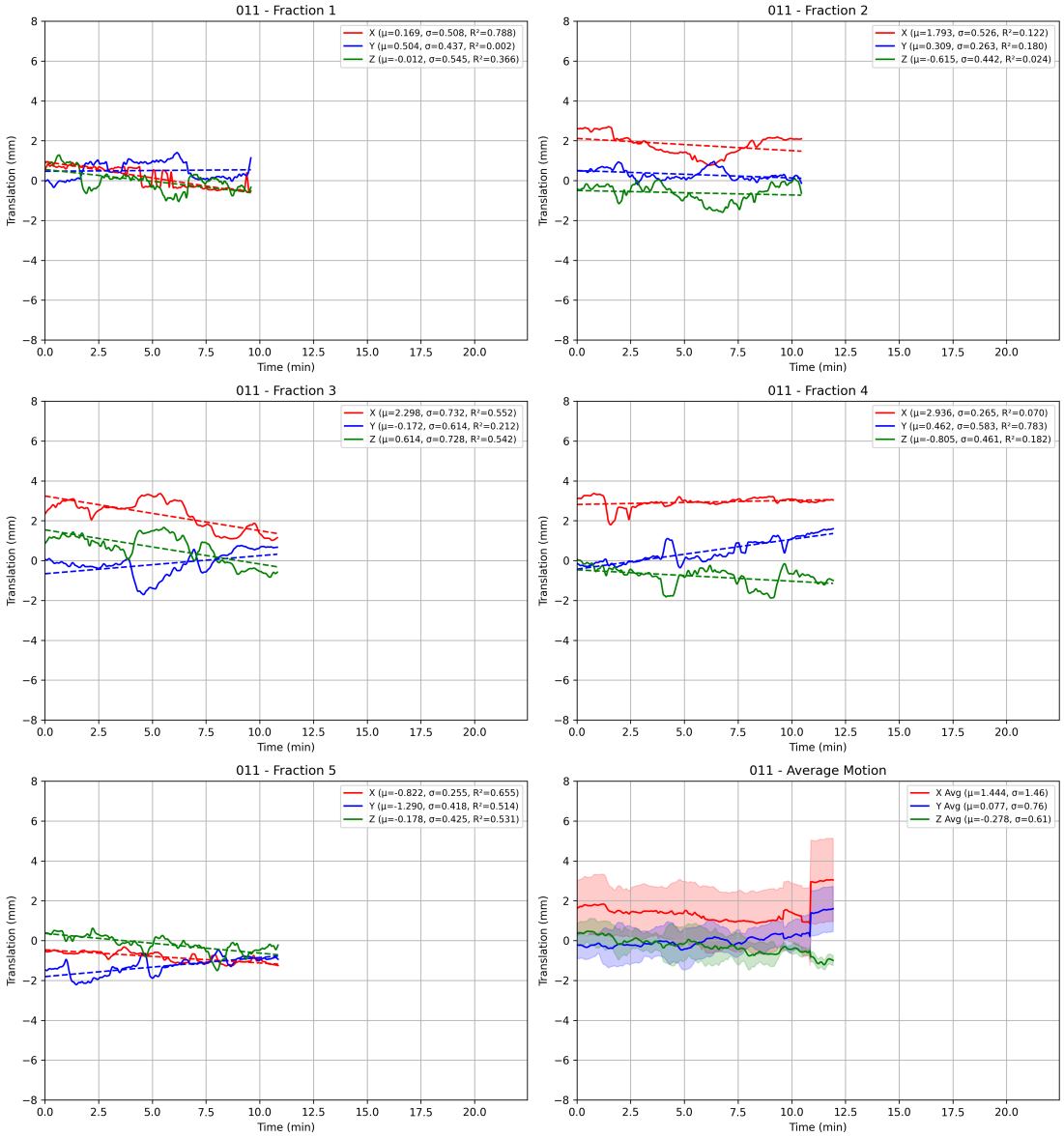

Figure B.11: Filtered traces plot for patient 011

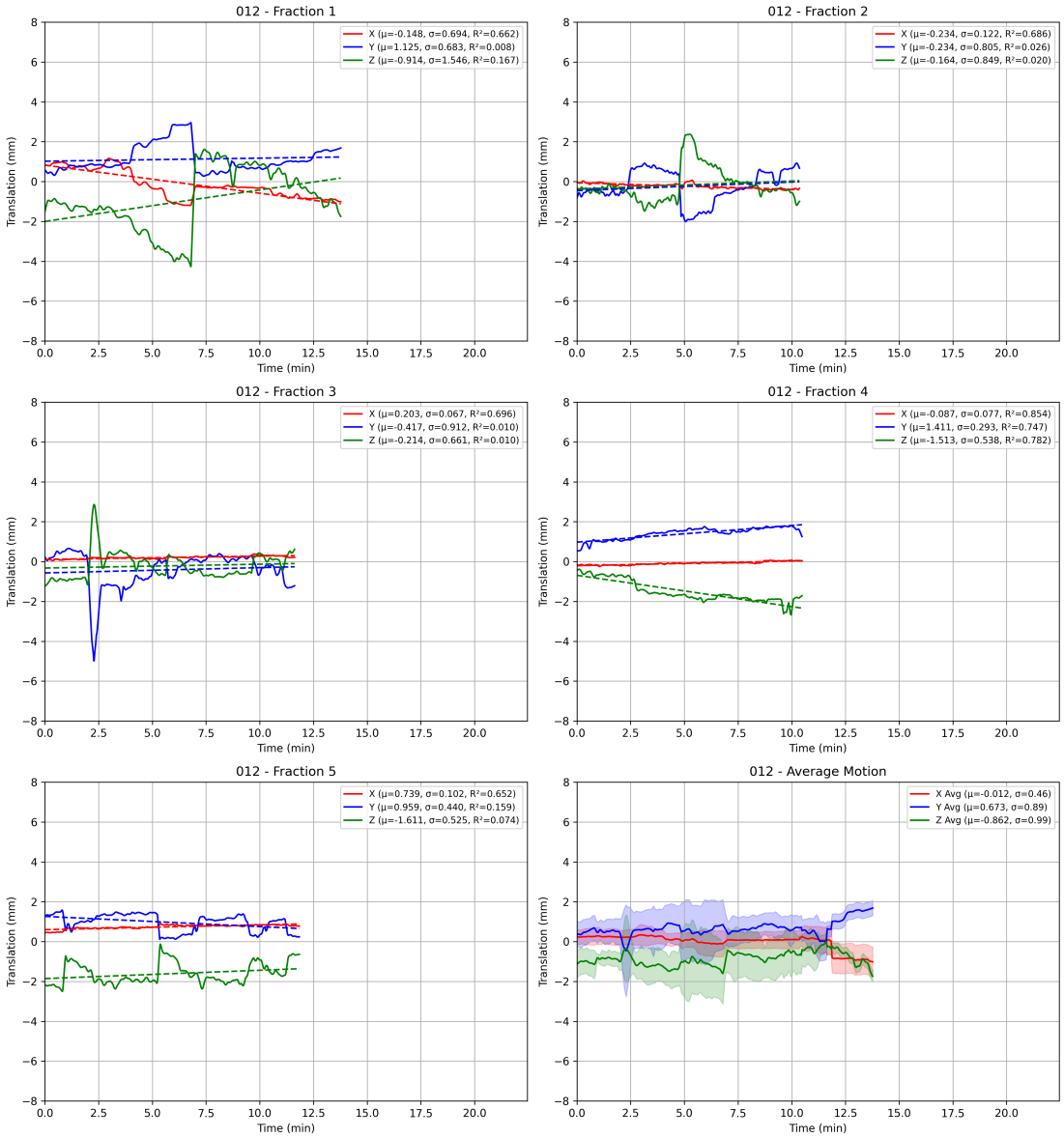

Figure B.12: Filtered traces plot for patient 012

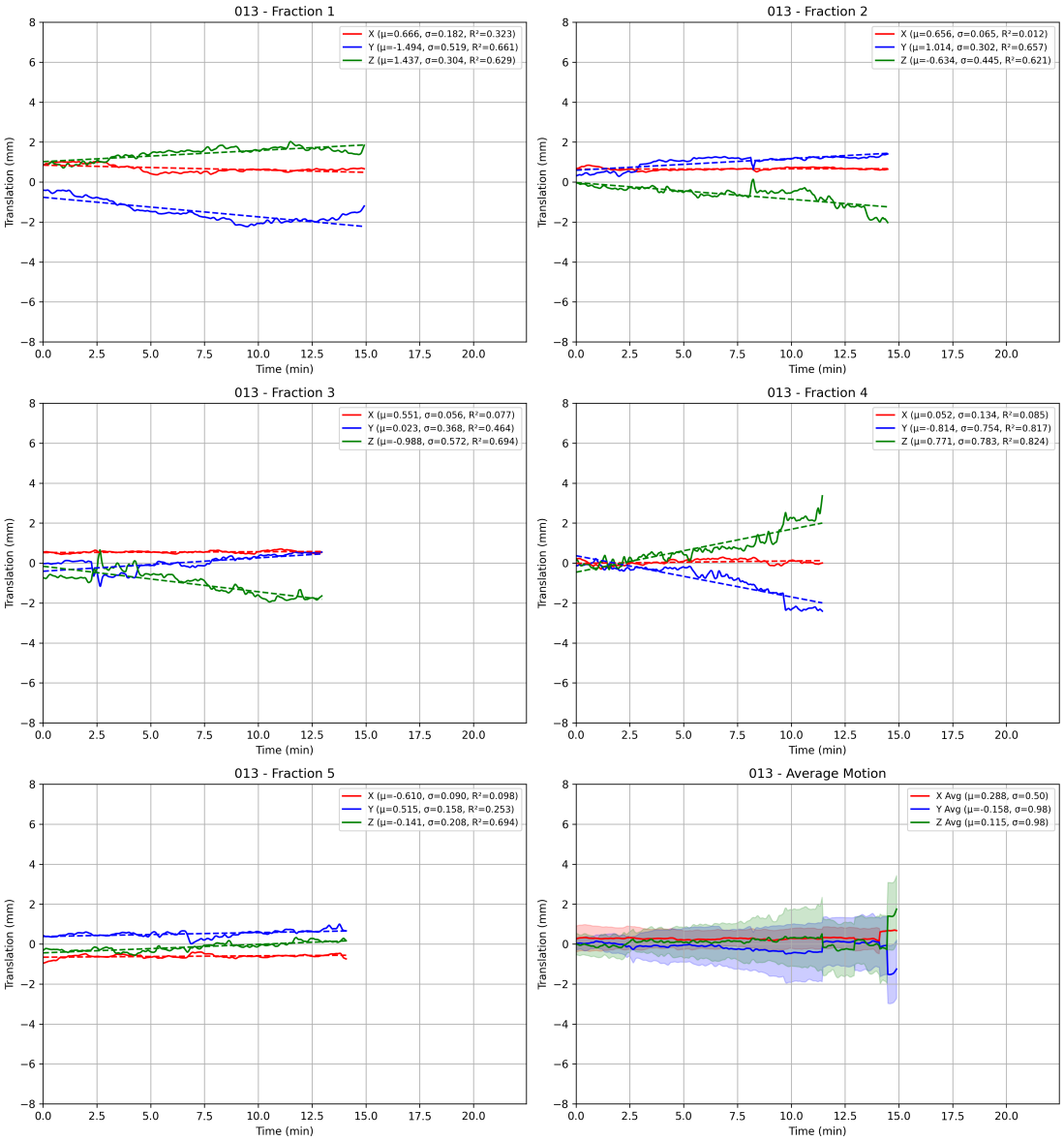

Figure B.13: Filtered traces plot for patient 013

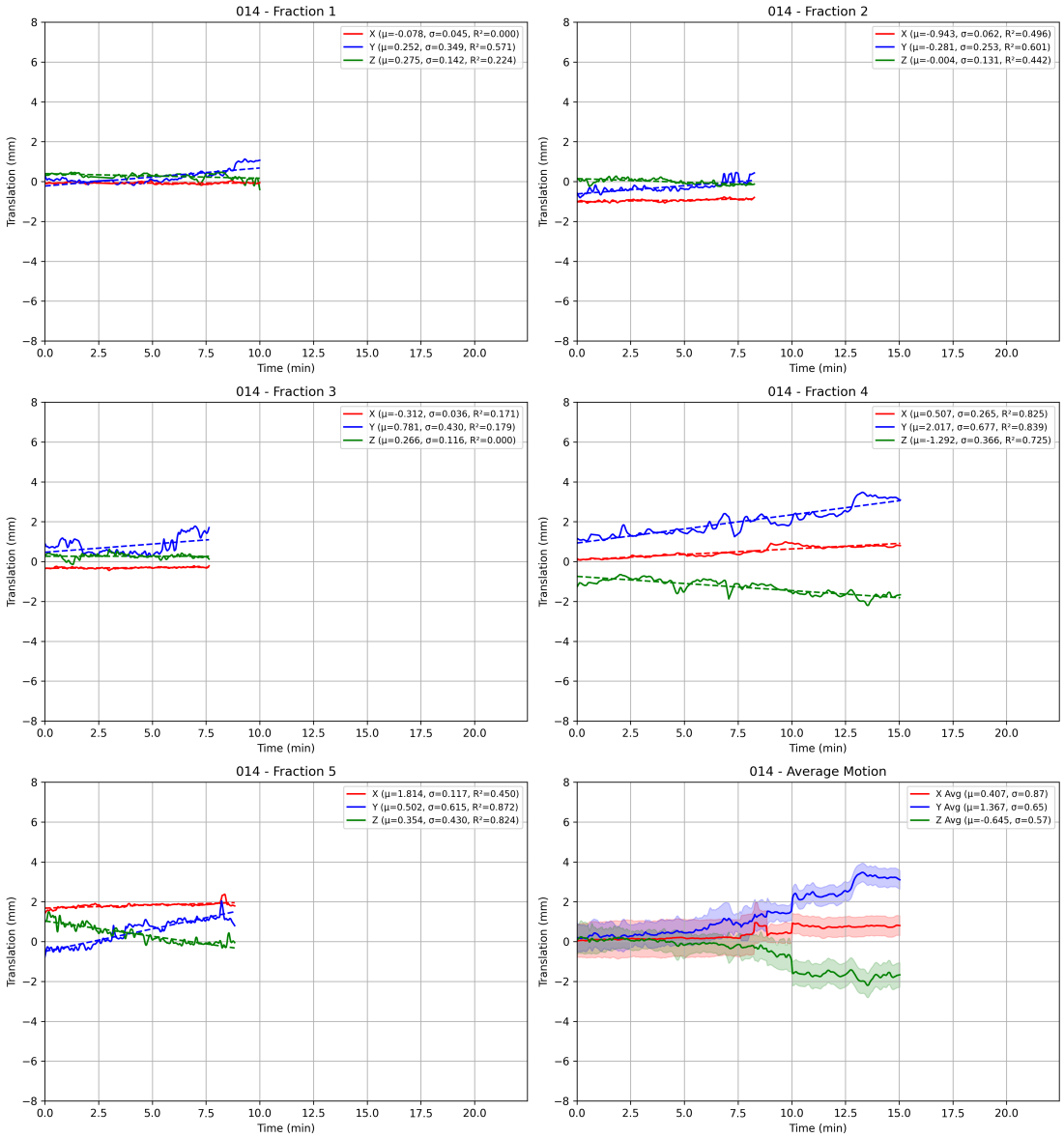

Figure B.14: Filtered traces plot for patient 014

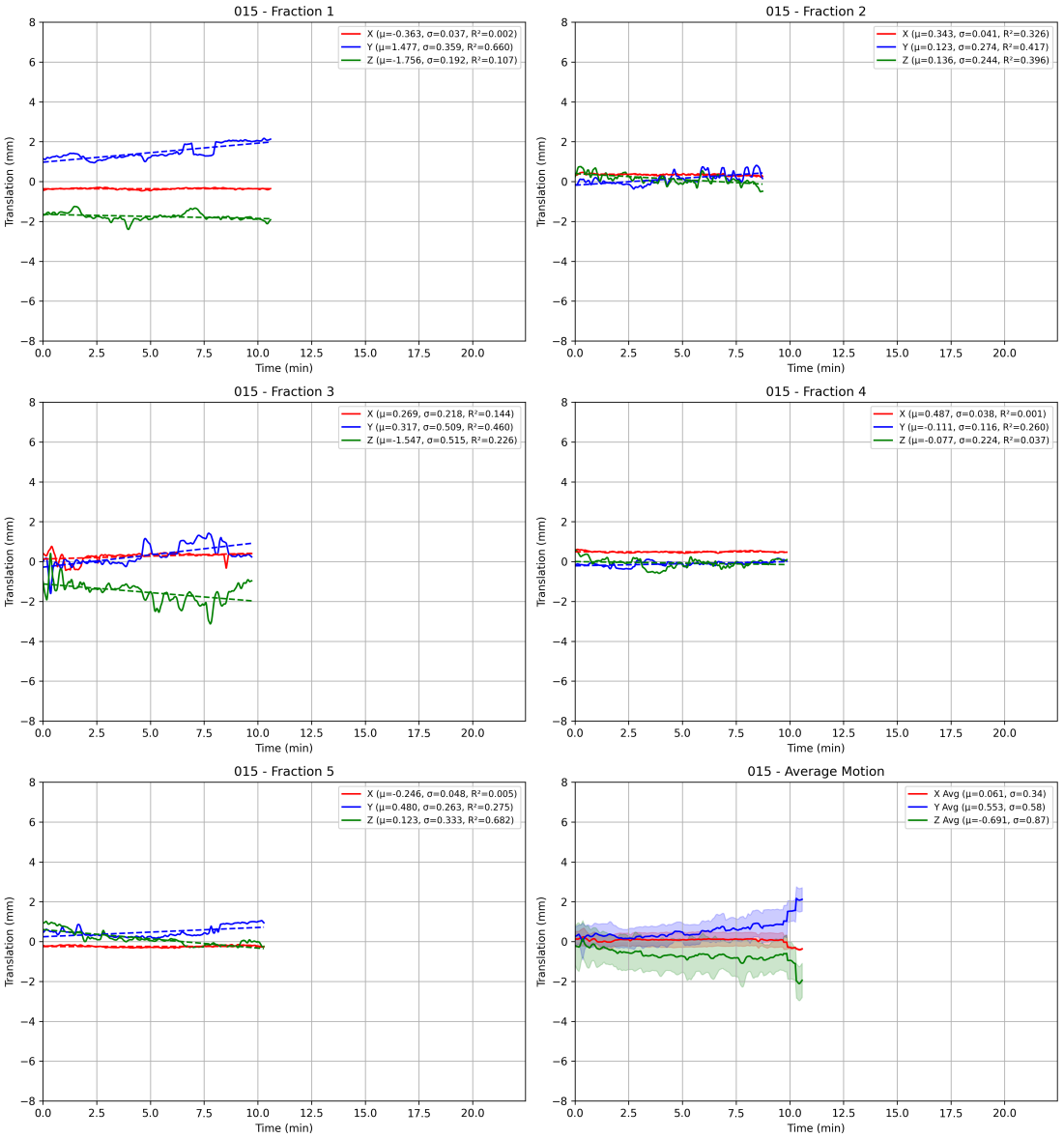

Figure B.15: Filtered traces plot for patient 015

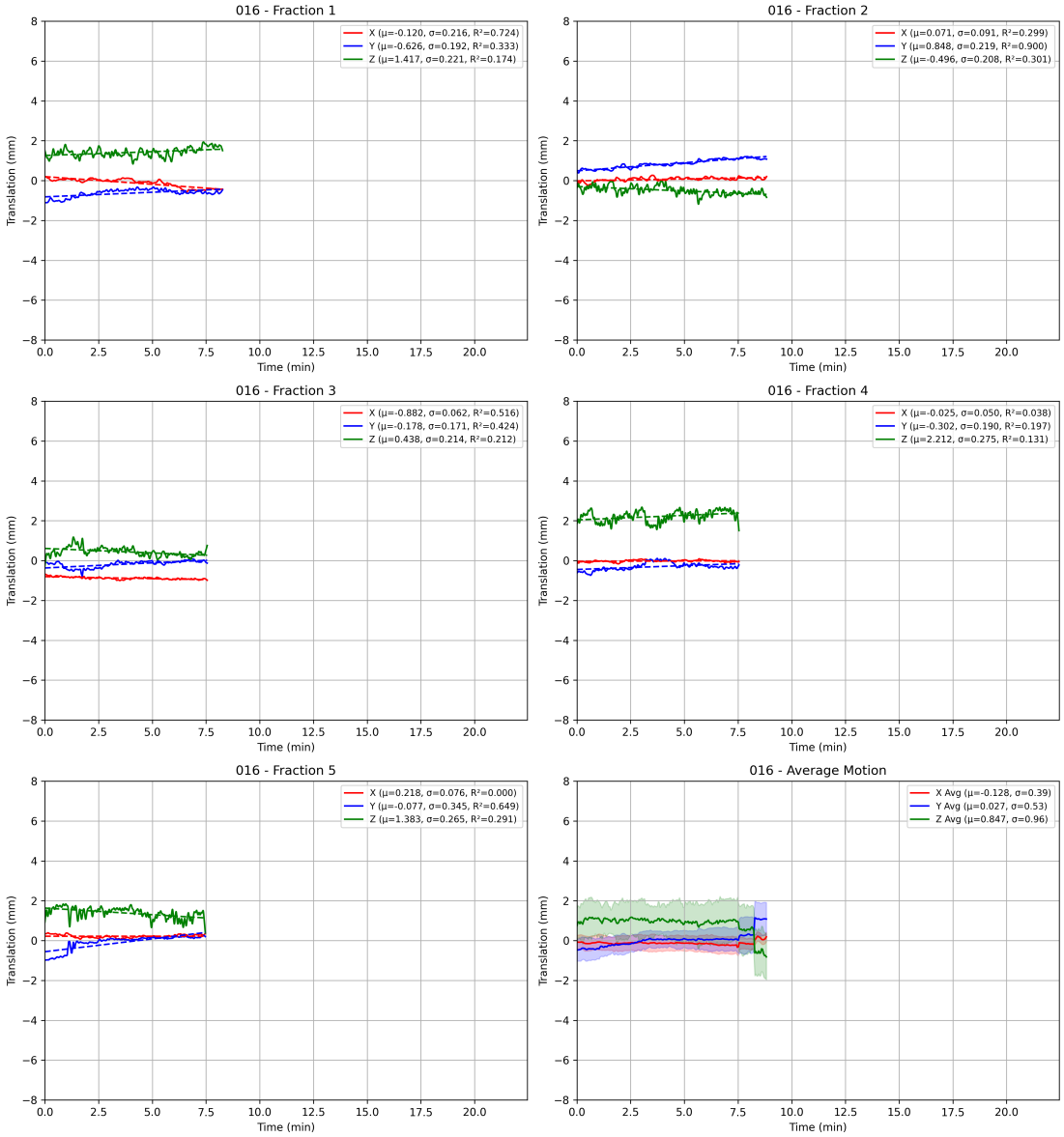

Figure B.16: Filtered traces plot for patient 016

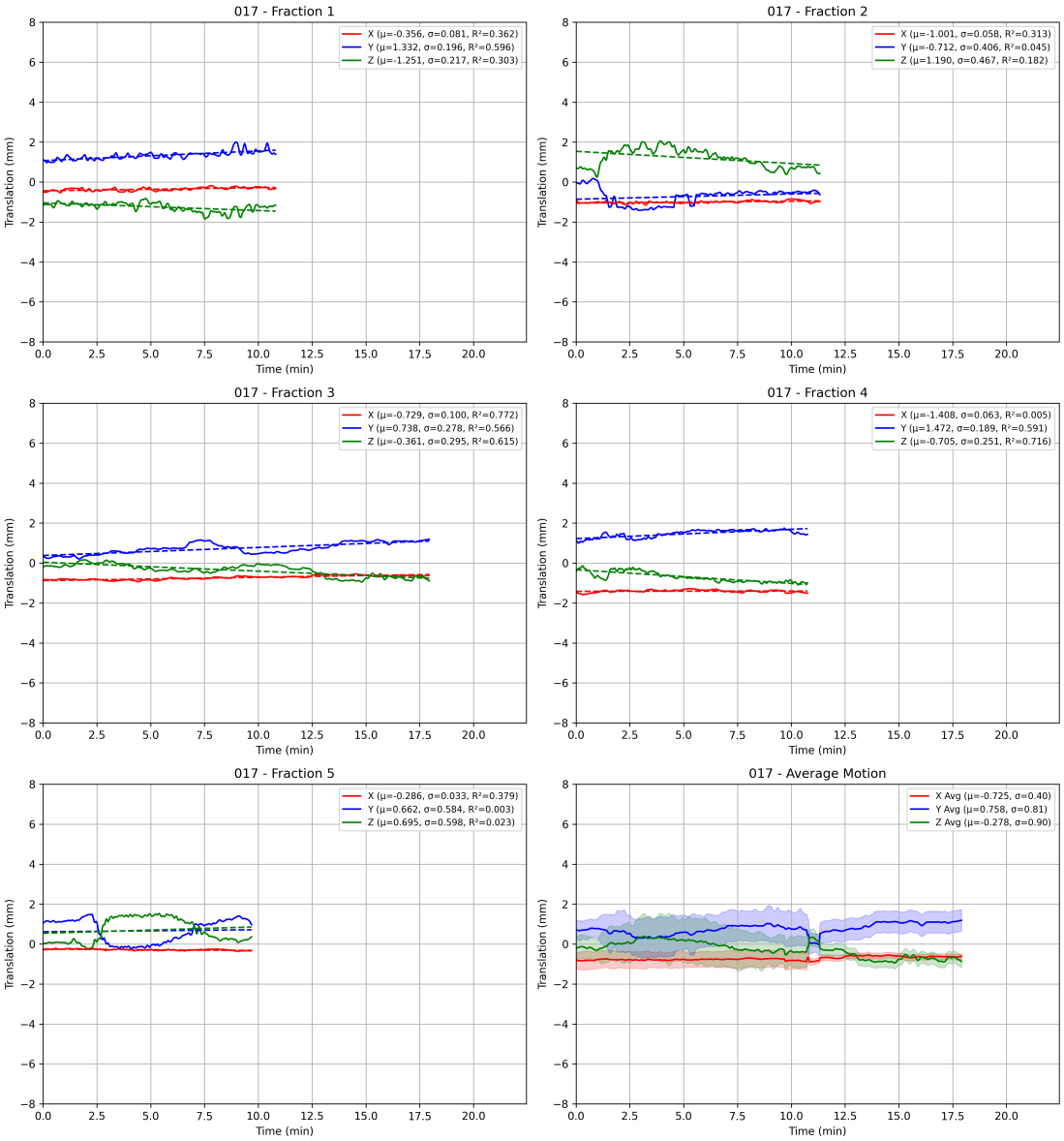

Figure B.17: Filtered traces plot for patient 017

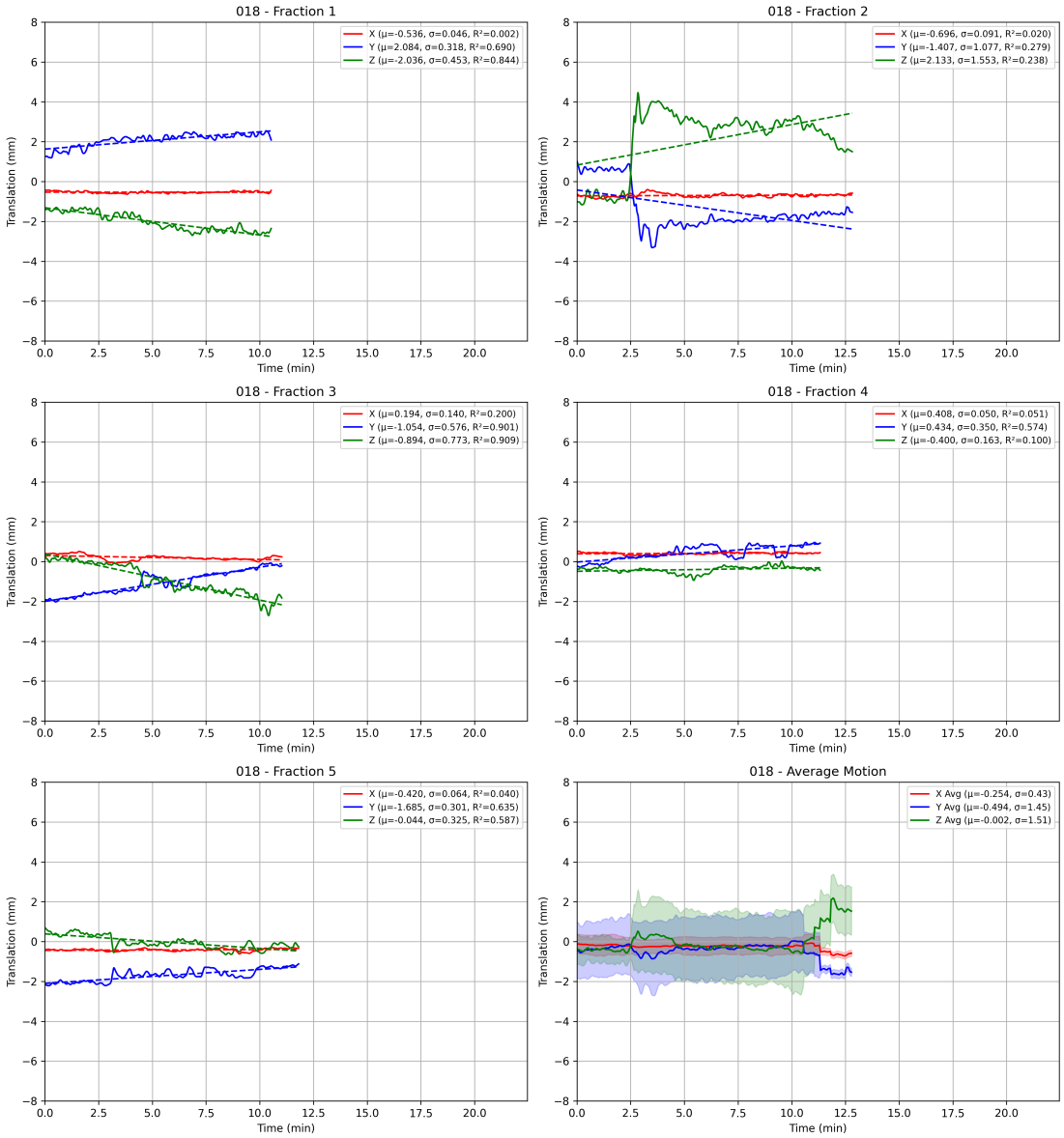

Figure B.18: Filtered traces plot for patient 018

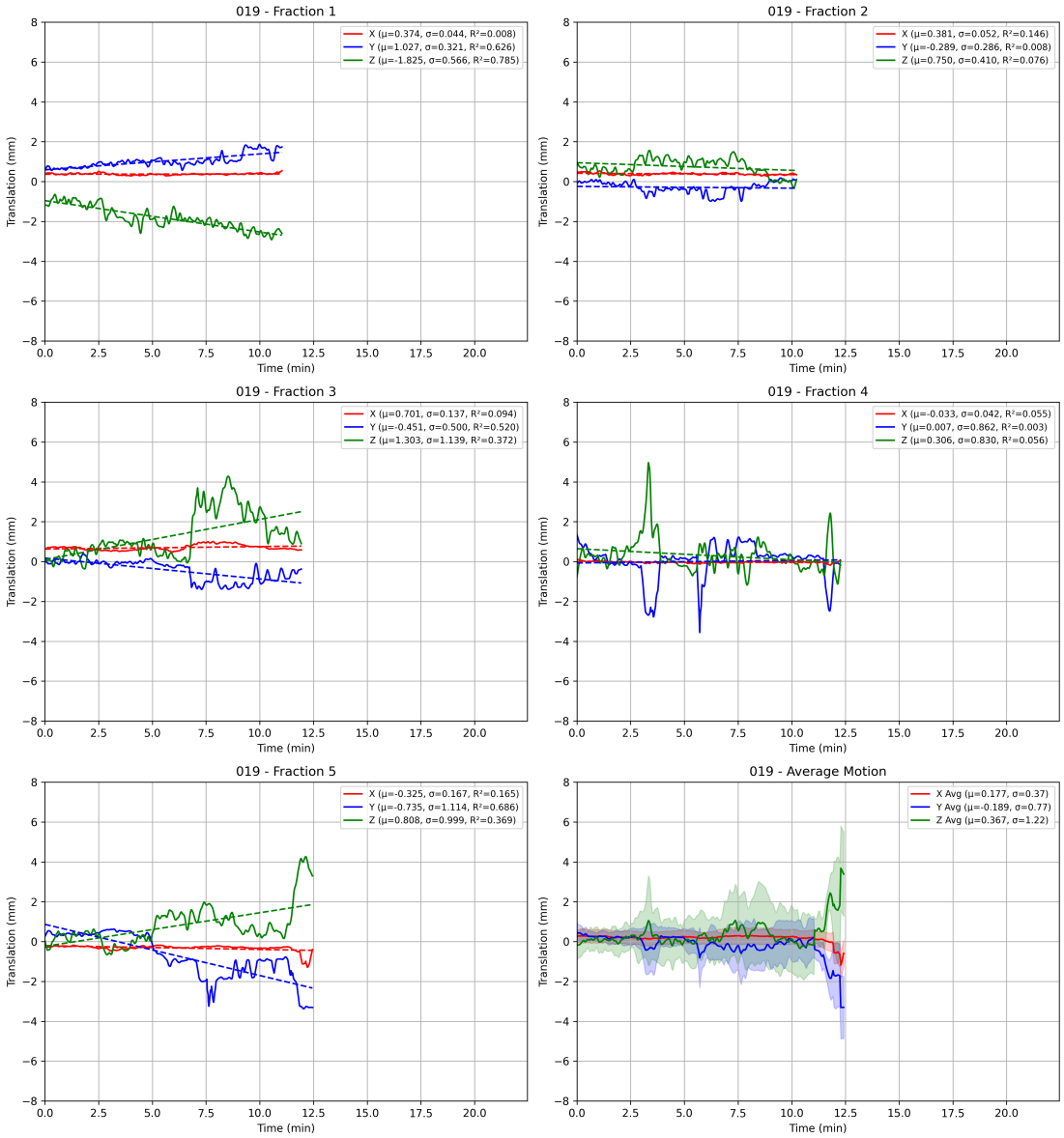

Figure B.19: Filtered traces plot for patient 019

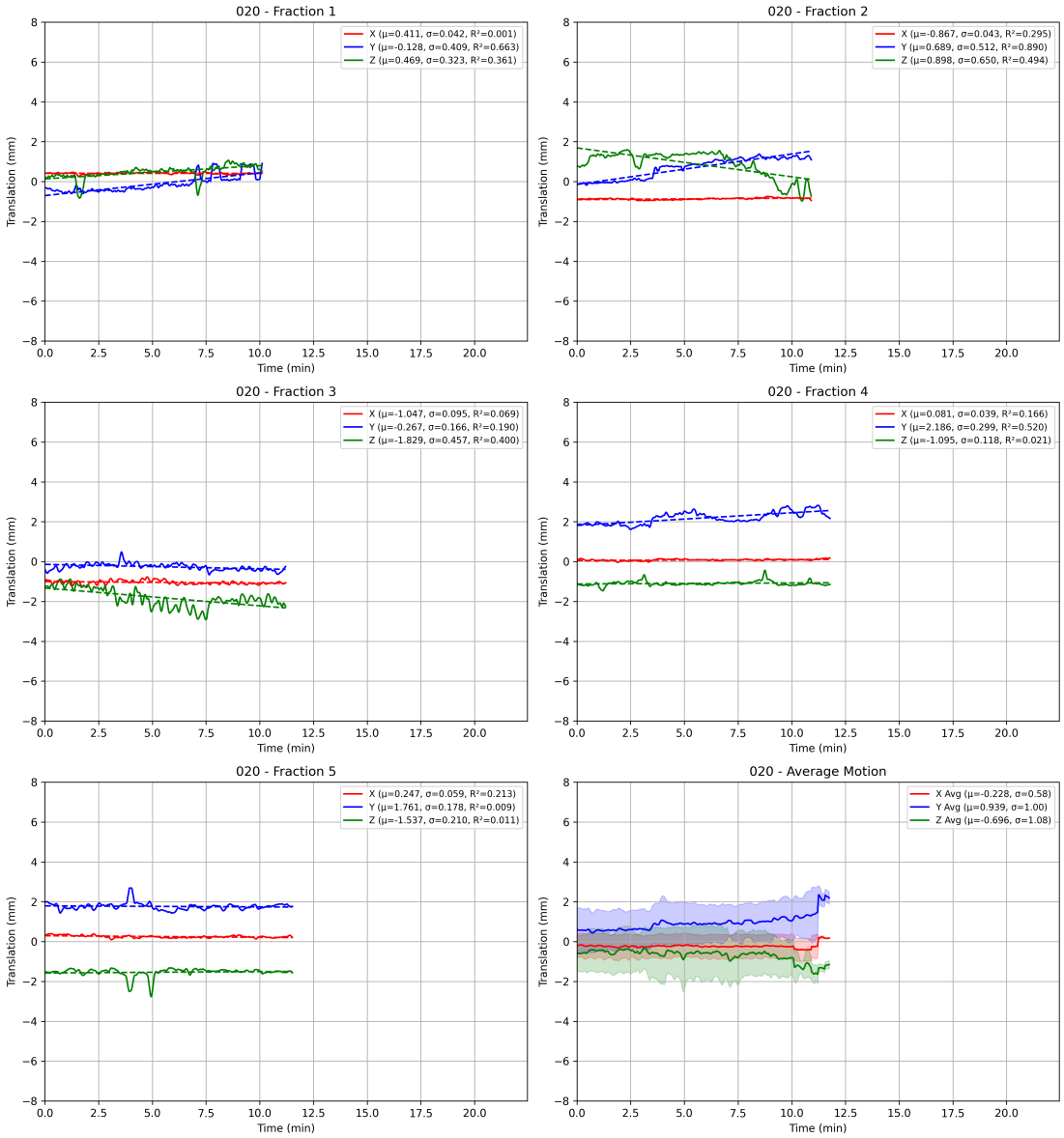

Figure B.20: Filtered traces plot for patient 020

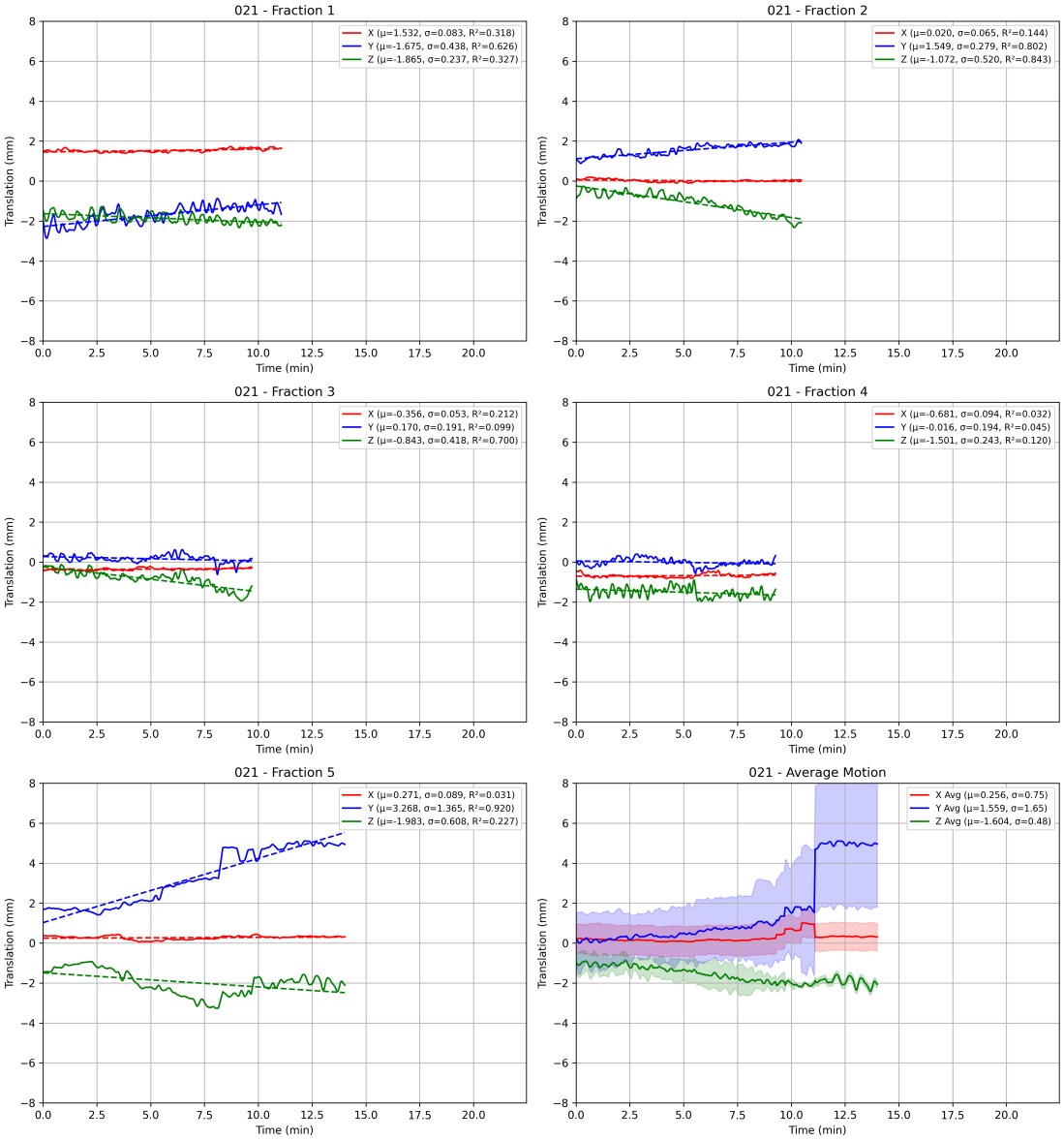

Figure B.21: Filtered traces plot for patient 021

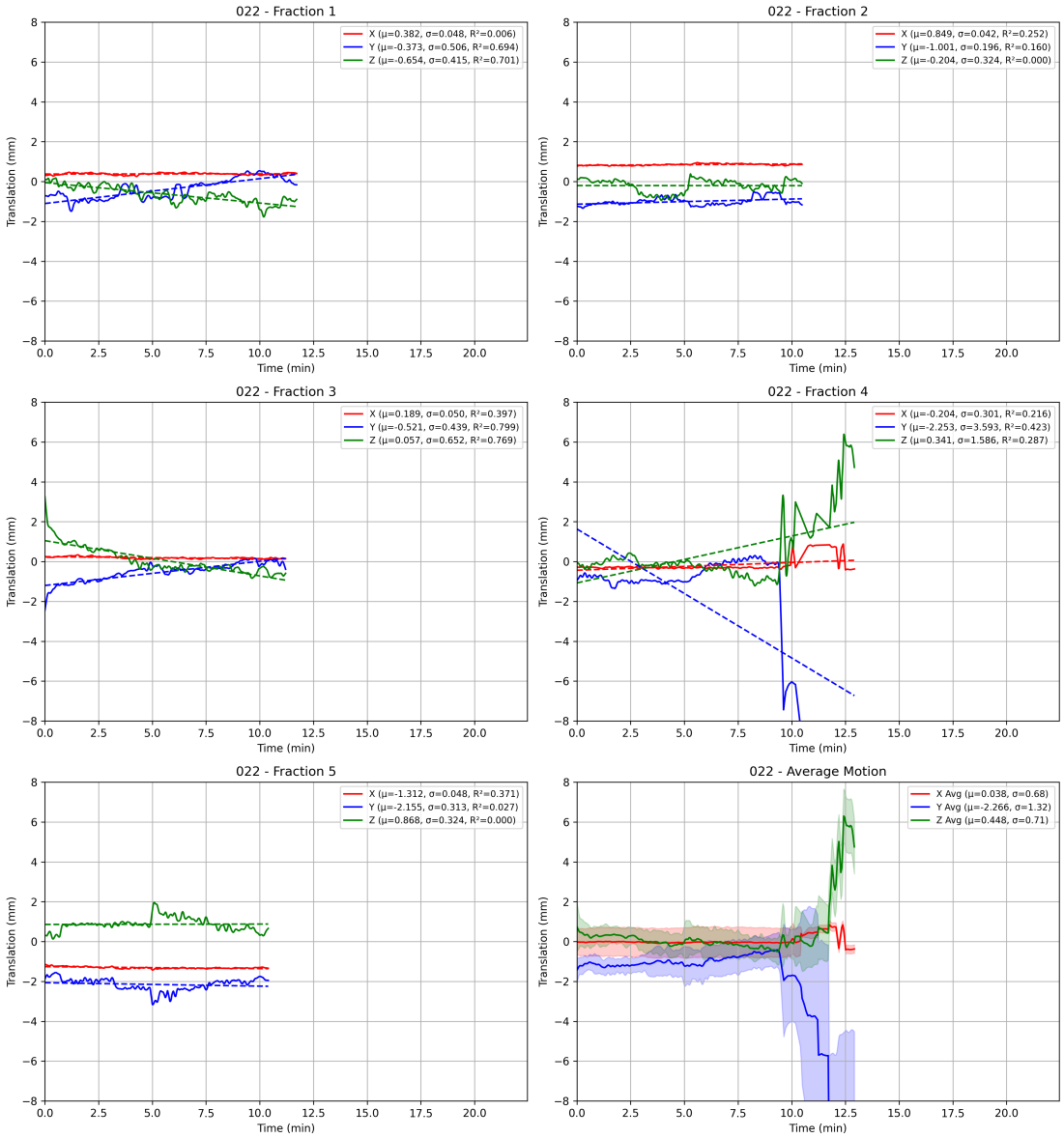

Figure B.22: Filtered traces plot for patient 022

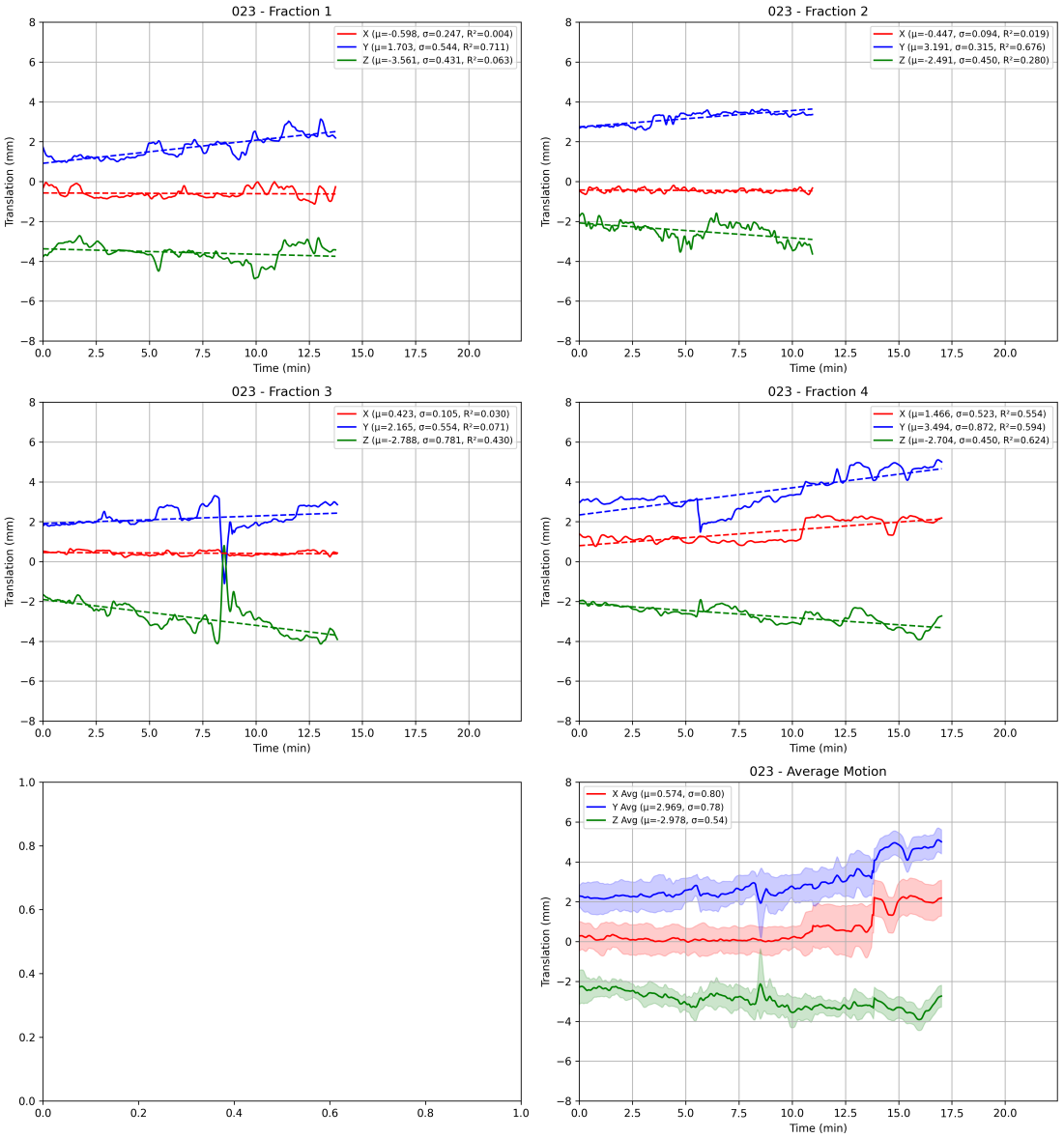

Figure B.23: Filtered traces plot for patient 023

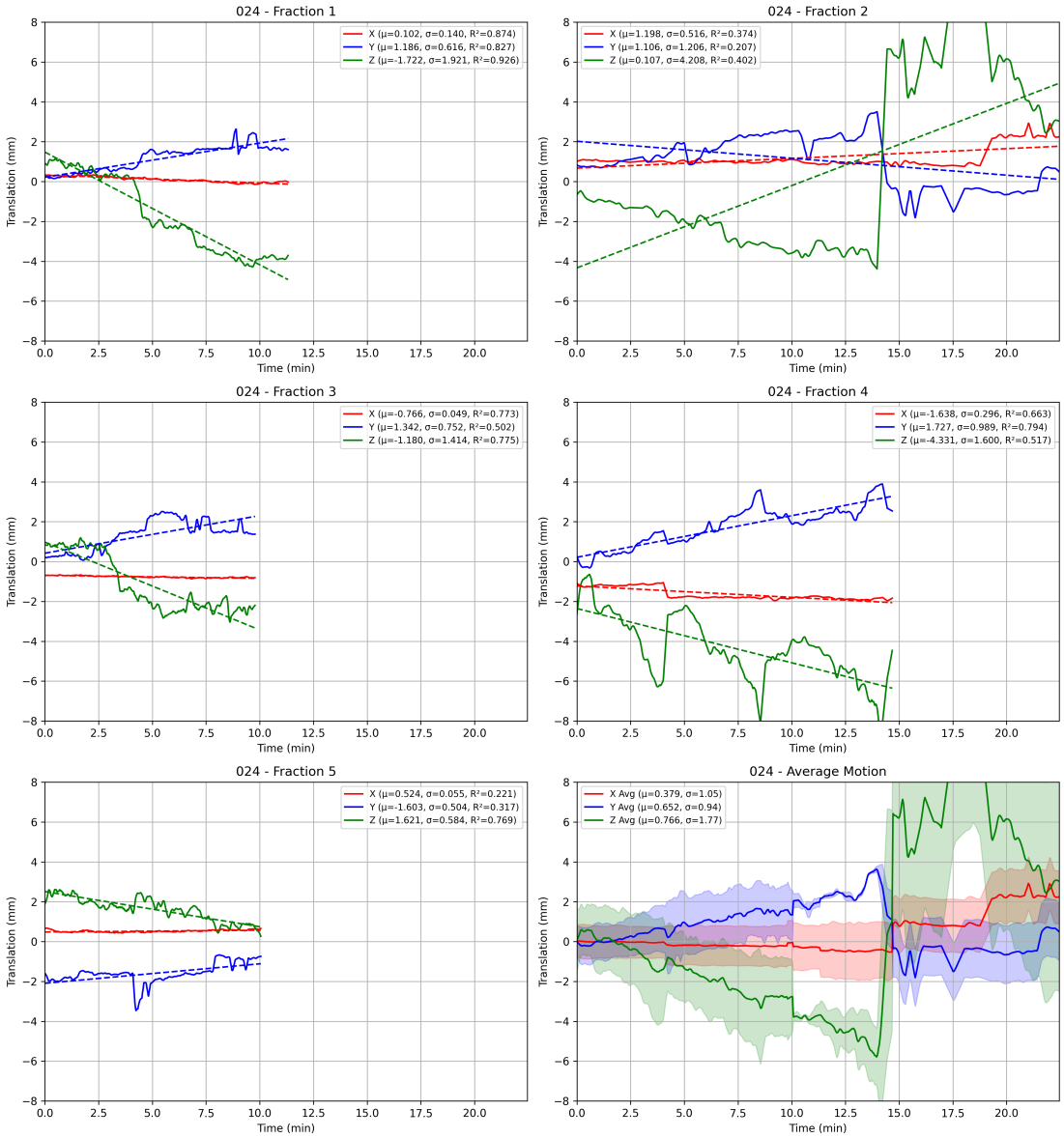

Figure B.24: Filtered traces plot for patient 024

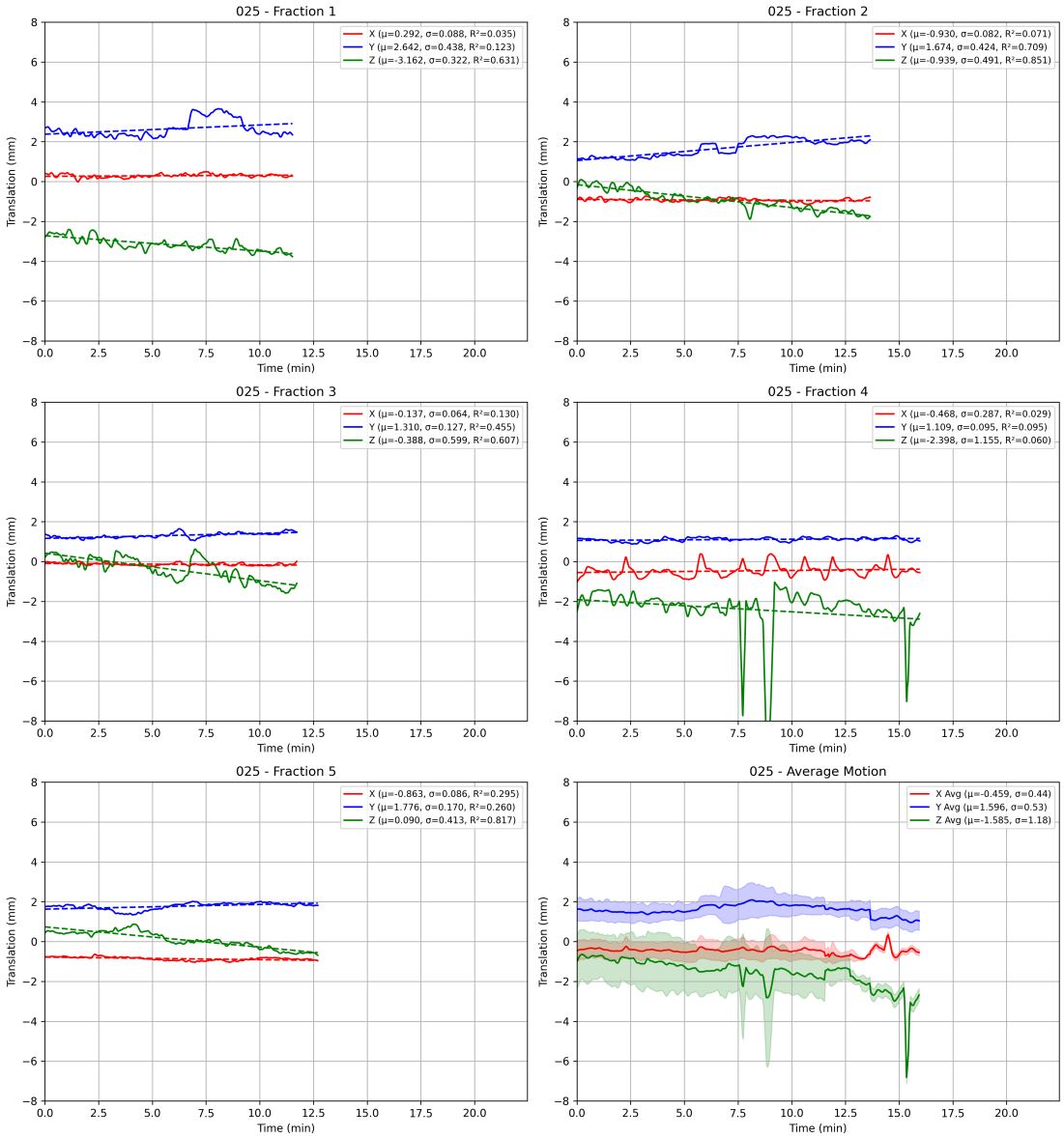

Figure B.25: Filtered traces plot for patient 025

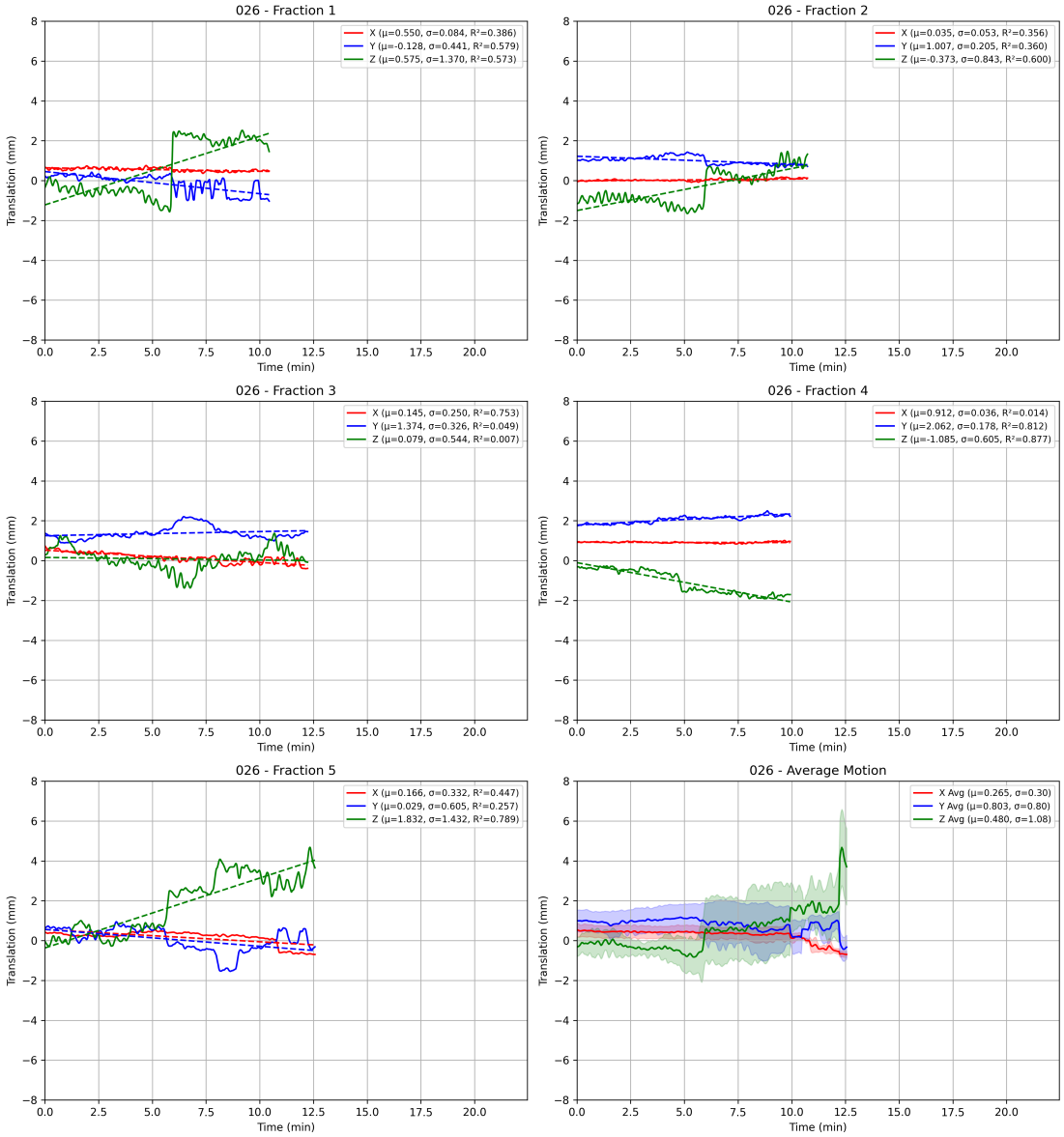

Figure B.26: Filtered traces plot for patient 026

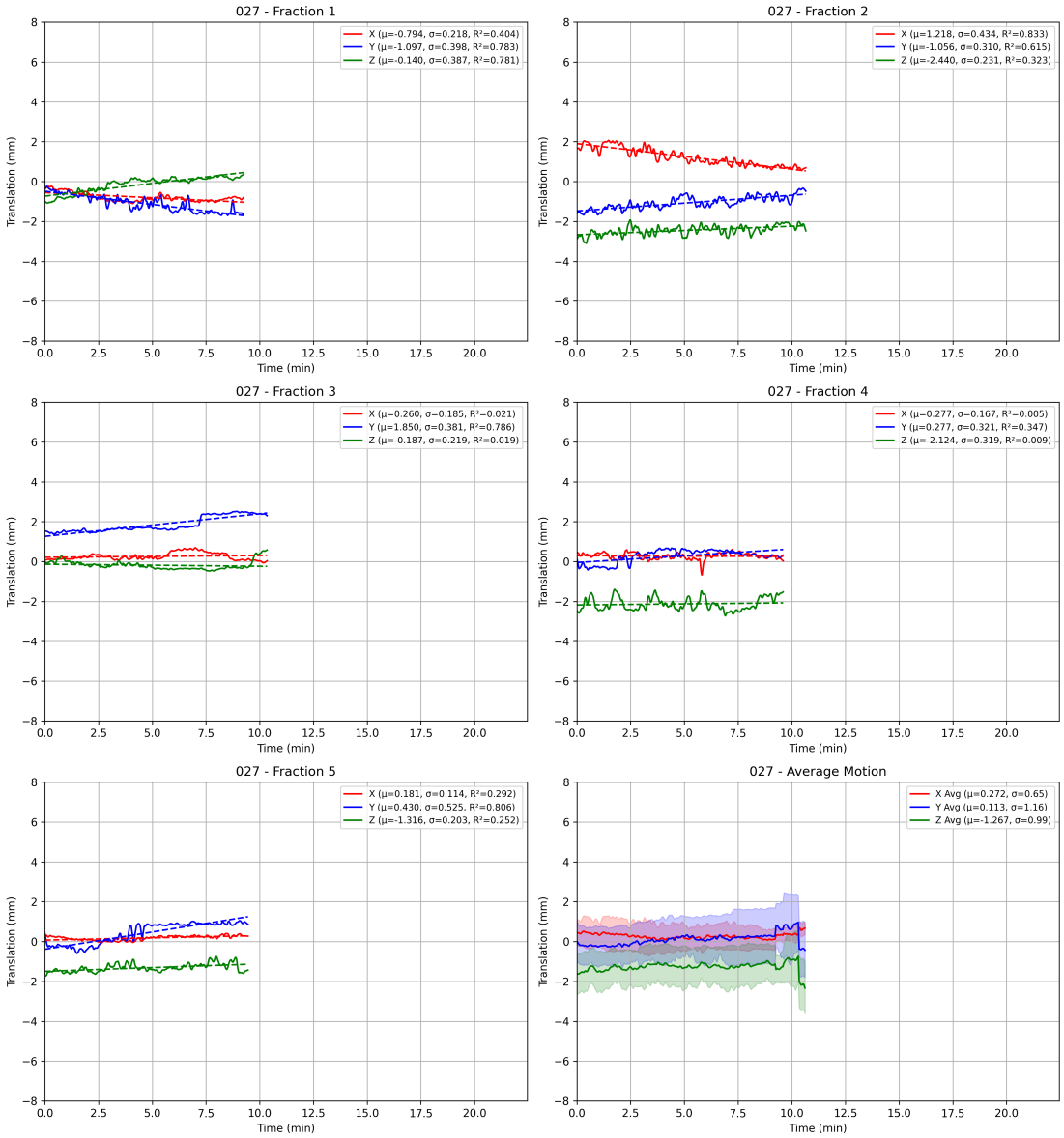

Figure B.27: Filtered traces plot for patient 027

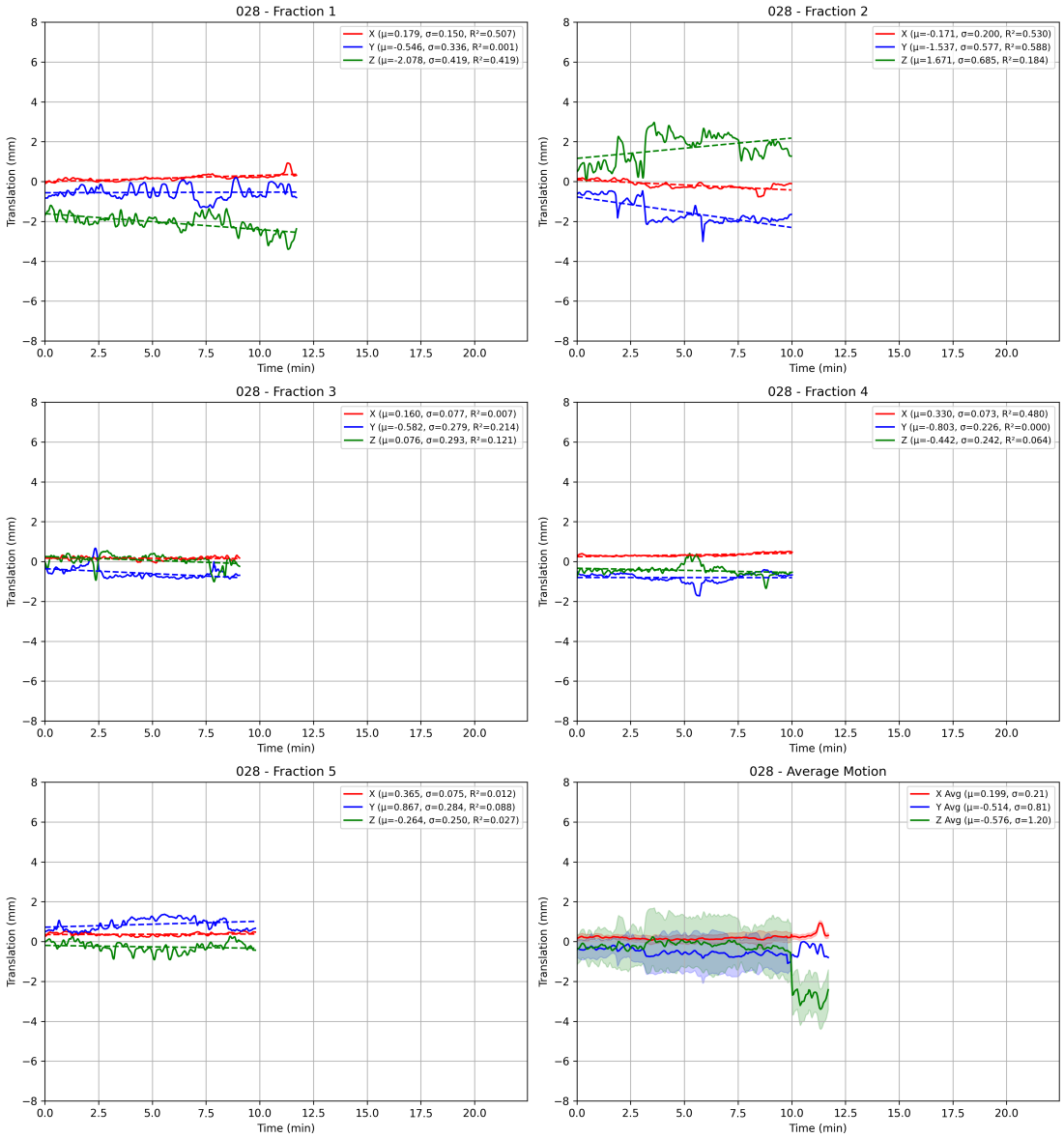

Figure B.28: Filtered traces plot for patient 028

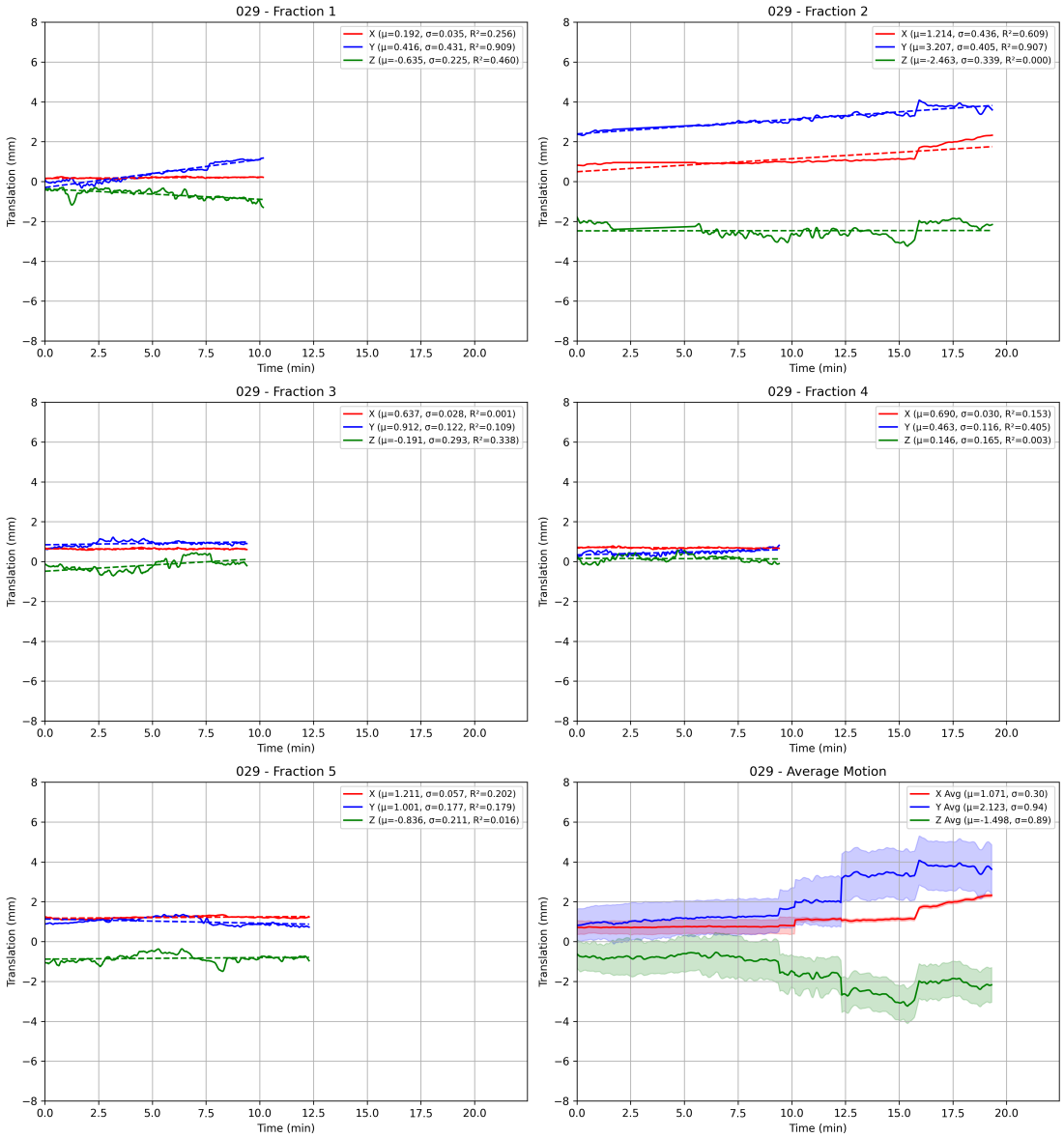

Figure B.29: Filtered traces plot for patient 029

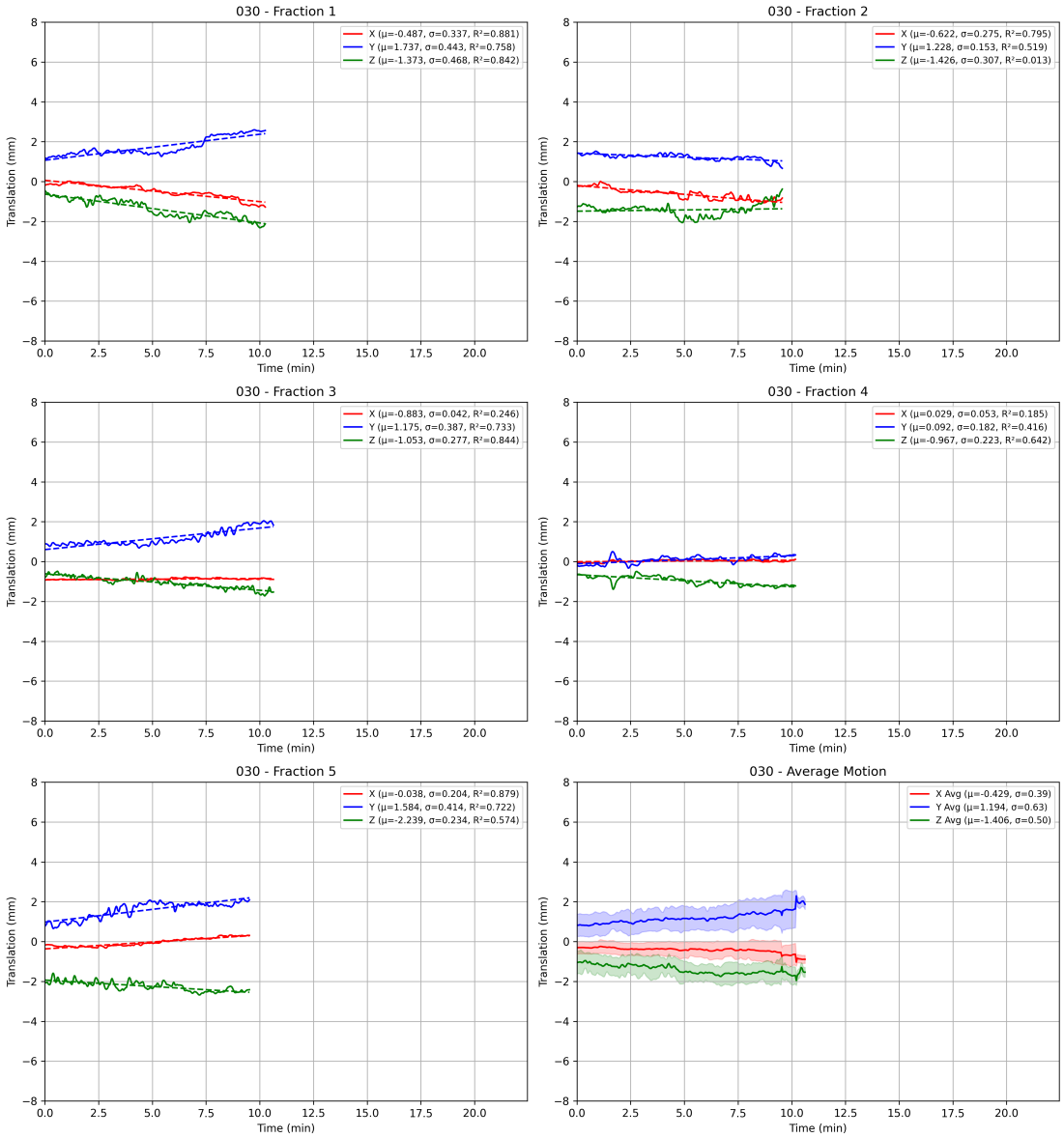

Figure B.30: Filtered traces plot for patient 030

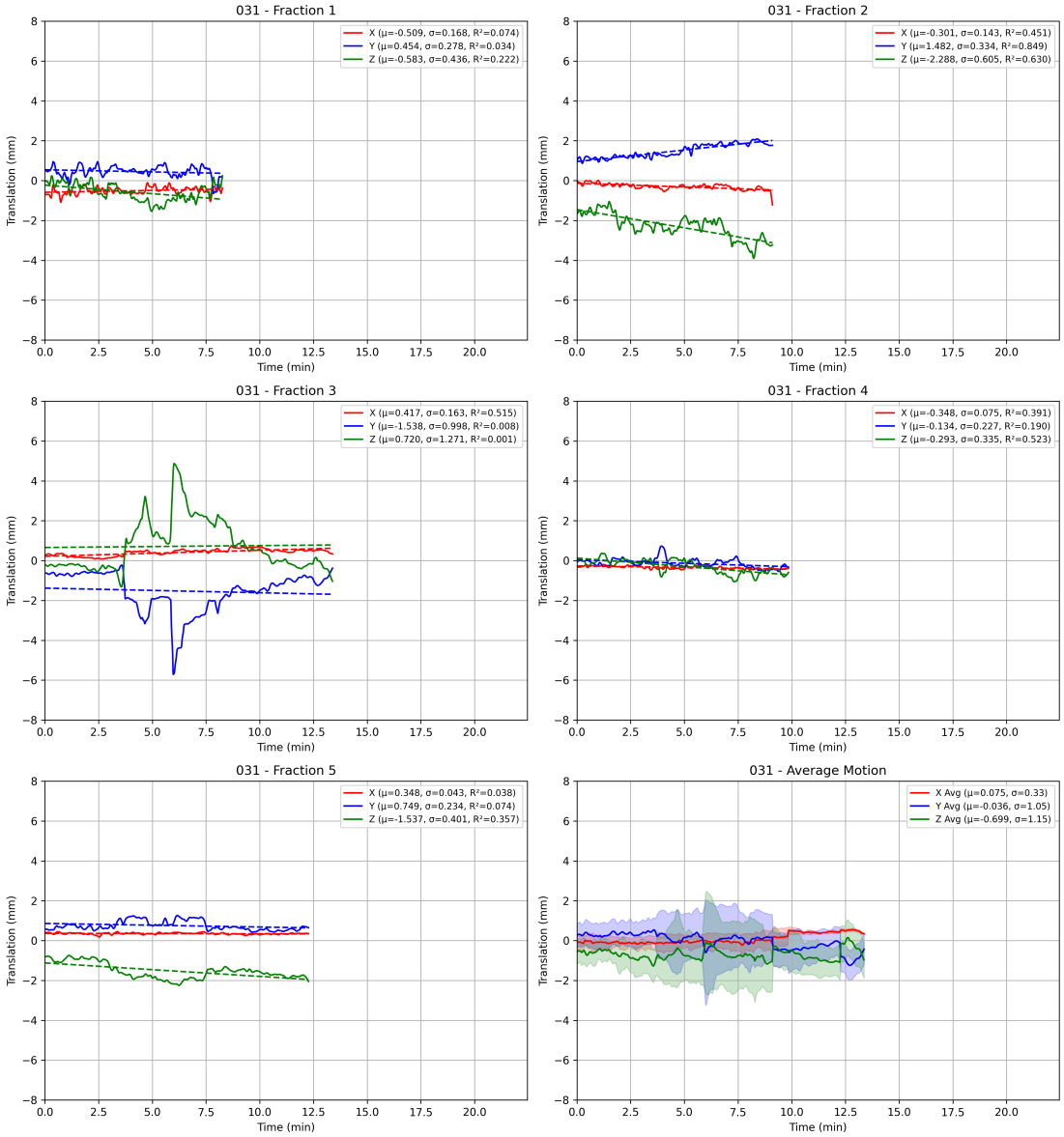

Figure B.31: Filtered traces plot for patient 031

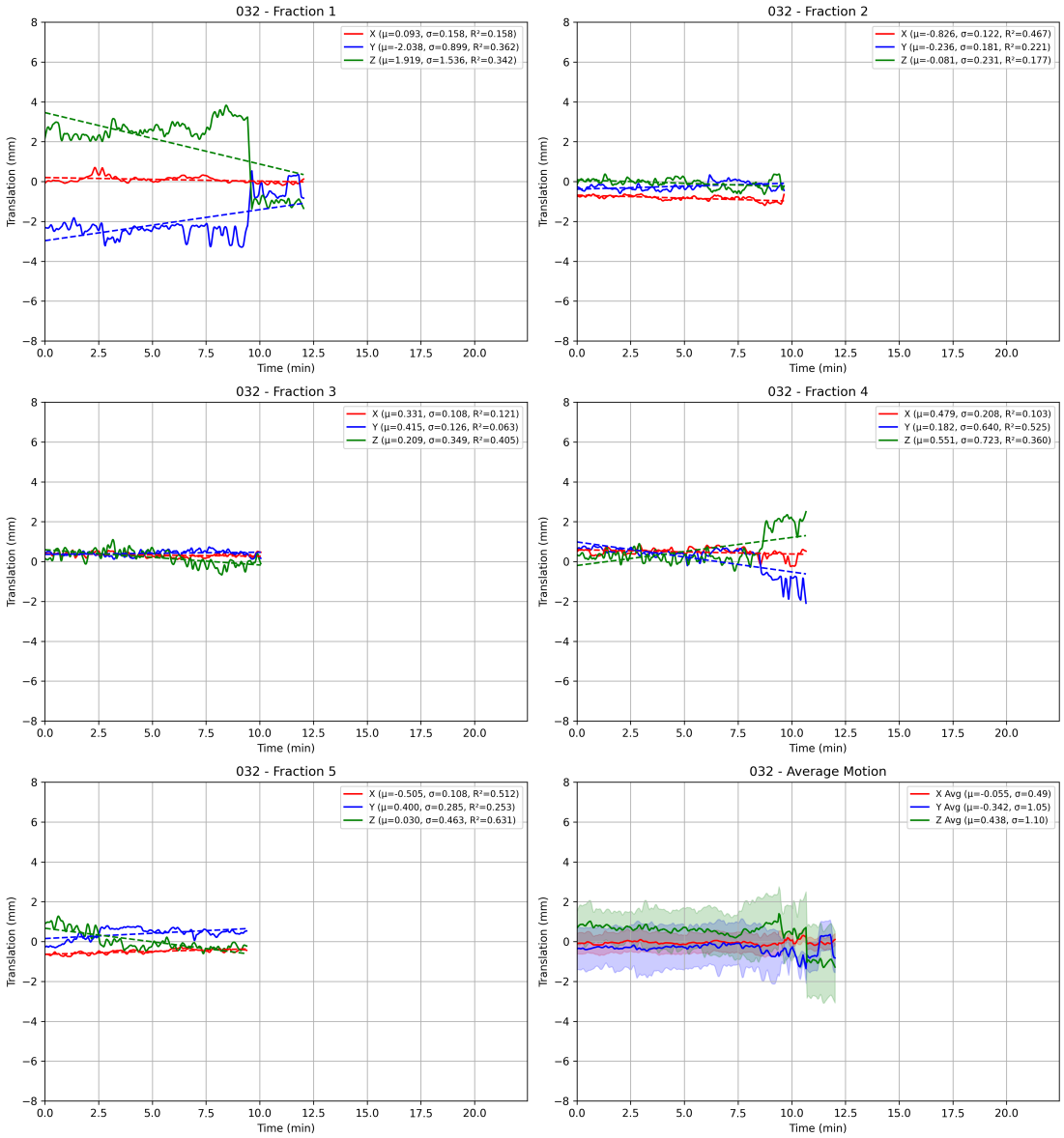

Figure B.32: Filtered traces plot for patient 032

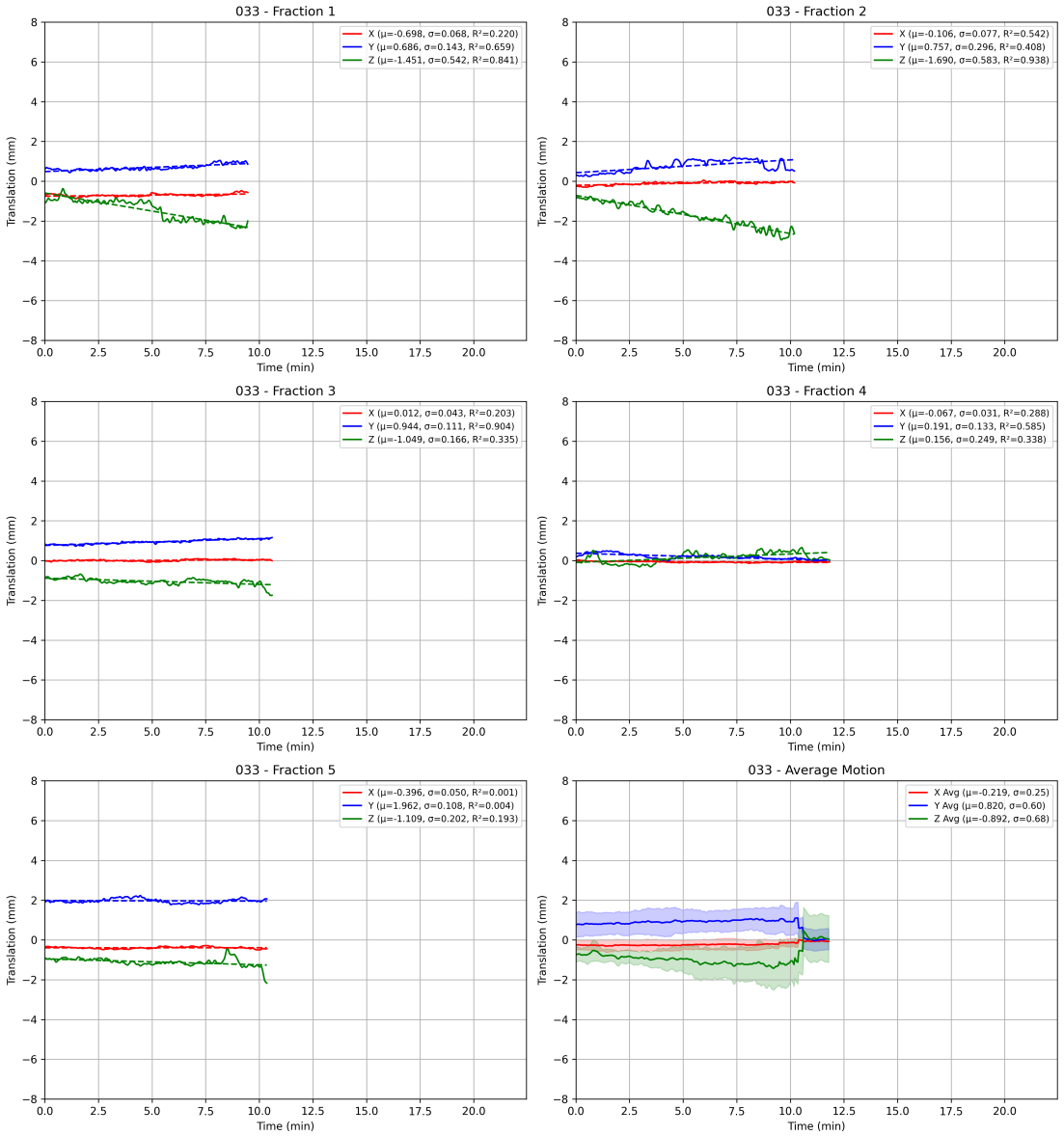

Figure B.33: Filtered traces plot for patient 033

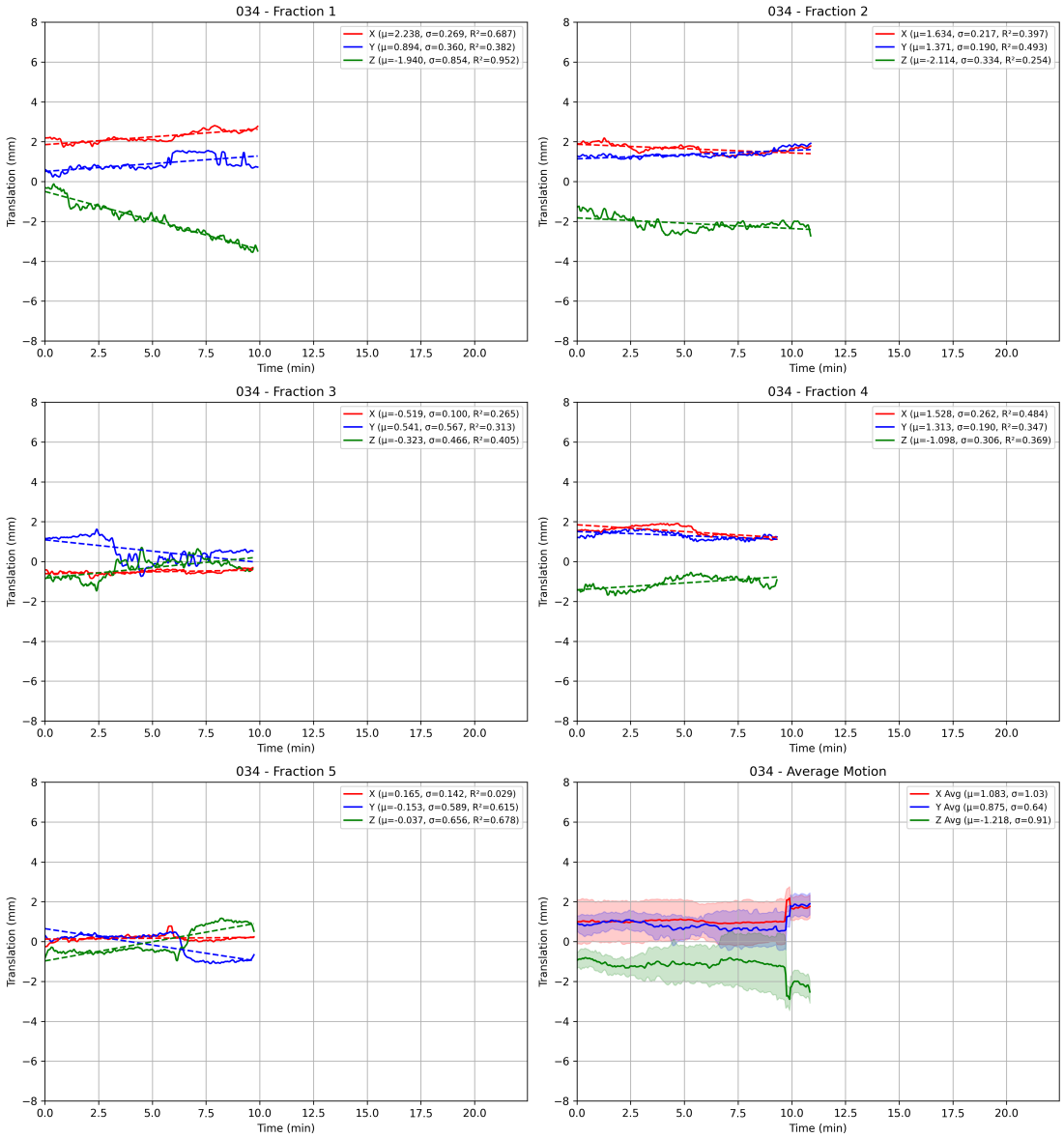

Figure B.34: Filtered traces plot for patient 034

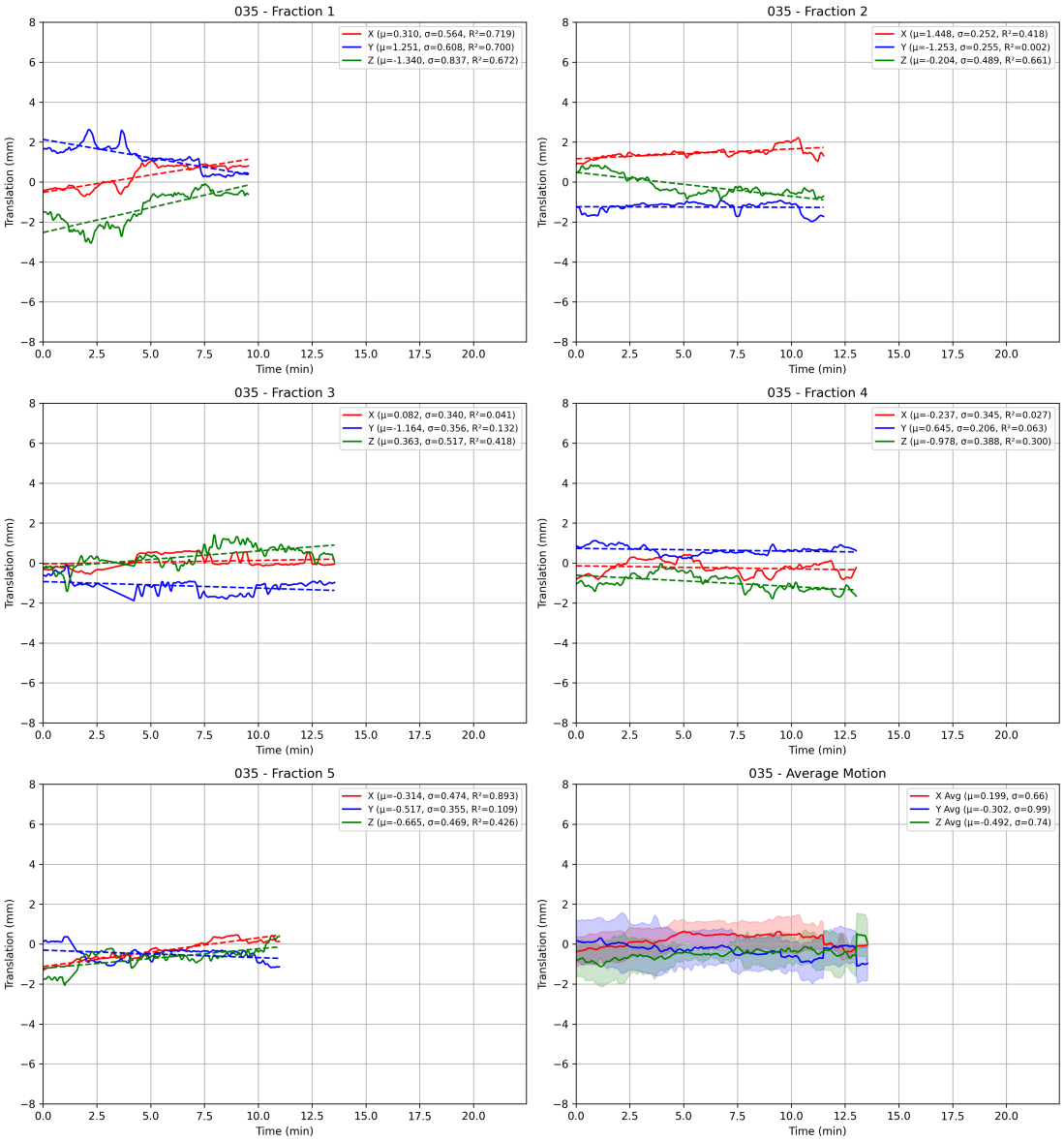

Figure B.35: Filtered traces plot for patient 035

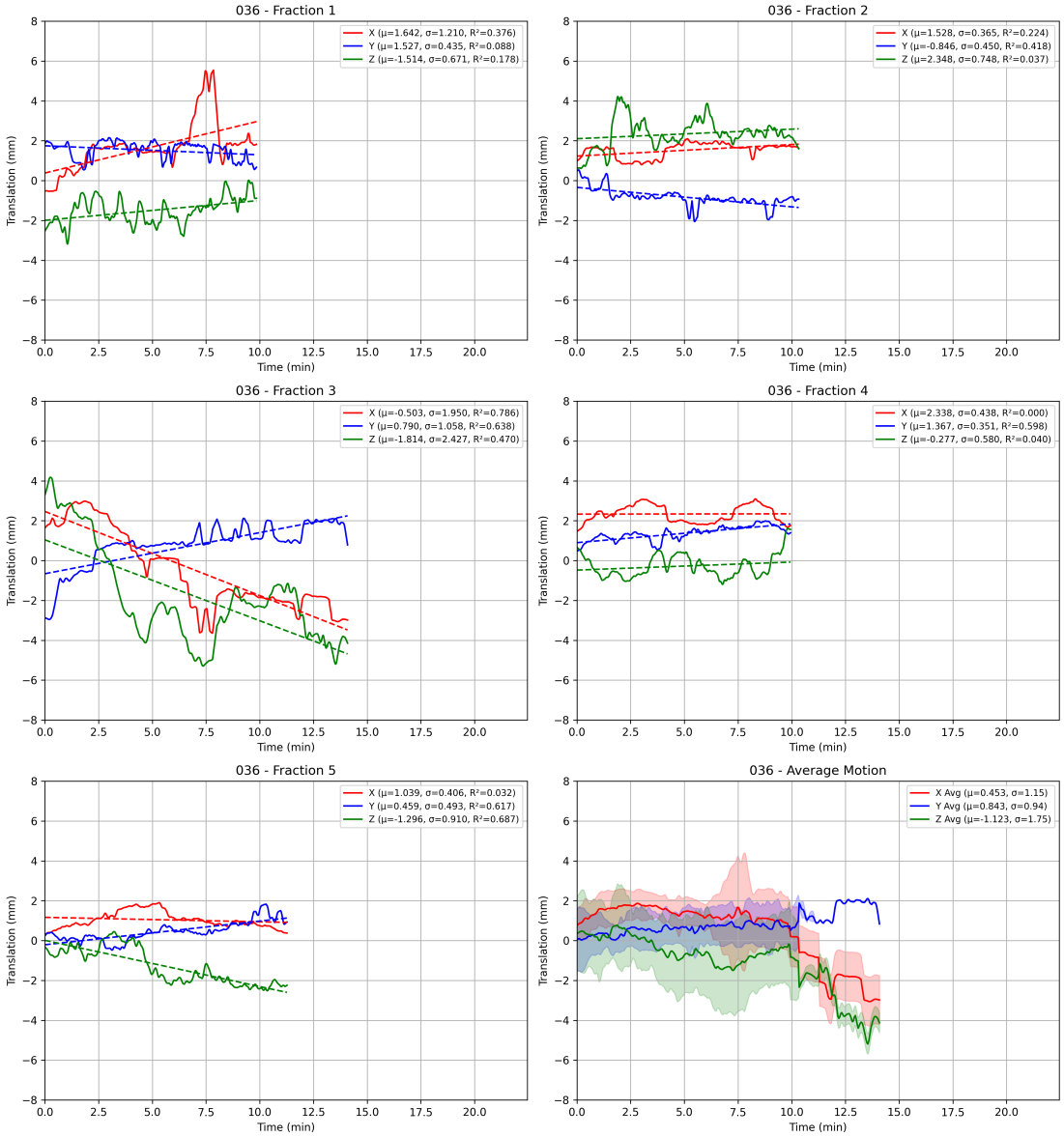

Figure B.36: Filtered traces plot for patient 036

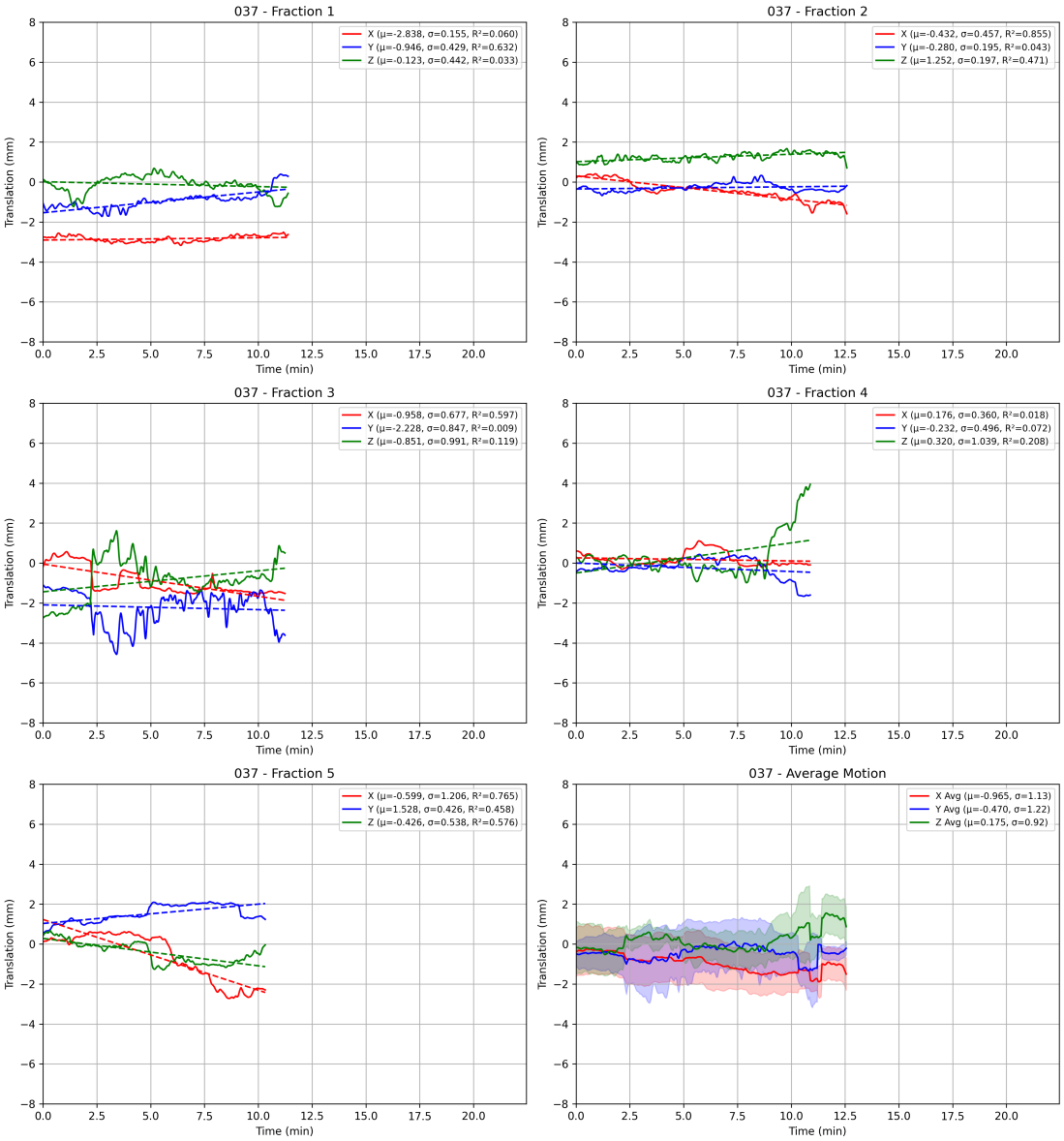

Figure B.37: Filtered traces plot for patient 037

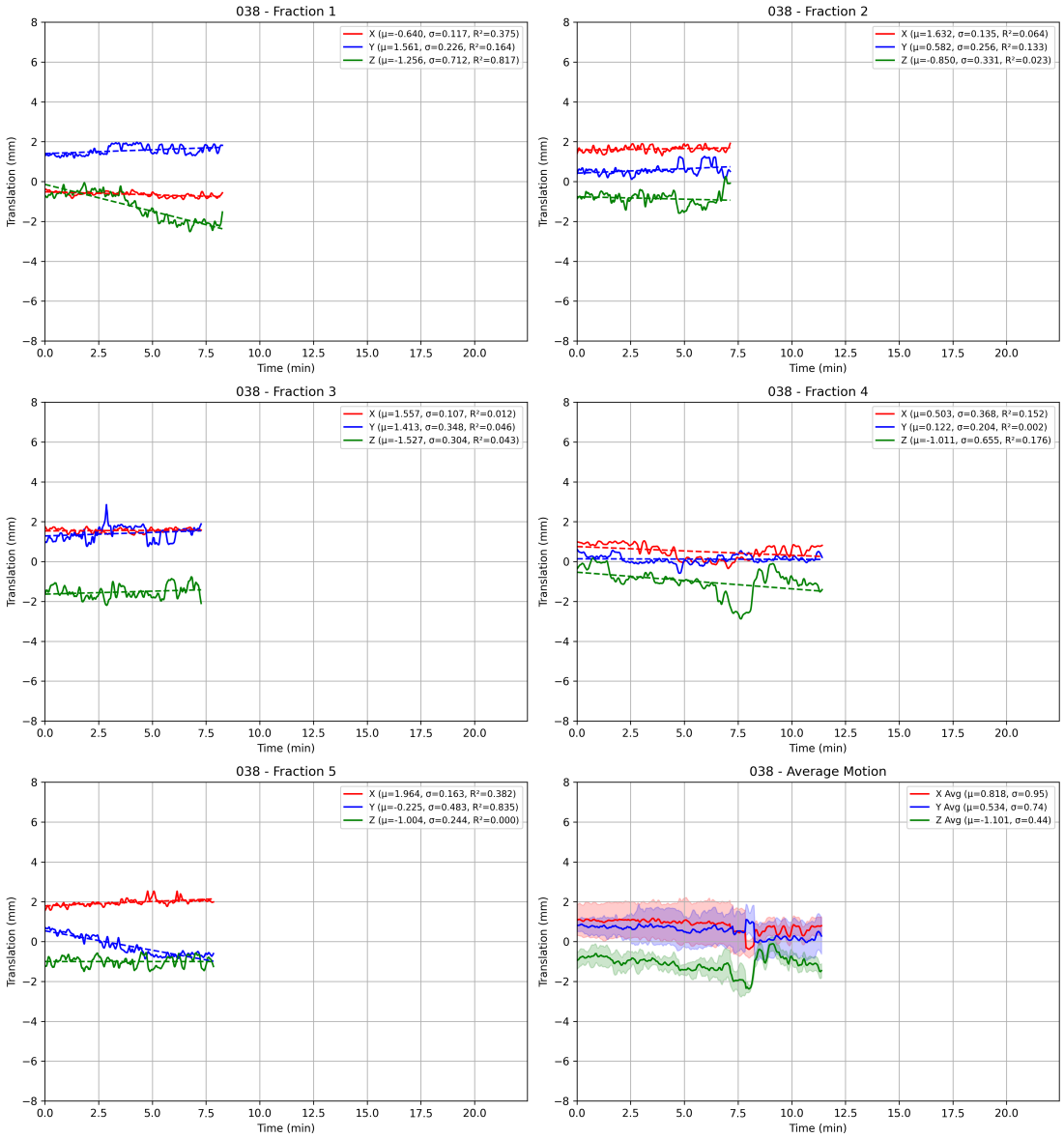

Figure B.38: Filtered traces plot for patient 038

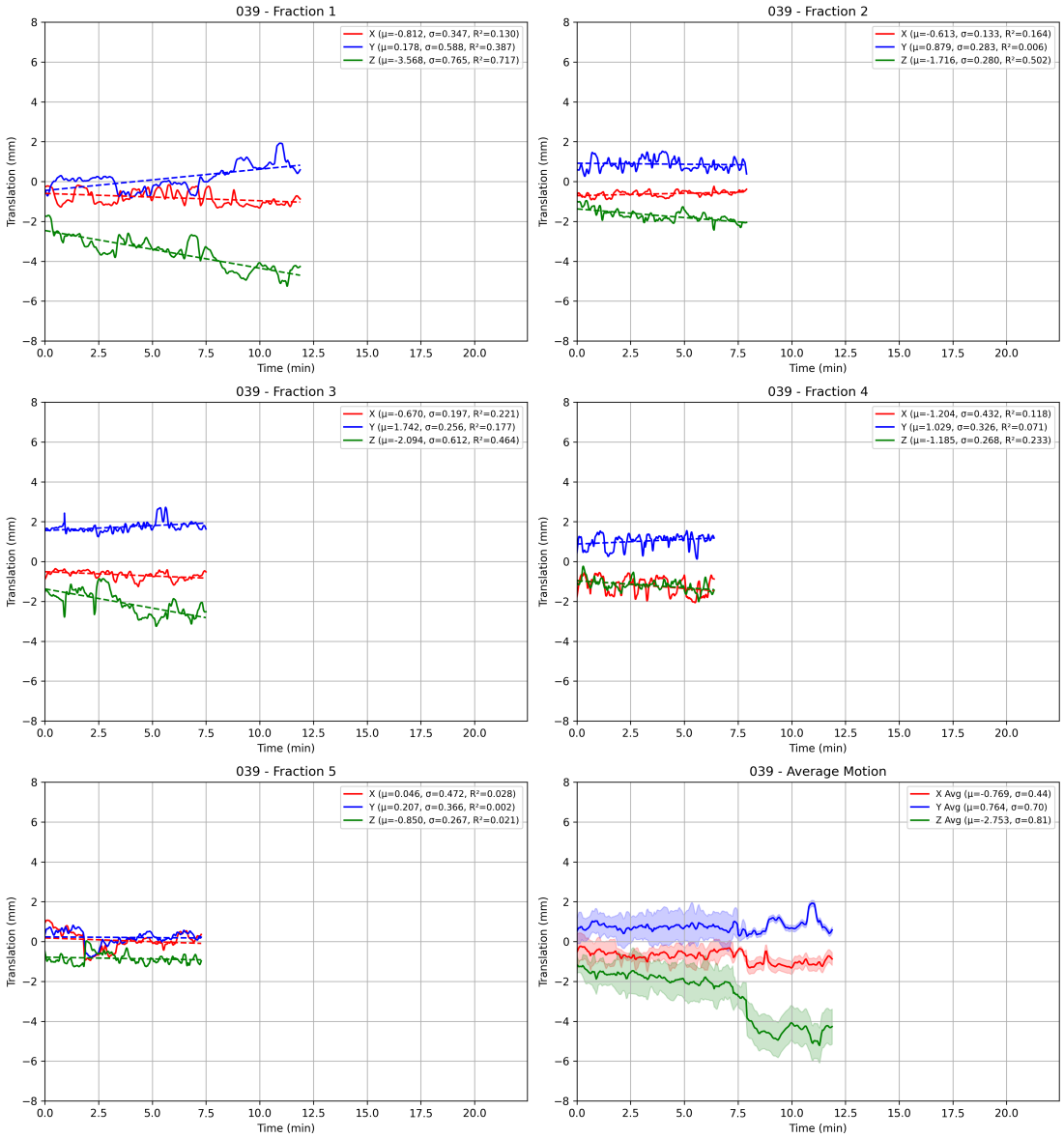

Figure B.39: Filtered traces plot for patient 039

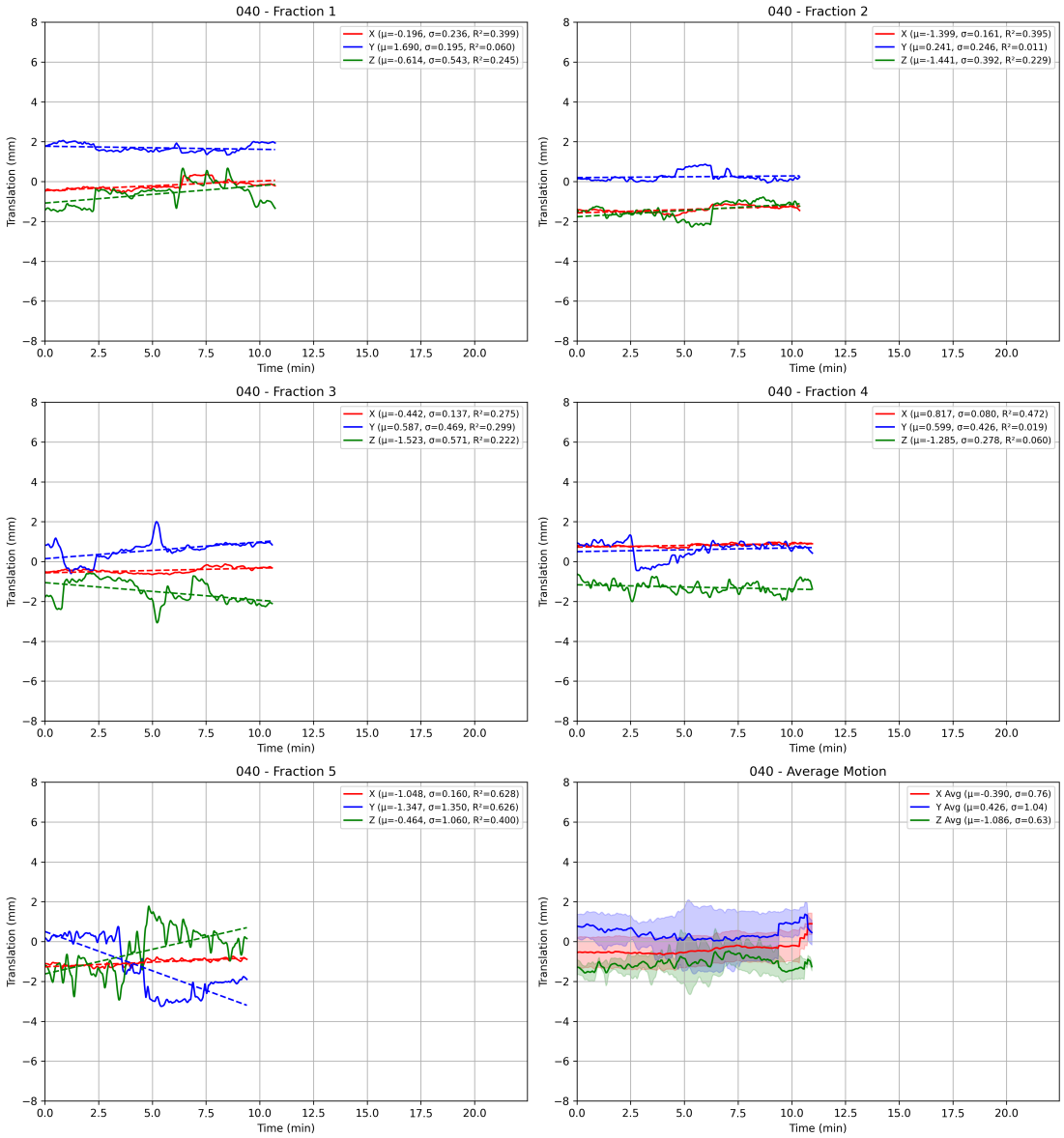

Figure B.40: Filtered traces plot for patient 040

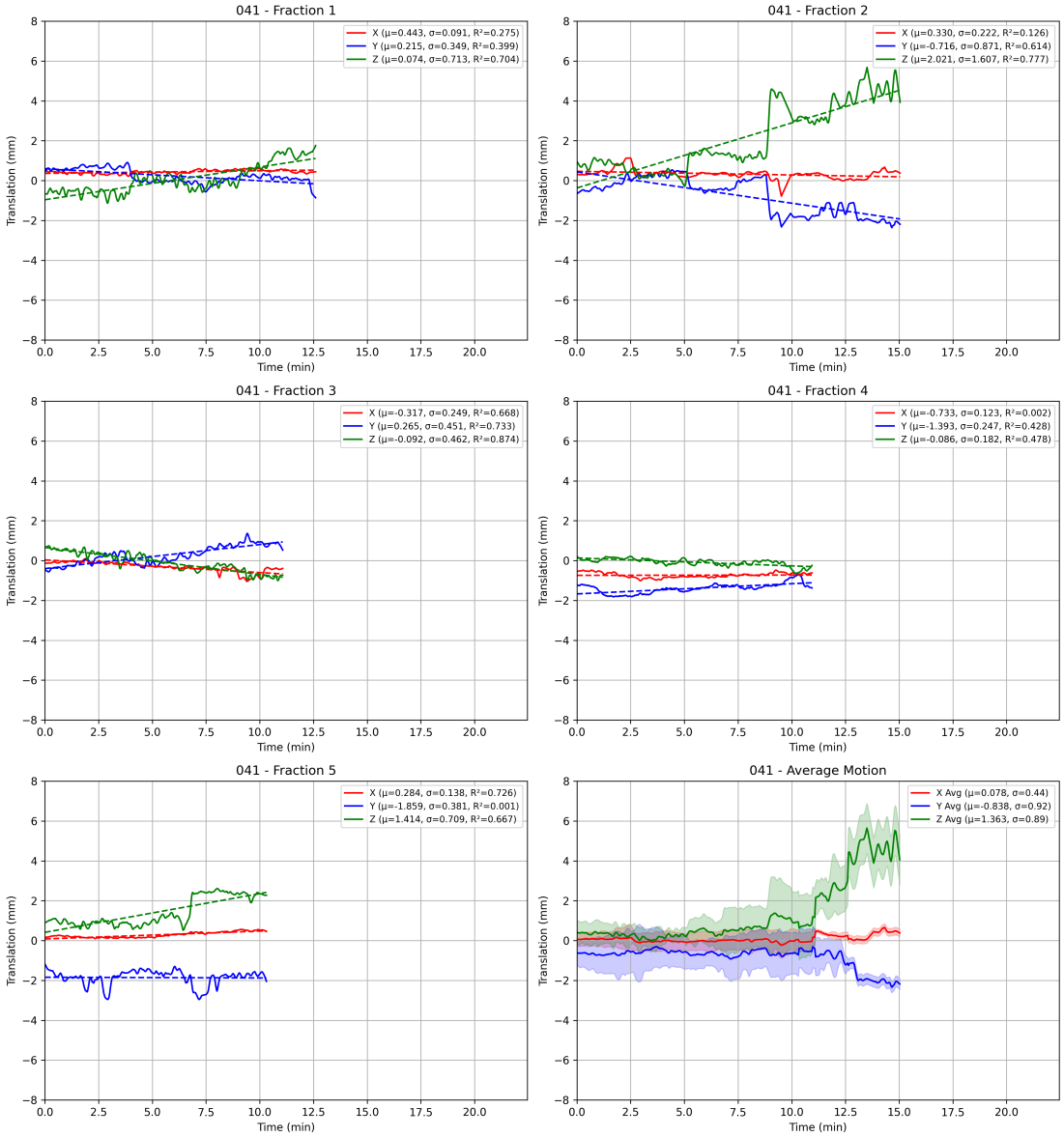

Figure B.41: Filtered traces plot for patient 041

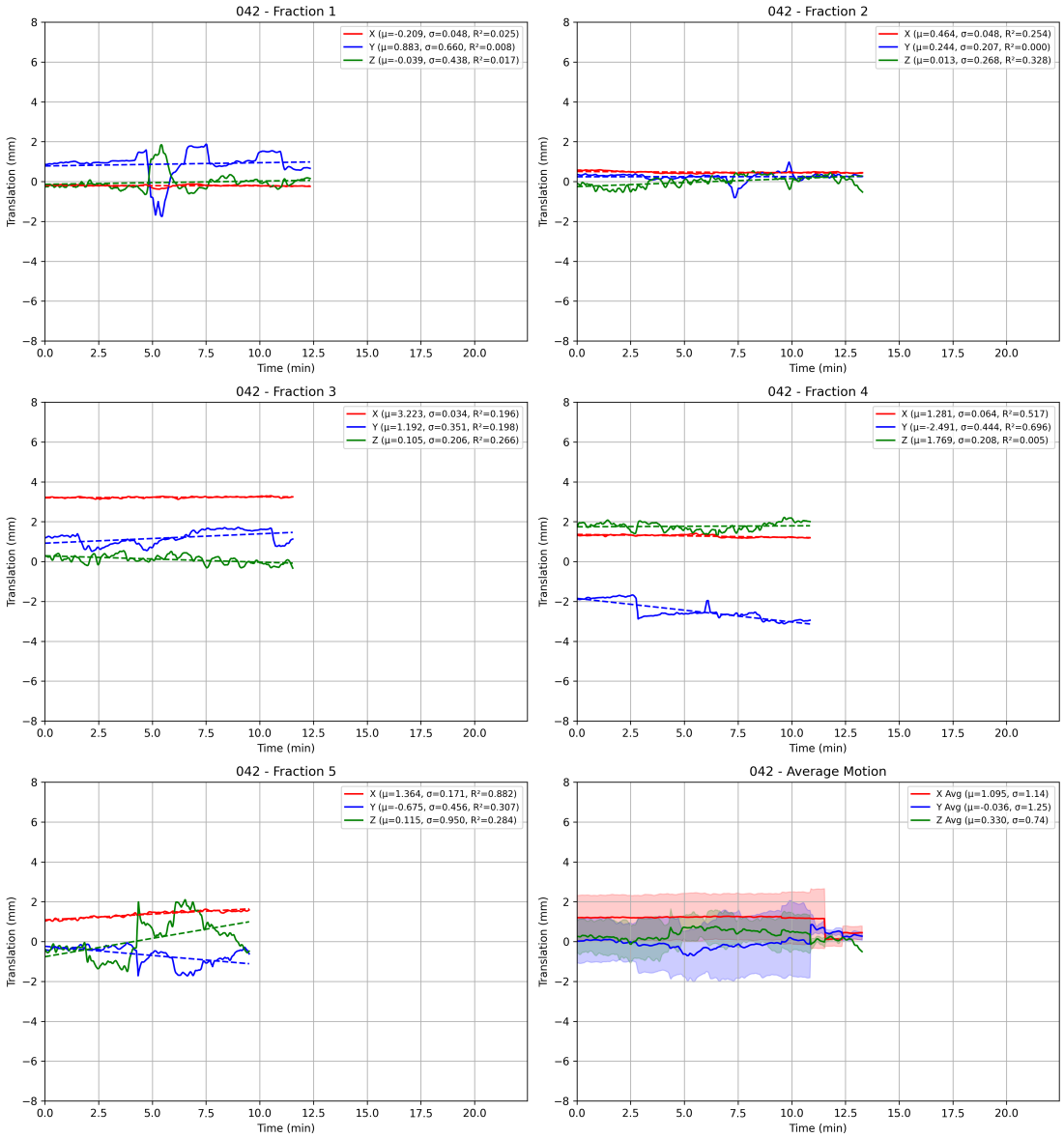

Figure B.42: Filtered traces plot for patient 042

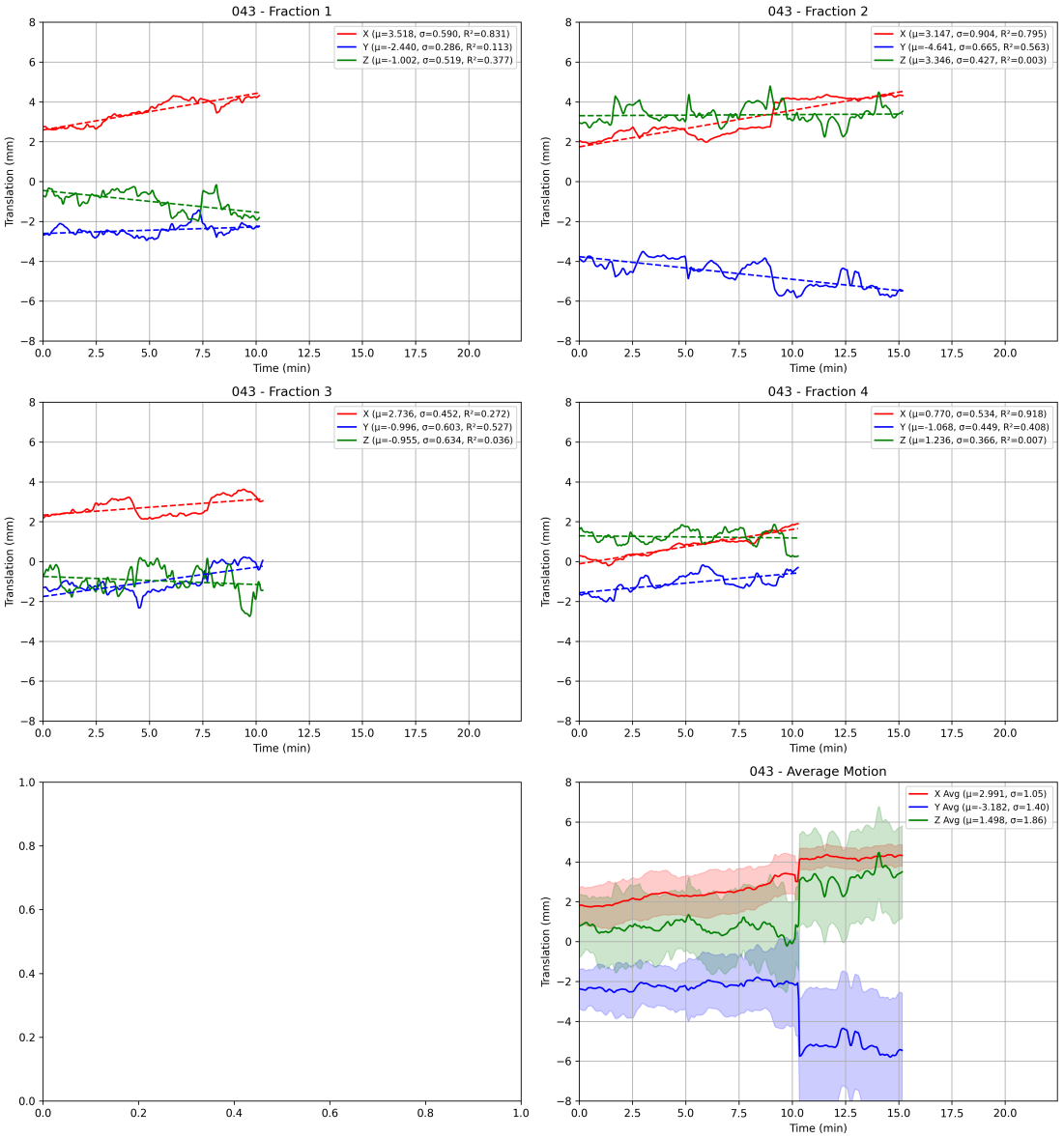

Figure B.43: Filtered traces plot for patient 043

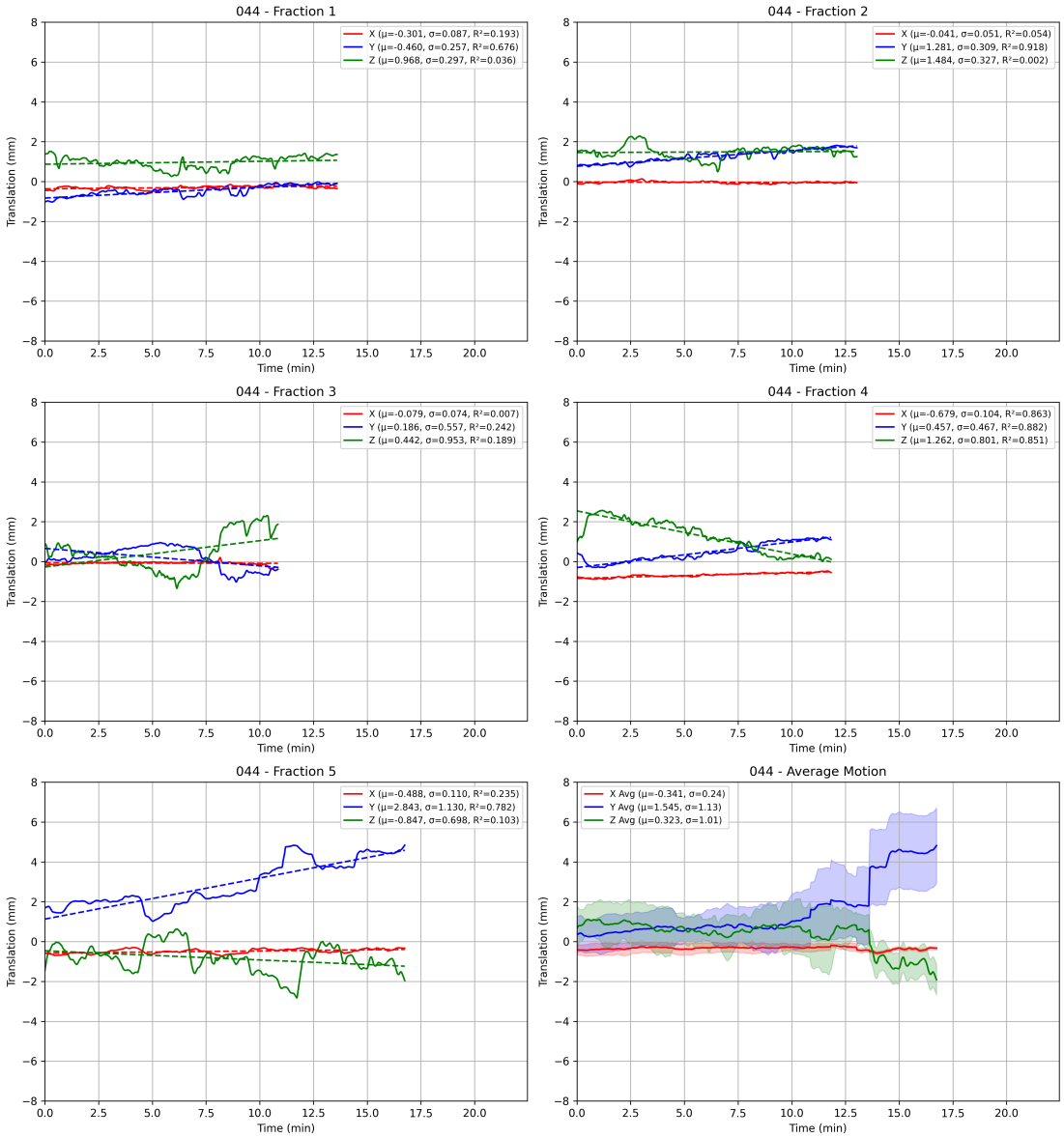

Figure B.44: Filtered traces plot for patient 044

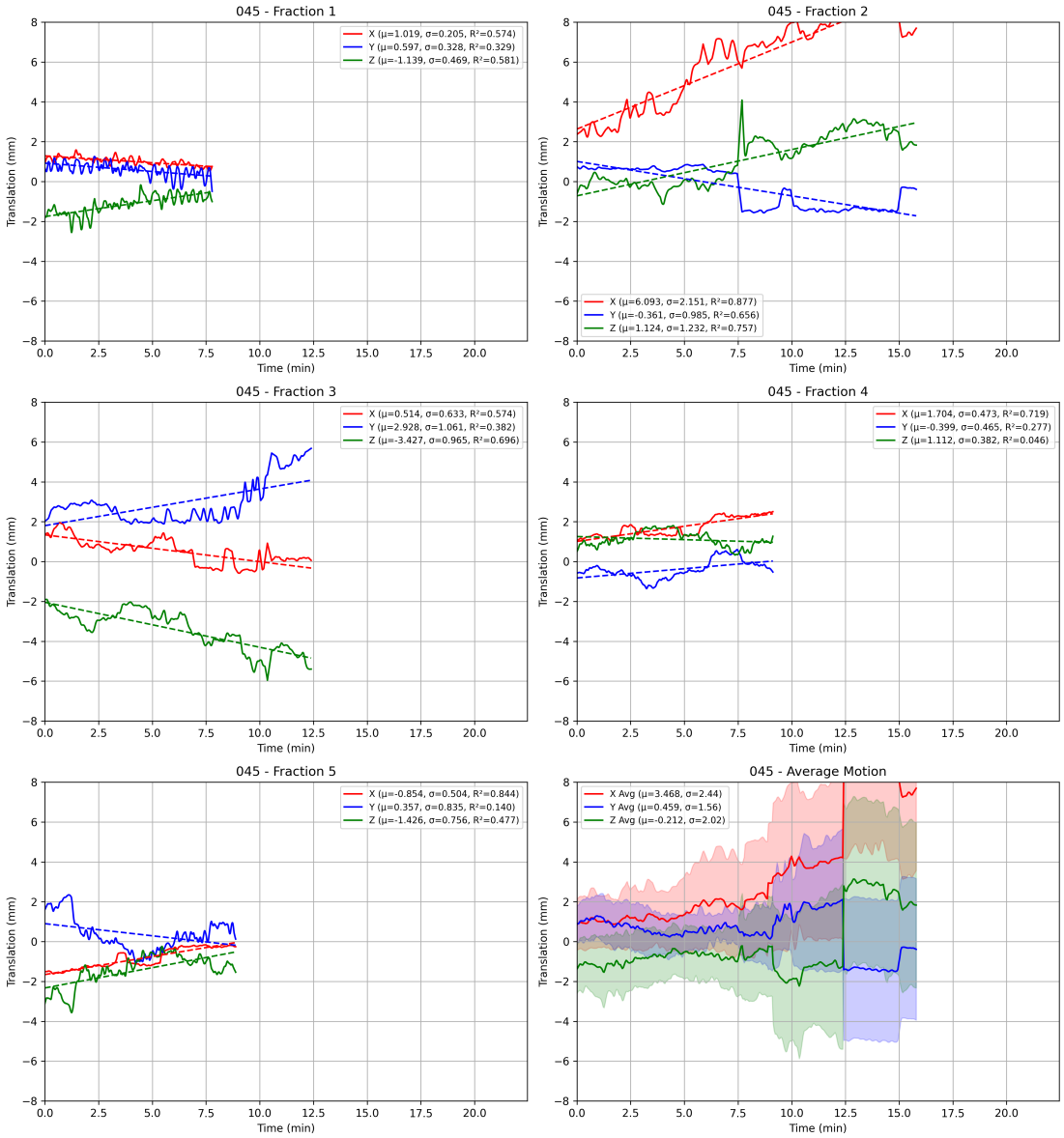

Figure B.45: Filtered traces plot for patient 045

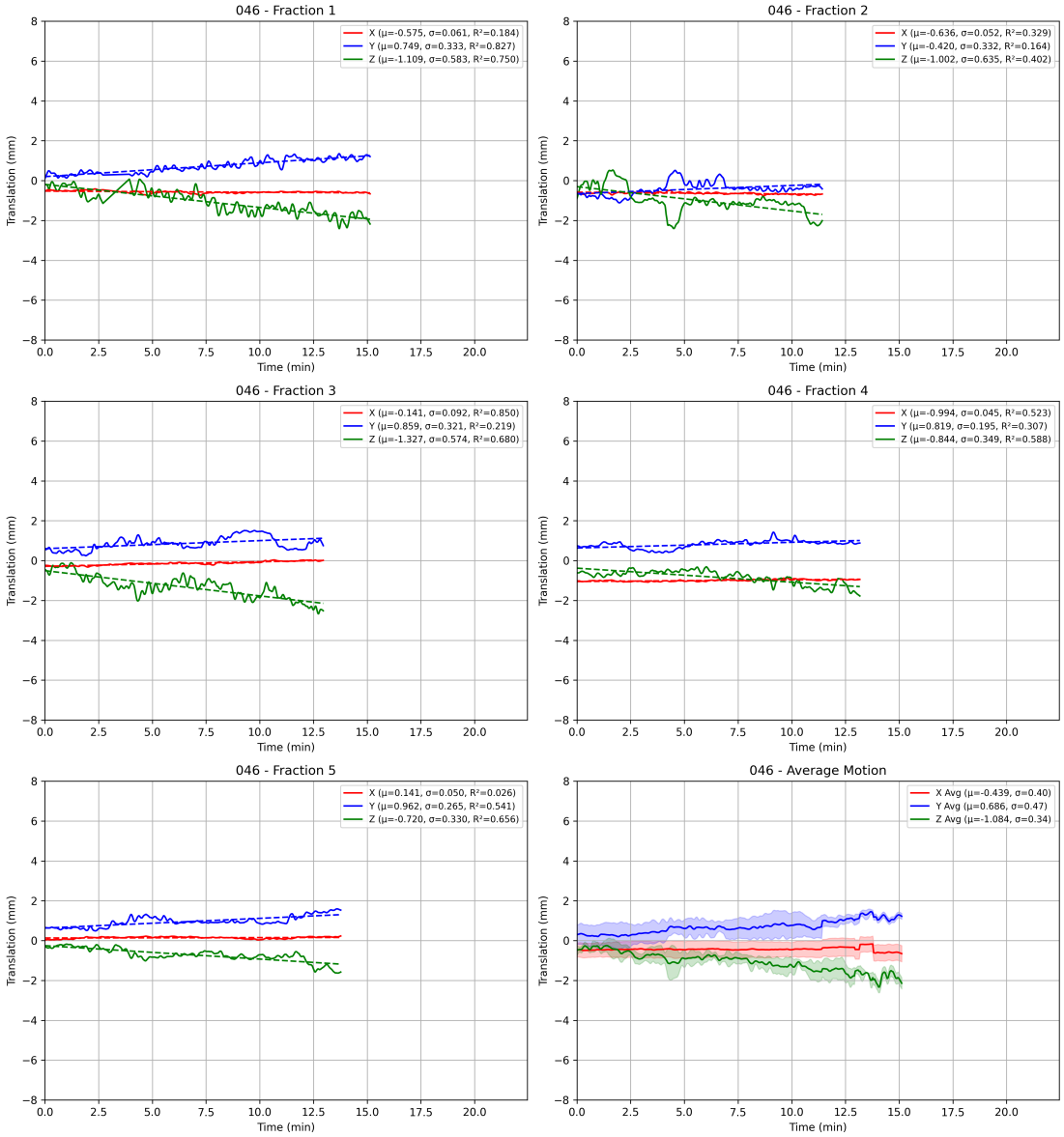

Figure B.46: Filtered traces plot for patient 046

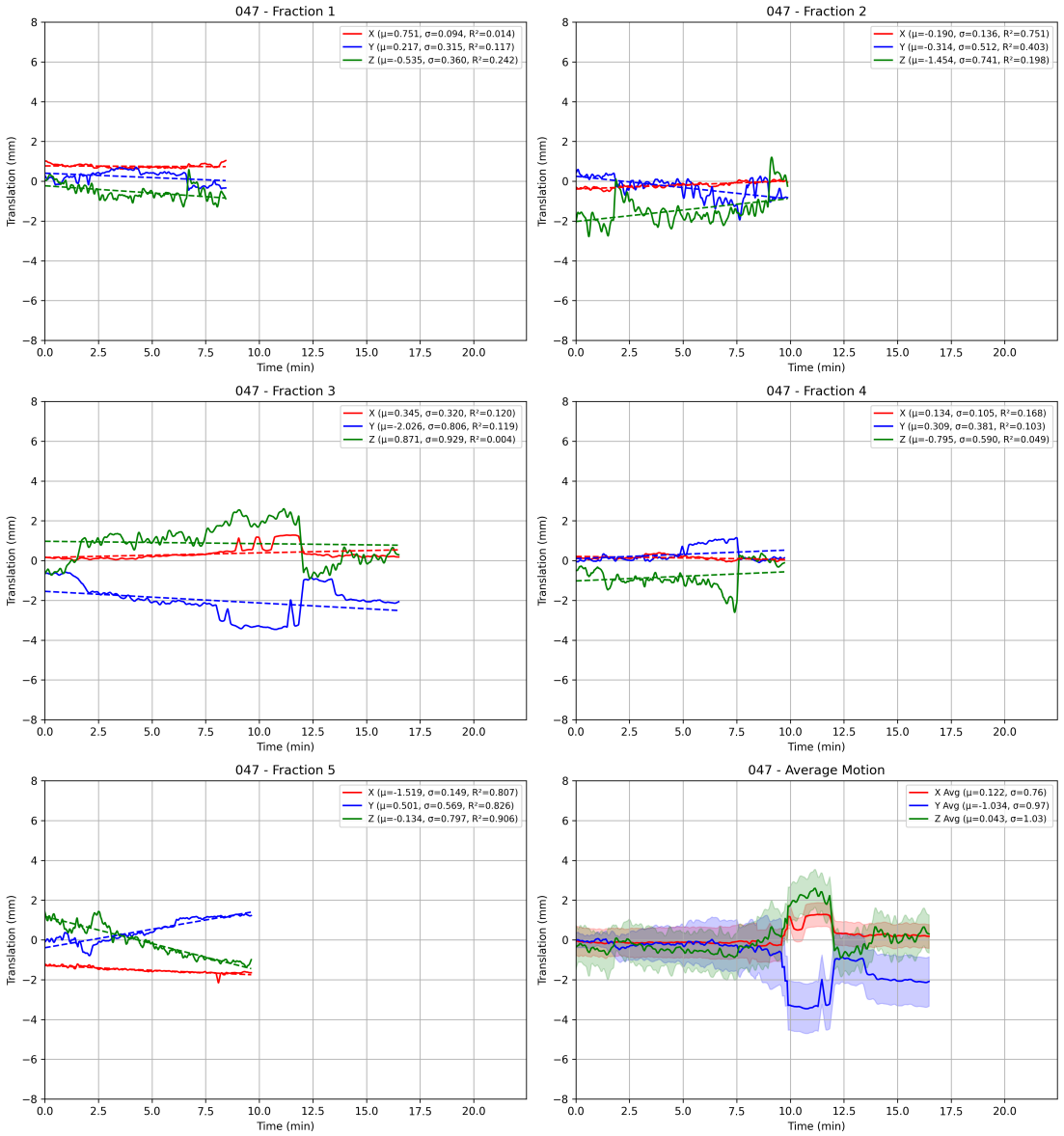

Figure B.47: Filtered traces plot for patient 047

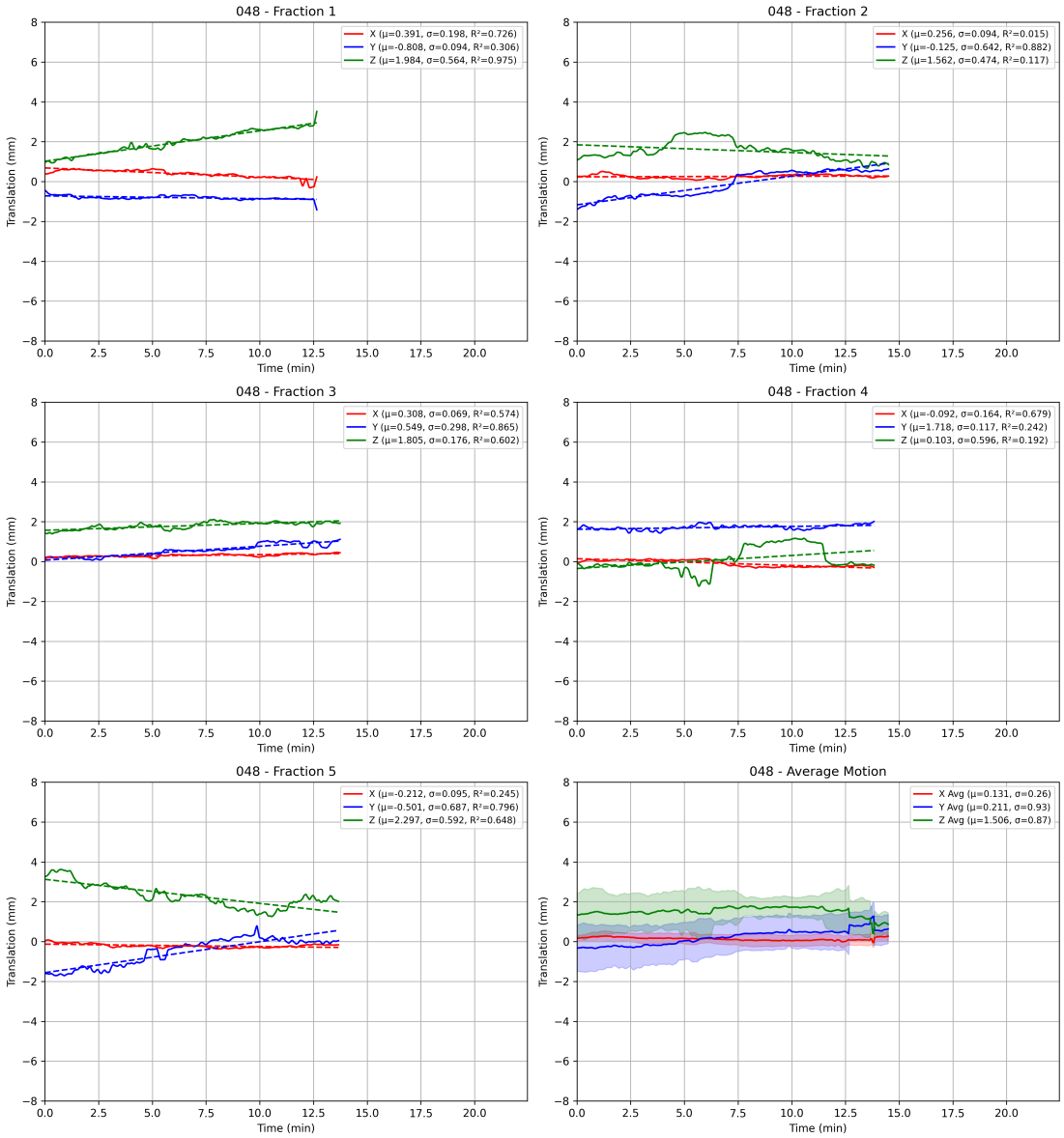

Figure B.48: Filtered traces plot for patient 048

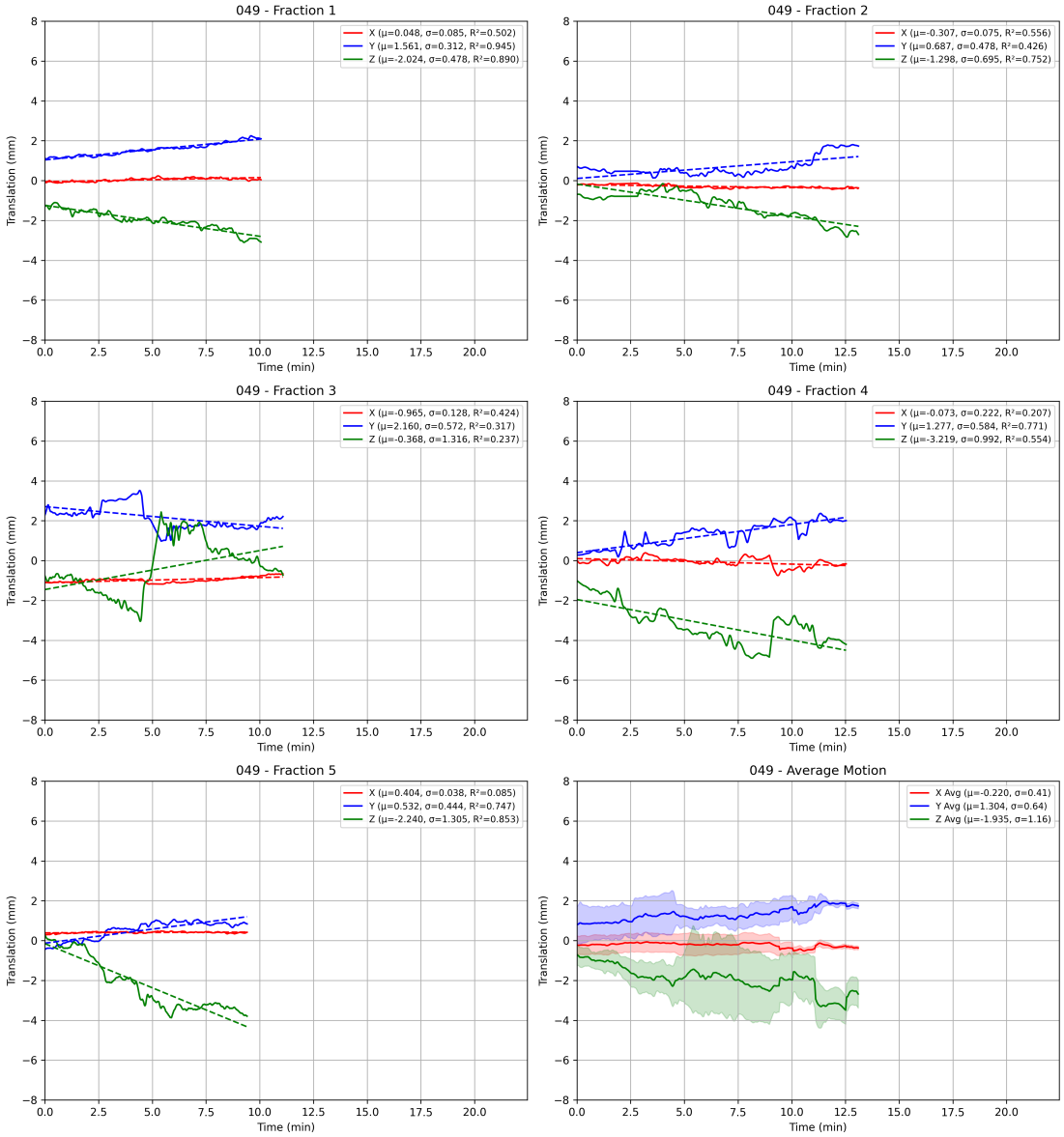

Figure B.49: Filtered traces plot for patient 049

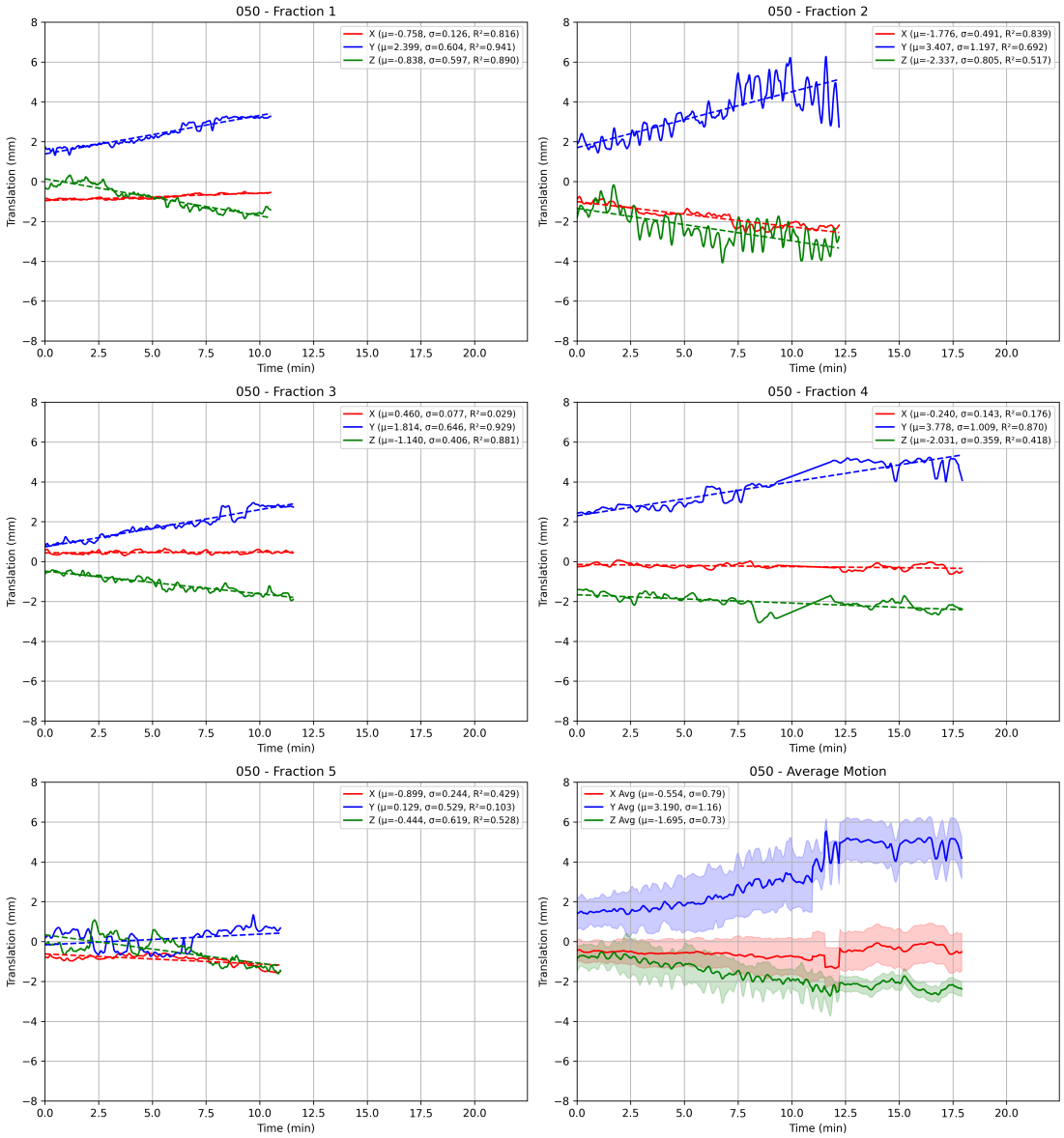

Figure B.50: Filtered traces plot for patient 050

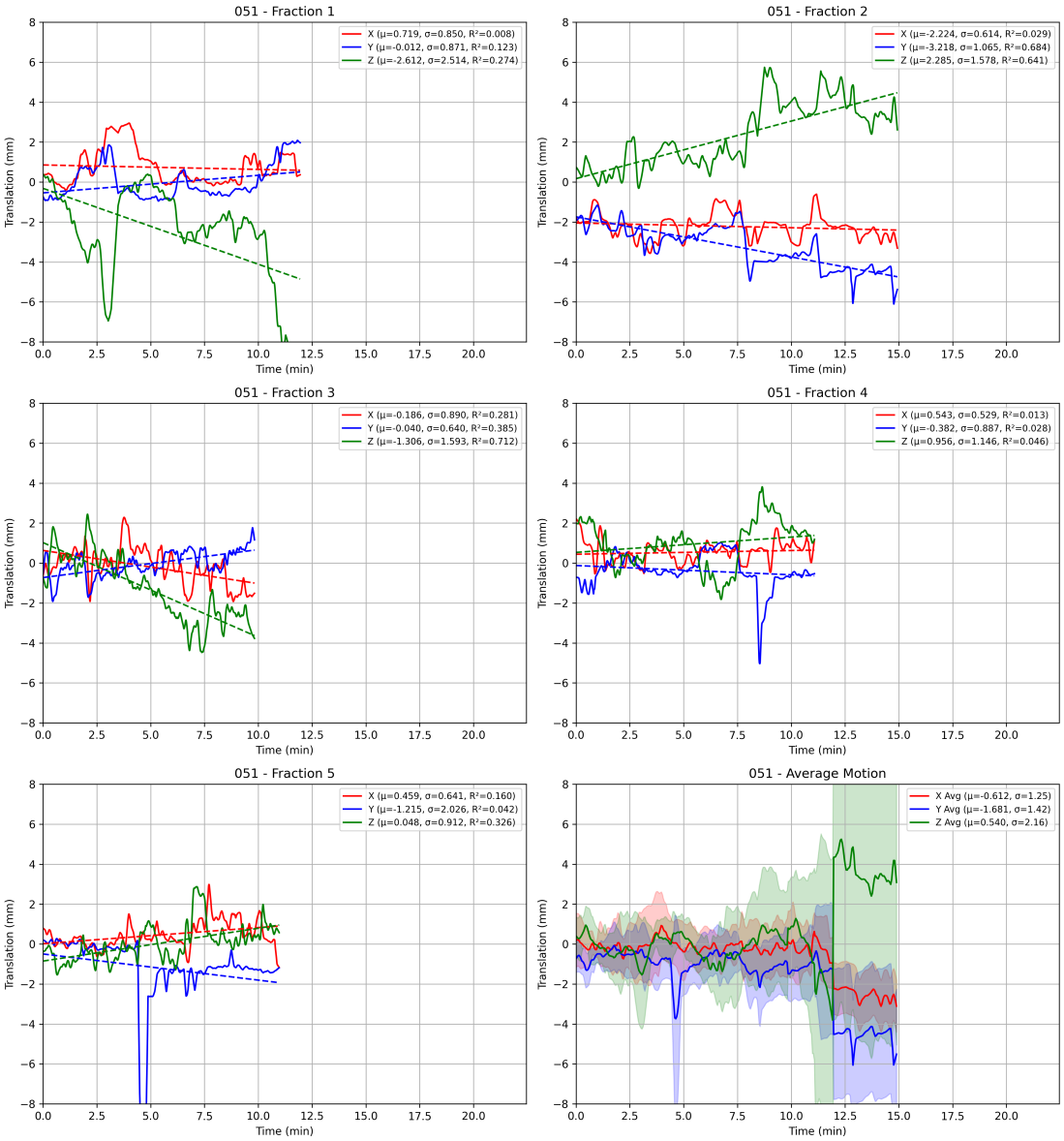

Figure B.51: Filtered traces plot for patient 051

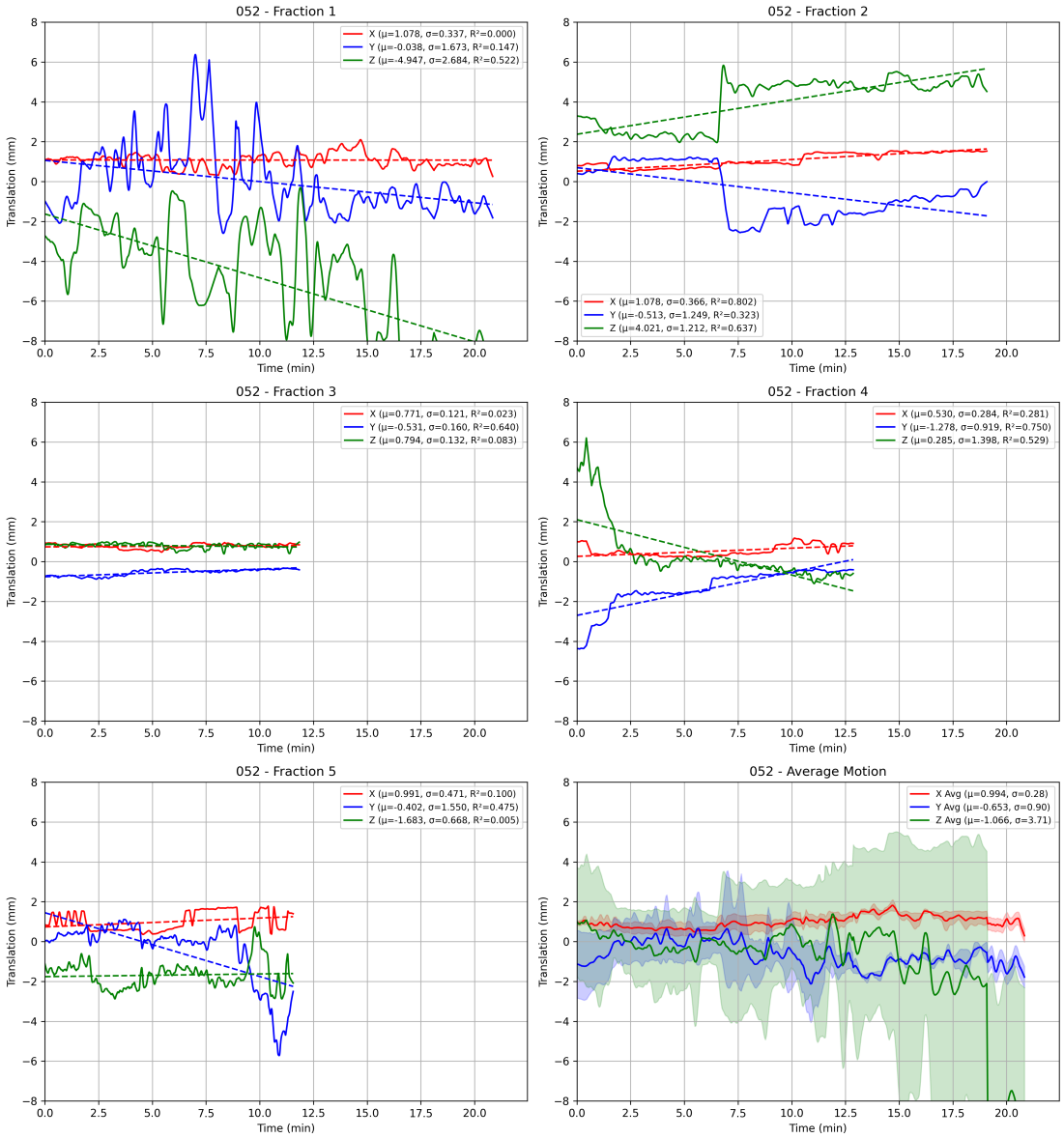

Figure B.52: Filtered traces plot for patient 052

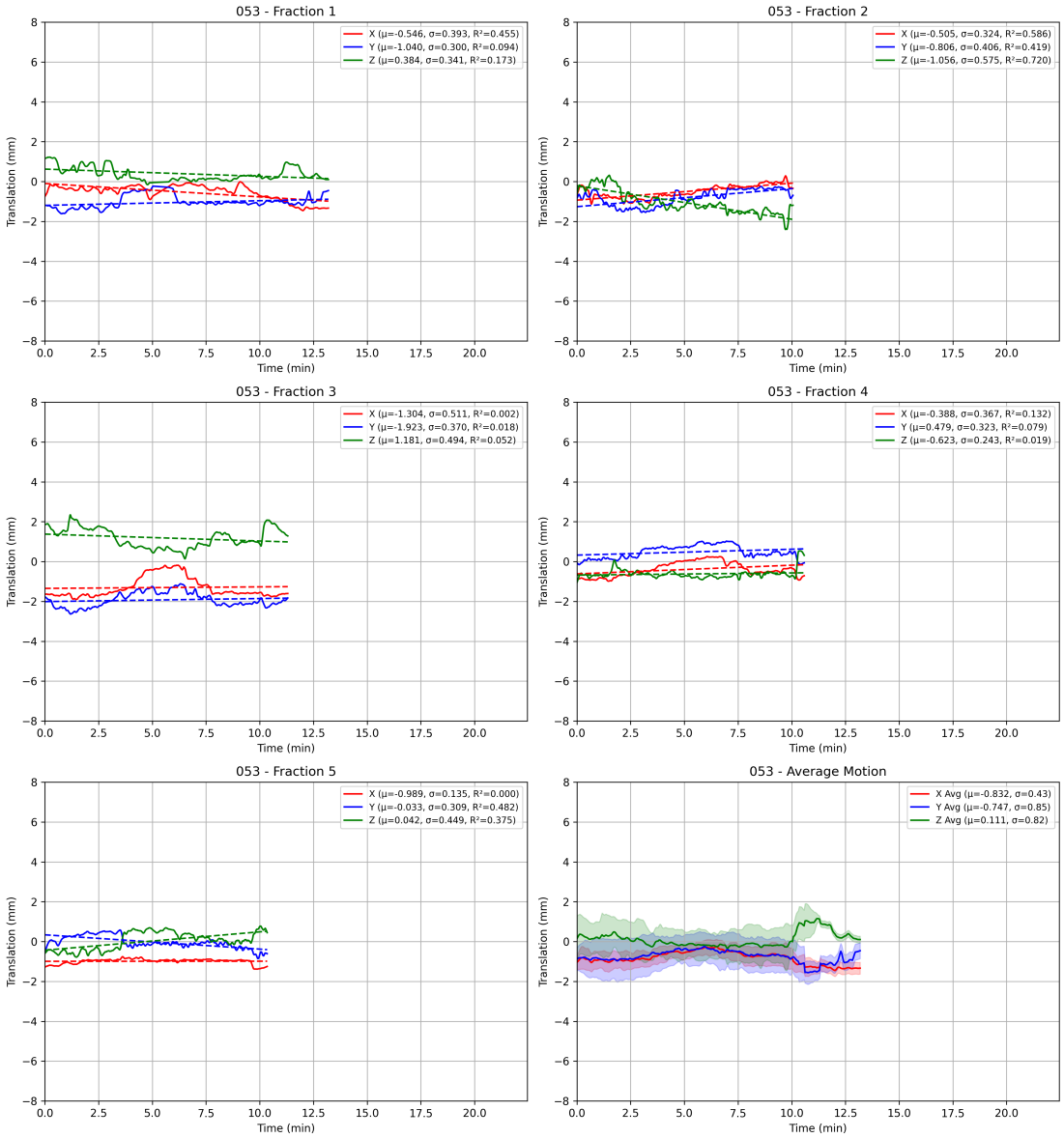

Figure B.53: Filtered traces plot for patient 053

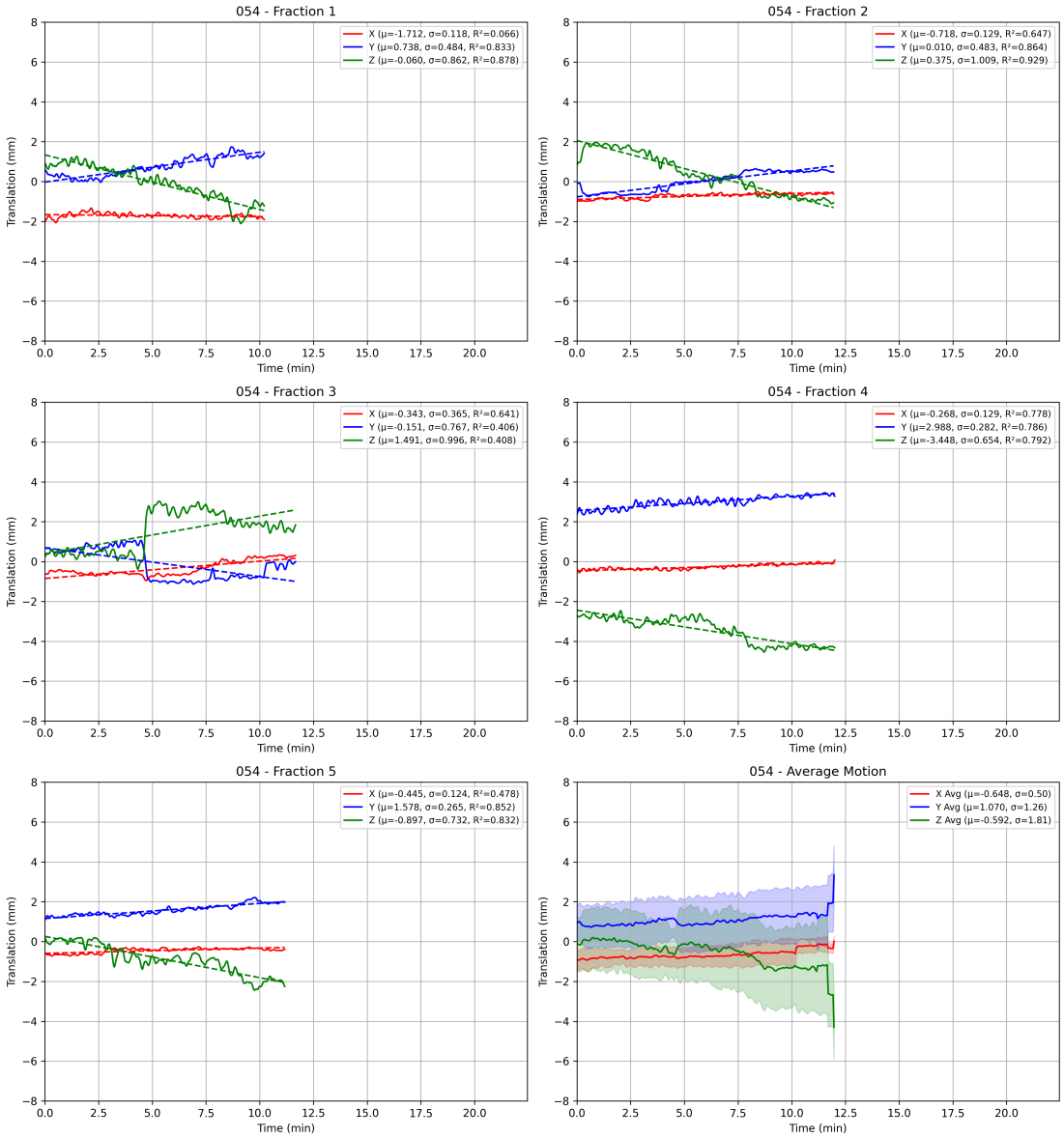

Figure B.54: Filtered traces plot for patient 054

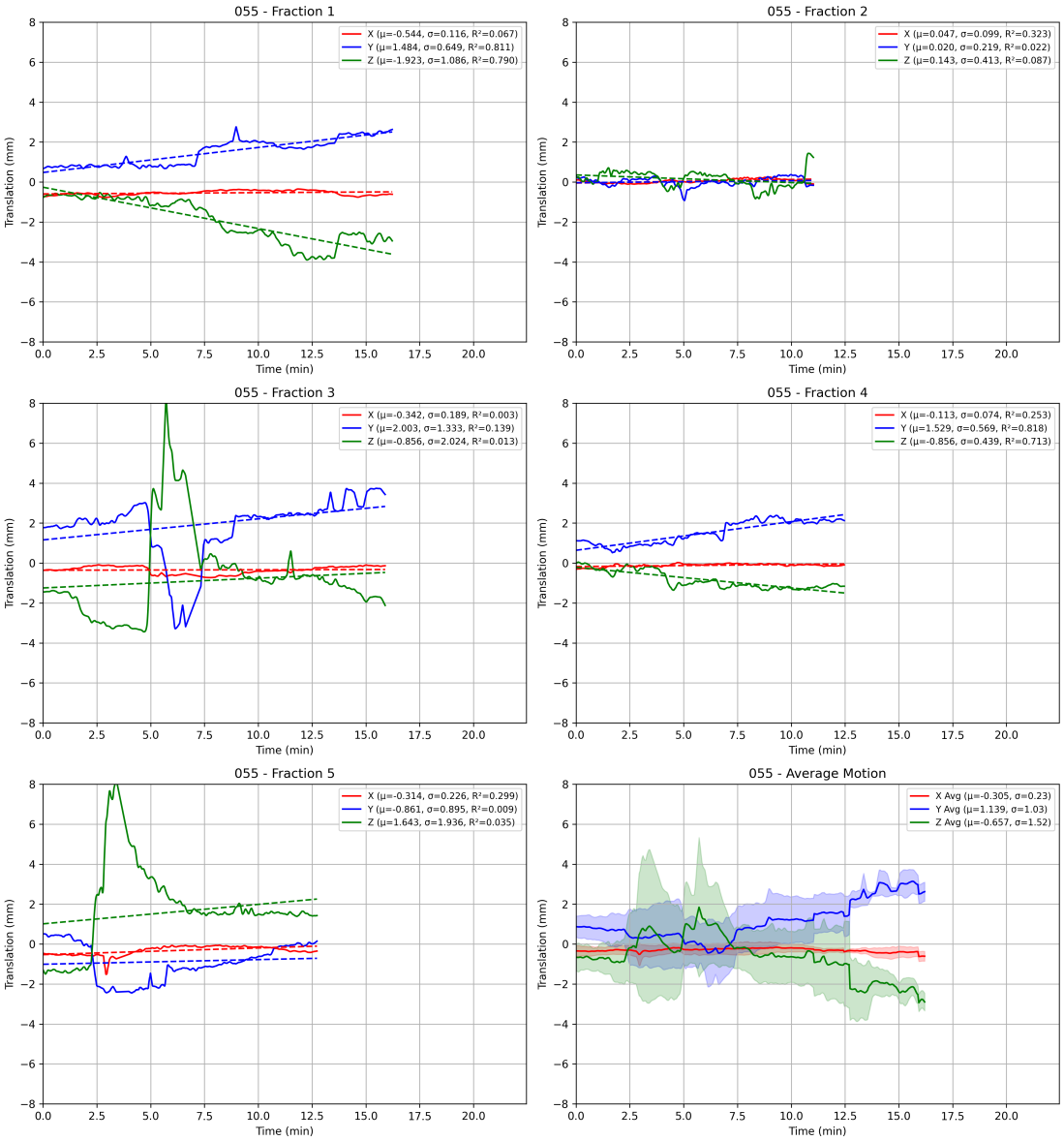

Figure B.55: Filtered traces plot for patient 055

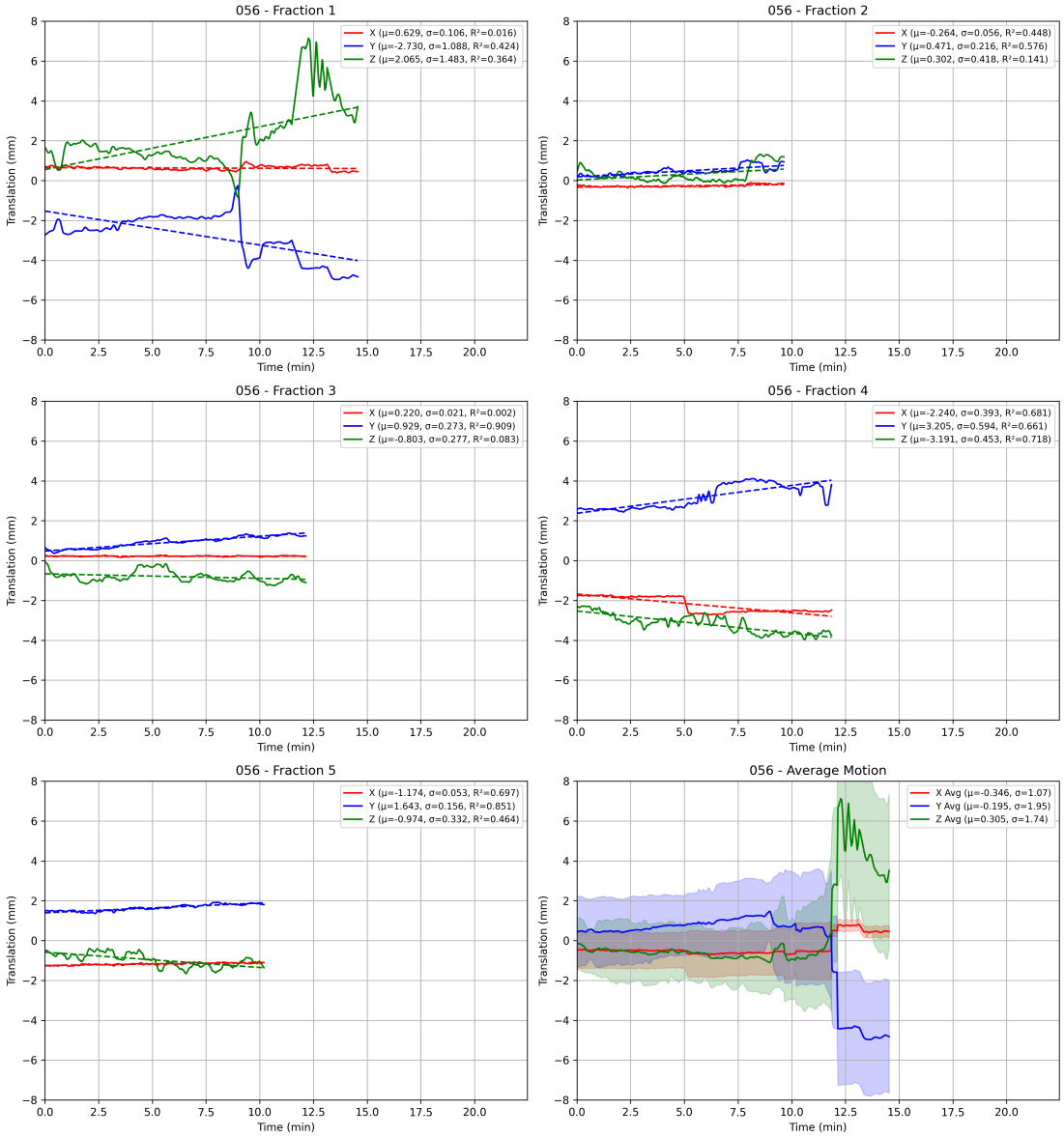

Figure B.56: Filtered traces plot for patient 056

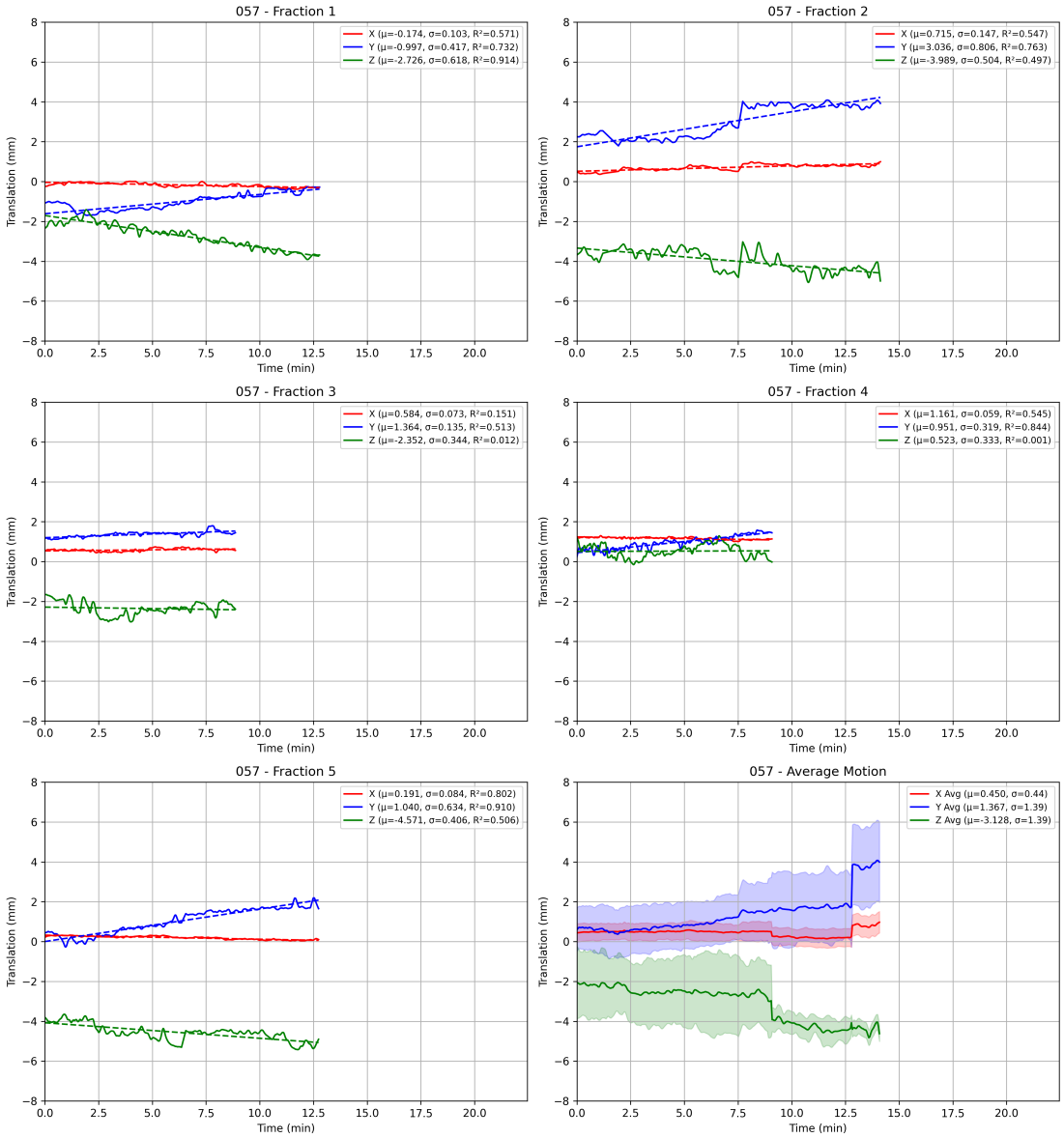

Figure B.57: Filtered traces plot for patient 057

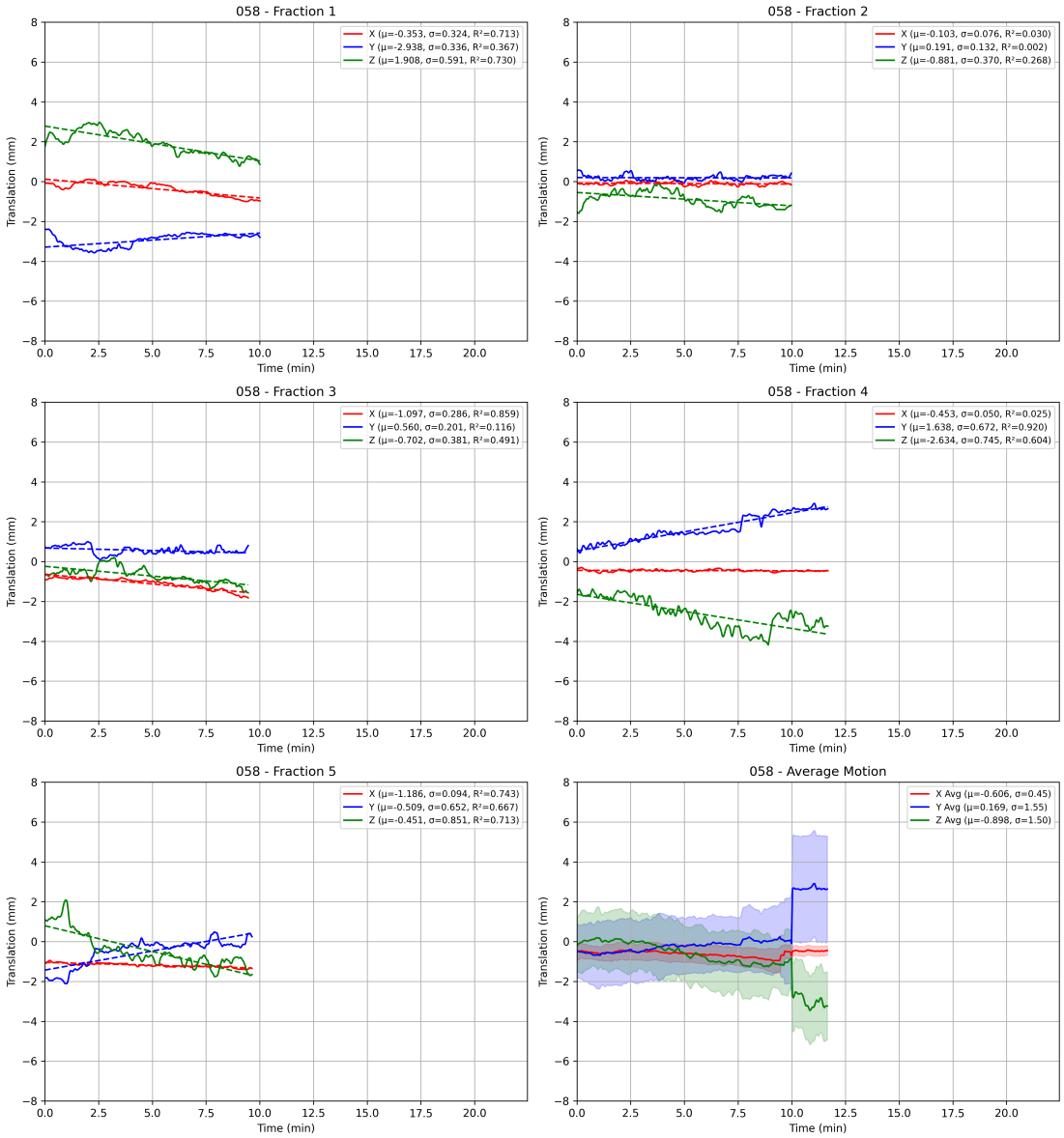

Figure B.58: Filtered traces plot for patient 058

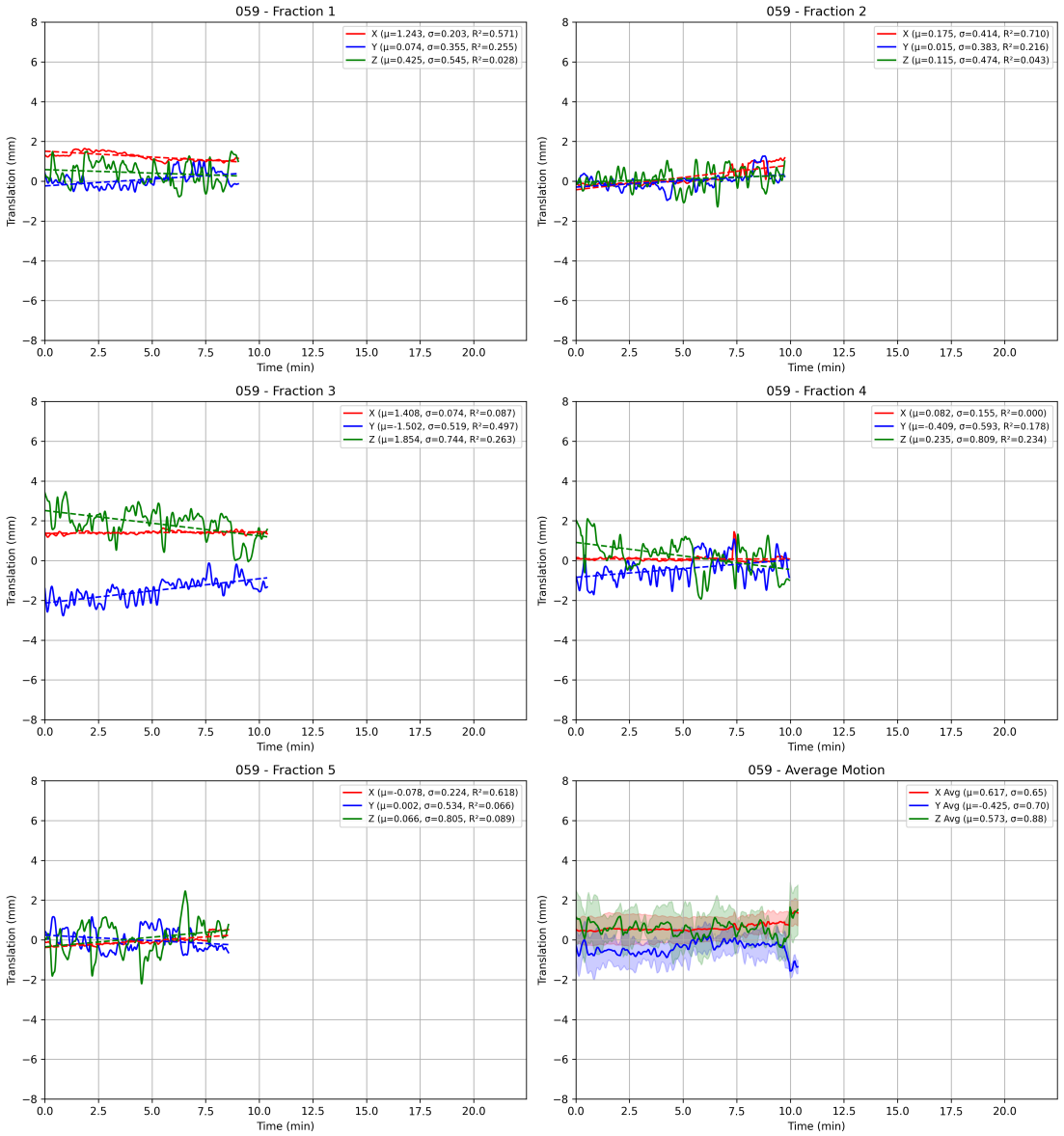

Figure B.59: Filtered traces plot for patient 059

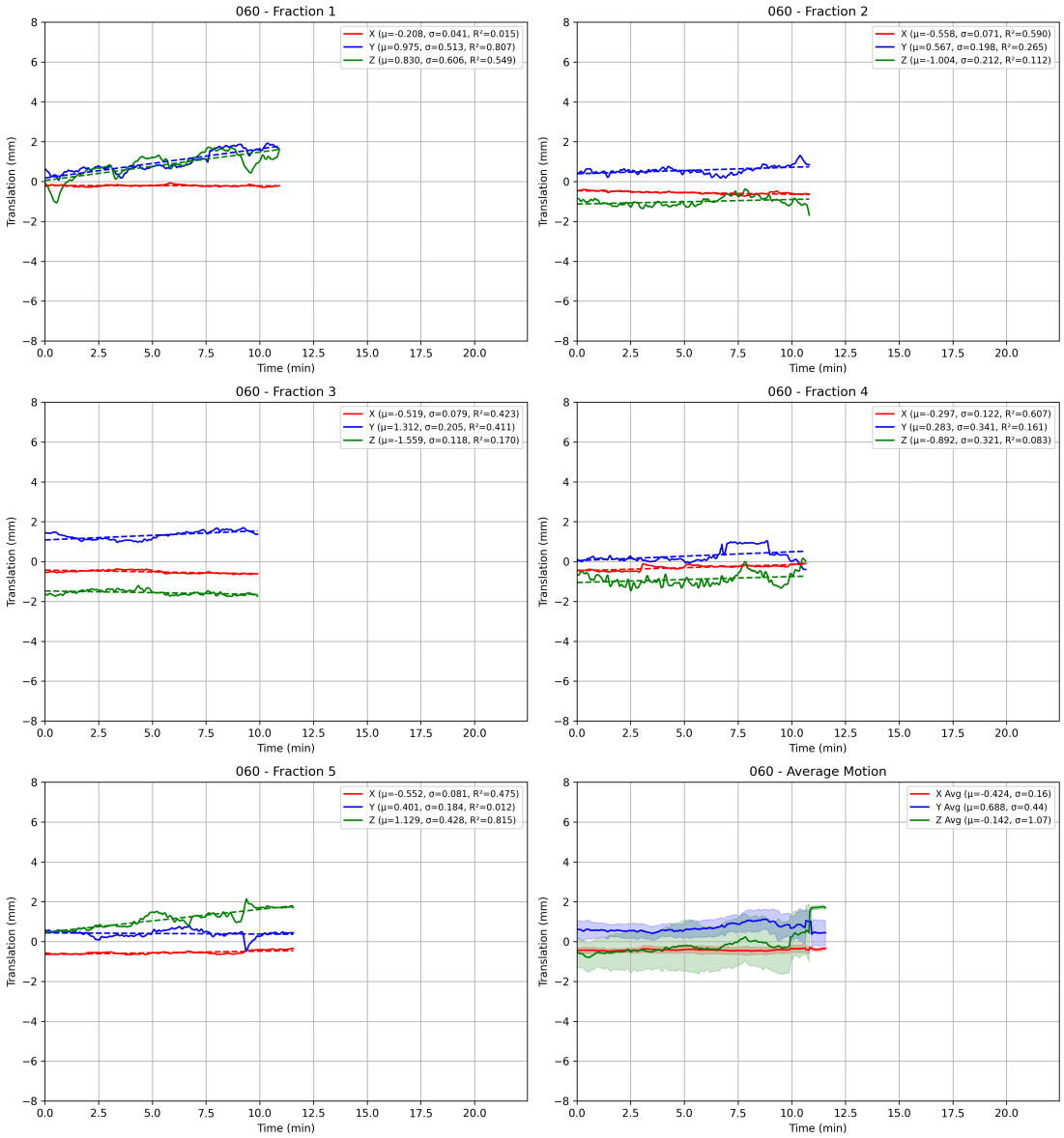

Figure B.60: Filtered traces plot for patient 060

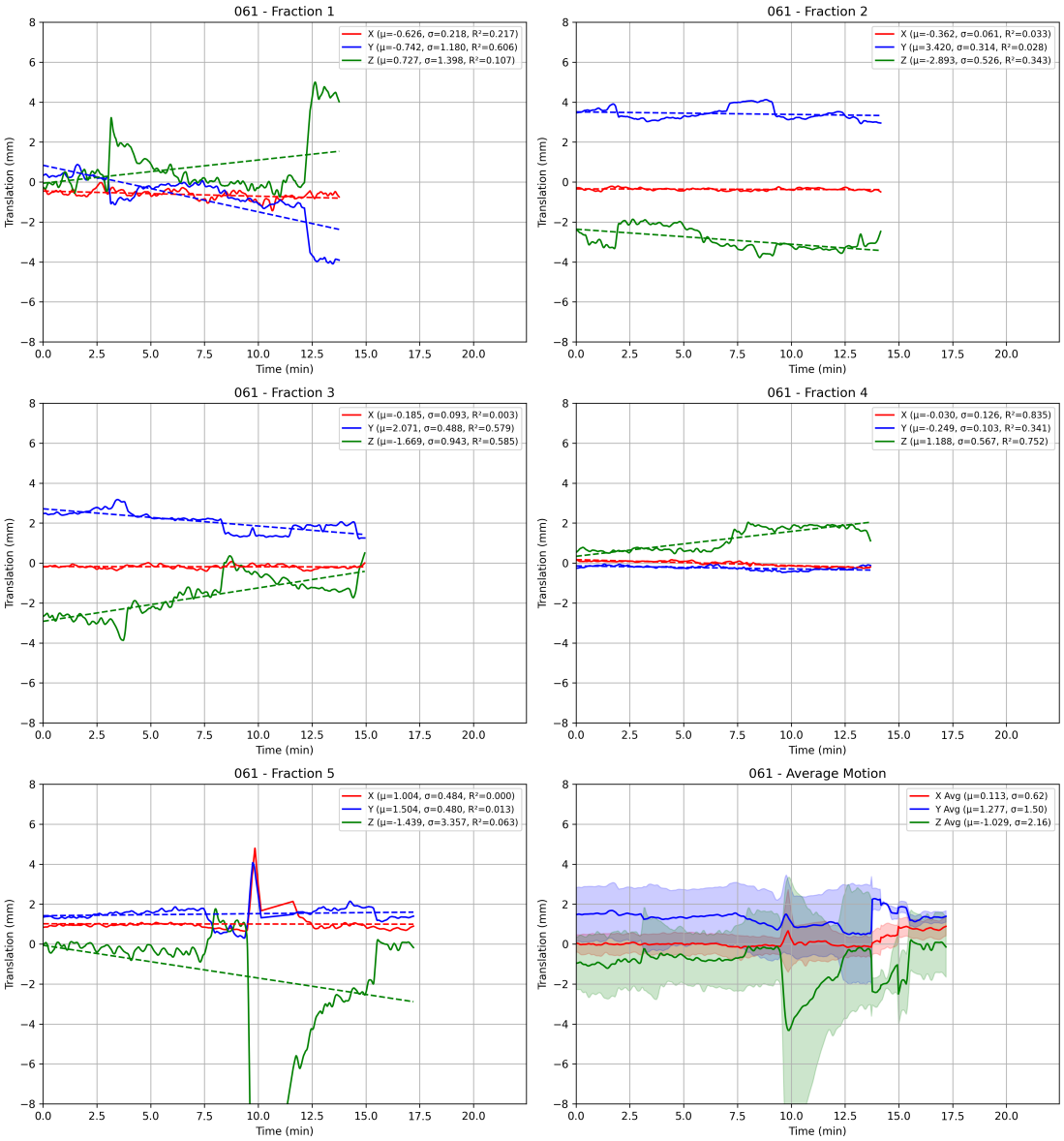

Figure B.61: Filtered traces plot for patient 061

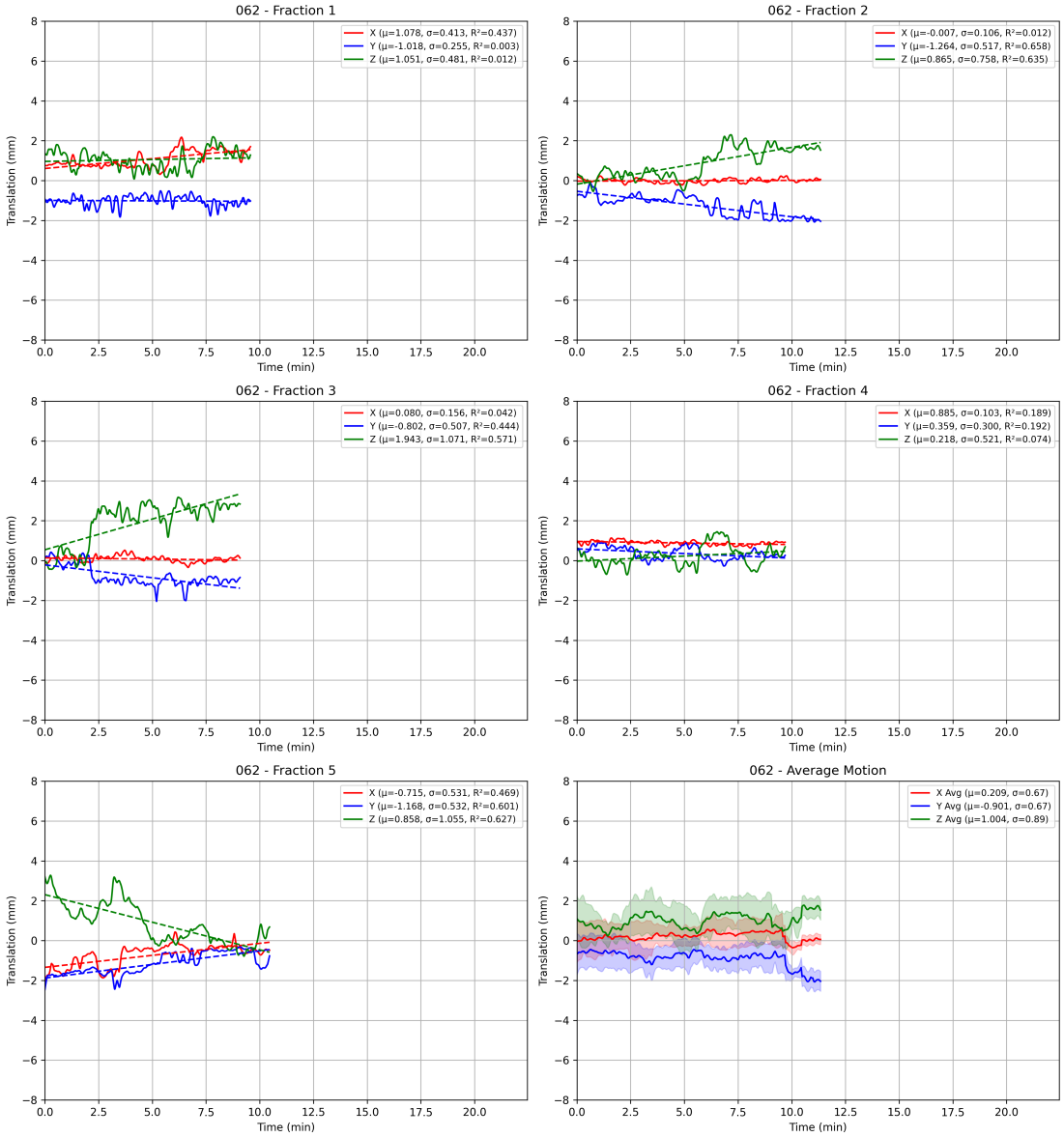

Figure B.62: Filtered traces plot for patient 062

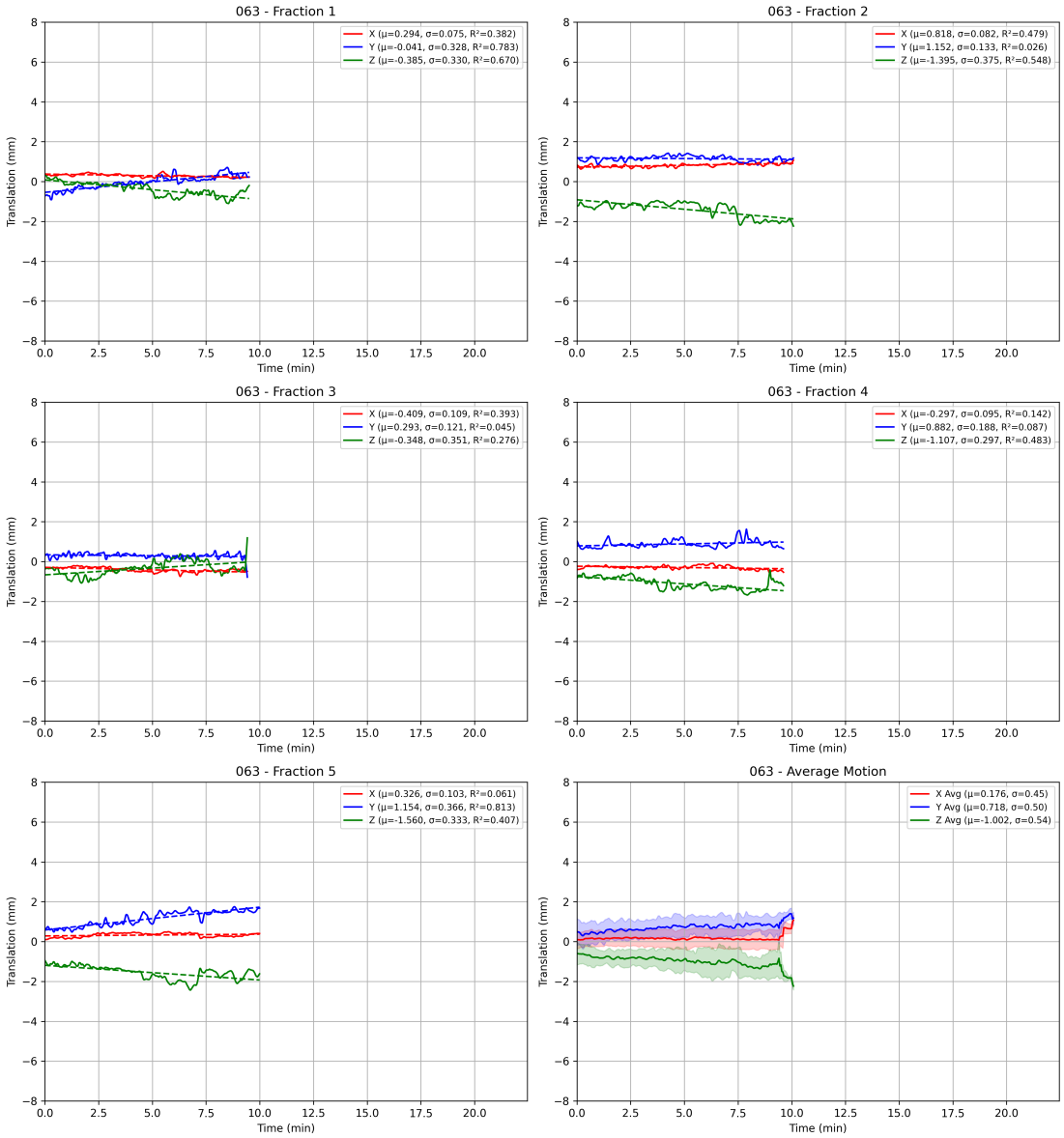

Figure B.63: Filtered traces plot for patient 063

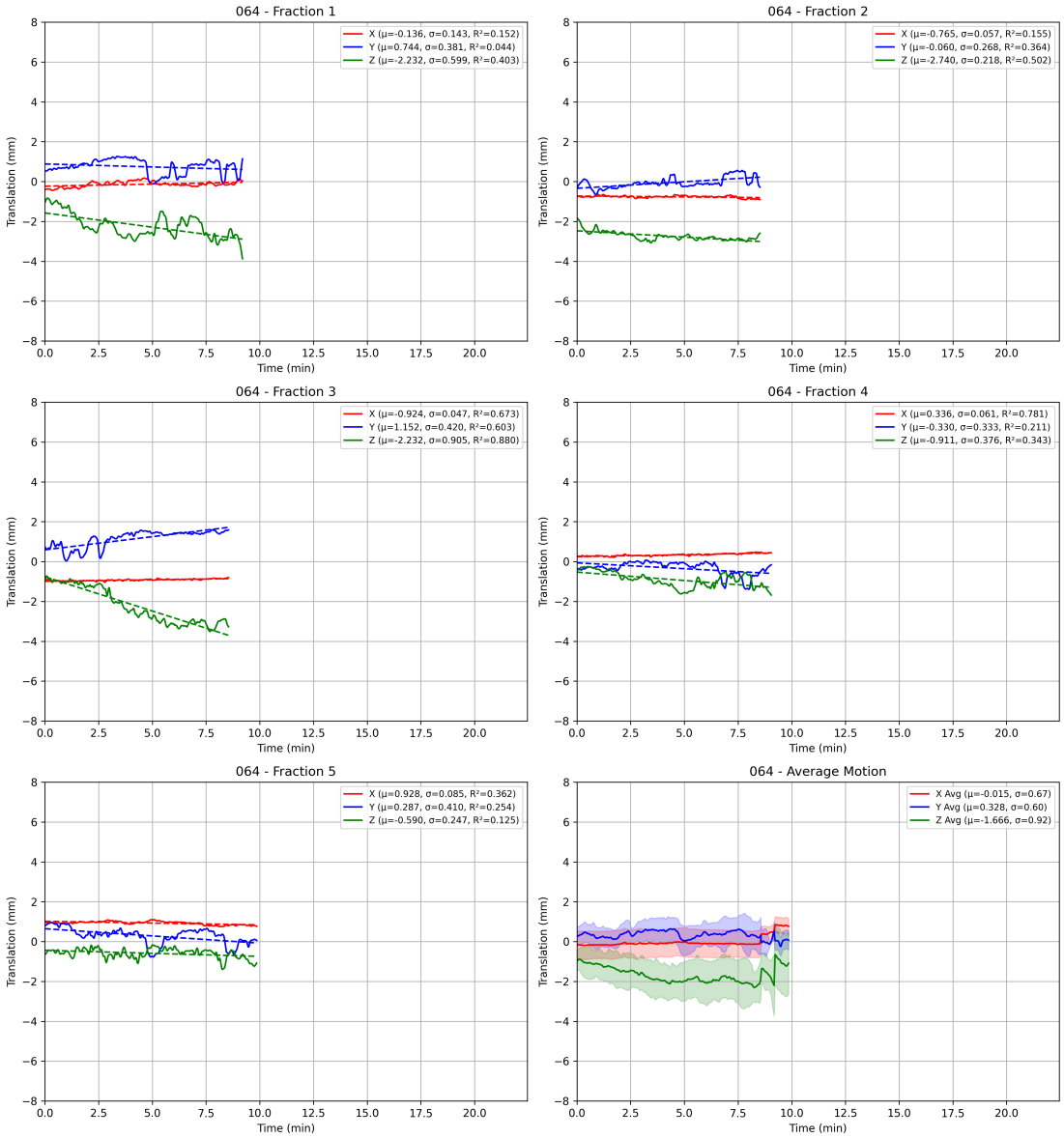

Figure B.64: Filtered traces plot for patient 064

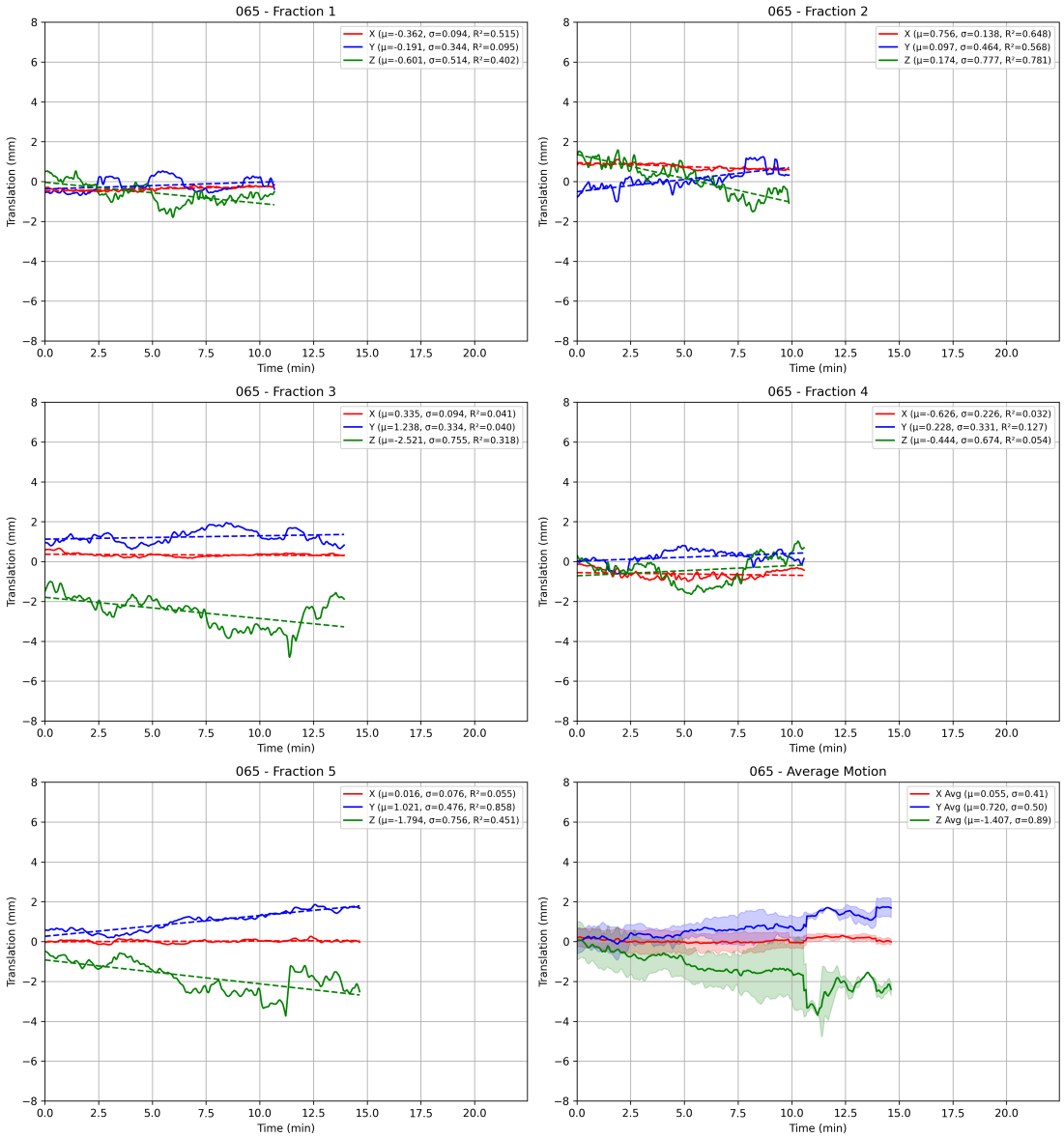

Figure B.65: Filtered traces plot for patient 065

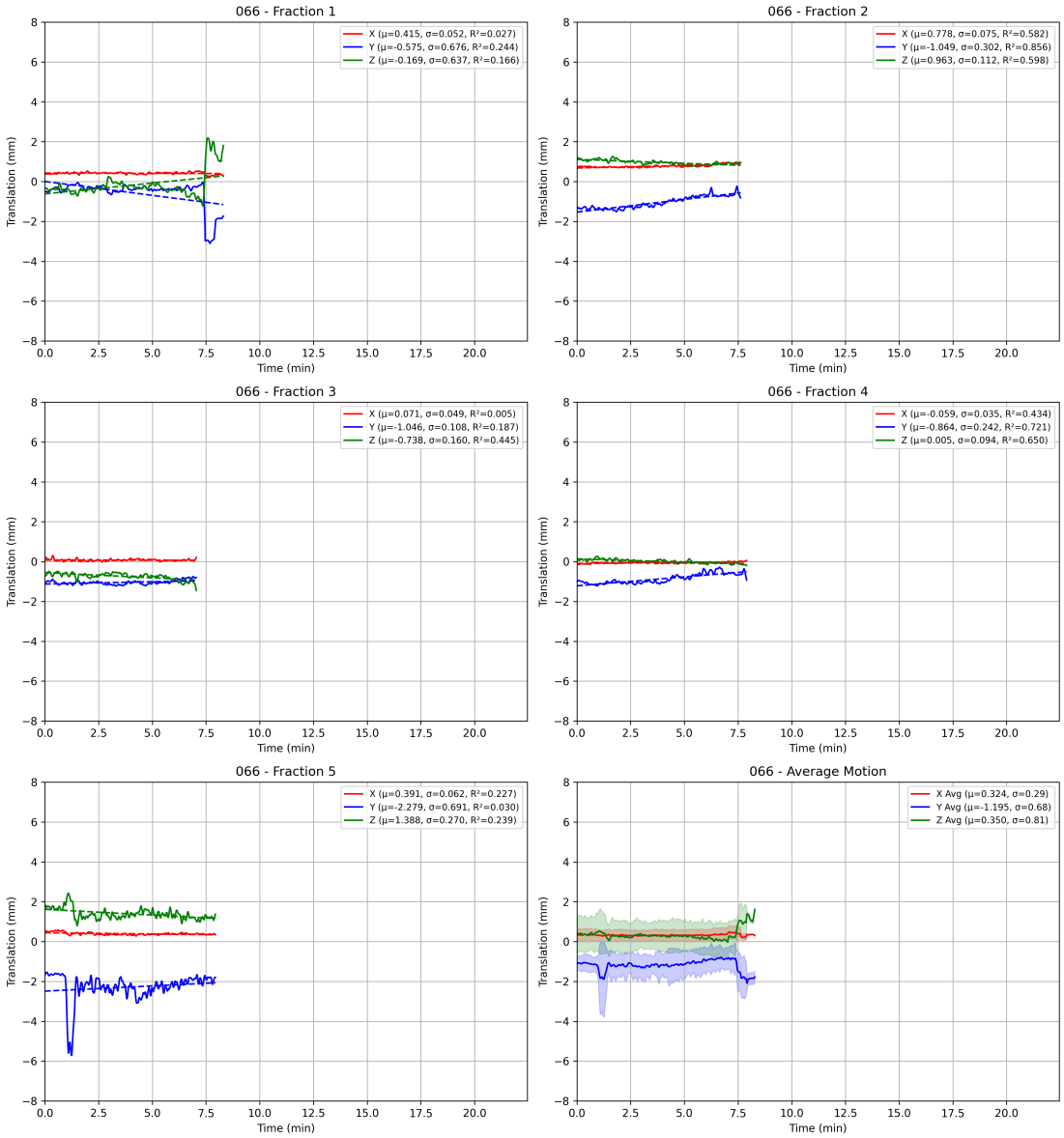

Figure B.66: Filtered traces plot for patient 066

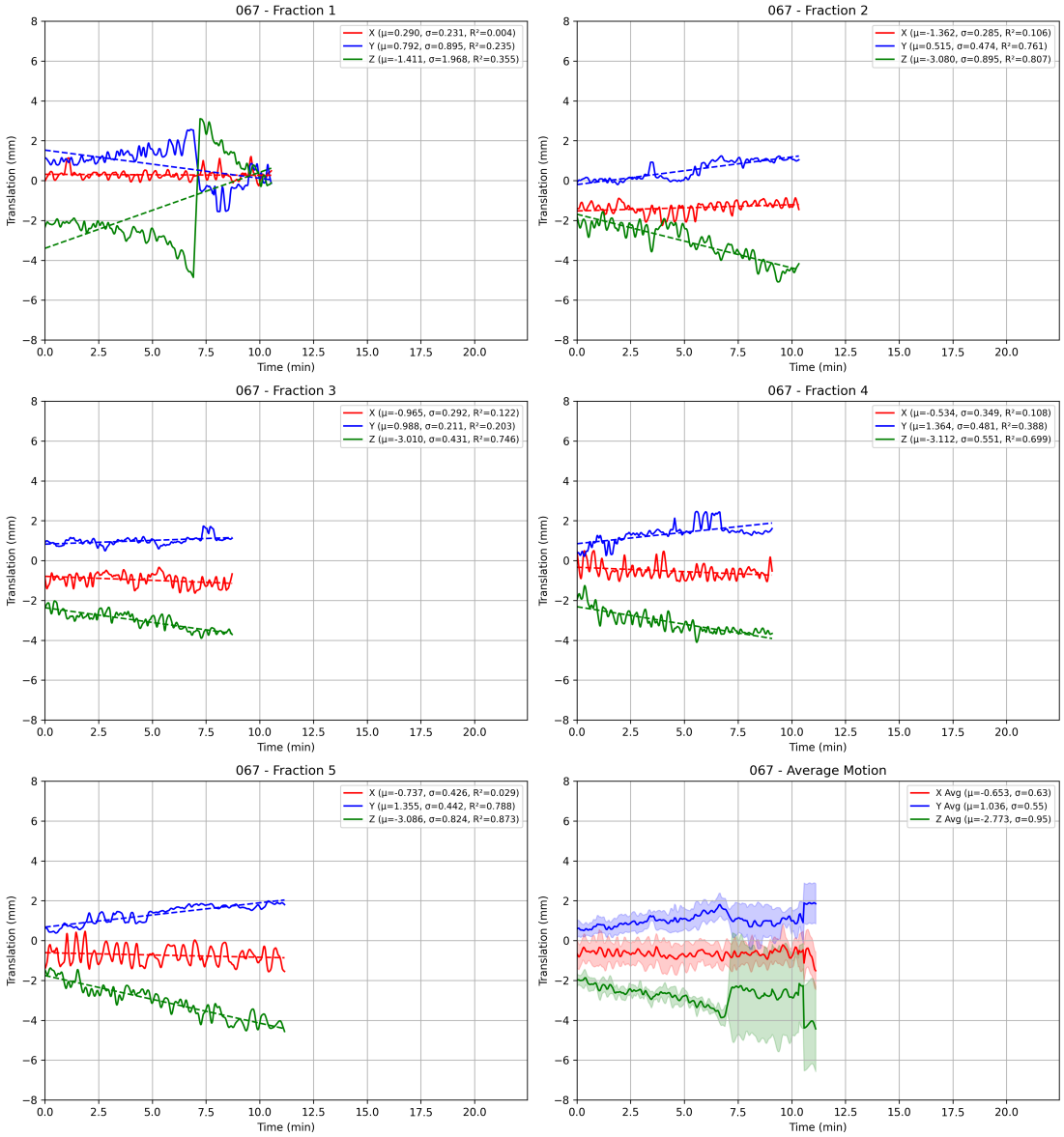

Figure B.67: Filtered traces plot for patient 067

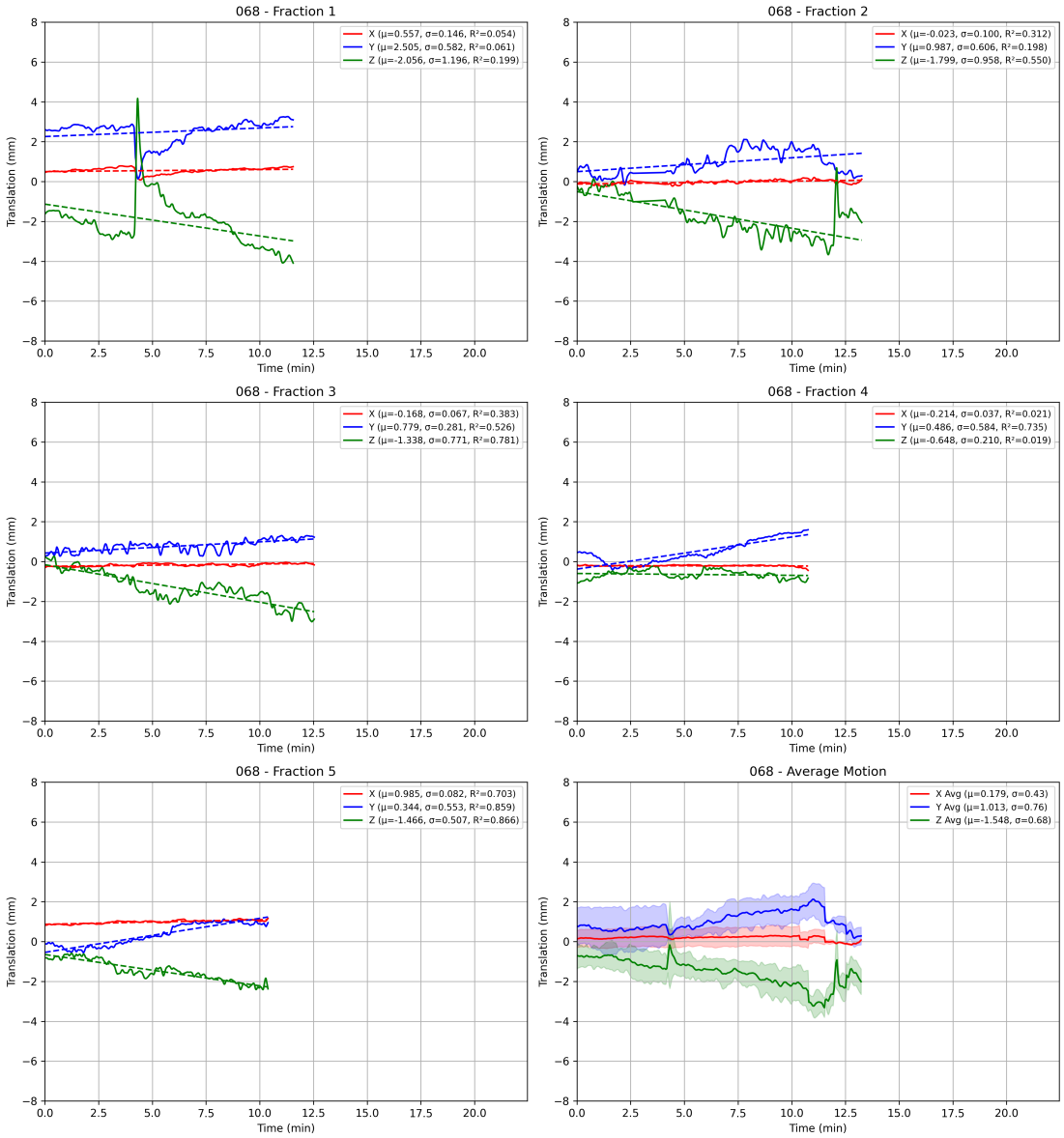

Figure B.68: Filtered traces plot for patient 068

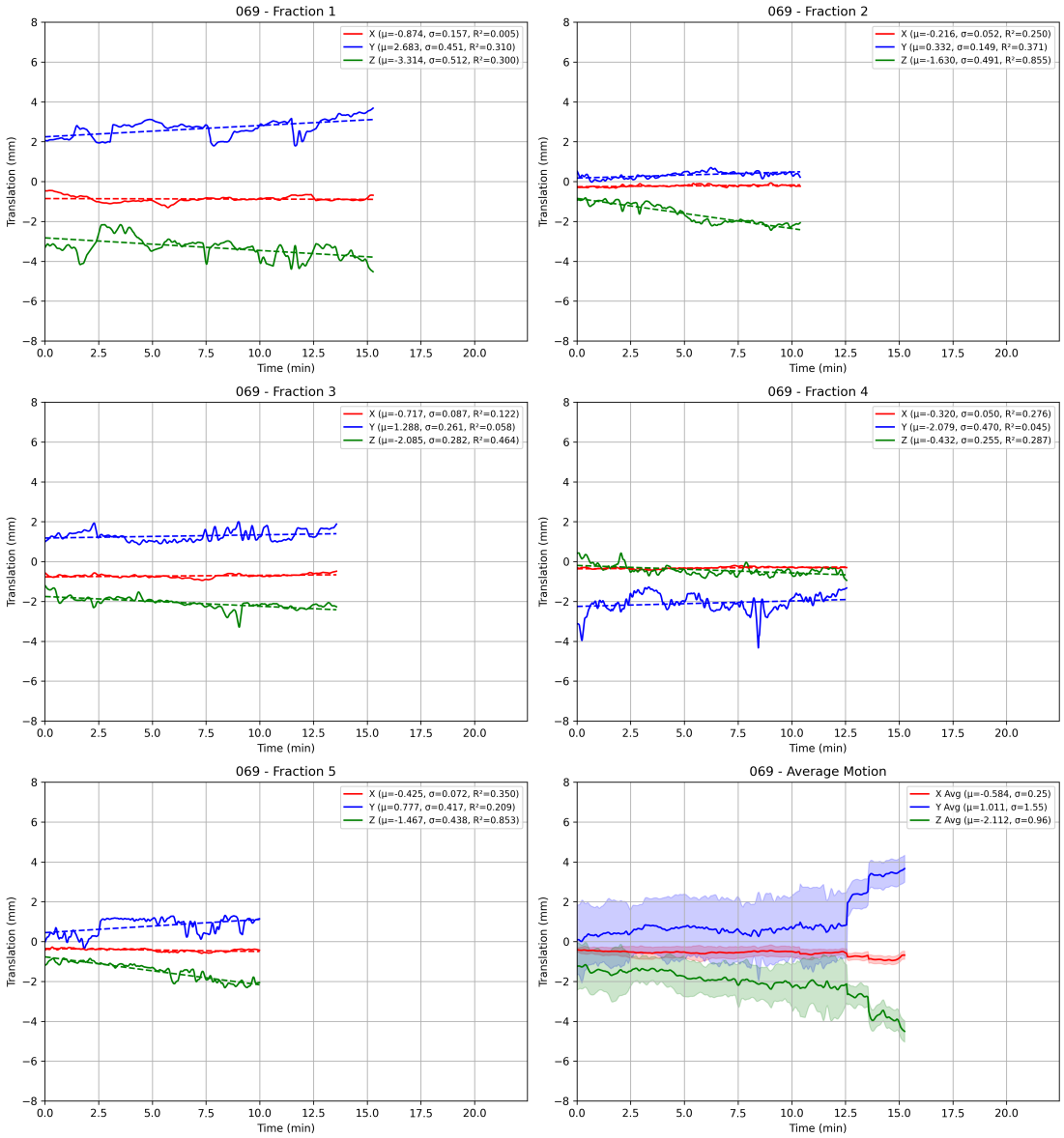

Figure B.69: Filtered traces plot for patient 069

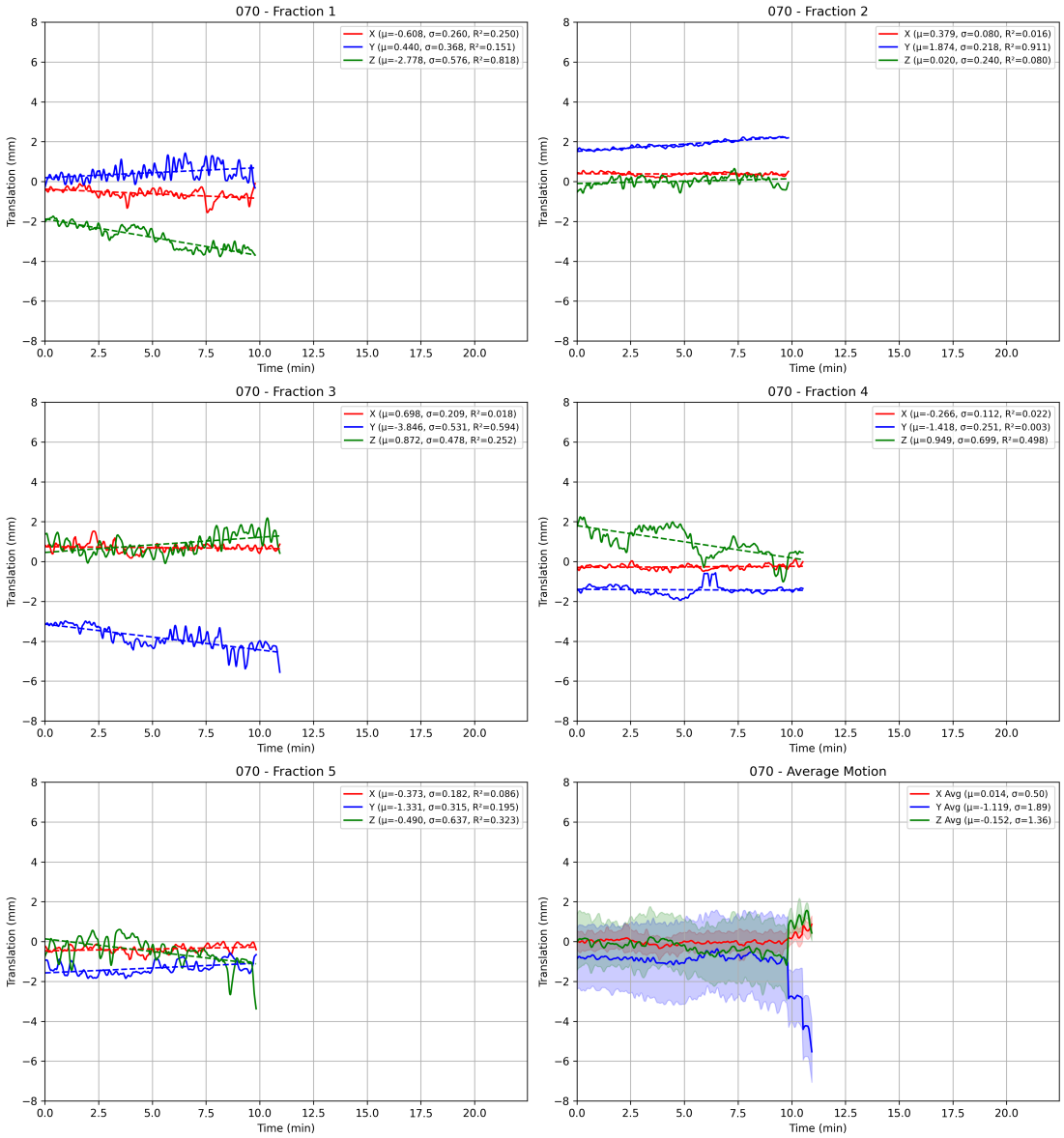

Figure B.70: Filtered traces plot for patient 070

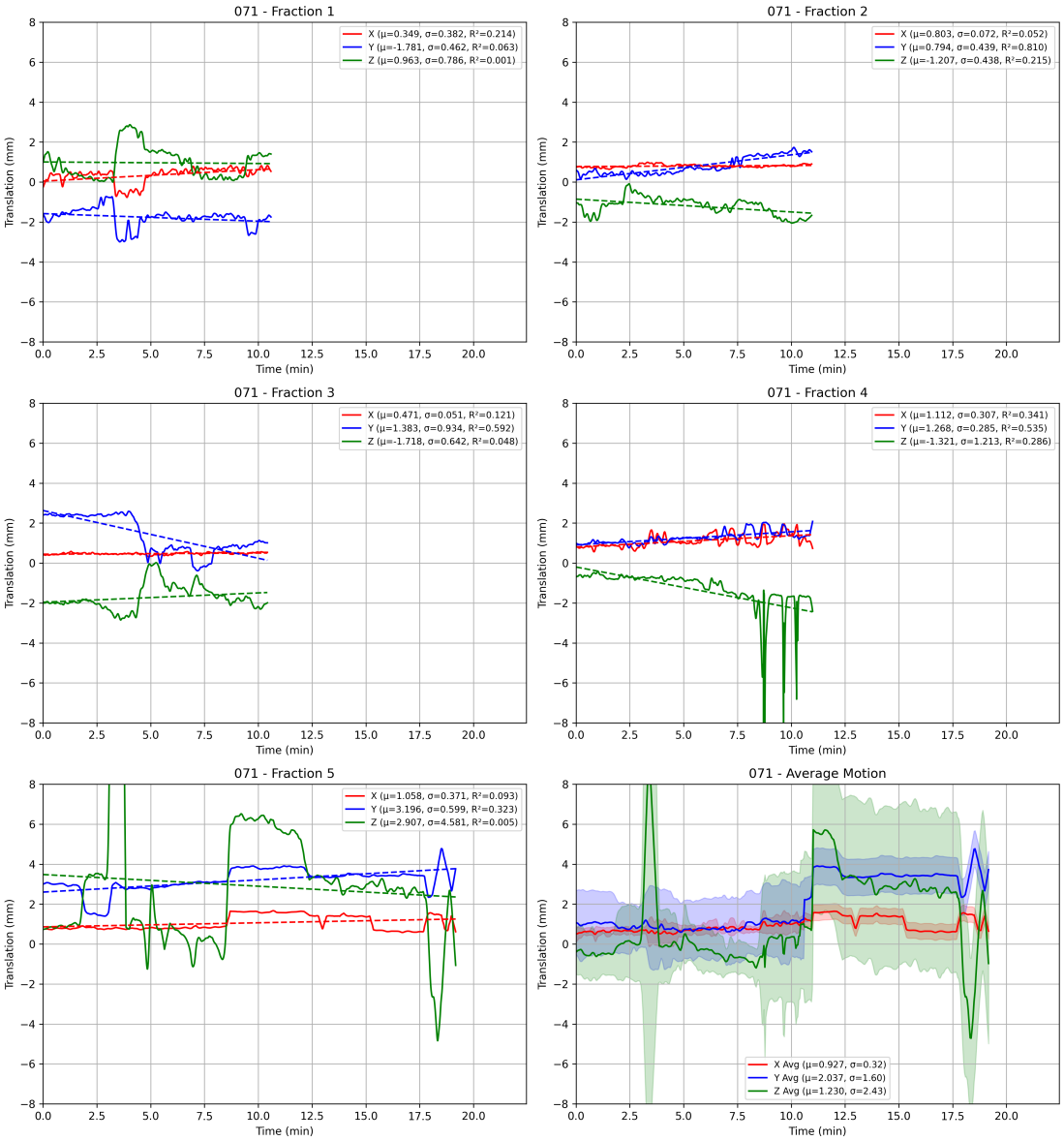

Figure B.71: Filtered traces plot for patient 071

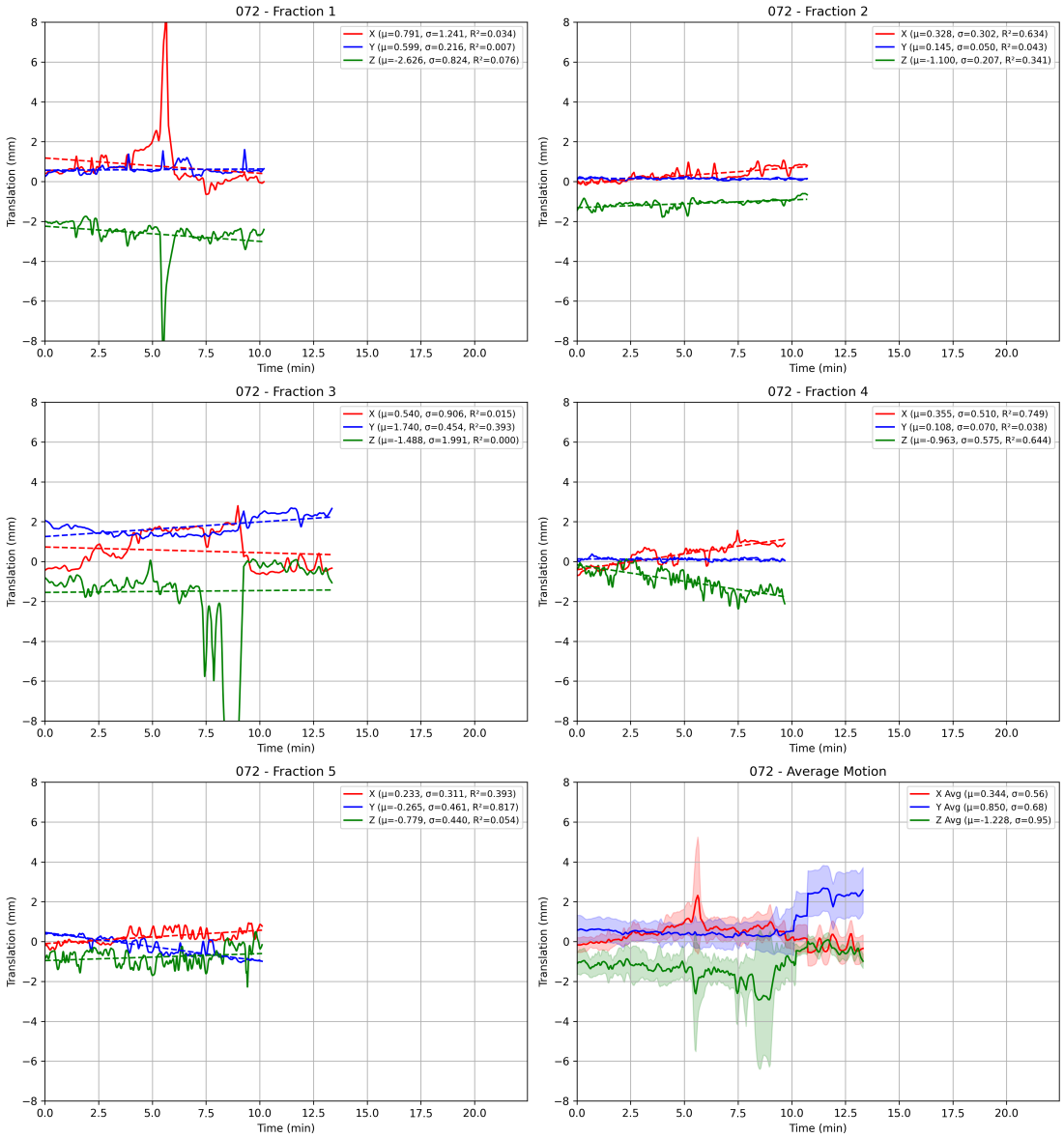

Figure B.72: Filtered traces plot for patient 072

C

Prostate Traces Legend Data

Table C.1: Patient statistics (X, Y, Z directions)

Patient	Fraction	Mean X	Std X	Slope X	R^2 X	Mean Y	Std Y	Slope Y	R^2 Y	Mean Z	Std Z	Slope Z	R^2 Z
001	1	-0.952	0.182	-0.033	0.265	1.142	1.125	0.295	0.563	-0.192	0.262	0.062	0.453
001	2	-0.272	0.254	-0.067	0.611	0.217	1.486	-0.069	0.019	0.054	0.136	0.019	0.171
001	3	0.372	0.301	-0.096	0.760	1.991	0.567	-0.002	0.000	-1.874	0.098	0.020	0.328
001	4	-1.072	0.274	-0.065	0.491	-1.180	0.683	-0.107	0.215	1.526	0.239	0.011	0.018
001	5	-1.258	0.089	-0.013	0.209	1.377	1.307	0.293	0.487	1.009	0.564	0.166	0.835
002	1	0.055	0.073	0.009	0.179	-0.645	0.218	0.034	0.318	-1.275	0.444	-0.110	0.776
002	2	0.064	0.055	0.008	0.506	0.579	0.449	0.076	0.709	-1.409	0.627	-0.118	0.873
002	3	0.299	0.043	0.007	0.448	1.250	0.417	0.073	0.503	-1.558	0.589	-0.127	0.756
002	4	0.713	0.034	0.009	0.657	0.625	0.259	0.060	0.541	0.414	0.138	-0.011	0.060
002	5	-0.282	0.021	-0.001	0.033	-0.587	0.116	0.009	0.064	-0.229	0.067	0.000	0.000
003	1	0.243	0.306	0.113	0.625	-1.892	0.283	0.073	0.303	0.640	0.324	0.010	0.005
003	2	-1.916	0.145	0.030	0.320	-2.096	0.251	0.030	0.107	2.100	0.297	-0.021	0.038
003	3	-0.179	0.082	-0.007	0.057	-0.900	0.136	0.032	0.457	0.709	0.271	-0.045	0.228
003	4	0.148	0.182	0.043	0.369	1.744	0.326	-0.024	0.034	-1.803	0.388	0.095	0.393
003	5	-0.706	0.095	-0.026	0.593	-0.731	0.286	0.015	0.021	-0.259	0.398	-0.093	0.414
004	1	4.298	1.199	0.233	0.633	-3.296	0.491	-0.046	0.149	-3.204	0.540	-0.120	0.832
004	2	0.077	0.146	0.001	0.001	-0.064	0.438	-0.114	0.617	-1.716	0.156	0.017	0.115
004	3	0.411	0.209	-0.003	0.003	2.027	0.317	0.044	0.373	-4.139	0.470	-0.085	0.635

Continued on next page

Patient	Fraction	Mean X	Std X	Slope X	R^2 X	Mean Y	Std Y	Slope Y	R^2 Y	Mean Z	Std Z	Slope Z	R^2 Z
004	4	0.008	0.182	0.015	0.071	0.742	0.286	0.022	0.066	-0.903	0.502	-0.133	0.772
004	5	-0.292	0.113	-0.018	0.232	-0.569	0.538	0.137	0.588	0.358	0.908	-0.284	0.891
005	1	-1.709	0.069	-0.012	0.153	-0.331	0.137	0.011	0.033	-0.819	0.308	-0.085	0.382
005	2	-1.228	0.078	-0.019	0.278	-0.239	0.148	-0.035	0.257	-0.159	0.265	-0.006	0.002
005	3	-0.503	0.090	-0.007	0.032	0.486	0.104	-0.021	0.203	-0.359	0.374	-0.138	0.692
005	4	-0.705	0.245	-0.031	0.066	-0.236	0.304	0.002	0.000	-0.477	0.223	-0.028	0.063
005	5	-0.603	0.049	-0.011	0.184	-1.062	0.405	0.000	0.000	0.722	0.219	0.007	0.004
006	1	0.369	0.674	-0.162	0.494	1.315	0.410	0.079	0.318	-1.704	0.632	-0.185	0.730
006	2	-1.135	0.230	0.005	0.004	2.180	0.495	0.139	0.702	0.343	0.431	-0.113	0.615
006	3	0.293	0.314	-0.088	0.686	1.878	0.242	0.063	0.604	-0.658	0.360	-0.108	0.798
006	4	2.105	0.222	-0.028	0.151	1.112	0.652	-0.006	0.001	-0.705	0.345	0.028	0.063
006	5	4.006	0.314	0.047	0.389	4.294	0.968	0.062	0.071	-3.904	0.590	-0.002	0.000
007	1	-0.486	0.781	-0.113	0.524	-1.128	0.812	-0.093	0.326	-0.183	2.299	0.302	0.431
007	2	1.658	0.314	0.023	0.053	1.134	0.275	-0.046	0.282	-1.701	0.321	0.018	0.031
007	3	-0.463	0.150	0.030	0.440	1.279	0.275	0.005	0.004	-0.909	0.277	0.012	0.019
007	4	0.144	0.142	0.021	0.177	-1.504	0.486	0.164	0.899	-0.269	0.654	-0.213	0.841
007	5	-0.773	0.331	-0.026	0.065	-1.290	0.383	0.090	0.609	1.778	0.660	-0.183	0.851
008	1	-0.393	0.254	-0.051	0.294	-0.798	0.558	-0.136	0.436	-0.152	0.627	-0.089	0.150
008	2	0.133	0.074	0.007	0.061	1.141	0.208	0.040	0.280	-0.407	0.626	-0.210	0.846

Continued on next page

Patient	Fraction	Mean X	Std X	Slope X	R^2 X	Mean Y	Std Y	Slope Y	R^2 Y	Mean Z	Std Z	Slope Z	R^2 Z
008	3	-0.071	0.107	-0.028	0.555	-0.883	0.226	0.000	0.000	-0.304	0.611	-0.055	0.064
008	4	-0.881	0.185	-0.028	0.442	1.311	0.285	0.062	0.904	-3.806	0.941	-0.201	0.868
008	5	-0.380	0.072	-0.009	0.116	1.004	0.326	0.104	0.832	-0.426	0.390	-0.129	0.894
009	1	-0.579	0.102	0.001	0.000	-1.030	0.356	0.102	0.674	-0.815	0.386	-0.123	0.834
009	2	-0.924	0.043	0.003	0.029	1.204	0.114	-0.009	0.045	-0.787	0.226	-0.072	0.736
009	3	-0.466	0.105	-0.006	0.030	-0.253	0.537	-0.135	0.519	-0.672	0.257	0.031	0.121
009	4	-0.423	0.120	-0.030	0.544	-0.692	0.278	0.051	0.281	-0.394	0.313	-0.085	0.625
009	5	1.852	0.094	0.005	0.017	-0.169	0.343	-0.050	0.119	-0.841	0.303	-0.070	0.302
010	1	0.415	0.211	-0.048	0.342	-0.272	0.676	-0.091	0.119	-1.407	0.441	-0.089	0.270
010	2	0.602	0.087	-0.027	0.596	-0.501	0.731	0.105	0.131	-1.107	0.666	-0.142	0.289
010	3	-0.015	0.082	-0.005	0.032	1.017	1.010	0.270	0.738	-1.314	0.913	-0.271	0.910
010	4	-0.518	0.212	0.061	0.555	-1.207	0.747	-0.060	0.044	-0.831	0.483	-0.054	0.084
010	5	0.563	0.043	0.002	0.020	0.021	0.117	-0.006	0.014	-1.655	0.123	-0.002	0.002
011	1	0.169	0.508	-0.163	0.788	0.504	0.437	0.008	0.002	-0.012	0.545	-0.119	0.366
011	2	1.793	0.526	-0.061	0.122	0.309	0.263	-0.037	0.180	-0.615	0.442	-0.023	0.024
011	3	2.298	0.732	-0.174	0.552	-0.172	0.614	0.090	0.212	0.614	0.728	-0.171	0.542
011	4	2.936	0.265	0.020	0.070	0.462	0.583	0.150	0.783	-0.805	0.461	-0.057	0.182
011	5	-0.822	0.255	-0.066	0.655	-1.290	0.418	0.096	0.514	-0.178	0.425	-0.099	0.531
012	1	-0.148	0.694	-0.141	0.662	1.125	0.683	0.015	0.008	-0.914	1.546	0.158	0.167

Continued on next page

Patient	Fraction	Mean X	Std X	Slope X	R^2 X	Mean Y	Std Y	Slope Y	R^2 Y	Mean Z	Std Z	Slope Z	R^2 Z
012	2	-0.234	0.122	-0.034	0.686	-0.234	0.805	0.043	0.026	-0.164	0.849	0.040	0.020
012	3	0.203	0.067	0.017	0.696	-0.417	0.912	0.027	0.010	-0.214	0.661	0.019	0.010
012	4	-0.087	0.077	0.023	0.854	1.411	0.293	0.084	0.747	-1.513	0.538	-0.157	0.782
012	5	0.739	0.102	0.024	0.652	0.959	0.440	-0.051	0.159	-1.611	0.525	0.042	0.074
013	1	0.666	0.182	-0.024	0.323	-1.494	0.519	-0.098	0.661	1.437	0.304	0.056	0.629
013	2	0.656	0.065	0.002	0.012	1.014	0.302	0.058	0.657	-0.634	0.445	-0.084	0.621
013	3	0.551	0.056	0.004	0.077	0.023	0.368	0.067	0.464	-0.988	0.572	-0.128	0.694
013	4	0.052	0.134	0.012	0.085	-0.814	0.754	-0.206	0.817	0.771	0.783	0.215	0.824
013	5	-0.610	0.090	0.007	0.098	0.515	0.158	0.020	0.253	-0.141	0.208	0.043	0.694
014	1	-0.078	0.045	0.000	0.000	0.252	0.349	0.090	0.571	0.275	0.142	-0.023	0.224
014	2	-0.943	0.062	0.018	0.496	-0.281	0.253	0.082	0.601	-0.004	0.131	-0.037	0.442
014	3	-0.312	0.036	0.007	0.171	0.781	0.430	0.083	0.179	0.266	0.116	0.000	0.000
014	4	0.507	0.265	0.055	0.825	2.017	0.677	0.142	0.839	-1.292	0.366	-0.071	0.725
014	5	1.814	0.117	0.031	0.450	0.502	0.615	0.225	0.872	0.354	0.430	-0.153	0.824
015	1	-0.363	0.037	0.001	0.002	1.477	0.359	0.095	0.660	-1.756	0.192	-0.021	0.107
015	2	0.343	0.041	-0.009	0.326	0.123	0.274	0.070	0.417	0.136	0.244	-0.061	0.396
015	3	0.269	0.218	0.029	0.144	0.317	0.509	0.123	0.460	-1.547	0.515	-0.087	0.226
015	4	0.487	0.038	0.000	0.001	-0.111	0.116	0.021	0.260	-0.077	0.224	-0.015	0.037
015	5	-0.246	0.048	0.001	0.005	0.480	0.263	0.046	0.275	0.123	0.333	-0.093	0.682

Continued on next page

Patient	Fraction	Mean X	Std X	Slope X	R^2 X	Mean Y	Std Y	Slope Y	R^2 Y	Mean Z	Std Z	Slope Z	R^2 Z
016	1	-0.120	0.216	-0.077	0.724	-0.626	0.192	0.046	0.333	1.417	0.221	0.038	0.174
016	2	0.071	0.091	0.020	0.299	0.848	0.219	0.081	0.900	-0.496	0.208	-0.045	0.301
016	3	-0.882	0.062	-0.020	0.516	-0.178	0.171	0.051	0.424	0.438	0.214	-0.045	0.212
016	4	-0.025	0.050	0.005	0.038	-0.302	0.190	0.039	0.197	2.212	0.275	0.046	0.131
016	5	0.218	0.076	0.000	0.000	-0.077	0.345	0.129	0.649	1.383	0.265	-0.066	0.291
017	1	-0.356	0.081	0.016	0.362	1.332	0.196	0.048	0.596	-1.251	0.217	-0.038	0.303
017	2	-1.001	0.058	0.010	0.313	-0.712	0.406	0.026	0.045	1.190	0.467	-0.061	0.182
017	3	-0.729	0.100	0.017	0.772	0.738	0.278	0.040	0.566	-0.361	0.295	-0.045	0.615
017	4	-1.408	0.063	0.001	0.005	1.472	0.189	0.047	0.591	-0.705	0.251	-0.068	0.716
017	5	-0.286	0.033	-0.007	0.379	0.662	0.584	0.011	0.003	0.695	0.598	0.032	0.023
018	1	-0.536	0.046	-0.001	0.002	2.084	0.318	0.087	0.690	-2.036	0.453	-0.137	0.844
018	2	-0.696	0.091	0.003	0.020	-1.407	1.077	-0.153	0.279	2.133	1.553	0.203	0.238
018	3	0.194	0.140	-0.020	0.200	-1.054	0.576	0.172	0.901	-0.894	0.773	-0.231	0.909
018	4	0.408	0.050	0.003	0.051	0.434	0.350	0.081	0.574	-0.400	0.163	0.016	0.100
018	5	-0.420	0.064	0.004	0.040	-1.685	0.301	0.070	0.635	-0.044	0.325	-0.073	0.587
019	1	0.374	0.044	0.001	0.008	1.027	0.321	0.080	0.626	-1.825	0.566	-0.157	0.785
019	2	0.381	0.052	-0.007	0.146	-0.289	0.286	-0.009	0.008	0.750	0.410	-0.038	0.076
019	3	0.701	0.137	0.012	0.094	-0.451	0.500	-0.105	0.520	1.303	1.139	0.201	0.372
019	4	-0.033	0.042	-0.003	0.055	0.007	0.862	0.013	0.003	0.306	0.830	-0.055	0.056

Continued on next page

Patient	Fraction	Mean X	Std X	Slope X	R^2 X	Mean Y	Std Y	Slope Y	R^2 Y	Mean Z	Std Z	Slope Z	R^2 Z
019	5	-0.325	0.167	-0.019	0.165	-0.735	1.114	-0.257	0.686	0.808	0.999	0.169	0.369
020	1	0.411	0.042	0.000	0.001	-0.128	0.409	0.114	0.663	0.469	0.323	0.066	0.361
020	2	-0.867	0.043	0.007	0.295	0.689	0.512	0.153	0.890	0.898	0.650	-0.145	0.494
020	3	-1.047	0.095	-0.008	0.069	-0.267	0.166	-0.022	0.190	-1.829	0.457	-0.089	0.400
020	4	0.081	0.039	0.005	0.166	2.186	0.299	0.063	0.520	-1.095	0.118	0.005	0.021
020	5	0.247	0.059	-0.008	0.213	1.761	0.178	-0.005	0.009	-1.537	0.210	0.007	0.011
021	1	1.532	0.083	0.015	0.318	-1.675	0.438	0.108	0.626	-1.865	0.237	-0.042	0.327
021	2	0.020	0.065	-0.008	0.144	1.549	0.279	0.083	0.802	-1.072	0.520	-0.158	0.843
021	3	-0.356	0.053	0.009	0.212	0.170	0.191	-0.021	0.099	-0.843	0.418	-0.125	0.700
021	4	-0.681	0.094	0.006	0.032	-0.016	0.194	-0.015	0.045	-1.501	0.243	-0.032	0.120
021	5	0.271	0.089	0.004	0.031	3.268	1.365	0.321	0.920	-1.983	0.608	-0.071	0.227
022	1	0.382	0.048	0.001	0.006	-0.373	0.506	0.125	0.694	-0.654	0.415	-0.103	0.701
022	2	0.849	0.042	0.007	0.252	-1.001	0.196	0.026	0.160	-0.204	0.324	0.000	0.000
022	3	0.189	0.050	-0.010	0.397	-0.521	0.439	0.121	0.799	0.057	0.652	-0.177	0.769
022	4	-0.204	0.301	0.039	0.216	-2.253	3.593	-0.647	0.423	0.341	1.586	0.235	0.287
022	5	-1.312	0.048	-0.010	0.371	-2.155	0.313	-0.017	0.027	0.868	0.324	0.002	0.000
023	1	-0.598	0.247	-0.004	0.004	1.703	0.544	0.116	0.711	-3.561	0.431	-0.027	0.063
023	2	-0.447	0.094	-0.004	0.019	3.191	0.315	0.082	0.676	-2.491	0.450	-0.075	0.280
023	3	0.423	0.105	-0.005	0.030	2.165	0.554	0.038	0.071	-2.788	0.781	-0.130	0.430

Continued on next page

Patient	Fraction	Mean X	Std X	Slope X	R^2 X	Mean Y	Std Y	Slope Y	R^2 Y	Mean Z	Std Z	Slope Z	R^2 Z
023	4	1.466	0.523	0.079	0.554	3.494	0.872	0.136	0.594	-2.704	0.450	-0.072	0.624
024	1	0.102	0.140	-0.040	0.874	1.186	0.616	0.171	0.827	-1.722	1.921	-0.565	0.926
024	2	1.198	0.516	0.049	0.374	1.106	1.206	-0.085	0.207	0.107	4.208	0.413	0.402
024	3	-0.766	0.049	-0.015	0.773	1.342	0.752	0.189	0.502	-1.180	1.414	-0.441	0.775
024	4	-1.638	0.296	-0.057	0.663	1.727	0.989	0.209	0.794	-4.331	1.600	-0.272	0.517
024	5	0.524	0.055	0.009	0.221	-1.603	0.504	0.098	0.317	1.621	0.584	-0.176	0.769
025	1	0.292	0.088	0.005	0.035	2.642	0.438	0.046	0.123	-3.162	0.322	-0.077	0.631
025	2	-0.930	0.082	-0.006	0.071	1.674	0.424	0.091	0.709	-0.939	0.491	-0.115	0.851
025	3	-0.137	0.064	-0.007	0.130	1.310	0.127	0.025	0.455	-0.388	0.599	-0.138	0.607
025	4	-0.468	0.287	0.011	0.029	1.109	0.095	0.006	0.095	-2.398	1.155	-0.061	0.060
025	5	-0.863	0.086	-0.013	0.295	1.776	0.170	0.024	0.260	0.090	0.413	-0.102	0.817
026	1	0.550	0.084	-0.017	0.386	-0.128	0.441	-0.111	0.579	0.575	1.370	0.344	0.573
026	2	0.035	0.053	0.010	0.356	1.007	0.205	-0.040	0.360	-0.373	0.843	0.211	0.600
026	3	0.145	0.250	-0.061	0.753	1.374	0.326	0.020	0.049	0.079	0.544	-0.013	0.007
026	4	0.912	0.036	-0.001	0.014	2.062	0.178	0.056	0.812	-1.085	0.605	-0.198	0.877
026	5	0.166	0.332	-0.061	0.447	0.029	0.605	-0.085	0.257	1.832	1.432	0.351	0.789
027	1	-0.794	0.218	-0.052	0.404	-1.097	0.398	-0.132	0.783	-0.140	0.387	0.128	0.781
027	2	1.218	0.434	-0.129	0.833	-1.056	0.310	0.079	0.615	-2.440	0.231	0.043	0.323
027	3	0.260	0.185	0.009	0.021	1.850	0.381	0.113	0.786	-0.187	0.219	-0.010	0.019

Continued on next page

Patient	Fraction	Mean X	Std X	Slope X	R^2 X	Mean Y	Std Y	Slope Y	R^2 Y	Mean Z	Std Z	Slope Z	R^2 Z
027	4	0.277	0.167	-0.004	0.005	0.277	0.321	0.068	0.347	-2.124	0.319	0.011	0.009
027	5	0.181	0.114	0.023	0.292	0.430	0.525	0.173	0.806	-1.316	0.203	0.037	0.252
028	1	0.179	0.150	0.032	0.507	-0.546	0.336	0.003	0.001	-2.078	0.419	-0.080	0.419
028	2	-0.171	0.200	-0.051	0.530	-1.537	0.577	-0.153	0.588	1.671	0.685	0.102	0.184
028	3	0.160	0.077	-0.002	0.007	-0.582	0.279	-0.049	0.214	0.076	0.293	-0.039	0.121
028	4	0.330	0.073	0.018	0.480	-0.803	0.226	-0.001	0.000	-0.442	0.242	-0.021	0.064
028	5	0.365	0.075	0.003	0.012	0.867	0.284	0.030	0.088	-0.264	0.250	-0.014	0.027
029	1	0.192	0.035	0.006	0.256	0.416	0.431	0.140	0.909	-0.635	0.225	-0.052	0.460
029	2	1.214	0.436	0.065	0.609	3.207	0.405	0.074	0.907	-2.463	0.339	0.001	0.000
029	3	0.637	0.028	0.000	0.001	0.912	0.122	0.015	0.109	-0.191	0.293	0.063	0.338
029	4	0.690	0.030	-0.004	0.153	0.463	0.116	0.027	0.405	0.146	0.165	-0.003	0.003
029	5	1.211	0.057	0.007	0.202	1.001	0.177	-0.021	0.179	-0.836	0.211	0.008	0.016
030	1	-0.487	0.337	-0.107	0.881	1.737	0.443	0.130	0.758	-1.373	0.468	-0.145	0.842
030	2	-0.622	0.275	-0.089	0.795	1.228	0.153	-0.040	0.519	-1.426	0.307	0.013	0.013
030	3	-0.883	0.042	0.007	0.246	1.175	0.387	0.108	0.733	-1.053	0.277	-0.083	0.844
030	4	0.029	0.053	0.008	0.185	0.092	0.182	0.040	0.416	-0.967	0.223	-0.061	0.642
030	5	-0.038	0.204	0.069	0.879	1.584	0.414	0.128	0.722	-2.239	0.234	-0.064	0.574
031	1	-0.509	0.168	0.019	0.074	0.454	0.278	-0.021	0.034	-0.583	0.436	-0.086	0.222
031	2	-0.301	0.143	-0.036	0.451	1.482	0.334	0.117	0.849	-2.288	0.605	-0.183	0.630

Continued on next page

Patient	Fraction	Mean X	Std X	Slope X	R^2 X	Mean Y	Std Y	Slope Y	R^2 Y	Mean Z	Std Z	Slope Z	R^2 Z
031	3	0.417	0.163	0.030	0.515	-1.538	0.998	-0.023	0.008	0.720	1.271	0.009	0.001
031	4	-0.348	0.075	-0.016	0.391	-0.134	0.227	-0.035	0.190	-0.293	0.335	-0.085	0.523
031	5	0.348	0.043	-0.002	0.038	0.749	0.234	-0.018	0.074	-1.537	0.401	-0.068	0.357
032	1	0.093	0.158	-0.018	0.158	-2.038	0.899	0.156	0.362	1.919	1.536	-0.258	0.342
032	2	-0.826	0.122	-0.030	0.467	-0.236	0.181	0.031	0.221	-0.081	0.231	-0.035	0.177
032	3	0.331	0.108	-0.013	0.121	0.415	0.126	0.011	0.063	0.209	0.349	-0.077	0.405
032	4	0.479	0.208	-0.022	0.103	0.182	0.640	-0.150	0.525	0.551	0.723	0.141	0.360
032	5	-0.505	0.108	0.028	0.512	0.400	0.285	0.053	0.253	0.030	0.463	-0.136	0.631
033	1	-0.698	0.068	0.012	0.220	0.686	0.143	0.043	0.659	-1.451	0.542	-0.182	0.841
033	2	-0.106	0.077	0.019	0.542	0.757	0.296	0.064	0.408	-1.690	0.583	-0.192	0.938
033	3	0.012	0.043	0.006	0.203	0.944	0.111	0.035	0.904	-1.049	0.166	-0.031	0.335
033	4	-0.067	0.031	-0.005	0.288	0.191	0.133	-0.030	0.585	0.156	0.249	0.042	0.338
033	5	-0.396	0.050	0.000	0.001	1.962	0.108	-0.002	0.004	-1.109	0.202	-0.030	0.193
034	1	2.238	0.269	0.078	0.687	0.894	0.360	0.078	0.382	-1.940	0.854	-0.291	0.952
034	2	1.634	0.217	-0.043	0.397	1.371	0.190	0.043	0.493	-2.114	0.334	-0.054	0.254
034	3	-0.519	0.100	0.018	0.265	0.541	0.567	-0.114	0.313	-0.323	0.466	0.106	0.405
034	4	1.528	0.262	-0.068	0.484	1.313	0.190	-0.042	0.347	-1.098	0.306	0.069	0.369
034	5	0.165	0.142	0.009	0.029	-0.153	0.589	-0.164	0.615	-0.037	0.656	0.192	0.678
035	1	0.310	0.564	0.174	0.719	1.251	0.608	-0.185	0.700	-1.340	0.837	0.249	0.672

Continued on next page

Patient	Fraction	Mean X	Std X	Slope X	R^2 X	Mean Y	Std Y	Slope Y	R^2 Y	Mean Z	Std Z	Slope Z	R^2 Z
035	2	1.448	0.252	0.049	0.418	-1.253	0.255	-0.003	0.002	-0.204	0.489	-0.120	0.661
035	3	0.082	0.340	0.017	0.041	-1.164	0.356	-0.033	0.132	0.363	0.517	0.084	0.418
035	4	-0.237	0.345	-0.015	0.027	0.645	0.206	-0.014	0.063	-0.978	0.388	-0.057	0.300
035	5	-0.314	0.474	0.144	0.893	-0.517	0.355	-0.038	0.109	-0.665	0.469	0.098	0.426
036	1	1.642	1.210	0.262	0.376	1.527	0.435	-0.045	0.088	-1.514	0.671	0.100	0.178
036	2	1.528	0.365	0.058	0.224	-0.846	0.450	-0.098	0.418	2.348	0.748	0.048	0.037
036	3	-0.503	1.950	-0.422	0.786	0.790	1.058	0.206	0.638	-1.814	2.427	-0.406	0.470
036	4	2.338	0.438	0.002	0.000	1.367	0.351	0.094	0.598	-0.277	0.580	0.041	0.040
036	5	1.039	0.406	-0.022	0.032	0.459	0.493	0.119	0.617	-1.296	0.910	-0.232	0.687
037	1	-2.838	0.155	0.012	0.060	-0.946	0.429	0.104	0.632	-0.123	0.442	-0.024	0.033
037	2	-0.432	0.457	-0.116	0.855	-0.280	0.195	0.011	0.043	1.252	0.197	0.037	0.471
037	3	-0.958	0.677	-0.161	0.597	-2.228	0.847	-0.024	0.009	-0.851	0.991	0.105	0.119
037	4	0.176	0.360	-0.015	0.018	-0.232	0.496	-0.042	0.072	0.320	1.039	0.151	0.208
037	5	-0.599	1.206	-0.354	0.765	1.528	0.426	0.097	0.458	-0.426	0.538	-0.137	0.576
038	1	-0.640	0.117	-0.030	0.375	1.561	0.226	0.038	0.164	-1.256	0.712	-0.270	0.817
038	2	1.632	0.135	0.017	0.064	0.582	0.256	0.045	0.133	-0.850	0.331	-0.024	0.023
038	3	1.557	0.107	0.006	0.012	1.413	0.348	0.035	0.046	-1.527	0.304	0.030	0.043
038	4	0.503	0.368	-0.044	0.152	0.122	0.204	-0.003	0.002	-1.011	0.655	-0.083	0.176
038	5	1.964	0.163	0.044	0.382	-0.225	0.483	-0.195	0.835	-1.004	0.244	0.000	0.000

Continued on next page

Patient	Fraction	Mean X	Std X	Slope X	R^2 X	Mean Y	Std Y	Slope Y	R^2 Y	Mean Z	Std Z	Slope Z	R^2 Z
039	1	-0.812	0.347	-0.037	0.130	0.178	0.588	0.107	0.387	-3.568	0.765	-0.189	0.717
039	2	-0.613	0.133	0.024	0.164	0.879	0.283	-0.010	0.006	-1.716	0.280	-0.087	0.502
039	3	-0.670	0.197	-0.043	0.221	1.742	0.256	0.050	0.177	-2.094	0.612	-0.192	0.464
039	4	-1.204	0.432	-0.080	0.118	1.029	0.326	0.047	0.071	-1.185	0.268	-0.070	0.233
039	5	0.046	0.472	-0.038	0.028	0.207	0.366	-0.007	0.002	-0.850	0.267	-0.018	0.021
040	1	-0.196	0.236	0.048	0.399	1.690	0.195	-0.015	0.060	-0.614	0.543	0.087	0.245
040	2	-1.399	0.161	0.034	0.395	0.241	0.246	0.008	0.011	-1.441	0.392	0.063	0.229
040	3	-0.442	0.137	0.024	0.275	0.587	0.469	0.084	0.299	-1.523	0.571	-0.088	0.222
040	4	0.817	0.080	0.017	0.472	0.599	0.426	0.018	0.019	-1.285	0.278	-0.021	0.060
040	5	-1.048	0.160	0.047	0.628	-1.347	1.350	-0.393	0.626	-0.464	1.060	0.247	0.400
041	1	0.443	0.091	0.013	0.275	0.215	0.349	-0.060	0.399	0.074	0.713	0.164	0.704
041	2	0.330	0.222	-0.018	0.126	-0.716	0.871	-0.157	0.614	2.021	1.607	0.326	0.777
041	3	-0.317	0.249	-0.064	0.668	0.265	0.451	0.121	0.733	-0.092	0.462	-0.135	0.874
041	4	-0.733	0.123	0.002	0.002	-1.393	0.247	0.051	0.428	-0.086	0.182	-0.040	0.478
041	5	0.284	0.138	0.040	0.726	-1.859	0.381	-0.004	0.001	1.414	0.709	0.194	0.667
042	1	-0.209	0.048	-0.002	0.025	0.883	0.660	0.016	0.008	-0.039	0.438	0.016	0.017
042	2	0.464	0.048	-0.006	0.254	0.244	0.207	0.001	0.000	0.013	0.268	0.040	0.328
042	3	3.223	0.034	0.005	0.196	1.192	0.351	0.047	0.198	0.105	0.206	-0.032	0.266
042	4	1.281	0.064	-0.015	0.517	-2.491	0.444	-0.118	0.696	1.769	0.208	0.005	0.005

Continued on next page

Patient	Fraction	Mean X	Std X	Slope X	R^2 X	Mean Y	Std Y	Slope Y	R^2 Y	Mean Z	Std Z	Slope Z	R^2 Z
042	5	1.364	0.171	0.058	0.882	-0.675	0.456	-0.092	0.307	0.115	0.950	0.184	0.284
043	1	3.518	0.590	0.183	0.831	-2.440	0.286	0.033	0.113	-1.002	0.519	-0.109	0.377
043	2	3.147	0.904	0.183	0.795	-4.641	0.665	-0.113	0.563	3.346	0.427	0.006	0.003
043	3	2.736	0.452	0.079	0.272	-0.996	0.603	0.147	0.527	-0.955	0.634	-0.040	0.036
043	4	0.770	0.534	0.172	0.918	-1.068	0.449	0.097	0.408	1.236	0.366	-0.011	0.007
044	1	-0.301	0.087	0.010	0.193	-0.460	0.257	0.054	0.676	0.968	0.297	0.014	0.036
044	2	-0.041	0.051	-0.003	0.054	1.281	0.309	0.079	0.918	1.484	0.327	0.004	0.002
044	3	-0.079	0.074	-0.002	0.007	0.186	0.557	-0.087	0.242	0.442	0.953	0.132	0.189
044	4	-0.679	0.104	0.028	0.863	0.457	0.467	0.128	0.882	1.262	0.801	-0.216	0.851
044	5	-0.488	0.110	0.011	0.235	2.843	1.130	0.206	0.782	-0.847	0.698	-0.046	0.103
045	1	1.019	0.205	-0.069	0.574	0.597	0.328	-0.084	0.329	-1.139	0.469	0.159	0.581
045	2	6.093	2.151	0.436	0.877	-0.361	0.985	-0.173	0.656	1.124	1.232	0.232	0.757
045	3	0.514	0.633	-0.134	0.574	2.928	1.061	0.184	0.382	-3.427	0.965	-0.226	0.696
045	4	1.704	0.473	0.152	0.719	-0.399	0.465	0.093	0.277	1.112	0.382	-0.031	0.046
045	5	-0.854	0.504	0.181	0.844	0.357	0.835	-0.122	0.140	-1.426	0.756	0.203	0.477
046	1	-0.575	0.061	-0.006	0.184	0.749	0.333	0.069	0.827	-1.109	0.583	-0.116	0.750
046	2	-0.636	0.052	-0.009	0.329	-0.420	0.332	0.041	0.164	-1.002	0.635	-0.122	0.402
046	3	-0.141	0.092	0.023	0.850	0.859	0.321	0.040	0.219	-1.327	0.574	-0.127	0.680
046	4	-0.994	0.045	0.009	0.523	0.819	0.195	0.028	0.307	-0.844	0.349	-0.070	0.588

Continued on next page

Patient	Fraction	Mean X	Std X	Slope X	R^2 X	Mean Y	Std Y	Slope Y	R^2 Y	Mean Z	Std Z	Slope Z	R^2 Z
046	5	0.141	0.050	0.002	0.026	0.962	0.265	0.049	0.541	-0.720	0.330	-0.067	0.656
047	1	0.751	0.094	-0.005	0.014	0.217	0.315	-0.044	0.117	-0.535	0.360	-0.073	0.242
047	2	-0.190	0.136	0.041	0.751	-0.314	0.512	-0.114	0.403	-1.454	0.741	0.116	0.198
047	3	0.345	0.320	0.023	0.120	-2.026	0.806	-0.058	0.119	0.871	0.929	-0.012	0.004
047	4	0.134	0.105	-0.015	0.168	0.309	0.381	0.044	0.103	-0.795	0.590	0.047	0.049
047	5	-1.519	0.149	-0.048	0.807	0.501	0.569	0.186	0.826	-0.134	0.797	-0.273	0.906
048	1	0.391	0.198	-0.046	0.726	-0.808	0.094	-0.014	0.306	1.984	0.564	0.152	0.975
048	2	0.256	0.094	0.003	0.015	-0.125	0.642	0.144	0.882	1.562	0.474	-0.039	0.117
048	3	0.308	0.069	0.013	0.574	0.549	0.298	0.070	0.865	1.805	0.176	0.034	0.602
048	4	-0.092	0.164	-0.034	0.679	1.718	0.117	0.014	0.242	0.103	0.596	0.065	0.192
048	5	-0.212	0.095	-0.012	0.245	-0.501	0.687	0.155	0.796	2.297	0.592	-0.121	0.648
049	1	0.048	0.085	0.021	0.502	1.561	0.312	0.104	0.945	-2.024	0.478	-0.155	0.890
049	2	-0.307	0.075	-0.015	0.556	0.687	0.478	0.084	0.426	-1.298	0.695	-0.162	0.752
049	3	-0.965	0.128	0.025	0.424	2.160	0.572	-0.099	0.317	-0.368	1.316	0.196	0.237
049	4	-0.073	0.222	-0.028	0.207	1.277	0.584	0.141	0.771	-3.219	0.992	-0.203	0.554
049	5	0.404	0.038	0.004	0.085	0.532	0.444	0.141	0.747	-2.240	1.305	-0.443	0.853
050	1	-0.758	0.126	0.037	0.816	2.399	0.604	0.193	0.941	-0.838	0.597	-0.186	0.890
050	2	-1.776	0.491	-0.127	0.839	3.407	1.197	0.280	0.692	-2.337	0.805	-0.163	0.517
050	3	0.460	0.077	0.004	0.029	1.814	0.646	0.187	0.929	-1.140	0.406	-0.114	0.881

Continued on next page

Patient	Fraction	Mean X	Std X	Slope X	R^2 X	Mean Y	Std Y	Slope Y	R^2 Y	Mean Z	Std Z	Slope Z	R^2 Z
050	4	-0.240	0.143	-0.011	0.176	3.778	1.009	0.170	0.870	-2.031	0.359	-0.042	0.418
050	5	-0.899	0.244	-0.051	0.429	0.129	0.529	0.054	0.103	-0.444	0.619	-0.142	0.528
051	1	0.719	0.850	-0.022	0.008	-0.012	0.871	0.088	0.123	-2.612	2.514	-0.380	0.274
051	2	-2.224	0.614	-0.024	0.029	-3.218	1.065	-0.201	0.684	2.285	1.578	0.288	0.641
051	3	-0.186	0.890	-0.166	0.281	-0.040	0.640	0.140	0.385	-1.306	1.593	-0.474	0.712
051	4	0.543	0.529	0.019	0.013	-0.382	0.887	-0.046	0.028	0.956	1.146	0.077	0.046
051	5	0.459	0.641	0.081	0.160	-1.215	2.026	-0.131	0.042	0.048	0.912	0.164	0.326
052	1	1.078	0.337	0.000	0.000	-0.038	1.673	-0.106	0.147	-4.947	2.684	-0.321	0.522
052	2	1.078	0.366	0.059	0.802	-0.513	1.249	-0.127	0.323	4.021	1.212	0.173	0.637
052	3	0.771	0.121	0.005	0.023	-0.531	0.160	0.038	0.640	0.794	0.132	-0.011	0.083
052	4	0.530	0.284	0.041	0.281	-1.278	0.919	0.218	0.750	0.285	1.398	-0.278	0.529
052	5	0.991	0.471	0.045	0.100	-0.402	1.550	-0.320	0.475	-1.683	0.668	0.014	0.005
053	1	-0.546	0.393	-0.067	0.455	-1.040	0.300	0.023	0.094	0.384	0.341	-0.036	0.173
053	2	-0.505	0.324	0.085	0.586	-0.806	0.406	0.090	0.419	-1.056	0.575	-0.168	0.720
053	3	-1.304	0.511	0.008	0.002	-1.923	0.370	0.015	0.018	1.181	0.494	-0.035	0.052
053	4	-0.388	0.367	0.044	0.132	0.479	0.323	0.030	0.079	-0.623	0.243	0.011	0.019
053	5	-0.989	0.135	0.001	0.000	-0.033	0.309	-0.072	0.482	0.042	0.449	0.092	0.375
054	1	-1.712	0.118	-0.010	0.066	0.738	0.484	0.150	0.833	-0.060	0.862	-0.274	0.878
054	2	-0.718	0.129	0.030	0.647	0.010	0.483	0.130	0.864	0.375	1.009	-0.282	0.929

Continued on next page

Patient	Fraction	Mean X	Std X	Slope X	R^2 X	Mean Y	Std Y	Slope Y	R^2 Y	Mean Z	Std Z	Slope Z	R^2 Z
054	3	-0.343	0.365	0.087	0.641	-0.151	0.767	-0.145	0.406	1.491	0.996	0.189	0.408
054	4	-0.268	0.129	0.033	0.778	2.988	0.282	0.072	0.786	-3.448	0.654	-0.168	0.792
054	5	-0.445	0.124	0.027	0.478	1.578	0.265	0.076	0.852	-0.897	0.732	-0.207	0.832
055	1	-0.544	0.116	0.006	0.067	1.484	0.649	0.125	0.811	-1.923	1.086	-0.207	0.790
055	2	0.047	0.099	0.018	0.323	0.020	0.219	0.010	0.022	0.143	0.413	-0.038	0.087
055	3	-0.342	0.189	0.002	0.003	2.003	1.333	0.105	0.139	-0.856	2.024	0.049	0.013
055	4	-0.113	0.074	0.010	0.253	1.529	0.569	0.143	0.818	-0.856	0.439	-0.103	0.713
055	5	-0.314	0.226	0.033	0.299	-0.861	0.895	0.023	0.009	1.643	1.936	0.097	0.035
056	1	0.629	0.106	-0.003	0.016	-2.730	1.088	-0.170	0.424	2.065	1.483	0.215	0.364
056	2	-0.264	0.056	0.014	0.448	0.471	0.216	0.059	0.576	0.302	0.418	0.056	0.141
056	3	0.220	0.021	0.000	0.002	0.929	0.273	0.074	0.909	-0.803	0.277	-0.023	0.083
056	4	-2.240	0.393	-0.094	0.681	3.205	0.594	0.140	0.661	-3.191	0.453	-0.111	0.718
056	5	-1.174	0.053	0.015	0.697	1.643	0.156	0.049	0.851	-0.974	0.332	-0.077	0.464
057	1	-0.174	0.103	-0.021	0.571	-0.997	0.417	0.097	0.732	-2.726	0.618	-0.160	0.914
057	2	0.715	0.147	0.027	0.547	3.036	0.806	0.176	0.763	-3.989	0.504	-0.089	0.497
057	3	0.584	0.073	0.011	0.151	1.364	0.135	0.038	0.513	-2.352	0.344	-0.015	0.012
057	4	1.161	0.059	-0.017	0.545	0.951	0.319	0.112	0.844	0.523	0.333	0.003	0.001
057	5	0.191	0.084	-0.020	0.802	1.040	0.634	0.163	0.910	-4.571	0.406	-0.078	0.506
058	1	-0.353	0.324	-0.095	0.713	-2.938	0.336	0.070	0.367	1.908	0.591	-0.175	0.730

Continued on next page

Patient	Fraction	Mean X	Std X	Slope X	R^2 X	Mean Y	Std Y	Slope Y	R^2 Y	Mean Z	Std Z	Slope Z	R^2 Z
058	2	-0.103	0.076	-0.005	0.030	0.191	0.132	-0.002	0.002	-0.881	0.370	-0.067	0.268
058	3	-1.097	0.286	-0.097	0.859	0.560	0.201	-0.025	0.116	-0.702	0.381	-0.098	0.491
058	4	-0.453	0.050	-0.002	0.025	1.638	0.672	0.191	0.920	-2.634	0.745	-0.171	0.604
058	5	-1.186	0.094	-0.029	0.743	-0.509	0.652	0.191	0.667	-0.451	0.851	-0.258	0.713
059	1	1.243	0.203	-0.059	0.571	0.074	0.355	0.069	0.255	0.425	0.545	-0.035	0.028
059	2	0.175	0.414	0.124	0.710	0.015	0.383	0.063	0.216	0.115	0.474	0.035	0.043
059	3	1.408	0.074	0.007	0.087	-1.502	0.519	0.122	0.497	1.854	0.744	-0.127	0.263
059	4	0.082	0.155	-0.001	0.000	-0.409	0.593	0.087	0.178	0.235	0.809	-0.136	0.234
059	5	-0.078	0.224	0.071	0.618	0.002	0.534	-0.056	0.066	0.066	0.805	0.097	0.089
060	1	-0.208	0.041	-0.002	0.015	0.975	0.513	0.146	0.807	0.830	0.606	0.143	0.549
060	2	-0.558	0.071	-0.018	0.590	0.567	0.198	0.033	0.265	-1.004	0.212	0.023	0.112
060	3	-0.519	0.079	-0.018	0.423	1.312	0.205	0.046	0.411	-1.559	0.118	-0.017	0.170
060	4	-0.297	0.122	0.031	0.607	0.283	0.341	0.044	0.161	-0.892	0.321	0.030	0.083
060	5	-0.552	0.081	0.017	0.475	0.401	0.184	-0.006	0.012	1.129	0.428	0.116	0.815
061	1	-0.626	0.218	-0.026	0.217	-0.742	1.180	-0.233	0.606	0.727	1.398	0.116	0.107
061	2	-0.362	0.061	-0.003	0.033	3.420	0.314	-0.013	0.028	-2.893	0.526	-0.075	0.343
061	3	-0.185	0.093	-0.001	0.003	2.071	0.488	-0.086	0.579	-1.669	0.943	0.167	0.585
061	4	-0.030	0.126	-0.029	0.835	-0.249	0.103	-0.015	0.341	1.188	0.567	0.125	0.752
061	5	1.004	0.484	-0.001	0.000	1.504	0.480	0.010	0.013	-1.439	3.357	-0.164	0.063

Continued on next page

Patient	Fraction	Mean X	Std X	Slope X	R^2 X	Mean Y	Std Y	Slope Y	R^2 Y	Mean Z	Std Z	Slope Z	R^2 Z
062	1	1.078	0.413	0.099	0.437	-1.018	0.255	-0.005	0.003	1.051	0.481	0.019	0.012
062	2	-0.007	0.106	0.004	0.012	-1.264	0.517	-0.128	0.658	0.865	0.758	0.184	0.635
062	3	0.080	0.156	-0.012	0.042	-0.802	0.507	-0.129	0.444	1.943	1.071	0.308	0.571
062	4	0.885	0.103	-0.016	0.189	0.359	0.300	-0.047	0.192	0.218	0.521	0.051	0.074
062	5	-0.715	0.531	0.120	0.469	-1.168	0.532	0.137	0.601	0.858	1.055	-0.277	0.627
063	1	0.294	0.075	-0.017	0.382	-0.041	0.328	0.105	0.783	-0.385	0.330	-0.098	0.670
063	2	0.818	0.082	0.019	0.479	1.152	0.133	-0.007	0.026	-1.395	0.375	-0.095	0.548
063	3	-0.409	0.109	-0.025	0.393	0.293	0.121	-0.009	0.045	-0.348	0.351	0.068	0.276
063	4	-0.297	0.095	-0.013	0.142	0.882	0.188	0.020	0.087	-1.107	0.297	-0.074	0.483
063	5	0.326	0.103	0.009	0.061	1.154	0.366	0.114	0.813	-1.560	0.333	-0.074	0.407
064	1	-0.136	0.143	0.021	0.152	0.744	0.381	-0.030	0.044	-2.232	0.599	-0.143	0.403
064	2	-0.765	0.057	-0.009	0.155	-0.060	0.268	0.066	0.364	-2.740	0.218	-0.063	0.502
064	3	-0.924	0.047	0.016	0.673	1.152	0.420	0.132	0.603	-2.232	0.905	-0.344	0.880
064	4	0.336	0.061	0.021	0.781	-0.330	0.333	-0.059	0.211	-0.911	0.376	-0.084	0.343
064	5	0.928	0.085	-0.018	0.362	0.287	0.410	-0.073	0.254	-0.590	0.247	-0.031	0.125
065	1	-0.362	0.094	0.022	0.515	-0.191	0.344	0.034	0.095	-0.601	0.514	-0.106	0.402
065	2	0.756	0.138	-0.039	0.648	0.097	0.464	0.123	0.568	0.174	0.777	-0.241	0.781
065	3	0.335	0.094	-0.005	0.041	1.238	0.334	0.017	0.040	-2.521	0.755	-0.107	0.318
065	4	-0.626	0.226	-0.013	0.032	0.228	0.331	0.039	0.127	-0.444	0.674	0.051	0.054

Continued on next page

Patient	Fraction	Mean X	Std X	Slope X	R^2 X	Mean Y	Std Y	Slope Y	R^2 Y	Mean Z	Std Z	Slope Z	R^2 Z
065	5	0.016	0.076	0.004	0.055	1.021	0.476	0.104	0.858	-1.794	0.756	-0.120	0.451
066	1	0.415	0.052	-0.004	0.027	-0.575	0.676	-0.139	0.244	-0.169	0.637	0.108	0.166
066	2	0.778	0.075	0.026	0.582	-1.049	0.302	0.127	0.856	0.963	0.112	-0.039	0.598
066	3	0.071	0.049	-0.002	0.005	-1.046	0.108	0.023	0.187	-0.738	0.160	-0.052	0.445
066	4	-0.059	0.035	0.010	0.434	-0.864	0.242	0.090	0.721	0.005	0.094	-0.033	0.650
066	5	0.391	0.062	-0.013	0.227	-2.279	0.691	0.052	0.030	1.388	0.270	-0.058	0.239
067	1	0.290	0.231	-0.005	0.004	0.792	0.895	-0.141	0.235	-1.411	1.968	0.382	0.355
067	2	-1.362	0.285	0.031	0.106	0.515	0.474	0.139	0.761	-3.080	0.895	-0.269	0.807
067	3	-0.965	0.292	-0.040	0.122	0.988	0.211	0.038	0.203	-3.010	0.431	-0.148	0.746
067	4	-0.534	0.349	-0.044	0.108	1.364	0.481	0.114	0.388	-3.112	0.551	-0.175	0.699
067	5	-0.737	0.426	-0.023	0.029	1.355	0.442	0.122	0.788	-3.086	0.824	-0.239	0.873
068	1	0.557	0.146	0.010	0.054	2.505	0.582	0.043	0.061	-2.056	1.196	-0.160	0.199
068	2	-0.023	0.100	0.014	0.312	0.987	0.606	0.070	0.198	-1.799	0.958	-0.184	0.550
068	3	-0.168	0.067	0.011	0.383	0.779	0.281	0.056	0.526	-1.338	0.771	-0.188	0.781
068	4	-0.214	0.037	-0.002	0.021	0.486	0.584	0.161	0.735	-0.648	0.210	-0.009	0.019
068	5	0.985	0.082	0.023	0.703	0.344	0.553	0.171	0.859	-1.466	0.507	-0.157	0.866
069	1	-0.874	0.157	-0.003	0.005	2.683	0.451	0.057	0.310	-3.314	0.512	-0.063	0.300
069	2	-0.216	0.052	0.009	0.250	0.332	0.149	0.030	0.371	-1.630	0.491	-0.151	0.855
069	3	-0.717	0.087	0.008	0.122	1.288	0.261	0.016	0.058	-2.085	0.282	-0.049	0.464

Continued on next page

Patient	Fraction	Mean X	Std X	Slope X	R^2 X	Mean Y	Std Y	Slope Y	R^2 Y	Mean Z	Std Z	Slope Z	R^2 Z
069	4	-0.320	0.050	0.007	0.276	-2.079	0.470	0.027	0.045	-0.432	0.255	-0.038	0.287
069	5	-0.425	0.072	-0.015	0.350	0.777	0.417	0.066	0.209	-1.467	0.438	-0.140	0.853
070	1	-0.608	0.260	-0.046	0.250	0.440	0.368	0.051	0.151	-2.778	0.576	-0.184	0.818
070	2	0.379	0.080	-0.004	0.016	1.874	0.218	0.073	0.911	0.020	0.240	0.024	0.080
070	3	0.698	0.209	-0.009	0.018	-3.846	0.531	-0.129	0.594	0.872	0.478	0.076	0.252
070	4	-0.266	0.112	0.006	0.022	-1.418	0.251	-0.005	0.003	0.949	0.699	-0.162	0.498
070	5	-0.373	0.182	0.019	0.086	-1.331	0.315	0.049	0.195	-0.490	0.637	-0.127	0.323
071	1	0.349	0.382	0.058	0.214	-1.781	0.462	-0.038	0.063	0.963	0.786	-0.008	0.001
071	2	0.803	0.072	0.005	0.052	0.794	0.439	0.125	0.810	-1.207	0.438	-0.064	0.215
071	3	0.471	0.051	0.006	0.121	1.383	0.934	-0.239	0.592	-1.718	0.642	0.047	0.048
071	4	1.112	0.307	0.056	0.341	1.268	0.285	0.066	0.535	-1.321	1.213	-0.204	0.286
071	5	1.058	0.371	0.020	0.093	3.196	0.599	0.061	0.323	2.907	4.581	-0.059	0.005
072	1	0.791	1.241	-0.077	0.034	0.599	0.216	0.006	0.007	-2.626	0.824	-0.076	0.076
072	2	0.328	0.302	0.078	0.634	0.145	0.050	-0.003	0.043	-1.100	0.207	0.039	0.341
072	3	0.540	0.906	-0.029	0.015	1.740	0.454	0.073	0.393	-1.488	1.991	0.009	0.000
072	4	0.355	0.510	0.158	0.749	0.108	0.070	-0.005	0.038	-0.963	0.575	-0.165	0.644
072	5	0.233	0.311	0.067	0.393	-0.265	0.461	-0.143	0.817	-0.779	0.440	0.035	0.054

D

Approved Template Coordinate Data

Table D.1: Patient data (column B excluded)

Patient ID	Fraction	X	Y	Z	Average Coordinates
001	1	-0.800	0.600	-0.600	
001	2	0.000	0.000	0.000	
001	3	0.900	2.300	-1.800	
001	4	-0.500	-0.500	1.500	
001	5	-1.100	0.500	0.100	-0.300, 0.580, -0.160
002	1	0.000	-1.000	-0.500	
002	2	0.000	0.100	-0.500	
002	3	0.200	0.700	0.000	
002	4	0.700	0.500	0.500	
002	5	-0.300	-0.500	-0.200	0.120, -0.040, -0.140
003	1	0.600	-1.500	0.100	
003	2	-1.800	-2.000	2.000	
003	3	-0.200	-0.800	0.900	
003	4	-0.700	1.400	-1.900	
003	5	-0.500	-0.800	0.400	-0.520, -0.740, 0.300

Patient ID	Fraction	X	Y	Z	Average Coordinates
004	1	2.700	-3.900	-1.500	
004	2	0.000	0.400	-1.900	
004	3	0.300	0.800	-3.100	
004	4	0.000	0.100	-0.300	
004	5	-0.100	0.000	-0.500	0.580, -0.520, -1.460
005	1	-1.500	-0.400	-0.500	
005	2	-1.100	-0.500	0.300	
005	3	-0.600	0.500	0.300	
005	4	-0.400	-0.400	0.200	
005	5	-0.600	-0.700	0.700	-0.840, -0.300, 0.200
006	1	0.800	0.800	-0.400	
006	2	-0.300	1.800	0.600	
006	3	0.800	1.400	-0.200	
006	4	2.300	0.700	-0.800	
006	5	3.700	2.900	-3.000	1.460, 1.520, -0.760
007	1	1.500	-2.000	0.200	
007	2	1.500	0.400	-1.200	
007	3	-0.400	0.500	-0.800	
007	4	-0.100	-2.200	0.600	
007	5	-1.200	-1.500	1.700	0.260, -0.960, 0.100
008	1	0.500	-1.000	1.500	
008	2	0.000	0.700	0.500	
008	3	0.100	0.400	-1.000	
008	4	-0.700	0.300	-0.500	
008	5	-0.300	0.400	0.500	-0.080, 0.160, 0.200
009	1	-0.600	-1.000	-0.600	

Patient ID	Fraction	X	Y	Z	Average Coordinates
009	2	-1.000	1.000	0.000	
009	3	-0.800	0.300	-0.500	
009	4	-0.200	-1.000	0.500	
009	5	1.900	-0.300	-0.400	-0.140, -0.200, -0.200
010	1	0.500	0.400	-0.800	
010	2	0.700	-1.000	-0.300	
010	3	0.000	-0.100	-0.100	
010	4	-0.900	0.000	-0.800	
010	5	0.500	-0.200	-1.600	0.160, -0.180, -0.720
011	1	0.800	0.000	0.300	
011	2	1.800	0.300	-0.200	
011	3	2.200	-0.200	1.000	
011	4	3.000	0.000	-0.600	
011	5	-0.200	-0.900	0.000	1.520, -0.160, 0.100
012	1	0.000	0.600	-1.300	
012	2	-0.100	-0.500	-0.200	
012	3	0.100	0.200	-0.800	
012	4	-0.200	0.100	-0.400	
012	5	0.400	0.000	-1.200	0.040, 0.080, -0.780
013	1	0.600	-0.500	0.300	
013	2	0.700	0.100	-0.300	
013	3	0.600	0.100	-0.800	
013	4	0.200	0.100	-0.500	
013	5	-0.600	0.200	-0.200	0.300, -0.000, -0.300
014	1	0.000	0.100	0.500	
014	2	-1.000	-0.500	-0.100	

Patient ID	Fraction	X	Y	Z	Average Coordinates
014	3	-0.500	0.200	0.300	
014	4	0.200	1.200	-1.000	
014	5	1.500	-0.200	0.500	0.040, 0.160, 0.040
015	1	-0.400	1.000	-1.600	
015	2	0.300	-0.200	0.800	
015	3	0.600	0.000	-0.700	
015	4	0.500	-0.100	0.600	
015	5	-0.100	0.000	0.800	0.180, 0.140, -0.020
016	1	-0.100	-0.500	0.700	
016	2	-0.100	0.100	0.000	
016	3	-0.800	-0.100	0.200	
016	4	-0.100	-0.300	1.400	
016	5	0.500	0.200	0.500	-0.120, -0.120, 0.560
017	1	-0.500	1.000	-0.900	
017	2	-1.000	-0.300	1.000	
017	3	-0.800	0.300	0.000	
017	4	-1.600	0.700	0.100	
017	5	-0.200	1.400	0.000	-0.820, 0.620, 0.040
018	1	-0.500	1.000	-1.000	
018	2	-0.500	0.500	0.100	
018	3	0.100	-1.700	1.500	
018	4	0.500	-0.100	-0.400	
018	5	-0.300	-2.200	0.700	-0.140, -0.500, 0.180
019	1	0.400	0.700	-0.600	
019	2	0.500	0.000	0.000	
019	3	0.900	0.000	0.000	

Patient ID	Fraction	X	Y	Z	Average Coordinates
019	4	0.100	0.000	0.500	
019	5	-0.200	0.600	-0.600	0.340, 0.260, -0.140
020	1	0.400	-0.200	-0.200	
020	2	-1.100	-0.200	0.600	
020	3	-0.900	-0.400	-1.000	
020	4	0.000	1.800	-1.300	
020	5	0.300	1.700	-1.500	-0.260, 0.540, -0.680
021	1	1.500	-2.600	-0.700	
021	2	0.100	0.800	-0.600	
021	3	-0.400	0.300	-0.100	
021	4	-0.400	0.100	-0.700	
021	5	0.200	1.800	-1.800	0.200, 0.080, -0.780
022	1	0.400	-1.100	0.500	
022	2	0.800	-1.400	0.300	
022	3	0.200	-0.800	0.600	
022	4	-0.300	-1.100	0.700	
022	5	-1.300	-2.000	1.000	-0.040, -1.280, 0.620
023	1	0.800	1.200	-1.500	
023	2	0.300	1.000	-2.900	
023	3	-0.500	2.400	-1.300	
023	4	0.600	1.800	-1.400	
023	5	1.200	3.000	-2.000	0.480, 1.880, -1.820
024	1	0.100	0.100	0.800	
024	2	1.000	0.900	-1.000	
024	3	-0.700	-0.100	0.700	
024	4	-1.000	0.000	-1.300	

Patient ID	Fraction	X	Y	Z	Average Coordinates
024	5	0.700	-1.800	2.200	0.020, -0.180, 0.280
025	1	0.300	2.300	-2.400	
025	2	-0.900	1.000	-0.200	
025	3	0.000	1.300	0.500	
025	4	-0.700	1.000	-1.600	
025	5	-0.700	1.700	0.500	-0.400, 1.460, -0.640
026	1	0.600	0.200	-0.400	
026	2	0.000	1.000	-0.800	
026	3	0.600	1.100	0.700	
026	4	0.900	1.800	-0.400	
026	5	0.400	0.900	-0.300	0.500, 1.000, -0.240
027	1	0.100	-0.400	-1.200	
027	2	0.900	-1.500	-1.900	
027	3	0.300	1.400	0.800	
027	4	0.200	-0.700	-1.300	
027	5	0.300	-0.200	-1.700	0.360, -0.280, -1.060
028	1	0.000	-1.100	-1.000	
028	2	0.100	-0.700	0.900	
028	3	0.300	-0.700	0.300	
028	4	0.300	-0.700	-0.400	
028	5	0.400	0.200	-0.200	0.220, -0.600, -0.080
029	1	0.200	0.100	-0.300	
029	2	1.000	2.200	-1.800	
029	3	0.600	0.500	-0.500	
029	4	0.700	0.400	0.100	

Patient ID	Fraction	X	Y	Z	Average Coordinates
029	5	1.200	0.400	-0.700	0.740, 0.720, -0.640
030	1	-0.300	1.400	-0.700	
030	2	-0.100	1.000	-0.600	
030	3	-0.900	0.900	-0.300	
030	4	0.300	0.000	-0.700	
030	5	-0.200	0.900	-1.900	-0.240, 0.840, -0.840
031	1	-0.300	0.500	-0.300	
031	2	-0.200	0.800	-1.000	
031	3	0.400	-0.400	-0.200	
031	4	-0.200	-0.200	0.300	
031	5	0.400	0.300	-0.600	0.020, 0.200, -0.360
032	1	-0.100	-2.100	1.800	
032	2	-0.800	-0.500	-0.100	
032	3	0.300	0.500	0.000	
032	4	0.700	0.600	0.900	
032	5	-0.500	-0.500	1.000	-0.080, -0.400, 0.720
033	1	-0.600	0.600	-1.000	
033	2	-0.300	0.200	-0.600	
033	3	-0.100	0.800	-0.700	
033	4	0.000	0.400	-0.200	
033	5	-0.300	1.900	-1.100	-0.260, 0.780, -0.720
034	1	2.300	0.500	-1.100	
034	2	1.500	0.900	-0.100	
034	3	-0.500	0.800	-0.400	
034	4	1.400	1.300	-1.800	

Patient ID	Fraction	X	Y	Z	Average Coordinates
034	5	-0.100	0.500	-0.300	0.920, 0.800, -0.740
035	1	-0.400	1.500	-1.800	
035	2	1.100	-0.800	0.100	
035	3	-0.400	-0.700	-0.100	
035	4	-1.200	0.700	-1.000	
035	5	-1.200	0.000	-1.700	-0.420, 0.140, -0.900
036	1	-0.900	1.900	-0.600	
036	2	0.700	0.500	-0.500	
036	3	2.800	-0.500	1.200	
036	4	1.700	1.600	-0.800	
036	5	0.700	0.500	-0.900	1.000, 0.800, -0.320
037	1	-2.900	-0.800	-0.200	
037	2	0.600	-0.500	1.800	
037	3	-0.200	-1.000	-2.800	
037	4	-0.300	-0.600	0.400	
037	5	0.200	1.000	1.300	-0.520, -0.380, 0.100
038	1	-0.500	1.000	-1.000	
038	2	1.700	0.300	-0.400	
038	3	1.400	0.600	-0.800	
038	4	1.200	0.300	0.100	
038	5	1.700	0.700	-1.000	1.100, 0.580, -0.620
039	1	0.000	-1.100	-1.200	
039	2	-0.500	0.400	-0.700	
039	3	-0.700	1.700	-0.900	
039	4	-0.700	0.100	-0.100	

Patient ID	Fraction	X	Y	Z	Average Coordinates
039	5	0.300	0.200	-0.100	-0.320, 0.260, -0.600
040	1	-0.500	1.600	-1.500	
040	2	-1.400	-0.200	-1.100	
040	3	-0.500	0.500	-2.000	
040	4	0.700	0.700	-0.600	
040	5	-1.000	-0.500	0.700	-0.540, 0.420, -0.900
041	1	0.600	0.300	-0.500	
041	2	0.300	-0.800	0.900	
041	3	0.000	-0.800	0.700	
041	4	-0.300	-1.700	0.400	
041	5	0.200	-1.600	1.200	0.160, -0.920, 0.540
042	1	-0.200	0.600	-0.100	
042	2	0.500	0.100	0.400	
042	3	3.200	0.700	0.700	
042	4	1.300	-0.300	1.300	
042	5	1.100	-0.500	-0.100	1.180, 0.120, 0.440
043	1	3.000	-2.500	-0.400	
043	2	2.600	-4.100	3.200	
043	3	1.900	-2.800	2.000	
043	4	2.100	-1.400	0.000	
043	5	0.300	-1.600	1.200	1.980, -2.480, 1.200
044	1	-0.300	-1.200	1.300	
044	2	-0.100	0.600	1.000	
044	3	-0.200	-0.300	1.200	
044	4	-0.800	0.100	1.400	

Patient ID	Fraction	X	Y	Z	Average Coordinates
044	5	-0.600	1.000	0.500	-0.400, 0.040, 1.080
045	1	0.800	0.800	-1.700	
045	2	0.700	0.700	-0.800	
045	3	2.100	1.700	-2.200	
045	4	0.900	-0.500	1.000	
045	5	-1.500	1.100	-0.800	0.600, 0.760, -0.900
046	1	-0.500	0.200	0.000	
046	2	-0.700	-0.700	0.200	
046	3	-0.300	0.300	0.000	
046	4	-1.000	0.600	-0.600	
046	5	0.100	0.500	-0.100	-0.480, 0.180, -0.100
047	1	0.600	0.700	0.000	
047	2	-0.300	0.200	-1.000	
047	3	0.200	-0.700	-0.200	
047	4	0.100	-0.100	-0.300	
047	5	-1.300	0.200	0.700	-0.140, 0.060, -0.160
048	1	0.600	-0.500	1.200	
048	2	0.200	-0.500	1.200	
048	3	0.200	0.200	1.300	
048	4	0.000	1.600	-0.100	
048	5	0.000	-1.300	2.600	0.200, -0.100, 1.240
049	1	-0.100	1.000	-1.000	
049	2	-0.300	0.500	-0.500	
049	3	-1.200	2.000	-0.300	
049	4	0.100	0.500	-2.300	

Patient ID	Fraction	X	Y	Z	Average Coordinates
049	5	0.300	-0.300	0.800	-0.240, 0.740, -0.660
050	1	-0.400	2.100	-0.500	
050	2	-0.800	1.800	-2.000	
050	3	0.500	0.500	-0.500	
050	4	0.000	1.400	-1.200	
050	5	-0.400	0.500	-1.300	-0.220, 1.260, -1.100
051	1	0.200	-0.600	-0.800	
051	2	-0.700	-1.200	0.100	
051	3	-0.400	-0.500	0.200	
051	4	0.800	0.800	-0.600	
051	5	0.200	0.000	-0.300	0.020, -0.300, -0.280
052	1	0.100	-1.200	1.200	
052	2	0.900	0.200	3.600	
052	3	1.000	-0.600	0.900	
052	4	0.000	-0.500	0.300	
052	5	1.800	-2.500	-1.800	0.760, -0.920, 0.840
053	1	-1.200	-1.400	1.300	
053	2	0.100	-1.300	0.400	
053	3	-1.700	-2.100	1.900	
053	4	-0.700	-0.300	-0.600	
053	5	-1.100	-0.400	-0.100	-0.920, -1.100, 0.580
054	1	-2.000	0.300	1.000	
054	2	-0.900	0.300	0.300	
054	3	-0.700	1.500	-0.900	
054	4	-0.500	2.400	-2.400	

Patient ID	Fraction	X	Y	Z	Average Coordinates
054	5	-0.700	1.000	0.000	-0.960, 1.100, -0.400
055	1	-0.600	0.500	-0.700	
055	2	0.000	0.000	0.000	
055	3	-0.400	2.100	-2.600	
055	4	-0.300	1.000	0.000	
055	5	-0.500	0.300	-1.500	-0.360, 0.780, -0.960
056	1	0.800	-2.900	1.600	
056	2	-0.300	0.100	0.100	
056	3	0.200	0.500	-1.000	
056	4	-1.800	2.500	-2.100	
056	5	-1.100	1.600	-1.500	-0.440, 0.360, -0.580
057	1	-0.200	-1.200	-1.800	
057	2	0.400	2.300	-3.400	
057	3	0.600	1.000	-1.600	
057	4	1.200	1.300	0.000	
057	5	0.200	0.500	-3.900	0.440, 0.780, -2.140
058	1	0.000	-2.500	1.800	
058	2	0.000	0.100	-0.600	
058	3	-1.100	1.300	-0.900	
058	4	-0.400	0.000	-0.800	
058	5	-1.000	-0.500	-0.500	-0.500, -0.320, -0.200
059	1	1.200	0.000	0.600	
059	2	-0.100	0.000	0.000	
059	3	1.300	-1.200	1.500	
059	4	0.000	-0.400	0.000	

Patient ID	Fraction	X	Y	Z	Average Coordinates
059	5	-0.400	-0.500	0.600	0.400, -0.420, 0.540
060	1	-0.100	0.700	0.600	
060	2	-0.500	0.400	-1.000	
060	3	-0.600	1.400	-1.700	
060	4	-0.400	0.000	-0.600	
060	5	-0.500	0.400	0.500	-0.420, 0.580, -0.440
061	1	-0.500	0.100	-0.300	
061	2	-0.300	3.100	-2.000	
061	3	-0.100	2.300	-2.600	
061	4	0.100	-0.300	0.700	
061	5	1.000	1.500	-0.800	0.040, 1.340, -1.000
062	1	0.500	-0.700	0.100	
062	2	0.100	-0.800	0.100	
062	3	-0.100	0.300	-0.200	
062	4	0.800	0.500	0.000	
062	5	-0.500	-1.500	2.200	0.160, -0.440, 0.440
063	1	0.400	-0.300	0.100	
063	2	0.700	1.000	-0.900	
063	3	-0.300	0.300	-0.100	
063	4	-0.300	0.700	-0.400	
063	5	0.200	0.500	-1.300	0.140, 0.440, -0.520
064	1	0.000	-0.100	-0.300	
064	2	-0.700	-0.500	-1.500	
064	3	-0.900	0.200	-0.400	
064	4	0.300	-0.300	-0.500	

Patient ID	Fraction	X	Y	Z	Average Coordinates
064	5	1.000	0.500	-0.400	-0.060, -0.040, -0.620
065	1	-0.100	-0.700	1.000	
065	2	0.800	0.100	0.900	
065	3	0.600	0.700	-0.600	
065	4	0.000	0.400	-0.100	
065	5	0.000	0.000	0.400	0.260, 0.100, 0.320
066	1	0.300	-0.500	-0.100	
066	2	0.700	-1.100	1.100	
066	3	0.200	-1.000	-0.500	
066	4	-0.100	-1.100	0.100	
066	5	0.100	-0.500	0.100	0.240, -0.840, 0.140
067	1	0.100	1.000	-2.000	
067	2	-1.100	-0.100	-1.700	
067	3	-0.500	0.700	-1.500	
067	4	-0.700	0.000	-1.000	
067	5	-0.400	0.500	-1.200	-0.520, 0.420, -1.480
068	1	0.500	2.800	-2.100	
068	2	-0.100	0.600	-0.200	
068	3	-0.300	-0.100	0.300	
068	4	-0.200	0.300	-1.100	
068	5	0.800	0.000	-1.200	0.140, 0.720, -0.860
069	1	-0.600	1.700	-3.100	
069	2	-0.300	0.300	-0.900	
069	3	-0.600	0.800	-0.900	
069	4	-0.300	0.000	-0.400	

Patient ID	Fraction	X	Y	Z	Average Coordinates
069	5	-0.600	0.000	-1.100	-0.480, 0.560, -1.280
070	1	-0.500	0.000	-1.000	
070	2	0.300	1.800	-0.600	
070	3	0.600	-2.900	1.600	
070	4	-0.300	-1.600	1.700	
070	5	-0.300	-0.500	-1.100	-0.040, -0.640, 0.120
071	1	0.600	-1.700	0.200	
071	2	0.600	0.300	-0.900	
071	3	0.500	2.200	-1.800	
071	4	0.700	1.000	-0.500	
071	5	0.800	2.900	1.000	0.640, 0.940, -0.400
072	1	0.300	0.400	-2.000	
072	2	-0.100	0.000	-0.900	
072	3	-0.800	1.400	-0.500	
072	4	-0.500	-0.100	0.100	
072	5	-0.200	0.400	-0.500	-0.260, 0.420, -0.760

E

Averaged Prostate Motion for Last 30 Seconds Data

Patient ID	Fraction	X	Y	Z	Average Coordinates
001	1	-1.224	1.844	-0.170	
001	2	-0.566	-0.082	0.153	
001	3	0.133	1.810	-1.623	
001	4	-1.568	-1.032	1.130	
001	5	-1.302	1.901	1.595	-0.905, 0.888, 0.217
002	1	0.149	-0.106	-2.366	
002	2	0.090	0.801	-2.177	
002	3	0.479	1.803	-2.897	
002	4	0.763	1.100	-0.097	
002	5	-0.280	-0.486	-0.298	0.240, 0.622, -1.567
003	1	0.387	-1.458	0.323	
003	2	-1.874	-1.796	1.872	
003	3	-0.248	-0.727	0.754	
003	4	-0.005	1.063	-0.836	

Patient ID	Fraction	X	Y	Z	Average Coordinates
003	5	-0.757	-0.427	-0.799	-0.500, -0.669, 0.263
004	1	1.140	-1.464	-0.212	
004	2	0.175	-0.234	-1.788	
004	3	0.144	0.196	-0.208	
004	4	0.337	0.683	-1.780	
004	5	-0.287	0.183	-1.059	0.302, -0.127, -1.009
005	1	-1.805	-0.393	-0.966	
005	2	-1.225	-0.312	-0.063	
005	3	-0.453	0.446	-0.879	
005	4	-0.919	-0.274	-0.482	
005	5	-0.610	-0.745	0.536	-1.002, -0.256, -0.371
006	1	-1.169	1.342	-1.951	
006	2	-1.366	2.851	-0.342	
006	3	0.025	2.023	-1.064	
006	4	1.936	2.054	-0.984	
006	5	0.872	-0.989	1.814	0.059, 1.456, -0.506
007	1	-0.824	-2.504	4.637	
007	2	2.302	0.738	-1.549	
007	3	-0.363	1.229	-0.632	
007	4	-0.044	-0.759	-0.726	
007	5	-1.359	-1.320	1.229	-0.058, -0.523, 0.592
008	1	-0.550	-1.393	-0.447	
008	2	0.173	1.331	-1.155	

Patient ID	Fraction	X	Y	Z	Average Coordinates
008	3	-0.104	-0.766	-0.839	
008	4	-0.387	0.220	-0.350	
008	5	-0.428	1.408	-0.863	-0.259, 0.160, -0.731
009	1	-0.492	-0.572	-1.423	
009	2	-0.978	0.948	-0.898	
009	3	-0.461	-0.707	-0.562	
009	4	-0.548	-0.663	-0.745	
009	5	1.850	-0.394	-1.105	-0.126, -0.278, -0.947
010	1	0.409	0.154	-1.712	
010	2	0.632	-2.305	-0.005	
010	3	0.079	2.141	-2.255	
010	4	-0.101	-0.616	-1.540	
010	5	0.605	0.054	-1.550	0.325, -0.114, -1.413
011	1	-0.382	0.407	-0.415	
011	2	2.094	0.131	-0.038	
011	3	1.137	0.686	-0.718	
011	4	2.891	1.485	-1.176	
011	5	-1.117	-0.914	-0.332	0.925, 0.359, -0.536
012	1	-0.772	1.557	-1.097	
012	2	-0.396	0.716	-0.683	
012	3	0.231	-1.307	0.116	
012	4	0.104	1.734	-2.175	
012	5	0.904	0.456	-1.028	0.014, 0.631, -0.974

Patient ID	Fraction	X	Y	Z	Average Coordinates
013	1	0.681	-1.513	1.516	
013	2	0.635	1.245	-1.843	
013	3	0.489	0.542	-1.678	
013	4	-0.007	-2.328	2.442	
013	5	-0.534	0.834	0.246	0.253, -0.244, 0.137
014	1	-0.067	0.988	0.023	
014	2	-0.895	0.054	-0.225	
014	3	-0.285	1.434	0.277	
014	4	0.243	0.889	-0.481	
014	5	2.010	1.336	-0.383	0.201, 0.940, -0.158
015	1	-0.371	1.950	-1.889	
015	2	0.284	0.587	-0.194	
015	3	0.234	0.292	-1.132	
015	4	0.462	0.121	0.094	
015	5	-0.224	1.001	-0.033	0.077, 0.790, -0.631
016	1	-0.429	-0.635	1.722	
016	2	0.171	1.086	-0.624	
016	3	-0.938	-0.038	0.314	
016	4	-0.071	-0.341	2.379	
016	5	0.271	0.147	1.248	-0.199, 0.044, 1.008
017	1	-0.312	1.606	-1.242	
017	2	-1.019	-0.487	0.710	
017	3	-0.625	1.060	-0.743	
017	4	-1.457	1.462	-1.005	

Patient ID	Fraction	X	Y	Z	Average Coordinates
017	5	-0.341	1.282	0.183	-0.751, 0.985, -0.419
018	1	-0.557	2.449	-2.599	
018	2	-0.154	0.781	-2.388	
018	3	0.273	-0.015	-2.274	
018	4	0.420	0.873	-0.576	
018	5	-0.335	-1.229	-0.174	-0.070, 0.572, -1.602
019	1	0.384	1.399	-2.697	
019	2	0.367	0.049	-0.101	
019	3	0.614	-0.572	1.170	
019	4	-0.085	-1.166	0.823	
019	5	-0.647	-2.744	3.412	0.127, -0.607, 0.522
020	1	0.409	0.528	0.835	
020	2	-0.796	1.307	-0.491	
020	3	-1.112	-0.672	-2.033	
020	4	0.146	2.557	-0.948	
020	5	0.226	2.035	-1.422	-0.225, 1.151, -0.812
021	1	1.664	-1.399	-2.086	
021	2	0.043	1.834	-2.208	
021	3	-0.298	0.046	-1.764	
021	4	-0.596	-0.060	-1.769	
021	5	0.107	1.739	1.051	0.184, 0.432, -1.355
022	1	0.439	-0.066	-1.212	
022	2	0.859	-1.018	-0.062	

Patient ID	Fraction	X	Y	Z	Average Coordinates
022	3	0.165	-0.072	-0.628	
022	4	0.890	-6.504	1.202	
022	5	-1.306	-1.828	0.362	0.209, -1.897, -0.067
023	1	0.771	2.378	-3.723	
023	2	-0.518	0.026	1.349	
023	3	-0.512	3.382	-3.170	
023	4	0.444	2.923	-3.529	
023	5	0.850	1.586	0.019	0.207, 2.059, -1.811
024	1	0.005	1.654	-3.946	
024	2	1.595	0.987	-1.143	
024	3	-0.793	1.498	-2.468	
024	4	-0.863	2.128	-2.312	
024	5	0.622	-0.987	0.653	0.113, 1.056, -1.843
025	1	0.251	2.392	-3.554	
025	2	-0.890	1.998	-1.763	
025	3	-0.160	1.577	-1.633	
025	4	-0.310	1.015	-4.301	
025	5	-0.898	1.828	-0.561	-0.402, 1.762, -2.363
026	1	0.499	-0.659	1.901	
026	2	0.123	0.622	0.885	
026	3	-0.186	1.351	0.009	
026	4	0.970	2.323	-1.772	
026	5	-0.478	0.019	3.817	0.186, 0.731, 0.968

Patient ID	Fraction	X	Y	Z	Average Coordinates
027	1	-0.788	-1.386	0.333	
027	2	0.699	-0.654	-2.248	
027	3	-0.040	2.341	0.309	
027	4	0.210	0.276	-1.769	
027	5	0.313	0.905	-1.358	0.079, 0.296, -0.946
028	1	0.345	-0.239	-2.674	
028	2	-0.164	-1.898	1.771	
028	3	0.161	-0.740	-0.142	
028	4	0.492	-0.701	-0.611	
028	5	0.463	0.625	-0.281	0.259, -0.591, -0.387
029	1	0.218	1.090	-1.038	
029	2	1.185	0.214	0.670	
029	3	0.640	0.912	-0.061	
029	4	0.693	0.697	-0.169	
029	5	1.194	0.762	-0.771	0.786, 0.735, -0.274
030	1	-1.135	2.556	-2.136	
030	2	-0.826	0.936	-0.891	
030	3	-0.858	1.993	-1.584	
030	4	-0.010	0.138	-1.230	
030	5	0.346	2.039	-2.516	-0.497, 1.533, -1.671
031	1	-0.570	-0.158	-0.132	
031	2	-0.493	1.846	-2.980	
031	3	0.518	-1.095	-0.237	
031	4	-0.432	-0.355	-0.604	

Patient ID	Fraction	X	Y	Z	Average Coordinates
031	5	0.358	0.557	-1.781	-0.124, 0.159, -1.147
032	1	-0.076	-0.098	-1.050	
032	2	-1.101	-0.265	-0.237	
032	3	0.319	0.252	-0.044	
032	4	0.348	-1.287	1.854	
032	5	-0.457	0.403	-0.281	-0.193, -0.199, 0.049
033	1	-0.529	0.976	-2.511	
033	2	-0.042	0.760	-2.667	
033	3	0.038	1.085	-1.384	
033	4	-0.058	-0.056	0.118	
033	5	-0.477	1.952	-1.404	-0.213, 0.943, -1.569
034	1	2.578	1.021	-3.387	
034	2	1.706	1.806	-2.154	
034	3	-0.340	0.537	-0.438	
034	4	1.127	1.270	-1.234	
034	5	0.267	-0.940	0.950	1.068, 0.739, -1.253
035	1	0.796	0.487	-0.556	
035	2	1.253	-1.804	-0.669	
035	3	-0.026	-1.092	0.440	
035	4	-0.715	0.812	-1.343	
035	5	0.170	-1.053	0.063	0.296, -0.530, -0.413
036	1	2.150	0.979	-0.422	
036	2	1.636	-1.007	2.130	

Patient ID	Fraction	X	Y	Z	Average Coordinates
036	3	-0.759	0.259	0.602	
036	4	1.847	1.515	0.891	
036	5	0.506	1.232	-2.139	1.076, 0.595, 0.212
037	1	-2.520	0.298	-1.044	
037	2	-1.141	-0.393	1.207	
037	3	-1.460	-3.525	0.367	
037	4	0.047	-1.621	3.485	
037	5	-2.245	1.408	-0.470	-1.464, -0.767, 0.709
038	1	-0.741	1.701	-2.226	
038	2	1.522	0.506	-0.578	
038	3	1.627	1.503	-1.109	
038	4	0.684	0.204	-1.147	
038	5	2.202	-0.666	-1.081	1.059, 0.650, -1.228
039	1	0.146	0.170	0.006	
039	2	-0.592	0.860	-2.000	
039	3	-0.654	1.765	-2.438	
039	4	-1.490	1.151	-1.285	
039	5	0.135	0.292	-0.922	-0.491, 0.847, -1.328
040	1	-0.145	1.966	-1.001	
040	2	-1.285	0.118	-1.100	
040	3	-0.288	0.980	-2.204	
040	4	0.909	0.673	-0.922	
040	5	-0.878	-2.018	-0.232	-0.337, 0.344, -1.092

Patient ID	Fraction	X	Y	Z	Average Coordinates
041	1	0.318	-0.232	1.324	
041	2	0.560	-2.260	4.716	
041	3	-0.584	0.888	-0.817	
041	4	-0.657	-1.057	-0.379	
041	5	0.545	-1.655	2.227	0.037, -0.863, 1.414
042	1	-0.228	0.627	0.114	
042	2	0.421	0.303	-0.135	
042	3	3.208	0.849	-0.019	
042	4	1.200	-2.950	2.034	
042	5	1.540	-0.409	-0.290	1.228, -0.316, 0.341
043	1	4.234	-2.283	-1.786	
043	2	1.612	-1.617	-0.621	
043	3	2.203	-1.488	-1.727	
043	4	3.264	-0.157	-1.772	
043	5	1.775	-0.472	0.483	2.618, -1.203, -1.085
044	1	-0.341	-0.128	1.358	
044	2	-0.020	1.747	1.511	
044	3	-0.284	-0.506	1.646	
044	4	-0.512	1.119	0.183	
044	5	-0.322	0.616	0.994	-0.296, 0.570, 1.138
045	1	0.662	0.371	-0.754	
045	2	2.453	-0.742	1.766	
045	3	0.551	2.660	-0.179	
045	4	2.474	-0.232	0.990	

Patient ID	Fraction	X	Y	Z	Average Coordinates
045	5	-0.223	0.703	-1.256	1.183, 0.552, 0.113
046	1	-0.590	1.077	-1.713	
046	2	-0.701	-0.244	-2.055	
046	3	0.074	0.969	-2.478	
046	4	-0.959	0.885	-1.443	
046	5	0.194	1.535	-1.527	-0.396, 0.844, -1.843
047	1	0.812	-0.106	-0.905	
047	2	0.117	-0.630	0.299	
047	3	0.249	-2.192	0.452	
047	4	0.005	0.134	-0.155	
047	5	-1.821	1.258	-1.191	-0.128, -0.307, -0.300
048	1	-0.085	-0.921	2.987	
048	2	0.223	0.532	0.976	
048	3	0.430	0.938	1.977	
048	4	-0.212	1.890	-0.455	
048	5	-0.160	-0.018	2.227	0.039, 0.484, 1.542
049	1	0.024	2.161	-2.916	
049	2	-0.336	1.759	-2.584	
049	3	-0.676	2.116	-0.481	
049	4	-0.162	0.198	0.668	
049	5	0.381	0.813	-3.548	-0.154, 1.410, -1.772
050	1	-0.580	3.203	-1.413	
050	2	-0.566	0.491	0.104	

Patient ID	Fraction	X	Y	Z	Average Coordinates
050	3	0.479	2.694	-1.682	
050	4	-0.371	1.177	0.792	
050	5	-1.524	0.700	-1.363	-0.512, 1.653, -0.712
051	1	0.708	2.332	-9.811	
051	2	0.137	-1.481	-0.643	
051	3	-1.667	0.368	-2.503	
051	4	0.777	-0.551	1.522	
051	5	-0.134	-1.570	0.806	-0.036, -0.181, -2.126
052	1	1.060	-1.141	-7.645	
052	2	0.521	0.984	0.282	
052	3	0.794	-0.395	0.663	
052	4	0.842	-0.432	-0.751	
052	5	1.039	-4.326	-1.712	0.851, -1.062, -1.833
053	1	-1.339	-0.682	0.221	
053	2	0.047	-0.345	-1.816	
053	3	-1.656	-2.035	1.576	
053	4	-0.683	0.171	-0.211	
053	5	-1.290	-0.592	0.270	-0.984, -0.697, 0.008
054	1	-1.784	1.213	-1.037	
054	2	-0.607	0.568	-1.025	
054	3	0.271	-0.302	1.724	
054	4	-0.084	3.382	-4.309	
054	5	-0.438	1.946	-1.963	-0.528, 1.361, -1.322

Patient ID	Fraction	X	Y	Z	Average Coordinates
055	1	-0.317	0.521	1.205	
055	2	-0.011	0.072	0.482	
055	3	-0.015	0.633	1.591	
055	4	-0.142	2.157	-0.999	
055	5	-0.396	0.013	1.509	-0.176, 0.679, 0.758
056	1	-0.428	0.000	-2.229	
056	2	-0.185	0.657	1.005	
056	3	0.237	1.268	-0.807	
056	4	-0.748	0.500	-0.668	
056	5	-1.121	1.853	-1.067	-0.449, 0.856, -0.753
057	1	-0.300	-0.276	-3.778	
057	2	0.169	1.119	0.157	
057	3	0.606	1.404	-2.130	
057	4	1.114	1.476	0.245	
057	5	-0.211	1.065	-0.604	0.276, 0.958, -1.222
058	1	-0.942	-2.726	1.162	
058	2	-0.052	0.270	-1.366	
058	3	-1.752	0.539	-1.433	
058	4	0.023	0.488	0.679	
058	5	-1.391	0.001	-1.188	-0.823, -0.286, -0.429
059	1	1.038	-0.049	0.818	
059	2	0.905	0.139	-0.409	
059	3	1.402	-1.458	1.330	
059	4	0.343	0.254	-1.647	

Patient ID	Fraction	X	Y	Z	Average Coordinates
059	5	0.398	-0.318	0.524	0.817, -0.286, 0.123
060	1	-0.249	1.841	1.096	
060	2	-0.618	1.066	-1.188	
060	3	-0.620	1.550	-1.646	
060	4	-0.112	-0.120	-0.272	
060	5	-0.390	0.427	1.675	-0.398, 0.953, -0.067
061	1	-0.638	-4.267	4.350	
061	2	-0.431	3.074	-3.058	
061	3	-0.188	1.734	-1.000	
061	4	-0.242	-0.142	1.521	
061	5	0.743	1.342	0.066	-0.151, 0.348, 0.376
062	1	1.328	-1.120	1.282	
062	2	0.058	-1.830	1.682	
062	3	0.031	-0.836	2.378	
062	4	0.927	0.227	0.333	
062	5	-0.603	-1.304	0.298	0.348, -0.973, 1.195
063	1	0.199	0.323	-0.529	
063	2	0.937	1.024	-1.969	
063	3	-0.412	0.309	-0.450	
063	4	-0.477	0.792	-0.832	
063	5	0.377	1.525	-1.530	0.125, 0.794, -1.062
064	1	-0.068	0.643	-2.598	
064	2	-0.868	0.167	-3.067	

Patient ID	Fraction	X	Y	Z	Average Coordinates
064	3	-0.855	1.467	-3.095	
064	4	0.443	-0.529	-1.212	
064	5	0.811	-0.063	-1.069	-0.107, 0.337, -2.208
065	1	-0.250	-0.057	-0.680	
065	2	0.592	0.464	-0.433	
065	3	0.338	0.752	-1.730	
065	4	-0.375	-0.033	0.776	
065	5	0.025	0.324	1.122	0.066, 0.290, -0.189
066	1	0.295	-2.747	1.858	
066	2	0.936	-0.586	0.773	
066	3	0.078	-0.820	-1.026	
066	4	-0.002	-0.597	-0.148	
066	5	0.421	-1.887	1.132	0.346, -1.327, 0.518
067	1	0.339	0.303	-0.050	
067	2	-1.100	1.028	-4.558	
067	3	-1.300	1.134	-3.584	
067	4	-0.682	1.517	-3.557	
067	5	-0.712	1.853	-4.180	-0.691, 1.167, -3.186
068	1	0.733	3.231	-3.913	
068	2	-0.116	0.322	-1.580	
068	3	-0.068	1.217	-2.267	
068	4	-0.298	1.478	-0.862	
068	5	1.030	0.812	-2.191	0.256, 1.412, -2.163

Patient ID	Fraction	X	Y	Z	Average Coordinates
069	1	-0.110	0.379	-0.049	
069	2	-0.202	0.393	-2.285	
069	3	-0.556	1.614	-2.168	
069	4	-0.322	-1.550	-0.665	
069	5	-0.405	0.976	-2.080	-0.319, 0.362, -1.449
070	1	-0.926	0.315	-3.567	
070	2	0.329	2.224	-0.290	
070	3	0.763	-4.553	1.267	
070	4	-0.050	-1.420	0.443	
070	5	-0.169	-1.357	-1.127	-0.011, -0.958, -0.655
071	1	0.705	-1.879	1.313	
071	2	0.942	1.462	-1.845	
071	3	0.538	1.064	-2.246	
071	4	1.246	1.353	-1.617	
071	5	0.272	0.724	-0.789	0.741, 0.545, -1.037
072	1	0.030	0.555	-2.655	
072	2	0.641	0.143	-0.829	
072	3	-0.055	2.225	-0.459	
072	4	0.885	0.127	-1.877	
072	5	0.567	-0.880	-0.831	0.413, 0.434, -1.330

F

Treatment Planning Study: Part 1

F.1 | DVH Statistics from TPS - Five Offsets from Prostate's Isocentre

Table F.1: A table of the DVH statistics for the CTV for each BLS, starting from a position of 4 cm inferior

Isocentre Offsets - 4 cm inf										
Plan Name	Direction	Adjust Tolerance/Plan (APM)			1_CTVpsv40					
		X (Lt/Rt) in cm	Z (Sup/Inf) in cm	Y (Ant/Post) in cm	D0.1cc	D95%	V40Gy	D99.9%	Dmean	V42Gy
					42.6Gy < D0.1cc < 48.3Gy	D95% > 40 Gy	V40Gy >95% (-5%)	D99.9% >= 40 Gy		V42Gy <=50%
v5ADT06	/	0.0	0.00	0.00	43.227	40.232	97.47	39.210	41.309	16.12
v5ADT06-BLS13	Inf Post Rt	0.20	-2.00	-1.00	41.553	38.050	36.57	36.152	39.612	0.01
v5ADT06-BLS12		0.20	-1.00	-0.50	43.046	39.142	76.46	37.179	40.745	9.65
v5ADT06-BLS11		0.20	-0.80	-0.40	43.165	39.383	87.55	37.248	41.004	12.84
v5ADT06-BLS10		0.20	-0.60	-0.60	43.292	39.506	87.97	37.638	41.081	17.83
v5ADT06-BLS09		0.15	-0.60	-0.40	43.248	39.508	88.51	37.748	41.123	19.00
v5ADT06-BLS08		0.10	-0.40	-0.30	43.285	39.569	88.28	38.088	41.073	16.61
v5ADT06-BLS07		0.08	-0.40	-0.20	43.086	39.835	93.01	38.298	41.117	13.71
v5ADT06-BLS06		0.08	-0.30	-0.30	43.134	39.749	91.80	38.188	41.177	19.33
v5ADT06-BLS05		0.05	-0.30	-0.15	43.125	39.899	93.66	38.478	41.127	14.62
v5ADT06-BLS04		0.05	-0.20	-0.20	43.425	39.976	94.67	38.548	41.281	20.25
v5ADT06-BLS03		0.03	-0.20	-0.10	43.210	40.070	95.75	38.948	41.266	17.11
v5ADT06-BLS02		0.03	-0.10	0.05	43.114	40.032	95.42	38.972	41.285	18.67
v5ADT06-BLS01	Center	0.00	0.00	0.00	43.065	40.045	95.57	38.707	41.263	18.45
v5ADT06-BLS14	Sup Ant Lt	-0.03	0.10	0.05	43.293	40.285	97.84	39.126	41.510	27.440
v5ADT06-BLS15		-0.03	0.20	0.10	43.558	40.491	98.61	39.278	41.740	37.160
v5ADT06-BLS16		-0.05	0.20	0.20	43.645	40.493	98.69	38.728	41.840	44.240
v5ADT06-BLS17		-0.05	0.30	0.15	43.680	40.548	98.84	39.112	41.864	45.710
v5ADT06-BLS18		-0.08	0.30	0.30	43.836	40.482	98.22	38.349	41.910	48.510
v5ADT06-BLS19		-0.08	0.40	0.20	43.803	40.630	98.82	38.698	41.936	49.200
v5ADT06-BLS20		-0.10	0.40	0.30	44.030	40.653	98.88	38.398	42.096	58.830
v5ADT06-BLS21		-0.15	0.60	0.40	43.767	40.638	98.73	39.006	42.053	54.230
v5ADT06-BLS22		-0.20	0.60	0.60	43.848	40.891	99.41	39.498	42.198	63.450
v5ADT06-BLS23		-0.20	0.80	0.40	44.275	40.911	99.34	38.987	42.343	70.180
v5ADT06-BLS24		-0.20	1.00	0.50	43.898	41.072	99.52	39.397	42.339	67.470
v5ADT06-BLS25		-0.20	2.00	1.00	44.705	41.667	99.66	39.048	43.026	90.510

Table F.2: A table of the DVH statistics for the PTV at 2 mm for each BLS, starting from a position of 4 cm inferior

Isocentre Offsets - 4 cm inf								
Plan Name	Direction	Adjust Tolerance/Plan (APM)			1_PTVpsv36_2mm			
		X (Lt/Rt) in cm	Z (Sup/Inf) in cm	Y (Ant/Post) in cm	D95%	D98%	V36.25Gy	V34.4Gy
					D95% > 36.25 Gy	D98% > 34.4 Gy	V36.25Gy >95% (-5%)	V34.4Gy >98%
v5ADT06	/	0.0	0.00	0.00	38.359	37.670	99.94	100.00
v5ADT06-BLS13	Inf Post Rt	0.20	-2.00	-1.00	36.286	35.458	95.17	99.67
v5ADT06-BLS12		0.20	-1.00	-0.50	37.395	36.586	98.65	99.87
v5ADT06-BLS11		0.20	-0.80	-0.40	37.562	36.699	98.81	99.85
v5ADT06-BLS10		0.20	-0.60	-0.60	37.690	36.839	99.12	99.95
v5ADT06-BLS09		0.15	-0.60	-0.40	37.807	36.955	99.18	99.91
v5ADT06-BLS08		0.10	-0.40	-0.30	37.784	37.012	99.46	100.00
v5ADT06-BLS07		0.08	-0.40	-0.20	37.906	37.098	99.43	99.98
v5ADT06-BLS06		0.08	-0.30	-0.30	37.875	37.014	99.48	100.00
v5ADT06-BLS05		0.05	-0.30	-0.15	38.079	37.325	99.69	100.00
v5ADT06-BLS04		0.05	-0.20	-0.20	38.063	37.290	99.60	100.00
v5ADT06-BLS03		0.03	-0.20	-0.10	38.266	37.539	99.84	100.00
v5ADT06-BLS02		0.03	-0.10	0.05	38.249	37.541	99.89	100.00
v5ADT06-BLS01	Center	0.00	0.00	0.00	38.189	37.464	99.80	100.00
v5ADT06-BLS14	Sup Ant Lt	-0.03	0.10	0.05	38.408	37.696	99.83	100.00
v5ADT06-BLS15		-0.03	0.20	0.10	38.627	37.897	99.91	100.00
v5ADT06-BLS16		-0.05	0.20	0.20	38.639	37.806	99.74	99.97
v5ADT06-BLS17		-0.05	0.30	0.15	38.702	37.883	97.79	100.00
v5ADT06-BLS18		-0.08	0.30	0.30	38.577	37.668	99.52	99.95
v5ADT06-BLS19		-0.08	0.40	0.20	38.698	37.879	99.75	99.96
v5ADT06-BLS20		-0.10	0.40	0.30	38.695	37.817	99.64	99.99
v5ADT06-BLS21		-0.15	0.60	0.40	38.670	37.745	99.80	100.00
v5ADT06-BLS22		-0.20	0.60	0.60	38.824	38.024	99.97	100.00
v5ADT06-BLS23		-0.20	0.80	0.40	38.840	38.017	99.80	100.00
v5ADT06-BLS24		-0.20	1.00	0.50	38.956	38.143	99.95	100.00
v5ADT06-BLS25		-0.20	2.00	1.00	39.524	38.561	99.76	99.97

Table F.3: A table of the DVH statistics for the urethra shifted (Urethra_XX) and unshifted (1_Urethra) for each BLS, starting from a position of 4 cm inferior

Isocentre Offsets - 4 cm inf								
Plan Name	Direction	Adjust Tolerance/Plan (APM)			1_Urethra (unshifted)		Urethra_XX (shifted)	
		X (Lt/Rt) in cm	Z (Sup/Inf) in cm	Y (Ant/Post) in cm	D50%	V42Gy	D50%	V42Gy
					D50% < 42 Gy	V42Gy < 50%	D50% <= 42 Gy	V42Gy <= 50%
v5ADT06	/	0.0	0.00	0.00	40.750	0.00	40.750	0.00
v5ADT06-BLS13	Inf Post Rt	0.20	-2.00	-1.00	36.718	0.00	39.177	0.00
v5ADT06-BLS12		0.20	-1.00	-0.50	40.179	0.00	39.909	0.00
v5ADT06-BLS11		0.20	-0.80	-0.40	40.570	0.00	40.603	0.00
v5ADT06-BLS10		0.20	-0.60	-0.60	40.464	0.00	40.347	0.00
v5ADT06-BLS09		0.15	-0.60	-0.40	40.456	0.00	40.459	0.00
v5ADT06-BLS08		0.10	-0.40	-0.30	40.217	0.00	40.386	0.05
v5ADT06-BLS07		0.08	-0.40	-0.20	40.504	0.00	40.550	0.00
v5ADT06-BLS06		0.08	-0.30	-0.30	40.454	0.00	40.565	0.19
v5ADT06-BLS05		0.05	-0.30	-0.15	40.658	0.00	40.666	0.00
v5ADT06-BLS04		0.05	-0.20	-0.20	40.628	0.48	40.711	0.66
v5ADT06-BLS03		0.03	-0.20	-0.10	40.817	0.00	40.810	0.00
v5ADT06-BLS02		0.03	-0.10	0.05	40.783	1.05	40.753	1.04
v5ADT06-BLS01	Center	0.00	0.00	0.00	40.751	1.81	40.751	1.81
v5ADT06-BLS14	Sup Ant Lt	-0.03	0.10	0.05	40.836	2.87	40.866	2.66
v5ADT06-BLS15		-0.03	0.20	0.10	41.192	5.21	41.185	5.63
v5ADT06-BLS16		-0.05	0.20	0.20	41.206	14.61	41.280	12.55
v5ADT06-BLS17		-0.05	0.30	0.15	41.268	8.98	41.312	15.96
v5ADT06-BLS18		-0.08	0.30	0.30	40.971	10.46	41.193	12.39
v5ADT06-BLS19		-0.08	0.40	0.20	41.236	15.43	41.283	19.34
v5ADT06-BLS20		-0.10	0.40	0.30	41.346	22.16	41.604	33.19
v5ADT06-BLS21		-0.15	0.60	0.40	41.091	19.77	41.488	30.35
v5ADT06-BLS22		-0.20	0.60	0.60	41.191	22.45	41.484	35.20
v5ADT06-BLS23		-0.20	0.80	0.40	41.169	20.73	41.911	43.84
v5ADT06-BLS24		-0.20	1.00	0.50	41.270	18.58	41.744	31.76
v5ADT06-BLS25		-0.20	2.00	1.00	25.180	10.36	42.724	79.56

Table F.4: A table of the DVH statistics for the CTV for each BLS, starting from a position of 2 cm inferior

Isocentre Offsets - 2 cm inf								
Plan Name	Direction	Adjust Tolerance/Plan (APM)			1_Urethra (unshifted)		Urethra_XX (shifted)	
		X (Lt/Rt) in cm	Z (Sup/Inf) in cm	Y (Ant/Post) in cm	D50%	V42Gy	D50%	V42Gy
					D50% < 42 Gy	V42Gy < 50%	D50% <= 42 Gy	V42Gy <= 50%
v5ADT05	/	0.0	0.00	0.00	40.670	0.00	40.670	0.00
v5ADT05-BLS13	Inf Post Rt	0.20	-2.00	-1.00	36.805	0.10	42.282	0.52
v5ADT05-BLS12		0.20	-1.00	-0.50	41.152	23.52	41.036	0.10
v5ADT05-BLS11		0.20	-0.80	-0.40	41.098	21.23	41.128	1.67
v5ADT05-BLS10		0.20	-0.60	-0.60	41.152	20.37	41.089	2.29
v5ADT05-BLS09		0.15	-0.60	-0.40	41.383	21.47	41.363	7.01
v5ADT05-BLS08		0.10	-0.40	-0.30	41.332	20.56	41.426	17.37
v5ADT05-BLS07		0.08	-0.40	-0.20	41.055	18.46	41.278	23.36
v5ADT05-BLS06		0.08	-0.30	-0.30	41.415	21.61	41.578	27.83
v5ADT05-BLS05		0.05	-0.30	-0.15	41.343	14.41	41.241	10.86
v5ADT05-BLS04		0.05	-0.20	-0.20	41.312	9.97	41.432	8.59
v5ADT05-BLS03		0.03	-0.20	-0.10	41.333	10.45	41.318	14.67
v5ADT05-BLS02		0.03	-0.10	0.05	41.099	5.44	41.059	5.64
v5ADT05-BLS01	Center	0.00	0.00	0.00	40.802	0.86	40.802	0.86
v5ADT05-BLS14	Sup Ant Lt	-0.03	0.10	0.05	41.087	7.68	41.060	8.93
v5ADT05-BLS15		-0.03	0.20	0.10	41.368	15.70	41.385	13.71
v5ADT05-BLS16		-0.05	0.20	0.20	41.576	18.03	41.508	14.59
v5ADT05-BLS17		-0.05	0.30	0.15	41.618	30.63	41.589	25.36
v5ADT05-BLS18		-0.08	0.30	0.30	42.047	52.53	41.984	49.19
v5ADT05-BLS19		-0.08	0.40	0.20	41.958	46.09	41.776	34.32
v5ADT05-BLS20		-0.10	0.40	0.30	41.745	37.02	41.634	26.70
v5ADT05-BLS21		-0.15	0.60	0.40	41.861	43.37	41.918	46.93
v5ADT05-BLS22		-0.20	0.60	0.60	41.496	23.43	41.460	27.51
v5ADT05-BLS23		-0.20	0.80	0.40	41.898	43.56	42.005	50.43
v5ADT05-BLS24		-0.20	1.00	0.50	41.512	38.45	42.037	51.96
v5ADT05-BLS25		-0.20	2.00	1.00	21.275	16.03	42.233	63.09

Table F.5: A table of the DVH statistics for the PTV at 2 mm for each BLS, starting from a position of 2 cm inferior

Isocentre Offsets - 2 cm inf								
Plan Name	Direction	Adjust Tolerance/Plan (APM)			1_PTVpsv36_2mm			
					D95%	D98%	V36.25Gy	V34.4Gy
		X (Lt/Rt) in cm	Z (Sup/Inf) in cm	Y (Ant/Post) in cm	D95% > 36.25 Gy	D98% > 34.4 Gy	V36.25Gy >95% (-5%)	V34.4Gy >98%
v5ADT05	/	0.0	0.00	0.00	38.299	37.701	99.96	100.00
v5ADT05-BLS13	Inf Post Rt	0.20	-2.00	-1.00	37.491	36.386	98.24	99.75
v5ADT05-BLS12		0.20	-1.00	-0.50	38.133	37.036	99.08	99.86
v5ADT05-BLS11		0.20	-0.80	-0.40	38.238	37.203	99.32	99.93
v5ADT05-BLS10		0.20	-0.60	-0.60	38.238	37.293	99.41	99.96
v5ADT05-BLS09		0.15	-0.60	-0.40	38.358	37.335	99.30	99.90
v5ADT05-BLS08		0.10	-0.40	-0.30	38.372	37.358	99.55	99.99
v5ADT05-BLS07		0.08	-0.40	-0.20	38.473	37.589	99.81	100.00
v5ADT05-BLS06		0.08	-0.30	-0.30	38.447	37.429	99.60	99.99
v5ADT05-BLS05		0.05	-0.30	-0.15	38.609	37.879	99.94	100.00
v5ADT05-BLS04		0.05	-0.20	-0.20	38.607	37.794	99.83	100.00
v5ADT05-BLS03		0.03	-0.20	-0.10	38.623	37.878	99.96	100.00
v5ADT05-BLS02		0.03	-0.10	0.05	38.682	37.946	99.99	100.00
v5ADT05-BLS01	Center	0.00	0.00	0.00	38.165	37.527	99.90	100.00
v5ADT05-BLS14	Sup Ant Lt	-0.03	0.10	0.05	38.314	37.637	99.93	100.00
v5ADT05-BLS15		-0.03	0.20	0.10	38.542	37.730	99.96	100.00
v5ADT05-BLS16		-0.05	0.20	0.20	38.379	37.566	99.84	100.00
v5ADT05-BLS17		-0.05	0.30	0.15	38.499	37.783	99.88	100.00
v5ADT05-BLS18		-0.08	0.30	0.30	38.430	37.539	99.72	100.00
v5ADT05-BLS19		-0.08	0.40	0.20	38.527	37.724	99.90	100.00
v5ADT05-BLS20		-0.10	0.40	0.30	38.354	37.484	99.68	100.00
v5ADT05-BLS21		-0.15	0.60	0.40	38.506	37.581	99.73	100.00
v5ADT05-BLS22		-0.20	0.60	0.60	38.480	37.717	99.89	100.00
v5ADT05-BLS23		-0.20	0.80	0.40	38.564	37.682	99.81	100.00
v5ADT05-BLS24		-0.20	1.00	0.50	38.553	37.709	99.90	100.00
v5ADT05-BLS25		-0.20	2.00	1.00	38.490	37.614	99.86	100.00

Table F.6: A table of the DVH statistics for the urethra shifted (Urethra_XX) and unshifted (1_Urethra) for each BLS, starting from a position of 2 cm inferior

Isocentre Offsets - 2 cm inf										
Plan Name	Direction	Adjust Tolerance/Plan (APM)			1_CTVpsv40					
		X (Lt/Rt) in cm	Z (Sup/Inf) in cm	Y (Ant/Post) in cm	D0.1cc	D95%	V40Gy	D99.9%	Dmean	V42Gy
					42.6Gy < D0.1cc < 48.3Gy	D95% > 40 Gy	V40Gy >95% (-5%)	D99.9% >= 40 Gy		V42Gy <=50%
v5ADT05	/	0.0	0.00	0.00	43.060	40.269	97.47	39.088	41.288	15.61
v5ADT05-BLS13	Inf Post Rt	0.20	-2.00	-1.00	42.634	39.546	89.21	37.059	40.907	7.20
v5ADT05-BLS12		0.20	-1.00	-0.50	43.582	40.230	96.54	37.649	41.687	37.45
v5ADT05-BLS11		0.20	-0.80	-0.40	43.515	40.372	97.25	38.256	41.771	42.33
v5ADT05-BLS10		0.20	-0.60	-0.60	43.555	40.264	96.74	38.009	41.801	46.30
v5ADT05-BLS09		0.15	-0.60	-0.40	43.753	40.509	97.74	37.804	41.935	49.98
v5ADT05-BLS08		0.10	-0.40	-0.30	43.707	40.397	97.65	38.529	41.954	51.80
v5ADT05-BLS07		0.08	-0.40	-0.20	43.590	40.534	98.29	38.957	41.947	51.40
v5ADT05-BLS06		0.08	-0.30	-0.30	43.971	40.524	97.82	38.439	42.040	55.21
v5ADT05-BLS05		0.05	-0.30	-0.15	43.663	40.599	98.43	39.067	41.913	48.41
v5ADT05-BLS04		0.05	-0.20	-0.20	43.675	40.712	98.82	38.990	42.027	56.15
v5ADT05-BLS03		0.03	-0.20	-0.10	43.390	40.690	98.99	39.337	41.911	48.06
v5ADT05-BLS02		0.03	-0.10	0.05	43.701	40.647	98.97	39.483	41.878	44.19
v5ADT05-BLS01	Center	0.00	0.00	0.00	43.410	40.161	96.60	38.859	41.285	15.88
v5ADT05-BLS14	Sup Ant Lt	-0.03	0.10	0.05	43.495	40.314	97.55	38.873	41.560	26.970
v5ADT05-BLS15		-0.03	0.20	0.10	43.822	40.498	98.34	39.112	41.772	36.010
v5ADT05-BLS16		-0.05	0.20	0.20	44.112	40.442	97.55	38.419	41.902	45.060
v5ADT05-BLS17		-0.05	0.30	0.15	43.901	40.540	98.02	38.700	41.908	46.180
v5ADT05-BLS18		-0.08	0.30	0.30	44.180	40.549	97.95	38.247	42.093	57.380
v5ADT05-BLS19		-0.08	0.40	0.20	44.041	40.507	97.96	38.429	42.024	53.100
v5ADT05-BLS20		-0.10	0.40	0.30	44.282	40.502	97.59	38.229	42.096	57.750
v5ADT05-BLS21		-0.15	0.60	0.40	44.195	40.584	98.00	38.569	42.197	62.860
v5ADT05-BLS22		-0.20	0.60	0.60	44.160	40.448	97.58	38.537	42.086	56.180
v5ADT05-BLS23		-0.20	0.80	0.40	44.265	40.614	97.88	38.422	42.258	65.280
v5ADT05-BLS24		-0.20	1.00	0.50	44.125	40.615	98.03	38.496	42.195	62.880
v5ADT05-BLS25		-0.20	2.00	1.00	45.002	40.396	97.15	38.279	42.451	65.160

Table F.7: A table of the DVH statistics for the CTV for each BLS, starting from a position of 0 cm

Isocentre Offsets - 0 cm										
Plan Name	Direction	Adjust Tolerance/Plan (APM)			1_CTVpsv40					
		X (Lt/Rt) in cm	Z (Sup/Inf) in cm	Y (Ant/Post) in cm	D0.1cc	D95%	V40Gy	D99.9%	Dmean	V42Gy
					42.6Gy < D0.1cc < 48.3Gy	D95% > 40 Gy	V40Gy >95% (-5%)	D99.9% >= 40 Gy		V42Gy <=50%
v5ADT03	/	0.0	0.00	0.00	42.900	40.206	97.41	39.150	41.332	18.59
v5ADT03 - BLS13	Inf Post Rt	0.20	-2.00	-1.00	44.861	38.992	88.46	38.992	41.905	51.19
v5ADT03 - BLS12		0.20	-1.00	-0.50	44.722	39.669	93.20	37.337	42.150	61.08
v5ADT03 - BLS11		0.20	-0.80	-0.40	44.990	39.776	93.91	37.219	42.415	68.84
v5ADT03 - BLS10		0.20	-0.60	-0.60	44.910	39.991	94.97	37.729	42.004	51.36
v5ADT03 - BLS09		0.15	-0.60	-0.40	44.972	39.719	93.26	37.197	42.285	65.12
v5ADT03 - BLS08		0.10	-0.40	-0.30	44.499	39.875	94.28	37.799	42.065	53.56
v5ADT03 - BLS07		0.08	-0.40	-0.20	44.570	40.256	96.55	38.429	42.017	50.17
v5ADT03 - BLS06		0.08	-0.30	-0.30	44.830	39.985	94.95	37.387	42.117	54.64
v5ADT03 - BLS05		0.05	-0.30	-0.15	44.096	40.475	97.39	38.129	41.948	48.96
v5ADT03 - BLS04		0.05	-0.20	-0.20	44.530	40.465	96.59	38.199	41.983	49.57
v5ADT03 - BLS03		0.03	-0.20	-0.10	43.679	40.460	98.13	38.997	41.767	40.05
v5ADT03 - BLS02		0.03	-0.10	0.05	43.668	40.424	98.27	39.120	41.723	36.52
v5ADT03 - BLS01	Center	0.01	0.00	0.00	43.217	40.038	95.42	38.776	41.338	20.87
v5ADT03 - BLS14	Sup Ant Lt	-0.03	0.10	0.05	43.639	40.453	98.36	38.979	41.772	38.72
v5ADT03 - BLS15		-0.03	0.20	0.10	43.682	40.362	97.83	38.999	41.812	40.89
v5ADT03 - BLS16		-0.05	0.20	0.20	44.680	40.399	97.02	38.329	42.151	57.62
v5ADT03 - BLS17		-0.05	0.30	0.15	44.148	40.423	97.57	38.659	41.941	46.44
v5ADT03 - BLS18		-0.08	0.30	0.30	45.030	40.096	95.59	38.127	42.441	68.36
v5ADT03 - BLS19		-0.08	0.40	0.20	44.243	40.243	96.42	38.222	42.039	54.23
v5ADT03 - BLS20		-0.10	0.40	0.30	44.958	40.071	95.37	38.019	42.386	67.02
v5ADT03 - BLS21		-0.15	0.60	0.40	44.411	40.027	95.18	38.182	42.063	56.39
v5ADT03 - BLS22		-0.20	0.60	0.60	43.953	40.453	97.72	38.499	42.040	57.42
v5ADT03 - BLS23		-0.20	0.80	0.40	44.392	40.002	95.01	38.990	41.971	51.37
v5ADT03 - BLS24		-0.20	1.00	0.50	43.885	40.253	96.60	38.412	41.905	47.85
v5ADT03 - BLS25		-0.20	2.00	1.00	44.431	39.677	92.61	39.677	37.779	41.80

Table F.8: A table of the DVH statistics for the PTV at 2 mm for each BLS, starting from a position of 0 cm

Isocentre Offsets - 0 cm								
Plan Name	Direction	Adjust Tolerance/Plan (APM)			1_PTVpsv36_2mm			
					D95%	D98%	V36.25Gy	V34.4Gy
		X (Lt/Rt) in cm	Z (Sup/Inf) in cm	Y (Ant/Post) in cm	D95% > 36.25 Gy	D98% > 34.4 Gy	V36.25Gy >95% (-5%)	V34.4Gy >98%
v5ADT03	/	0.0	0.00	0.00	38.369	37.723	99.91	100.00
v5ADT03 - BLS13	Inf Post Rt	0.20	-2.00	-1.00	37.468	36.249	98.00	99.75
v5ADT03 - BLS12		0.20	-1.00	-0.50	38.037	36.832	98.71	99.86
v5ADT03 - BLS11		0.20	-0.80	-0.40	38.090	36.887	99.80	99.88
v5ADT03 - BLS10		0.20	-0.60	-0.60	38.276	37.223	99.30	99.97
v5ADT03 - BLS09		0.15	-0.60	-0.40	38.041	36.832	98.72	99.86
v5ADT03 - BLS08		0.10	-0.40	-0.30	38.173	37.132	99.23	100.00
v5ADT03 - BLS07		0.08	-0.40	-0.20	38.339	37.484	99.70	100.00
v5ADT03 - BLS06		0.08	-0.30	-0.30	38.173	37.140	99.17	99.98
v5ADT03 - BLS05		0.05	-0.30	-0.15	38.432	37.605	99.79	100.00
v5ADT03 - BLS04		0.05	-0.20	-0.20	38.350	37.567	99.75	100.00
v5ADT03 - BLS03		0.03	-0.20	-0.10	38.449	37.665	99.86	100.00
v5ADT03 - BLS02		0.03	-0.10	0.05	38.425	37.679	99.84	100.00
v5ADT03 - BLS01	Center	0.01	0.00	0.00	38.270	37.666	99.85	100.00
v5ADT03 - BLS14	Sup Ant Lt	-0.03	0.10	0.05	38.525	37.838	99.88	100.00
v5ADT03 - BLS15		-0.03	0.20	0.10	38.522	37.883	99.88	100.00
v5ADT03 - BLS16		-0.05	0.20	0.20	38.415	37.488	99.63	100.00
v5ADT03 - BLS17		-0.05	0.30	0.15	38.485	37.701	99.72	100.00
v5ADT03 - BLS18		-0.08	0.30	0.30	38.230	37.226	99.43	100.00
v5ADT03 - BLS19		-0.08	0.40	0.20	38.352	37.487	99.62	100.00
v5ADT03 - BLS20		-0.10	0.40	0.30	38.287	37.309	99.46	100.00
v5ADT03 - BLS21		-0.15	0.60	0.40	38.102	37.190	99.48	100.00
v5ADT03 - BLS22		-0.20	0.60	0.60	38.348	37.555	99.79	100.00
v5ADT03 - BLS23		-0.20	0.80	0.40	38.138	37.154	99.41	100.00
v5ADT03 - BLS24		-0.20	1.00	0.50	38.199	37.425	99.77	100.00
v5ADT03 - BLS25		-0.20	2.00	1.00	37.602	36.589	98.63	99.97

Table F.9: A table of the DVH statistics for the rectum and bladder at 2 mm for each BLS, starting from a position of 0 cm

Isocentre Offsets - 0 cm								
Plan Name	Direction	Adjust Tolerance/Plan (APM)			1_Rectum		1_Bladder	
		X (Lt/Rt) in cm	Z (Sup/Inf) in cm	Y (Ant/Post) in cm	D1cc	V36Gy	D5cc	V36Gy
					D1cc < 36 Gy	V36Gy < 1cc	D5cc < 37 Gy	V37Gy < 5cc
v5ADT03	/	0.0	0.00	0.00	33.880	0.476	21.418	0.243
v5ADT03 - BLS13	Inf Post Rt	0.2	-2.00	-1.00	43.749	9.359	1.448	0.000
v5ADT03 - BLS12		0.2	-1.00	-0.50	42.098	5.200	7.798	0.000
v5ADT03 - BLS11		0.2	-0.80	-0.40	41.545	4.107	11.076	0.000
v5ADT03 - BLS10		0.2	-0.60	-0.60	41.847	5.155	13.015	0.000
v5ADT03 - BLS09		0.2	-0.60	-0.40	40.980	3.674	13.812	0.000
v5ADT03 - BLS08		0.1	-0.40	-0.30	39.688	2.585	16.428	0.000
v5ADT03 - BLS07		0.1	-0.40	-0.20	38.378	1.916	17.123	0.000
v5ADT03 - BLS06		0.1	-0.30	-0.30	39.375	2.349	17.411	0.000
v5ADT03 - BLS05		0.1	-0.30	-0.15	37.213	1.434	18.351	0.000
v5ADT03 - BLS04		0.1	-0.20	-0.20	37.555	1.570	18.813	0.006
v5ADT03 - BLS03		0.0	-0.20	-0.10	35.974	0.993	19.415	0.023
v5ADT03 - BLS02		0.0	-0.10	0.05	34.933	0.663	20.478	0.119
v5ADT03 - BLS01	Center	0.0	0.00	0.00	33.744	0.456	21.435	0.219
v5ADT03 - BLS14	Sup Ant Lt	0.0	0.10	0.05	33.273	0.338	22.842	0.524
v5ADT03 - BLS15		0.0	0.20	0.10	32.155	0.215	24.260	0.923
v5ADT03 - BLS16		-0.1	0.20	0.20	30.365	0.031	25.175	1.231
v5ADT03 - BLS17		-0.1	0.30	0.15	30.771	0.082	25.780	1.354
v5ADT03 - BLS18		-0.1	0.30	0.30	28.040	0.000	27.601	1.952
v5ADT03 - BLS19		-0.1	0.40	0.20	29.182	0.014	27.570	1.848
v5ADT03 - BLS20		-0.1	0.40	0.30	27.520	0.000	28.988	2.275
v5ADT03 - BLS21		-0.2	0.60	0.40	25.548	0.000	33.338	3.449
v5ADT03 - BLS22		-0.2	0.60	0.60	23.128	0.000	35.539	4.270
v5ADT03 - BLS23		-0.2	0.80	0.40	24.872	0.000	35.618	4.306
v5ADT03 - BLS24		-0.2	1.00	0.50	23.184	0.000	38.325	5.862
v5ADT03 - BLS25		-0.2	2.00	1.00	18.816	0.000	42.411	15.780

Table F.10: A table of the DVH statistics for the urethra shifted (Urethra_XX) and unshifted (1_Urethra) for each BLS, starting from a position of 0 cm

Isocentre Offsets - 0 cm								
Plan Name	Direction	Adjust Tolerance/Plan (APM)			1_Urethra (unshifted)		Urethra_XX (shifted)	
		X (Lt/Rt) in cm	Z (Sup/Inf) in cm	Y (Ant/Post) in cm	D50%	V42Gy	D50%	V42Gy
					D50% < 42 Gy	V42Gy < 50%	D50% <= 42 Gy	V42Gy <= 50%
v5ADT03	/	0.0	0.00	0.00	40.723	0.00	40.723	0.00
v5ADT03 - BLS13	Inf Post Rt	0.20	-2.00	-1.00	38.093	0.00	40.527	25.59
v5ADT03 - BLS12		0.20	-1.00	-0.50	41.687	31.49	40.703	11.08
v5ADT03 - BLS11		0.20	-0.80	-0.40	41.764	39.53	40.997	25.50
v5ADT03 - BLS10		0.20	-0.60	-0.60	41.171	10.18	41.053	0.00
v5ADT03 - BLS09		0.15	-0.60	-0.40	41.730	30.73	40.754	13.49
v5ADT03 - BLS08		0.10	-0.40	-0.30	41.484	16.56	41.061	16.84
v5ADT03 - BLS07		0.08	-0.40	-0.20	41.374	6.95	41.367	7.78
v5ADT03 - BLS06		0.08	-0.30	-0.30	41.556	21.79	41.250	25.55
v5ADT03 - BLS05		0.05	-0.30	-0.15	41.306	7.99	41.258	10.57
v5ADT03 - BLS04		0.05	-0.20	-0.20	41.451	17.51	41.314	9.63
v5ADT03 - BLS03		0.03	-0.20	-0.10	41.020	6.52	41.077	9.11
v5ADT03 - BLS02		0.03	-0.10	0.05	41.000	4.23	41.084	3.28
v5ADT03 - BLS01	Center	0.00	0.00	0.00	40.724	0.10	40.724	0.10
v5ADT03 - BLS14	Sup Ant Lt	-0.03	0.10	0.05	41.410	13.46	41.379	12.73
v5ADT03 - BLS15		-0.03	0.20	0.10	41.247	1.00	41.307	1.15
v5ADT03 - BLS16		-0.05	0.20	0.20	41.597	19.27	41.683	22.50
v5ADT03 - BLS17		-0.05	0.30	0.15	41.237	4.66	41.366	8.14
v5ADT03 - BLS18		-0.08	0.30	0.30	41.224	33.40	41.684	36.30
v5ADT03 - BLS19		-0.08	0.40	0.20	41.323	15.84	41.384	11.75
v5ADT03 - BLS20		-0.10	0.40	0.30	41.046	31.26	41.647	35.39
v5ADT03 - BLS21		-0.15	0.60	0.40	40.843	33.25	41.778	36.99
v5ADT03 - BLS22		-0.20	0.60	0.60	41.368	22.41	41.644	26.93
v5ADT03 - BLS23		-0.20	0.80	0.40	40.277	23.60	41.480	20.08
v5ADT03 - BLS24		-0.20	1.00	0.50	39.698	20.50	41.464	13.75
v5ADT03 - BLS25		-0.20	2.00	1.00	21.980	2.00	41.098	9.09

Table F.11: A table of the DVH statistics for the CTV for each BLS, starting from a position of 2 cm superior

Isocentre Offsets - 2 cm sup										
Plan Name	Direction	Adjust Tolerance/Plan (APM)			1_CTVpsv40					
		X (Lt/Rt) in cm	Z (Sup/Inf) in cm	Y (Ant/Post) in cm	D0.1cc	D95%	V40Gy	D99.9%	Dmean	V42Gy
					42.6Gy < D0.1cc < 48.3Gy	D95% > 40 Gy	V40Gy >95% (-5%)	D99.9% >= 40 Gy		V42Gy <=50%
v5ADT15	/	0.0	0.00	0.00	43.013	40.276	97.98	39.102	41.291	16.86
v5ADT15 - BLS16	Inf Post Rt	0.20	-2.00	-1.00	46.195	40.264	95.99	37.189	42.853	78.92
v5ADT15 - BLS15		0.20	-1.00	-0.50	45.209	40.759	97.73	38.127	42.637	74.52
v5ADT15 - BLS14		0.20	-0.80	-0.40	45.135	40.665	97.54	38.198	42.560	72.66
v5ADT15 - BLS13		0.20	-0.60	-0.60	45.035	40.546	97.47	38.348	42.310	64.37
v5ADT15 - BLS12		0.15	-0.60	-0.40	44.812	40.594	97.69	38.067	42.494	71.93
v5ADT15 - BLS11		0.10	-0.40	-0.30	45.025	40.608	98.14	38.478	42.311	64.79
v5ADT15 - BLS10		0.08	-0.40	-0.20	44.567	40.653	98.37	38.818	42.223	61.74
v5ADT15 - BLS9		0.08	-0.30	-0.30	44.820	40.519	97.88	38.348	42.233	61.62
v5ADT15 - BLS8		0.05	-0.30	-0.15	44.565	40.675	98.62	39.149	42.173	60.09
v5ADT15 - BLS7		0.05	-0.20	-0.20	44.758	40.548	98.31	38.928	42.129	56.61
v5ADT15 - BLS6		0.03	-0.20	-0.10	44.065	40.631	98.84	39.137	41.977	50.06
v5ADT15 - BLS5		0.03	-0.10	0.05	43.601	40.209	97.34	39.103	41.404	21.52
v5ADT15 - BLS01	Center	0.01	0.00	0.00	43.477	40.142	96.62	38.972	41.299	18.29
v5ADT15 - BLS02	Sup Ant Lt	-0.03	0.10	0.05	43.175	40.194	97.03	38.917	41.382	23.040
v5ADT15 - BLS03		-0.03	0.20	0.10	44.037	40.204	96.84	38.872	41.724	40.020
v5ADT15 - BLS04		-0.05	0.20	0.20	44.115	40.220	96.29	37.938	41.897	48.980
v5ADT15 - BLS17		-0.05	0.30	0.15	44.014	40.342	97.08	38.608	41.844	44.570
v5ADT15 - BLS18		-0.08	0.30	0.30	44.017	40.068	95.39	37.948	41.897	50.230
v5ADT15 - BLS19		-0.08	0.40	0.20	43.692	40.203	96.38	38.159	41.734	40.880
v5ADT15 - BLS20		-0.10	0.40	0.30	44.118	40.020	95.15	37.968	41.850	47.410
v5ADT15 - BLS21		-0.15	0.60	0.40	43.845	39.944	94.65	37.507	41.729	42.380
v5ADT15 - BLS22		-0.20	0.60	0.60	43.745	40.098	95.73	38.138	41.636	35.860
v5ADT15 - BLS23		-0.20	0.80	0.40	44.035	39.744	93.04	37.338	41.527	32.000
v5ADT15 - BLS24		-0.20	1.00	0.50	43.846	39.712	92.33	37.708	41.366	22.570
v5ADT15 - BLS25		-0.20	2.00	1.00	42.482	39.015	78.09	39.015	37.258	5.180

Table F.12: A table of the DVH statistics for the PTV at 2 mm for each BLS, starting from a position of 2 cm superior

Isocentre Offsets - 2cm sup								
Plan Name	Direction	Adjust Tolerance/Plan (APM)			1_PTVpsv36_2mm			
					D95%	D98%	V36.25Gy	V34.4Gy
		X (Lt/Rt) in cm	Z (Sup/Inf) in cm	Y (Ant/Post) in cm	D95% > 36.25 Gy	D98% > 34.4 Gy	V36.25Gy >95% (-5%)	V34.4Gy >98%
v5ADT15	/	0.0	0.00	0.00	38.379	37.710	99.89	100.00
v5ADT15 - BLS16	Inf Post Rt	0.20	-2.00	-1.00	38.579	36.961	98.75	99.73
v5ADT15 - BLS15		0.20	-1.00	-0.50	38.692	37.383	99.26	99.92
v5ADT15 - BLS14		0.20	-0.80	-0.40	38.665	37.467	99.30	99.87
v5ADT15 - BLS13		0.20	-0.60	-0.60	38.604	37.504	99.54	99.95
v5ADT15 - BLS12		0.15	-0.60	-0.40	38.652	37.443	99.30	99.88
v5ADT15 - BLS11		0.10	-0.40	-0.30	38.664	37.728	99.63	99.91
v5ADT15 - BLS10		0.08	-0.40	-0.20	38.733	37.825	99.71	99.98
v5ADT15 - BLS9		0.08	-0.30	-0.30	38.657	37.751	99.67	99.92
v5ADT15 - BLS8		0.05	-0.30	-0.15	38.800	37.962	99.92	100.00
v5ADT15 - BLS7		0.05	-0.20	-0.20	38.620	37.777	99.81	99.99
v5ADT15 - BLS6		0.03	-0.20	-0.10	38.604	37.766	98.82	100.00
v5ADT15 - BLS5		0.03	-0.10	0.05	38.448	37.777	98.83	100.00
v5ADT15 - BLS01	Center	0.01	0.00	0.00	38.296	37.595	99.89	100.00
v5ADT15 - BLS02	Sup Ant Lt	-0.03	0.10	0.05	38.289	37.605	99.86	100.00
v5ADT15 - BLS03		-0.03	0.20	0.10	38.378	37.604	99.80	99.99
v5ADT15 - BLS04		-0.05	0.20	0.20	38.336	37.286	99.40	99.96
v5ADT15 - BLS17		-0.05	0.30	0.15	38.474	37.617	99.76	99.99
v5ADT15 - BLS18		-0.08	0.30	0.30	38.076	37.087	99.17	99.91
v5ADT15 - BLS19		-0.08	0.40	0.20	38.171	37.177	99.36	99.96
v5ADT15 - BLS20		-0.10	0.40	0.30	38.010	36.997	99.13	99.91
v5ADT15 - BLS21		-0.15	0.60	0.40	37.919	36.905	99.01	99.85
v5ADT15 - BLS22		-0.20	0.60	0.60	38.060	37.168	99.32	99.99
v5ADT15 - BLS23		-0.20	0.80	0.40	37.805	36.812	98.91	99.81
v5ADT15 - BLS24		-0.20	1.00	0.50	37.700	36.811	98.92	99.91
v5ADT15 - BLS25		-0.20	2.00	1.00	36.963	36.053	97.43	99.86

Table F.13: A table of the DVH statistics for the urethra shifted (Urethra_XX) and unshifted (1_Urethra) for each BLS, starting from a position of 2 cm superior

Isocentre Offsets - 2cm sup								
Plan Name	Direction	Adjust Tolerance/Plan (APM)			1_Urethra (unshifted)		Urethra_XX (shifted)	
		X (Lt/Rt) in cm	Z (Sup/Inf) in cm	Y (Ant/Post) in cm	D50%	V42Gy	D50%	V42Gy
					D50% < 42 Gy	V42Gy < 50%	D50% <= 42 Gy	V42Gy <= 50%
v5ADT15	/	0.0	0.00	0.00	40.478	0.00	40.478	0.00
v5ADT15 - BLS16	Inf Post Rt	0.20	-2.00	-1.00	39.645	30.94	41.722	34.39
v5ADT15 - BLS15		0.20	-1.00	-0.50	42.493	63.79	41.770	32.57
v5ADT15 - BLS14		0.20	-0.80	-0.40	42.447	65.66	41.775	32.23
v5ADT15 - BLS13		0.20	-0.60	-0.60	41.895	46.26	41.227	4.41
v5ADT15 - BLS12		0.15	-0.60	-0.40	42.177	56.85	41.661	30.78
v5ADT15 - BLS11		0.10	-0.40	-0.30	42.175	54.93	41.636	30.80
v5ADT15 - BLS10		0.08	-0.40	-0.20	42.118	56.03	41.879	43.65
v5ADT15 - BLS9		0.08	-0.30	-0.30	42.153	55.32	41.708	36.97
v5ADT15 - BLS8		0.05	-0.30	-0.15	41.992	49.43	41.833	41.40
v5ADT15 - BLS7		0.05	-0.20	-0.20	48.280	41.98	41.723	35.09
v5ADT15 - BLS6		0.03	-0.20	-0.10	46.550	41.95	41.828	39.83
v5ADT15 - BLS5		0.03	-0.10	0.05	40.523	0.10	40.532	0.00
v5ADT15 - BLS01	Center	0.01	0.00	0.00	40.527	0.00	40.527	0.00
v5ADT15 - BLS02	Sup Ant Lt	-0.03	0.10	0.05	40.669	0.00	40.593	0.00
v5ADT15 - BLS03		-0.03	0.20	0.10	40.858	0.00	40.765	0.00
v5ADT15 - BLS04		-0.05	0.20	0.20	40.935	1.29	40.911	1.77
v5ADT15 - BLS17		-0.05	0.30	0.15	40.882	0.38	40.921	0.00
v5ADT15 - BLS18		-0.08	0.30	0.30	40.773	4.69	40.873	1.81
v5ADT15 - BLS19		-0.08	0.40	0.20	40.741	0.00	40.777	1.15
v5ADT15 - BLS20		-0.10	0.40	0.30	40.801	1.58	41.047	2.58
v5ADT15 - BLS21		-0.15	0.60	0.40	40.855	2.39	41.045	3.26
v5ADT15 - BLS22		-0.20	0.60	0.60	40.480	2.06	41.048	10.72
v5ADT15 - BLS23		-0.20	0.80	0.40	40.149	0.10	40.552	3.35
v5ADT15 - BLS24		-0.20	1.00	0.50	39.163	0.00	40.673	5.22
v5ADT15 - BLS25		-0.20	2.00	1.00	20.055	0.00	40.206	2.54

Table F.14: A table of the DVH statistics for the CTV for each BLS, starting from a position of 4 cm superior

Isocentre Offsets - 4 cm sup										
Plan Name	Direction	Adjust Tolerance/Plan (APM)			1_CTVpsv40					
		X (Lt/Rt) in cm	Z (Sup/Inf) in cm	Y (Ant/Post) in cm	D0.1cc	D95%	V40Gy	D99.9%	Dmean	V42Gy
					42.6Gy < D0.1cc < 48.3Gy	D95% > 40 Gy	V40Gy >95% (-5%)	D99.9% >= 40 Gy		V42Gy <=50%
v5ADT01	/	0.0	0.00	0.00	42.913	40.433	98.92	39.188	41.327	15.53
v5ADT01-BLS13	Inf Post Rt	0.20	-2.00	-1.00	46.919	41.939	99.47	38.780	44.189	94.70
v5ADT01-BLS12		0.20	-1.00	-0.50	45.348	41.363	99.13	38.170	43.078	87.65
v5ADT01-BLS11		0.20	-0.80	-0.40	45.511	41.054	99.13	38.140	43.010	84.56
v5ADT01-BLS10		0.20	-0.60	-0.60	44.998	41.004	98.89	38.400	42.656	79.89
v5ADT01-BLS09		0.15	-0.60	-0.40	45.091	40.854	98.26	37.960	42.683	78.09
v5ADT01-BLS08		0.10	-0.40	-0.30	45.046	40.746	97.90	37.860	42.545	76.11
v5ADT01-BLS07		0.08	-0.40	-0.20	44.579	41.019	98.59	38.540	42.509	77.44
v5ADT01-BLS06		0.08	-0.30	-0.30	44.963	40.740	97.85	38.000	42.587	76.29
v5ADT01-BLS05		0.05	-0.30	-0.15	44.030	40.945	99.08	38.967	42.273	67.25
v5ADT01-BLS04		0.05	-0.20	-0.20	44.830	40.890	98.67	38.687	42.426	73.72
v5ADT01-BLS03		0.03	-0.20	-0.10	43.876	40.819	99.43	39.320	42.091	55.28
v5ADT01-BLS02		0.03	-0.10	0.05	43.382	40.599	98.82	39.037	41.751	37.21
v5ADT01-BLS01	Center	0.01	0.00	0.00	43.194	40.315	98.04	39.120	41.358	16.48
v5ADT01-BLS14	Sup Ant Lt	-0.03	0.10	0.05	43.520	40.247	97.03	38.882	41.568	30.820
v5ADT01-BLS15		-0.03	0.20	0.10	43.307	40.354	97.72	38.767	41.584	27.980
v5ADT01-BLS16		-0.05	0.20	0.20	43.698	40.254	96.80	38.130	41.652	35.020
v5ADT01-BLS17		-0.05	0.30	0.15	43.493	40.257	97.20	38.390	41.526	27.040
v5ADT01-BLS18		-0.08	0.30	0.30	43.933	40.033	95.33	37.472	41.669	36.970
v5ADT01-BLS19		-0.08	0.40	0.20	43.600	40.000	95.00	37.977	41.486	28.540
v5ADT01-BLS20		-0.10	0.40	0.30	43.732	39.611	91.48	37.090	41.433	28.530
v5ADT01-BLS21		-0.15	0.60	0.40	43.834	36.609	92.09	37.110	41.510	29.740
v5ADT01-BLS22		-0.20	0.60	0.60	43.655	39.978	94.82	37.702	41.525	27.100
v5ADT01-BLS23		-0.20	0.80	0.40	43.885	39.558	91.44	36.960	41.535	32.610
v5ADT01-BLS24		-0.20	1.00	0.50	43.361	39.394	88.41	37.150	41.067	16.970
v5ADT01-BLS25		-0.20	2.00	1.00	/	/	/	/	/	/

Table F.15: A table of the DVH statistics for the PTV at 2 mm for each BLS, starting from a position of 4 cm superior

Isocentre Offsets - 4 cm sup								
Plan Name	Direction	Adjust Tolerance/Plan (APM)			1_PTVpsv36_2mm			
					D95%	D98%	V36.25Gy	V34.4Gy
		X (Lt/Rt) in cm	Z (Sup/Inf) in cm	Y (Ant/Post) in cm	D95% > 36.25 Gy	D98% > 34.4 Gy	V36.25Gy >95% (-5%)	V34.4Gy >98%
v5ADT01	/	0.0	0.00	0.00	38.324	37.703	99.88	100.00
v5ADT01-BLS13	Inf Post Rt	0.20	-2.00	-1.00	39.634	38.244	99.49	99.92
v5ADT01-BLS12		0.20	-1.00	-0.50	39.281	38.040	99.47	99.91
v5ADT01-BLS11		0.20	-0.80	-0.40	38.980	37.637	99.22	99.84
v5ADT01-BLS10		0.20	-0.60	-0.60	39.031	37.824	99.51	99.95
v5ADT01-BLS09		0.15	-0.60	-0.40	38.709	37.376	99.10	99.79
v5ADT01-BLS08		0.10	-0.40	-0.30	38.449	37.314	99.23	99.86
v5ADT01-BLS07		0.08	-0.40	-0.20	38.633	37.500	99.40	99.96
v5ADT01-BLS06		0.08	-0.30	-0.30	38.486	38.798	99.84	99.21
v5ADT01-BLS05		0.05	-0.30	-0.15	38.591	37.573	99.56	99.99
v5ADT01-BLS04		0.05	-0.20	-0.20	38.529	37.498	99.46	99.96
v5ADT01-BLS03		0.03	-0.20	-0.10	38.525	37.814	99.81	100.00
v5ADT01-BLS02		0.03	-0.10	0.05	38.487	37.755	99.70	100.00
v5ADT01-BLS01	Center	0.00	0.00	0.00	38.207	37.620	99.87	100.00
v5ADT01-BLS14	Sup Ant Lt	-0.03	0.10	0.05	38.198	37.445	99.72	100.00
v5ADT01-BLS15		-0.03	0.20	0.10	38.257	37.517	99.70	100.00
v5ADT01-BLS16		-0.05	0.20	0.20	38.206	37.270	99.29	99.90
v5ADT01-BLS17		-0.05	0.30	0.15	38.161	37.304	99.52	99.97
v5ADT01-BLS18		-0.08	0.30	0.30	37.845	37.765	98.72	99.75
v5ADT01-BLS19		-0.08	0.40	0.20	37.982	36.976	99.03	99.87
v5ADT01-BLS20		-0.10	0.40	0.30	38.553	36.392	98.19	99.66
v5ADT01-BLS21		-0.15	0.60	0.40	37.247	36.052	97.64	99.58
v5ADT01-BLS22		-0.20	0.60	0.60	37.666	36.686	98.62	99.87
v5ADT01-BLS23		-0.20	0.80	0.40	37.217	36.063	97.69	99.57
v5ADT01-BLS24		-0.20	1.00	0.50	37.015	35.901	97.28	99.57
v5ADT01-BLS25		-0.20	2.00	1.00	/	/	/	/

Table F.16: A table of the DVH statistics for the urethra shifted (Urethra_XX) and unshifted (1_Urethra) for each BLS, starting from a position of 4 cm superior

Isocentre Offsets - 4 cm sup								
Plan Name	Direction	Adjust Tolerance/Plan (APM)			1_Urethra (unshifted)		Urethra_XX (shifted)	
		X (Lt/Rt) in cm	Z (Sup/Inf) in cm	Y (Ant/Post) in cm	D50%	V42Gy	D50%	V42Gy
					D50% < 42 Gy	V42Gy < 50%	D50% <= 42 Gy	V42Gy <= 50%
v5ADT01	/	0.0	0.00	0.00	40.736	0.00	40.736	0.00
v5ADT01-BLS13	Inf Post Rt	0.20	-2.00	-1.00	39.270	39.18	43.201	79.33
v5ADT01-BLS12		0.20	-1.00	-0.50	42.809	65.30	42.321	70.73
v5ADT01-BLS11		0.20	-0.80	-0.40	42.956	72.45	42.522	77.36
v5ADT01-BLS10		0.20	-0.60	-0.60	42.213	56.48	41.868	39.85
v5ADT01-BLS09		0.15	-0.60	-0.40	42.398	65.44	42.037	53.57
v5ADT01-BLS08		0.10	-0.40	-0.30	42.008	50.67	42.029	51.91
v5ADT01-BLS07		0.08	-0.40	-0.20	41.932	44.09	41.992	49.00
v5ADT01-BLS06		0.08	-0.30	-0.30	41.904	40.75	42.055	53.81
v5ADT01-BLS05		0.05	-0.30	-0.15	41.576	27.07	41.680	32.38
v5ADT01-BLS04		0.05	-0.20	-0.20	41.780	37.65	41.800	37.25
v5ADT01-BLS03		0.03	-0.20	-0.10	41.319	16.87	41.316	16.38
v5ADT01-BLS02		0.03	-0.10	0.05	40.846	9.25	40.826	8.06
v5ADT01-BLS01	Center	0.01	0.00	0.00	40.660	0.00	40.660	0.00
v5ADT01-BLS14	Sup Ant Lt	-0.03	0.10	0.05	40.998	2.14	41.023	3.49
v5ADT01-BLS15		-0.03	0.20	0.10	41.008	3.62	41.078	4.81
v5ADT01-BLS16		-0.05	0.20	0.20	40.801	1.81	41.058	1.62
v5ADT01-BLS17		-0.05	0.30	0.15	40.786	0.67	40.829	1.99
v5ADT01-BLS18		-0.08	0.30	0.30	40.988	3.72	41.510	18.67
v5ADT01-BLS19		-0.08	0.40	0.20	40.519	1.72	40.844	1.00
v5ADT01-BLS20		-0.10	0.40	0.30	40.376	3.24	41.059	4.58
v5ADT01-BLS21		-0.15	0.60	0.40	41.016	0.38	41.348	4.23
v5ADT01-BLS22		-0.20	0.60	0.60	40.980	10.96	41.063	0.24
v5ADT01-BLS23		-0.20	0.80	0.40	40.601	1.33	41.274	1.43
v5ADT01-BLS24		-0.20	1.00	0.50	39.848	0.00	40.695	0.00
v5ADT01-BLS25		-0.20	2.00	1.00	/	/	/	/

Table F.17: A table summarising the rectum and bladder's DVH statistics for each plan with different offset from the prostate's isocentre

Plan Name	Direction	Adjust Tolerance/Plan (APM)			1_Rectum	
		X (Lt/Rt) in cm	Z (Sup/Inf) in cm	Y (Ant/Post) in cm	D1cc	V36Gy
					D1cc < 36 Gy	V36Gy < 1cc
v5ADT01	4cm sup	0.0	0.00	0.00	32.253	0.287
v4ADT15	2cm sup				33.267	0.403
v4ADT03	0cm				33.880	0.476
v4ADT05	2cm inf				34.505	0.636
v4ADT06	4cm inf				34.635	0.670
Plan Name	**Direction**	**Adjust Tolerance/Plan (APM)**			**1_Bladder**	
		X (Lt/Rt) in cm	**Z (Sup/Inf) in cm**	**Y (Ant/Post) in cm**	**D5cc**	**V36Gy**
					D5cc < 37 Gy	V37Gy < 5cc
v5ADT01	4cm sup	0.0	0.00	0.00	19.074	0.233
v4ADT15	2cm sup				20.180	0.290
v4ADT03	0cm				21.418	0.243
v4ADT05	2cm inf				21.865	0.259
v4ADT06	4cm inf				20.939	0.376

G

Treatment Planning Study: Part 2

G.1 | CTV movement within PTV

Table G.1: A table of the dosimetric criteria for the Urethra when CTV lies within PTV

CTV within PTV					
Direction	Adjust Tolerance/Plan (APM)			1_Urethra_x	
	X (Lt/Rt) in cm	Z (Sup/Inf) in cm	Y (Ant/Post) in cm	D50%	V42Gy
				D50% < 42 Gy	V42Gy < 50%
Inf Post Rt	0.200	-0.200	-0.200	40.582	0.29
	0.075	-0.350	-0.175	40.596	0.09
	0.050	-0.250	-0.125	40.547	0.00
	0.050	-0.200	-0.200	40.584	0.19
	0.025	-0.200	-0.100	40.551	0.00
	0.025	-0.100	0.050	40.546	0.00
Center	0.000	0.000	0.000	40.583	0.00
Sup Ant Lt	-0.025	0.100	0.050	40.895	0.00
	-0.025	0.200	0.100	40.619	0.00
	-0.050	0.200	0.200	40.702	0.00
	-0.050	0.250	0.125	40.613	0.00
	-0.075	0.350	0.175	40.653	0.09
	-0.200	0.200	0.200	40.783	0.00

Table G.2: A table of the dosimetric criteria for the CTV within PTV

CTV within PTV									
Direction	Adjust Tolerance/Plan (APM)			1_CTVpsv40_x					
	X (Lt/Rt) in cm	Z (Sup/Inf) in cm	Y (Ant/Post) in cm	D0.1cc	D95%	V40Gy	D99.9%	Dmean	V42Gy
				42.6Gy < D0.1cc < 48.3Gy	D95% > 40 Gy	V40Gy >95% (-5%)	D99.9% >= 40 Gy		V42Gy <=50%
Inf Post Rt	0.200	-0.200	-0.200	42.801	38.021	81.61	34.680	40.807	13.21
	0.075	-0.350	-0.175	42.798	37.552	79.69	30.840	40.663	12.30
	0.050	-0.250	-0.125	42.805	38.581	84.60	34.117	40.895	13.25
	0.050	-0.200	-0.200	42.804	38.481	84.31	35.000	40.905	13.46
	0.025	-0.200	-0.100	42.805	39.132	87.89	36.113	41.022	13.87
	0.025	-0.100	0.050	42.800	39.727	92.36	37.560	41.145	14.55
Center	0.000	0.000	0.000	42.799	40.015	95.18	38.702	41.204	14.71
Sup Ant Lt	-0.025	0.100	0.050	42.799	40.065	95.94	38.868	41.218	14.82
	-0.025	0.200	0.100	42.799	39.820	93.13	38.373	41.163	14.69
	-0.050	0.200	0.200	42.785	39.434	89.92	37.693	41.069	13.79
	-0.050	0.250	0.125	42.789	38.650	89.16	37.630	41.060	14.08
	-0.075	0.350	0.175	42.774	38.407	83.86	35.920	40.882	13.39
	-0.200	0.200	0.200	42.791	39.165	87.43	37.120	41.005	13.82

H

Film Dosimetry - Scaling Data

Table H.1: Scaling: Static 0 mm film scaling with morning films

Pixel Dimensions	Half Image	Full Image		Conversion			W/O Scaling		Percentage Error W/O Scaling		With Scaling	Percentage Error With Scaling
Horizontal (X)	1046	2092	px	1px ='	0.2 mm							
Vertical (Y)	661.5	1323	px									
Film	Coordinates											
Static 0mm	morning	evening	morning	evening	morning	evening	morning	evening	morning	evening	morning	morning
7.25	from centre (mm)		px from top right corner		percentage		dose		error		dose	error
x1	-58	3.7	756	1064.5	36.14	50.88	7.4161	7.4178	-2.3%	-2.3%	7.2864	0.5%
x2	-48	13.7	806	1114.5	38.53	53.27						
y1	-11	-10.3	606.5	610	45.84	46.11						
y2	-21	-20.3	556.5	560	42.06	42.33						
8	morning	evening	morning	evening	morning	evening	morning	evening	morning	evening	morning	morning
x1	-88	51.7	606	1304.5	28.97	62.36	8.2111	8.0805	-2.6%	-1.0%	7.9950	0.1%
x2	-78	61.7	656	1354.5	31.36	64.75						
y1	-9	-8.6	616.5	618.5	46.60	46.75						
y2	-19	-18.6	566.5	568.5	42.82	42.97						
9	morning	evening	morning	evening	morning	evening	morning	evening	morning	evening	morning	morning
x1	-152.9	98.9	281.5	1540.5	13.46	73.64	9.2036	9.0743	-2.3%	-0.8%	9.0859	1.0%
x2	-142.9	108.9	331.5	1590.5	15.85	76.03						
y1	-11.4	-7.2	604.5	625.5	45.69	47.28						
y2	-21.4	-17.2	554.5	575.5	41.91	43.50						

Table H.2: Scaling: Static 8.5 mm inf shift film scaling with morning films

Static 8.5mm inf shift	morning	evening	morning	evening	morning	evening	morning	evening	morning	evening	morning	morning
7.25	from centre		from top right corner		percentage		dose		error			error
x1	-57.2	0.7	760	1049.5	**36.33**	**50.17**	**7.4226**	**7.4297**	**-2.4%**	**-2.5%**	**7.2744**	**0.3%**
x2	-47.2	10.7	810	1099.5	**38.72**	**52.56**						
y1	-11	-9.9	606.5	612	**45.84**	**46.26**						
y2	-21	-20	556.5	561.5	**42.06**	**42.44**						
8	**morning**	**evening**	**morning**	**evening**	**morning**	**evening**	**morning**	**evening**	**morning**	**evening**	**morning**	**morning**
x1	-96	51.4	566	1303	**27.06**	**62.60**	**8.1911**	**8.0879**	**-2.4%**	**-1.1%**	**7.9770**	**-0.3%**
x2	-86	61.4	616	1353	**29.45**	**65.00**						
y1	-13	-6.5	596.5	629	**45.09**	**53.70**						
y2	-23	-16.5	546.5	579	**41.31**	**57.50**						
9	**morning**	**evening**	**morning**	**evening**	**morning**	**evening**	**morning**	**evening**	**morning**	**evening**	**morning**	**morning**
x1	-151.8	94	287	1516	**13.72**	**72.47**	**9.2094**	**9.0803**	**-2.3%**	**-0.9%**	**9.0852**	**0.9%**
x2	-141.8	104	337	1566	**16.11**	**74.86**						
y1	-13.5	-8	594	621.5	**44.90**	**46.98**						
y2	-23.5	-18	544	571.5	**41.12**	**43.20**						

Table H.3: Scaling: Static VOICE 97% film with evening films

Static VOICE 97	morning	evening	morning	evening	morning	evening	morning	evening	morning	evening	evening	evening
7.25	from centre		from top right corner		percentage		dose		error			error
x1	-58.8	2	752	1056	**35.95**	**50.48**	**7.4289**	**7.4330**	**-2.5%**	**-2.5%**	**7.3616**	**1.5%**
x2	-48.7	12	802.5	1106	**38.36**	**52.87**						
y1	-12	-10.2	601.5	610.5	**45.46**	**46.15**						
y2	-22	-20.1	551.5	561	**41.69**	**42.40**						
8	**morning**	**evening**	**morning**	**evening**	**morning**	**evening**	**morning**	**evening**	**morning**	**evening**	**evening**	**evening**
x1	-94	50.9	576	1300.5	**25.60**	**62.60**	**8.2024**	**8.0922**	**-2.5%**	**-1.2%**	**7.9951**	**0.1%**
x2	-84	60.8	626	1350	**28.00**	**65.00**						
y1	-14.4	-7.8	589.5	622.5	**54.00**	**53.70**						
y2	-24.3	-17.8	540	572.5	**57.90**	**57.50**						
9	**morning**	**evening**	**morning**	**evening**	**morning**	**evening**	**morning**	**evening**	**morning**	**evening**	**evening**	**evening**
x1	-151.9	94.7	286.5	1519.5	**13.70**	**72.63**	**9.2135**	**9.1053**	**-2.4%**	**-1.2%**	**8.9345**	**0.7%**
x2	-142	104.8	336	1570	**16.06**	**75.05**						
y1	-13.2	-4.8	595.5	637.5	**45.01**	**48.19**						
y2	-23.2	-14.8	545.5	587.5	**41.23**	**44.41**						

Table H.4: Scaling: Motion 2 BLS film with evening films

Motion 2BLS	morning	evening	morning	evening	morning	evening	morning	evening	morning	evening	evening	evening
7.25	from centre		from top right corner		percentage		dose		error			error
x1	-59.4	0	749	1046	**35.80**	**50.00**	**7.4299**	**7.4392**	**-2.5%**	**-2.6%**	**7.3592**	**-1.5%**
x2	-49.4	10	799	1096	**38.19**	**52.39**						
y1	-11.2	-14	605.5	591.5	**45.77**	**44.71**						
y2	-21.2	-24	555.5	541.5	**41.99**	**40.93**						
8	**morning**	**evening**	**morning**	**evening**	**morning**	**evening**	**morning**	**evening**	**morning**	**evening**	**evening**	**evening**
x1	-96.5	50.3	563.5	1297.5	**26.94**	**62.02**	**8.1774**	**8.1009**	**-2.2%**	**-1.3%**	**8.0120**	**-0.2%**
x2	-86.6	60.3	613	1347.5	**29.30**	**64.41**						
y1	-14.8	-8.8	587.5	617.5	**44.41**	**46.67**						
y2	-24.7	-18.7	538	568	**40.67**	**42.93**						
9	**morning**	**evening**	**morning**	**evening**	**morning**	**evening**	**morning**	**evening**	**morning**	**evening**	**evening**	**evening**
x1	-152.2	94.9	285	1520.5	**13.62**	**72.68**	**9.2261**	**9.1096**	**-2.5%**	**-1.2%**	**8.9595**	**0.4%**
x2	-142.3	104.9	334.5	1570.5	**15.99**	**75.07**						
y1	-14	-3.4	591.5	644.5	**44.71**	**48.72**						
y2	-23.9	-13.4	542	594.5	**40.97**	**44.94**						

Table H.5: Scaling: Motion 3 BLS film with evening films

Motion 3BLS	morning	evening	morning	evening	morning	evening	morning	evening	morning	evening	evening	evening
7.25	from centre		from top right corner		percentage		dose		error			error
x1	-58.1	1.3	755.5	1052.5	**36.11**	**50.31**	**7.4529**	**7.4531**	**-2.8%**	**-2.8%**	**7.3589**	**-1.5%**
x2	-48.1	11.2	805.5	1102	**38.50**	**52.68**						
y1	-12.7	-11.6	598	603.5	**45.20**	**45.62**						
y2	-22.7	-21.5	548	554	**41.42**	**41.87**						
8	**morning**	**evening**	**morning**	**evening**	**morning**	**evening**	**morning**	**evening**	**morning**	**evening**	**evening**	**evening**
x1	-96.5	51.3	563.5	1302.5	**26.94**	**62.60**	**8.2106**	**8.1107**	**-2.6%**	**-1.4%**	**8.0100**	**-0.1%**
x2	-86.4	61.2	614	1352	**29.35**	**65.00**						
y1	-13.3	-9.8	595	612.5	**44.97**	**53.70**						
y2	-23.3	-19.7	545	563	**41.19**	**57.50**						
9	**morning**	**evening**	**morning**	**evening**	**morning**	**evening**	**morning**	**evening**	**morning**	**evening**	**evening**	**evening**
x1	-153	97.6	281	1534	**13.43**	**73.33**	**9.0895**	**9.2325**	**-1.0%**	**-2.6%**	**8.9366**	**0.7%**
x2	-143	107.7	331	1584.5	**15.82**	**75.74**						
y1	-11.7	-10.1	603	611	**45.58**	**46.18**						
y2	-21.6	-20.1	553.5	561	**41.84**	**42.40**						

References

Berberoğlu, K. (2016). Use of positron emission tomography/computed tomography in radiation treatment planning for lung cancer. *Molecular Imaging and Radionuclide Therapy*, 25:50–62.

Bertholet, J., Knopf, A., Eiben, B., McClelland, J., Grimwood, A., Harris, E., Menten, M., Poulsen, P., Nguyen, D. T., Keall, P., and Oelfke, U. (2019). Real-time intrafraction motion monitoring in external beam radiotherapy. *Physics in Medicine amp; Biology*, 64:15TR01.

Bosma, L. S., Zachiu, C., Ries, M., , D., and Raaymakers, B. W. (2021). Quantitative investigation of dose accumulation errors from intra-fraction motion in mrgrt for prostate cancer. *Physics in Medicine and Biology*, 66:065002–065002.

Brown, K. and Corbett, J. (2025). Elekta unity comprehensive motion management-explained.

Chetcuti, M. (2025). Extended commissioning and validation of the comprehensive motion management system on an elekta unity mrl. Master's thesis, University of Malta.

de Muinck Keizer, D., Kerkmeijer, L., Willigenburg, T., van Lier, A., Hartogh, M. d., van der Voort van Zyp, J., de Groot-van Breugel, E., Raaymakers, B., Lagendijk, J., and de Boer, J. (2020a). Prostate intrafraction motion during the preparation and delivery of mr-guided radiotherapy sessions on a 1.5t mr-linac. *Radiotherapy and Oncology*, 151:88–94.

de Muinck Keizer, D. M., Kontaxis, C., Kerkmeijer, L. G. W., van der Voort van Zyp, J. R. N., van der Berg, C. A. T., Raaymakers, B. W., Lagendijk, J., and de Boer, J. C. J. (2020b). Dosimetric impact of soft-tissue based intrafraction motion from 3d cine-mr in prostate sbrt. 65:025012–025012.

ELEKTA, S. A. (2023). User manual: Mosaiq 3.2.1.0 instructions for use.

ELEKTA, S. A. (2024). User manual: Monaco instructions for use for: Monaco 6.2.

EMITEL, E. (2016). Emitel. *www.emitel2.eu*, Last Accessed on 15th July 2025.

Faccenda, V., Panizza, D., Daniotti, M. C., Pellegrini, R., Trivellato, S., Caricato, P., Lucchini, R., De Ponti, E., and Arcangeli, S. (2023). Dosimetric impact of intrafraction prostate motion and interfraction anatomical changes in dose-escalated linac-based sbrt. *Cancers*, 15:1153.

Grams, M. (n.d). Do's and don'ts of gafchromic film dosimetry.

Kishan, A. U., Martin Ma, T., Lamb, J., Casado, M., Wilhalme, H., Low, D. A., Sheng, K., Sharma, S., Nickols, N. G., Pham, J., Yang, Y., Gao, Y. T., Neylon, J., Basehart, V., Cao, M., and Steinberg, M. L. (2023). Magnetic resonance imaging–guided vs computed tomography–guided stereotactic body radiotherapy for prostate cancer. *JAMA Oncology*, 9:365–365.

Kontaxis, C., de Muinck Keizer, D. M., Kerkmeijer, L. G., Willigenburg, T., den Hartogh, M. D., van der Voort van Zyp, J. R., de Groot-van Breugel, E. N., Hes, J., Raaymakers, B. W., Lagendijk, J. J., and de Boer, H. C. (2020). Delivered dose quantification in prostate radiotherapy using online 3d cine imaging and treatment log files on a combined 1.5t magnetic resonance imaging and linear accelerator system. *Physics and Imaging in Radiation Oncology*, 15:23–29.

Ladbury, C., Amini, A., Schwer, A., Liu, A., Williams, T., and Lee, P. (2023). Clinical applications of magnetic resonance-guided radiotherapy: A narrative review. *Cancers*, 15:2916.

Lawes, R., Barnes, H., Herbert, T., Mitchell, A., Nill, S., Oelfke, U., Pathmanathan, A., Smith, G. A., Sritharan, K., Tree, A., McNair, H., and Dunlop, A. (2022). Mri-guided adaptive radiotherapy for prostate cancer: When do we need to account for intra-fraction motion? *Clinical and Translational Radiation Oncology*, 37:85–88.

Legge, K., Nguyen, D., Ng, J. A., Wilton, L., Richardson, M., Booth, J., Keall, P., O'Connor, D. J., Greer, P., and Martin, J. (2017). Real-time intrafraction prostate motion during linac based stereotactic radiotherapy with rectal displacement. *Journal of Applied Clinical Medical Physics*, 18:130–136.

Mastella, E., Epile, J. E., Guglielmo, E. D., Fabbri, S., Calderoni, F., Manco, L., Szilagyi, K. E., Malorgio, A., Turra, A., and Stefanelli, A. (2024). Stereotactic body radiation therapy (sbrt) for prostate cancer: Improving treatment delivery efficiency and accuracy. *Technical Innovations Patient Support in Radiation Oncology*, 30:100253–100253.

Menten, M. J., Mohajer, J. K., Nilawar, R., Bertholet, J., Dunlop, A., Pathmanathan, A. U., Moreau, M., Marshall, S., Wetscherek, A., Nill, S., Tree, A. C., and Oelfke, U. (2020). Automatic reconstruction of the delivered dose of the day using mr-linac treatment log files and online mr imaging. *Radiotherapy and Oncology*, 145:88–94.

Munther, M., Zyoud, M. M., Tahani, R. K., and Dweikat, K. (2024). Quantitative research methods: Maximizing benefits, addressing limitations, and advancing methodological...

Ocanto, A., Torres, L., Montijano, M., Rincón, D., Fernández, C., Sevilla, B., Gonsalves, D., Teja, M., Guijarro, M., Glaría, L., Hernánz, R., Zafra-Martin, J., Sanmamed, N., Kishan, A., Alongi, F., Moghanaki, D., Nagar, H., and Couñago, F. (2024). Mr-linac, a new partner in radiation oncology: Current landscape. *Cancers*, 16:270.

Oehler, C., Roehner, N., Sumila, M., Curschmann, J., Storelli, F., Zwahlen, D. R., and Schneider, U. (2022). Intrafraction prostate motion management for ultra-hypofractionated radiotherapy of prostate cancer. *Current Oncology*, 29:6314–6324.

Smith, B., Allen, B., Rusu, S., St-Aubin, J., and Hyer, D. (2025). Real-time tracking of lung tumors using a 1.5t elekta unity mr-linac: first clinical experiences. *Frontiers in Oncology*, 15.

Snyder, J., Smith, B., Aubin, J. S., Shepard, A., and Hyer, D. (2024). Simulating an intra-fraction adaptive workflow to enable ptv margin reduction in mrigart volumetric modulated arc therapy for prostate sbrt. *Frontiers in Oncology*, 13.

Tetar, S. U., Bruynzeel, A. M., Verweij, L., Bohoudi, O., Slotman, B. J., Rosario, T., Palacios, M. A., and Lagerwaard, F. J. (2022). Magnetic resonance imaging-guided radiotherapy for intermediate- and high-risk prostate cancer: Trade-off between planning target volume margin and online plan adaption. *Physics and Imaging in Radiation Oncology*, 23:92–96.

Tsekas, G., Zachiu, C., Bol, G. H., van den Dobbelsteen, M., Meijers, L. T., van Lier, A. L., de Boer, J. C., and Raaymakers, B. W. (2024). Investigating the use of comprehensive motion monitoring for intrafraction 3d drift assessment of hypofractionated prostate cancer patients on a 1.5t magnetic resonance imaging radiotherapy system. *Physics and Imaging in Radiation Oncology*, 31:100596.

Uijtewaal, P., Borman, P., Cote, B., LeChasseur, Y., Therriault-Proulx, F., Flores, R., Smith, S., Koenig, G., Raaymakers, B., and Fast, M. (2023). Performance characterization of a novel hybrid dosimetry insert for simultaneous spatial, temporal, and motion-included dosimetry for mr-linac. *Medical Physics*, 51:2983–2997.

Uno, T., Tsuneda, M., Abe, K., Fujita, Y., Harada, R., Saito, M., Kanazawa, A., Kodate, A., Abe, Y., Ikeda, Y., Nemoto, M. W., and Yokota, H. (2023). A new workflow of the on-line 1.5-t mr-guided adaptive radiation therapy. *Japanese Journal of Radiology*, 41:1316–1322.

van As, N. and Tree, A. (2020). Pace radiotherapy planning and delivery guidelines version 2.2 the pace trial (prostate advances in comparative evidence) international randomised study of prostatectomy

vs stereotactic body radiotherapy (sbrt) and conventional radiotherapy vs sbrt for early stage organ-confined prostate cancer radiotherapy planning and delivery guidelines (pace-a and pace-c).

Vanhanen, A., Poulsen, P., and Kapanen, M. (2020). Dosimetric effect of intrafraction motion and different localization strategies in prostate sbrt. *Physica Medica*, 75:58–68.

Willigenburg, T., Zachiu, C., Bol, G. H., de Groot-van Beugel, E. N., Lagendijk, J. J., van der Voort van Zyp, J. R., Raaymakers, B. W., and de Boer, J. C. (2022). Clinical application of a sub-fractionation workflow for intrafraction re-planning during prostate radiotherapy treatment on a 1.5 tesla mr-linac: A practical method to mitigate intrafraction motion. *Radiotherapy and Oncology*, 176:25–30.

Winkel, D., Bol, G. H., Kroon, P. S., van Asselen, B., Hackett, S. S., Werensteijn-Honingh, A. M., Intven, M. P., Eppinga, W. S., Tijssen, R. H., Kerkmeijer, L. G., de Boer, H. C., Mook, S., Meijer, G. J., Hes, J., Willemsen-Bosman, M., de Groot-van Breugel, E. N., Jürgenliemk-Schulz, I. M., and Raaymakers, B. W. (2019). Adaptive radiotherapy: The elekta unity mr-linac concept. *Clinical and Translational Radiation Oncology*, 18:54–59.

Xiong, Y., Rabe, M., Nierer, L., Kawula, M., Corradini, S., Belka, C., Riboldi, M., Landry, G., and Kurz, C. (2022). Assessment of intrafractional prostate motion and its dosimetric impact in mri-guided online adaptive radiotherapy with gating. *Strahlentherapie und Onkologie*, 199:544–553.

Zwierzchowski, G., Bielƒôda, G., Skowronek, J., and Mazur, M. (2016). Film based verification of calculation algorithms used for brachytherapy planning-getting ready for upcoming challenges of mbdca. *Journal of Contemporary Brachytherapy*, 4:326–335.